TOPOLOGICAL STATES OF MATTER IN TWO-DIMENSIONAL FERMIONIC SYSTEMS

printed by Ipskamp Drukkers BV
ISBN: 978-94-6191-394-4

TOPOLOGICAL STATES OF MATTER IN TWO-DIMENSIONAL FERMIONIC SYSTEMS

Topologische toestanden
in tweedimensionale fermionische systemen

(met een samenvatting in het Nederlands)

Proefschrift

ter verkrijging van de graad van doctor aan de Universiteit Utrecht op gezag van de rector magnificus, prof. dr. G. J. van der Zwaan, ingevolge het besluit van het college voor promoties in het openbaar te verdedigen op woensdag 19 september 2012 des middags te 2.30 uur

door

WOUTER BEUGELING

geboren op 21 maart 1982 te Niedorp

Promotor: Prof. dr. C. Morais Smith

Contents

Chapter 1

Introduction

Two-dimensional systems exhibit specific quantum phenomena that are not present in systems with other dimensionality, and as such they form a very rich field of study in physics. This field has been opened by the realisation of the quantum Hall effect in the early 1980s. The experimental evidence of this effect in a GaAs/AlGaAs semiconductor heterostructure has been provided by Von Klitzing [1], who has been awarded the 1985 Nobel Prize in Physics for this achievement. The system studied by Von Klitzing is the Hall system, where an electric current is applied to a two-dimensional electron gas (2DEG), subjected to a perpendicular magnetic field. Classically, the Lorentz force deflects the electrons, so that a voltage is measured in the transverse direction, as demonstrated in Fig. 1.1. In 1879, Hall demonstrated by a conductance measurement on gold leaf, that this transverse (or Hall) voltage is proportional to the magnetic field strength [2]. Von Klitzing showed that in pure systems at low temperatures, this proportionality is no longer valid; instead, the measured voltage comes in steps, such that the ratio between the applied current and the voltage is an integer multiple of a fixed conductance value; see Fig. 1.2(a). The independence of the quantised Hall conductance on the system's size and shape and the ability to measure it very precisely has led to the proposal of using the Von Klitzing constant $h/e^2 = 25812.807\ \Omega$ as the standard for resistance measurements.

The novelty of the quantum Hall state lies in the fact that the bulk and the edges exhibit different properties: The bulk is insulating, and only the edges of the system carry the current. Due to the quantisation of the electron motion, the transverse (Hall) conductivity is quantised: The currents propagate in edge channels, each of which contributes one conductivity quantum e^2/h to the Hall conductivity. These edge states are *chiral*, i.e., all edge currents on a single edge propagate in the same direction. As there are no edge states with oppositely propagating currents, backward scattering is not possible. Thus, the Hall conductivity is immune to disorder effects and to local perturbations in the geometry in the system. The Hall conductivity is therefore a *topologically protected* quantity.

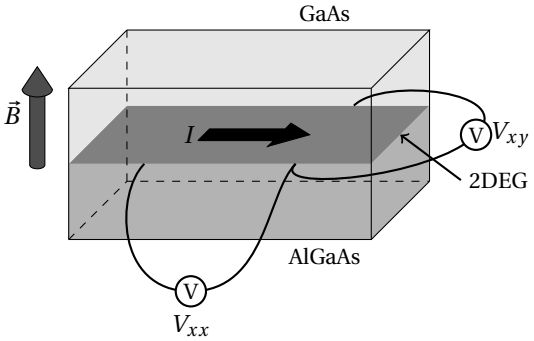

Figure 1.1: Schematic view of a 2DEG at the interface of a GaAs/AlGaAs heterostructure. We indicate the magnetic field **B**, the current I, the longitudinal voltage V_{xx} and transverse (or Hall) voltage V_{xy}.

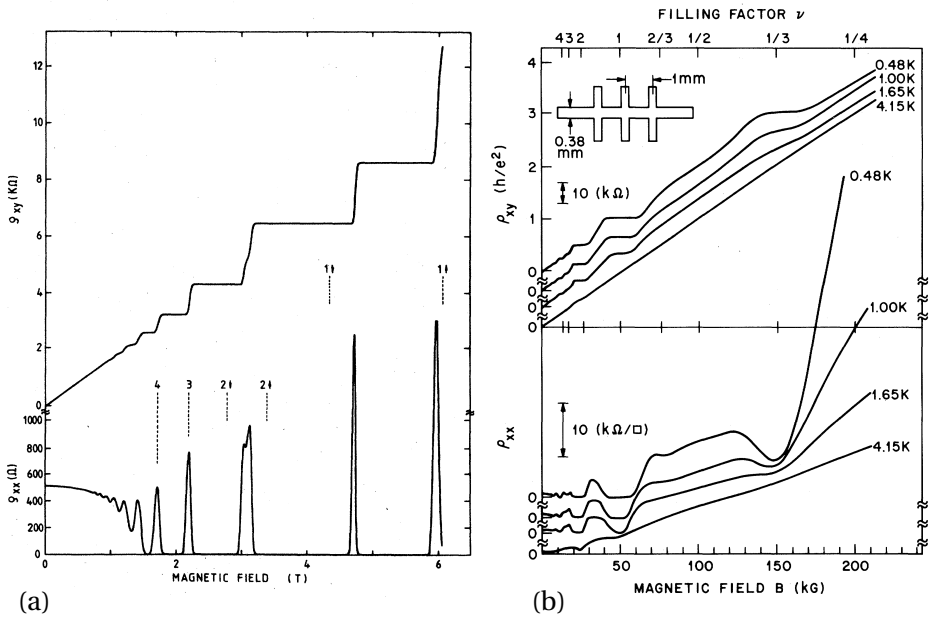

Figure 1.2: (a) Measurements of the longitudinal and transverse (Hall) resistance by Von Klitzing *et al.* [3], showing the integer quantum Hall effect. (b) Measurements of the longitudinal and transverse resistance by Tsui *et al.* [4], showing the fractional quantum Hall effect.

In the theory of quantum Hall physics, the quantisation of the electron motion is known as the *Landau-level* quantisation. In a magnetic field, the electrons move in circular *cyclotron orbits* due to the Lorentz force. In quantum mechanics, the radii of these orbits can take only specific values, i.e., the orbits are quantised. Each of the cyclotron radii has an energy associated to it, $\hbar\omega_c(n+\frac{1}{2})$, where $\omega_c = eB/m$ is the cyclotron frequency (in terms of the electron charge e, mass m, and magnetic field strength B), and $n = 0, 1, 2, \ldots$ is the quantum number enumerating the increasing values for the radius. Each Landau level has a large degeneracy, since there are many cyclotron orbits at different positions in the system, all carrying the same energy. The electrons performing the circular cyclotron motion in the bulk do not contribute to the Hall conductivity, but those near the edge cannot complete their circular orbits, and they will "skip" forward along the edge, giving rise to a net current. There is one edge channel per Landau level, so that the Hall conductivity is ne^2/h when n Landau levels are completely occupied [5, 6].

Nowadays, the quantised Hall conductivity is also understood as a topological invariant known as the *Chern number*, which is a winding number for a vector bundle on the (two-dimensional) first Brillouin zone. In physics, this number is evaluated through the integration of the curl of the so-called Berry connection over the first Brillouin zone. The Berry connection, in turn, is defined in terms of the eigenstates of the Hamiltonian. As a winding number, the Chern number is always an integer. In quantum Hall physics, the Chern number that defines the Hall conductivity is known as the TKNN integer (after Thouless, Kohmoto, Nightingale, and Den Nijs [7]), which is equal to the number of edge channels on each edge. The fact that this number is an integer means that it cannot be perturbed by small (i.e., continuous) deformations of the system, i.e., it is topologically protected. Physically speaking, the topological protection is provided by the property that the number of edge channels cannot be modified as long as the bulk of the system remains gapped.

Soon after the experimental verification and theoretical description of the quantum Hall effect, it has been shown in experiments with improved samples that the Hall conductivity can also be quantised at noninteger values times the conductivity quantum [4, 8], see Fig. 1.2(b). In these experiments, the Hall conductivity also shows quantisation at fractional numbers times e^2/h. For this reason, this effect has been dubbed the *fractional quantum Hall effect* (FQHE), as opposed to the *integer quantum Hall effect* (IQHE) discussed earlier. Importantly, the theoretical explanation of the FQHE requires to take into account interparticle interactions, unlike the IQHE, which may be understood within a single-particle perspective. The interacting (strongly correlated) nature of the FQHE theory prevents an exact description of such a system, due to the huge amount of particles involved. Instead of exact descriptions, the first theories of the FQHE, pioneered by Laughlin [9], rely on *trial wave functions*. These trial wave functions are not derived from first principles, but they are postulated, and it is shown that they lead to a good agreement in terms of physical observables. The

Laughlin wave functions are compatible with a framework in which the FQHE is explained through *flux attachments* [10, 11]. Here, the electrons pair up with several flux quanta to form a *composite fermion* [10–12]. The key point is that the FQHE of electrons can now be understood as an IQHE of composite fermions, which is a non-interacting theory, much simpler than the strongly correlated FQHE theory. Although the description of the system in terms of the flux attachment is only approximate, one is able to compute physical observables in the thermodynamic limit (many-particle limit). This should be contrasted to exact numerical studies, which can be performed only up to tens of particles, because the involved Hilbert-space dimension increases exponentially with the number of particles [13–15]. Besides the ability to go into the thermodynamic limit, another motivation to use the theory of flux attachments is that it provides an intuitive way to understand the physics that is involved, which would be much harder in a numerical study.

The flux attachment is rigorously described by a *Chern-Simons* transformation on the wave functions [6, 16, 17]. This Chern-Simons transformation generates an additional gauge field, that renormalises the original (external) magnetic field. The composite fermions "feel" this renormalised field, so that their effective filling factor (which depends on the magnetic field) differs from the electron filling factor. Within the framework of the Chern-Simons theory, one encounters field operators which neither commute nor anticommute (like bosons and fermions, respectively), but which pick up a certain phase $e^{i\alpha}$ when interchanged. Such fields are said to obey *anyonic statistics* if α is not an integer multiple of π, which is a property that appears exclusively in two-dimensional systems. In addition, some quantum Hall states (e.g., at filling factor 5/2) are described by theories featuring *nonabelian anyons*, where the statistical phases are given by matrices rather than numbers [18, 19]. The nonabelian exchange of particles, also known as *braiding*, has potential applications in quantum computation [20].

There have been several approaches to describe the fractional quantum Hall system with Chern-Simons theory. The most common way is to treat the system within the Lagrangian formalism, i.e., by including the (topological) Chern-Simons action [16, 21, 22]. A different perspective is obtained in a Hamiltonian formulation of the theory [23–28]. The aim of such a description is to provide the composite-fermion operators and the correct form factors to construct a Hamiltonian for the composite-fermion system. The resulting Hamiltonian is of the same form as the original one before the flux attachment has been applied, but it describes the dynamics of the composite fermions rather than that of the electrons. The flux attachment may then be repeated: Additional flux may be attached to the composite fermions, so as to create *second generation* composite fermions. This construction has been used to explain, e.g., the plateau at the filling fraction $\nu = 4/11$, which does appear in the framework of a single flux attachment [29, 30]. The idea of higher generation composite fermions provides a hierarchy of quantum Hall states that explains the self-similarity of the Hall

conductivity curve [30, 31]. Although the values obtained for the gaps are sometimes less precise than those obtained from the numerical calculations based on the wave functions, the Chern-Simons theory has the merit that it may be applied in a parameter regime where numerical calculations are unreliable, as e.g. for the $\nu = 4/11$ state. Because the gap of this state is small, the size of the system to be considered numerically, which grows with the inverse of the excitation gap, is two orders of magnitude beyond the limits for which numerical calculations are feasible [30, 32, 33].

The field of quantum Hall physics has gained renewed interest since the experimental isolation of graphene, the two-dimensional form of carbon, and the subsequent observation of the quantum Hall effect in this material [34, 35]. In graphene samples, the IQHE is extremely robust, and appears even at room temperature [36]. The quantum Hall effect in graphene differs essentially from the one observed in semiconductor heterostructures, due to the difference in the dispersion relations. In semiconductors, the dispersion is quadratic in the momentum, and the Landau levels show a linear dependence on the magnetic field strength, $E_n \propto B(n+\frac{1}{2})$. In graphene, the electrons obey a *Dirac* dispersion, which is linear around zero energy, due to the honeycomb lattice structure. As a consequence, the Landau-level energies scale as $E_n \propto \pm\sqrt{nB}$. A second difference is that in graphene each Landau level is fourfold degenerate due to two spin and two *valley* degrees of freedom. The latter derives from the fact that the first Brillouin zone features two inequivalent points, around which the dispersion exhibits the linear behaviour. Due to the differences in the energy dependence and conductivity steps with respect to those in semiconductor 2DEGs, this behaviour has been dubbed the *anomalous quantum Hall effect* (not to be confused with the quantum version of the anomalous Hall effect).

Recent experiments have also shown evidence for the FQHE in graphene [37, 38]. In order to explain the FQHE in graphene theoretically using the argument of flux attachments, one would require a Chern-Simons theory that includes multiple internal degrees of freedom (e.g., spin and valley pseudospin). For semiconductors, these theories have been developed with two internal degrees of freedom (spin only) [39–41]. Motivated by the four internal degrees of freedom in graphene, we extend these theories to systems with an arbitrary number of internal degrees of freedom. In Chapter 4, we generalise the Hamiltonian theory by Shankar and Murthy and we show that it recovers the known single- and two-component theories as special cases. Here, we show that the matrix K, that describes the number of attached flux quanta to one type of particle due to the presence of another type of particle, plays the same role as the even integer that connects the Laughlin wave function of the composite fermions to that of the electrons, as described by Jain for the single-component case [10, 11]. In particular, the interpretation of the wave functions by means of the *plasma analogy* [9] remains valid for multi-component systems. Furthermore, we generalise the decoupling procedure proposed by Shankar and Murthy [24], and we recover a set of excitation energies that obeys Kohn's theorem, namely, one of them equals the cyclotron energy, asso-

ciated to a mode where all components contribute equally. In addition, we identify the other energy eigenvalues and connect the corresponding modes to other linear combination of the componentwise Hall currents. We also explore the several "singular" cases, e.g., the **SU**(2)-symmetric two-component system. In our formalism, these cases are characterised by states with singular exponent matrix, and the corresponding flux attachments are described by singular matrices K. In particular, we explore the various possibilities for the flux attachments (both singular and nonsingular) in the four-component case, relevant for graphene.

In 1988, Haldane [42] has described a mechanism to obtain a quantum Hall effect in zero net magnetic field in a honeycomb lattice, by applying local flux of alternating sign within different parts of the lattice unit cell. Initially, his paper did not receive much interest, until the point that Kane and Mele realised that intrinsic spin-orbit coupling in graphene is equivalent to two copies of the Haldane model with opposite signs for spin up and down [43, 44]. Thus, the system is time-reversal symmetric. At zero energy the bulk of the system is gapped, but the edge carries two edge states, of opposite spin and propagating in opposite directions, so-called *helical* edge states, see Fig. 1.3. The contributions to the Hall currents therefore cancel, but those to the spin current add up. This state is known as the *quantum spin Hall* state, referring to the quantised spin Hall conductivity. The latter is a topologically protected quantity. The protection is provided by time-reversal symmetry (unlike the quantum Hall effect where this symmetry is absent), due to the fact that backscattered electrons interfere destructively with each other [45]. The relevant topological invariant is known as the spin Chern number. Unlike the ordinary Chern number which can take any integer value (i.e., in $\mathbb{Z}$), the spin Chern number can take only two values, and is therefore known as a $\mathbb{Z}_2$ topological invariant. This property derives from an even-odd effect that may be explained as follows. (See Fig. 1.4 for an illustration.) A single *Kramers pair* (a time-reversal invariant pair of edge states) cannot be gapped out while preserving time-reversal symmetry, since they cross only at zero momentum. If there are two Kramers pairs, then there are crossings at other (non-time-reversal invariant) momenta, which are unprotected, i.e., they can be gapped out by disorder to form a trivial state. Thus, an even number of Kramers pairs can all be gapped out and the system is topologically equivalent to the trivial state. On the other hand, when the number of Kramers pairs is odd, one cannot gap out all of them, and then the spin Hall conductivity is nonzero. The two elements of the group $\mathbb{Z}_2$ ("integers modulo 2") exactly represent these two inequivalent topological classes.

Although the model proposed by Kane and Mele provides an elegant way to describe the quantum spin Hall effect, it is unresolvable in graphene (for which their model was proposed), because this material has a very weak spin-orbit coupling [46]. In order to observe the quantum spin Hall effect, one should resort to materials with much stronger spin-orbit coupling, using the heavier elements in the periodic table. In 2005, the group led by Molenkamp has found experimental evidence for the quantum

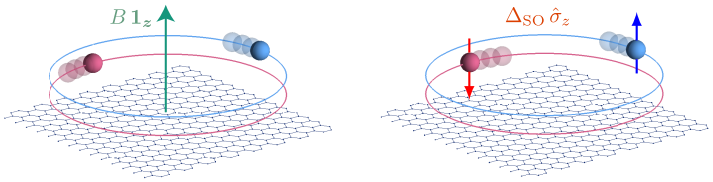

(a) Chiral (Quantum Hall) (b) Helical (Quantum spin Hall)

Figure 1.3: (a) A magnetic field induces the integer quantum Hall state, an example of a chiral state: All edge states propagate in the same direction. (b) Spin-orbit coupling induces the quantum spin Hall state which exhibits the helical edge-state structure: Edge states with opposite spins propagate in opposite directions.

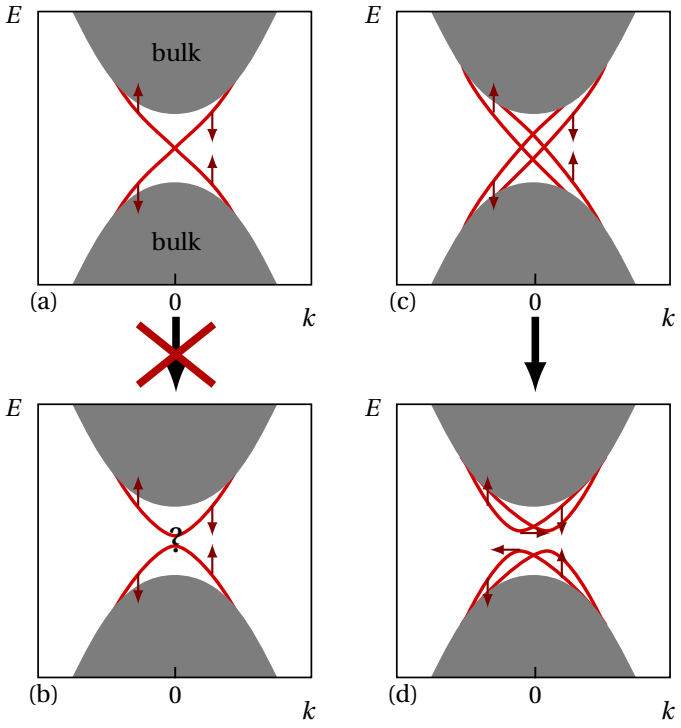

Figure 1.4: Explanation of the $\mathbb{Z}_2$ topological invariant. (a) When there is one Kramers pair, they cross at zero momentum ($k = 0$). (b) One cannot gap out the edge states at this crossing, while keeping time-reversal symmetry. Thus, the configuration (b) is forbidden if time-reversal symmetry is present, and the crossing in (a) is protected. (c) When the number of edge states is even, there are crossings at nonzero momenta. (d) These crossings can be gapped out without violating time-reversal symmetry.

spin Hall effect in quantum wells composed of a HgTe layer between HgCdTe layers [47]. The existence of the quantum spin Hall state in these systems depends on the thickness of the central HgTe layer. This behaviour can be understood from the band structures of HgTe and HgCdTe: The former has an inverted band structure (in other words, a negative gap), while the latter has a normal one. Only if the central layer has sufficient thickness, the quantum spin Hall effect is observed. Theoretically, this behaviour can been described by the four-band effective low-energy model proposed by Bernevig, Hughes, and Zhang (BHZ) [48]. The parameters of this model control the nature of the gap (either quantum spin Hall or trivial), and can be derived numerically by integrating out the perpendicular direction, and by taking into account the high-energy bands within perturbation theory [49].

An interesting question arises at this point: What happens if the elements triggering the quantum Hall and quantum spin Hall effects, namely the magnetic field and spin-orbit coupling, are combined? Arguing from the quantum spin Hall perspective, one could naively expect that an additional magnetic field would break the time-reversal symmetry and destroy the quantum spin Hall state, so that a trivial state remains. However, when one looks at the problem from the quantum Hall perspective, namely adding spin-orbit coupling to a system in a magnetic field, one observes that this naive expectation is false in some cases: If the spin components in the system are not coupled, i.e., the Hamiltonian is diagonal in the spin components and there are no magnetic impurities, then the Hamiltonian may be decomposed into two spin sectors, both of which exhibit quantum Hall states. Taking these two sectors together, one may end up with quantum spin Hall states surviving in the presence of a magnetic field. The existence of such phases in the simultaneous presence of magnetic field and spin-orbit coupling has, somewhat remarkably, been studied only recently [50, 51]. In Chapter 2 of this thesis (Refs. [51, 52]), we explore the various topological phases in a model for the honeycomb lattice in a magnetic field. The spinless version of this model already shows very rich physics, where the energy bands as a function of the magnetic field show a fractal structure, known as the Hofstadter butterfly [53, 54]. Adding the Zeeman effect and *intrinsic* spin-orbit coupling to this model, we observe the time-reversal symmetry broken quantum spin Hall phase, among several other quantum Hall-like states. Tuning the spin-orbit strength induces phase transitions, where the gaps close and change their edge-state structure. If the Rashba spin-orbit coupling is also included, the spin components become coupled, so that the spins no longer reside in the up or down state. As a consequence, the spin Hall conductivity is no longer well-defined, and for instance the quantum spin Hall state becomes a trivial one.

In ferromagnetic materials (and paramagnetic ones in an external magnetic field), the Hall conductivity is affected by a contribution from the magnetisation of the material, much stronger than would be expected on the basis of the magnetic field generated by this magnetisation. This effect is known as the *anomalous Hall effect*, and was originally observed by Hall in 1892 [55]. (For a review, see e.g. Ref. [56].) Its quan-

tum counterpart, the *quantum anomalous Hall effect* can generate a topologically nontrivial bulk gap, and consequently a nonzero quantised Hall conductivity, without the presence of a magnetic field and consequently without Landau levels [57]. In this case, the magnetisation provides the breaking of time-reversal symmetry. In this aspect, the quantum Hall effect at zero magnetic field described by Haldane in Ref. [42] could also be understood as an example of the quantum anomalous Hall effect [57].

Now, a similar question arises as before: What is the effect of combining the magnetic field, magnetisation, and spin-orbit coupling? The answer to this question is relevant for the Mn-doped HgTe quantum well, where the central layer is doped with a small fraction of Mn ions. In this system, the magnetisation is provided by the Mn ions, while HgTe provides the spin-orbit coupling. If the Mn doping fraction is less than 0.07, the *exchange coupling* between the magnetic ions induces a paramagnetic response to the magnetic field [58, 59]. The paramagnetic behaviour can be conveniently described in the four-band model as an effective Zeeman interaction, with a field-dependent Landé g factor. Thus, the combination of the linear Zeeman effect and the exchange coupling leads to an effective nonlinear Zeeman effect. In addition, the Mn doping modifies the parameters of the four-band model. Most importantly, with increasing doping, the size of the inverted gap decreases, or the trivial gap increases in size. In Chapter 3, we show that the nonlinear Zeeman effect induces a bending of the Landau levels in a way that the Hall conductivity and spin Hall conductivity show reentrant behaviour for increasing magnetic field. This reentrant effect should be contrasted to that in semiconductor quantum Hall systems, where it arises due to interparticle interactions, whereas in HgTe quantum wells, it appears at the single-particle level. In addition, when the gap is inverted, the spectra of these quantum wells exhibit a Landau-level crossing which also give rise to a reentrant quantum Hall conductivity. In fact, this mechanism has been employed as an indirect manner to detect the quantum spin Hall effect in these systems, as it is experimentally easier to measure charge currents than spin currents [47]. In Chapter 3, we explain how the reentrant effects from the bending and from the crossings of the Landau levels differ, and we show that these two features can be present simultaneously in the spectrum. In that case, the (quantised) Hall and spin Hall conductivity show more intricate reentrant behaviour. From computation of the band parameters as a function of the well thickness, the Mn concentration, and the temperature, we have identified the regimes where either mechanism (or both) gives rise to reentrant behaviour. Furthermore, from the Landau level energies, it is determined how well the reentrant effect could be resolved in an experimental measurement.

As argued before, the quantum Hall and quantum spin Hall states differ in the sense that only the latter preserves time-reversal symmetry, and this difference is reflected in the different topological invariants ($\mathbb{Z}$ and $\mathbb{Z}_2$, respectively). This link between the symmetries and the topology of the system exists in more generality: For single-particle Hamiltonians, the invariance properties under time reversal $\mathscr{T}$, charge conjugation $\mathscr{C}$,

and the parity operation $\mathscr{P}$ completely determine the topological nature of the system [60, 61]. The system may either break time-reversal symmetry, or preserve it, where $\mathscr{T}^2$ can have eigenvalues $+1$ or -1. The same holds for charge conjugation. The parity symmetry (also called chiral or inversion symmetry) is determined by the invariance $\mathscr{T}$ and $\mathscr{C}$ unless the system breaks both the $\mathscr{T}$ and $\mathscr{C}$ invariances. Thus, ten different symmetry classes may be obtained for a specific number of dimensions. For each symmetry class, the topological property is described by the homotopy group of the symmetry group of the Hamiltonian, which can be either $\mathbb{Z}$, $\mathbb{Z}_2$, or the trivial group. The homotopy group determines the topological invariant of the system. In the case of the quantum Hall effect, the homotopy group is $\mathbb{Z}$, which is linked to the TKNN topological invariant. For the quantum spin Hall effect, the homotopy group is $\mathbb{Z}_2$, related to the spin Hall conductivity. The classification based on the symmetry properties is known as the *periodic table* of topological states or as the *ten-fold way* [60, 61]. The mathematical properties of the homotopy groups are responsible for the highly ordered structure of this classification. For instance, in each dimension, there are exactly five symmetry classes with a nontrivial homotopy group. In addition, the classification is periodic, because the homotopy groups only depend on the dimension modulo 2 or 8 (depending on the symmetry class), a feature known as Bott periodicity [61]. Furthermore, these mathematical properties allow for the method of *dimensional reduction*, where a d-dimensional theory is understood in terms of a $(d+1)$-dimensional theory where one dimension has been integrated out [61, 62].

The topological states described in this thesis do not always fit directly in this symmetry classification. For instance, the weak quantum spin Hall effect of Chapters 2 and 3 does not preserve time-reversal symmetry, so in that sense it would be in the same class as the quantum Hall effect. In fact, the weak quantum spin Hall effect may be regarded as two copies of the quantum Hall effect, which are uncoupled. In this case, the topological invariant lives in $\mathbb{Z} \times \mathbb{Z}$, i.e., both spin components have a separate TKNN integer associated with them. If the spin components are coupled, e.g., by Rashba spin-orbit coupling, then this invariant breaks down to $\mathbb{Z}$, namely, the TKNN integer that describes the charge Hall conductivity.

The outline of this thesis is as follows. In Chapter 2, we investigate the topological states in the fermionic honeycomb lattice in the presence of a perpendicular magnetic field within a tight-binding approach incorporating nearest-neighbour hopping, Rashba and intrinsic spin-orbit coupling, and the Zeeman effect. In Chapter 3, we study the reentrant effects of the charge and spin Hall conductivity in Mn-doped HgTe quantum wells. In Chapter 4, we discuss the generalisation of the Hamiltonian Chern-Simons theory formulated by Shankar and Murthy to systems with multiple internal degrees of freedom. We present the conclusions and an outlook in Chapter 5.

Chapter 2

Topological phases in the fermionic honeycomb lattice

In this chapter, we explore the rich variety of topological states that arise in two-dimensional systems, by considering the competing effects of spin-orbit couplings and a perpendicular magnetic field on a honeycomb lattice. Unlike earlier approaches, we investigate minimal models in order to clarify the effects of the intrinsic and Rashba spin-orbit couplings, and also of the Zeeman splitting, on the quantum Hall states generated by the magnetic field. In this sense, our work provides an interesting path connecting quantum Hall and quantum spin Hall physics. First, we consider the properties of each term individually and we analyse their similarities and differences. Secondly, we investigate the subtle competitions that arise when these effects are combined. We finally explore the various possible experimental realisations of our model.[1]

2.1 Introduction

Today, unprecedented efforts are devoted to the study of novel topological insulating phases, which exhibit remarkable properties at their boundaries [63, 64]. In two dimensions, these quantum states are characterised by propagating edge states, which carry dissipationless currents along one-dimensional boundaries. From a theoretical point of view, these transport properties rely on the existence of large bulk gaps in the energy spectrum, which host robust and gapless edge excitations. Different edge-state structures and transport properties can be realised according to the nature of the gaps: A magnetic field breaks time-reversal symmetry (TRS) and leads to chiral edge states (i.e., particles propagating in a given direction) and quantised Hall currents

[1] This chapter is based on *Topological phase transitions between chiral and helical spin textures in a lattice with spin-orbit coupling and a magnetic field*, N. Goldman, W. Beugeling, and C. Morais Smith, EPL **97**, 23003 (2012) [51] and *Topological phases in a two-dimensional lattice: Magnetic field versus spin-orbit coupling*, W. Beugeling, N. Goldman, and C. Morais Smith, Phys. Rev. B **86**, 075118 (2012) [52].

[1], whereas a large spin-orbit coupling preserves the TRS and produces helical edge structures [43, 44]. In the latter situation, referred to as the quantum spin Hall (QSH) effect, edge states with opposite spins counterpropagate and contribute to a vanishing Hall current, while producing a spin Hall current [47, 48]. The origins of the quantum Hall (QH) and QSH phases are fundamentally different, as the former is produced by an external field, whereas the latter relies on the intrinsic properties of the material. However, one can interpret the QSH phase as being two opposite QH phases, one for each spin component. This observation is easily shown through the Kane-Mele lattice model [43, 44], which realises the QSH effect by the inclusion of the intrinsic spin-orbit coupling (ISO), and corresponds to two copies of the (QH) Haldane model [42].

In recent works, the ISO coupling has been combined with a magnetic field [51, 65], or with a constant exchange term [50], in order to study the effect of the TRS breaking on the QSH effect. It has been shown that the QSH effect persists in the presence of magnetic field, leading to the "TRS-broken" [50] or "weak" QSH effect [51]. The term "weak" refers to the absence of robustness against spin-flip scattering due to magnetic disorder. In absence of this scattering process, the Hall and spin Hall conductivities are protected and quantised.

In this work, we present a different approach to study the interplay between QH and QSH physics. Contrarily to the general trend in the field of topological insulators, which is to include many terms and study complicated Hamiltonians, here we investigate the minimal models that can produce topological phases. We consider a tight-binding model of the honeycomb lattice under a perpendicular magnetic field, which includes the ISO coupling, the Rashba spin-orbit (RSO) coupling, and the Zeeman effect. This spin-$\frac{1}{2}$ model was introduced in one of our recent papers [51], where we already studied the combined effects of some of these terms. Here, instead, we first investigate the effect of each of these terms individually on the QH phases generated by the magnetic field, in order to distill the problem. In particular, we demonstrate the equivalence of the ISO and Zeeman terms in generating the weak QSH phase at zero energy in the presence of a magnetic field. Then, we show that the ISO coupling can drive topological phase transitions between different topological insulating phases, an effect which totally relies on the combination of the ISO coupling and the magnetic field.

Secondly, we study the interplay between the terms incorporated in our model. For example, we discuss the competition between the ISO coupling and Zeeman effect, motivated by the similarity of these terms for generating the weak QSH effect. We show that the combination of these terms does not necessarily lead to a larger regime of parameters where the weak QSH effect is observed, which reveals the subtle competition between each of these terms and the magnetic field. We also study the exquisite effects produced by the Rashba coupling in the presence of a large exchange field, which is shown to generate several QH gaps, even in the absence of a magnetic field. From another perspective, we also discuss the fate of the weak QSH phase, as the RSO coupling

is turned on, which introduces spin-flip terms into the Hamiltonian, so that the spins are no longer aligned perpendicularly to the plane, and the spin Hall conductivity is no longer protected.

An important motivation for the investigation of these topological phases and phase transitions is the rich variety of systems where they may be observed. Despite its weak ISO coupling, graphene remains an appealing candidate for the observation of these phases, e.g., by increasing the ISO coupling artificially by adatoms [66]. Secondly, several experimental groups have reported on synthetic honeycomb lattices in a condensed matter system, for instance arrays of quantum dots on a GaAs substrate [67], and "molecular graphene", where the lattice is created by using the repulsive interactions of CO molecules deposited in a triangular array on a Cu(111) surface [68]. These systems have larger lattice constants, which lead to a higher flux per plaquette at realistic magnetic field values, and allow for a more flexible control over the parameters than in real graphene. A third type of experiments that motivate our studies is the recent realisation of a honeycomb optical lattice for ultracold atoms [69–71]. In cold-atom systems, large magnetic fields [72] and spin-orbit couplings [73] are produced synthetically by adjustable lasers (see Ref. [74] for a review). In particular, such artificial gauge potentials could be produced in optical lattices [74–80], thus leading to the possibility to probe the high-flux regime. Furthermore, we note that optical *square* lattices subjected to well-designed gauge potentials can reproduce the properties of honeycomb lattice systems, exhibiting Dirac-type physics [81–85]. Cold-atoms systems carry the advantages of high tunability, necessary for studying phase transitions, and allow for the study of topological phases in absence of interparticle interactions [86] and disorder [87]. These possible experimental realisations are explored in detail in the final part of this work.

This chapter is structured as follows. We introduce the lattice model in Sec. 2.2 and present the four terms characterising our tight-binding Hamiltonian: the usual hopping term, the two spin-orbit terms as well as the Zeeman splitting. Then, in Sec. 2.3, we review the techniques used for our investigation and characterisation of topological phases. Section 2.4 discusses the combined effect of the magnetic field and spin-orbit coupling. Then, the combined effects of spin-orbit couplings, Zeeman splitting and uniform magnetic flux are explored in Sec. 2.5. The possible experimental realisations of our model, as well as the possibility to detect the effects presented in Secs. 2.4 and 2.5, are reported in Sec. 2.6. Finally, the conclusions are drawn in Sec. 2.7. The Appendices provides further mathematical details of the calculations.

2.2 Model

We consider a tight-binding model of spinful electrons in a two-dimensional honeycomb lattice, subjected to a uniform perpendicular magnetic field $\mathbf{B} = B\mathbf{e}_z$. This model

was introduced in Ref. [51] to investigate the effects of an external magnetic field on the Kane-Mele model (cf. Refs. [43, 44]). The magnetic field induces a Zeeman effect, and causes the hopping terms to acquire a phase. This phase is encoded by the so-called Peierls substitution, where one replaces the momentum $\mathbf{p}$ by $\mathbf{p} - e\mathbf{A}$, where $\mathbf{A}$ is the gauge potential associated with the magnetic field. Thus, any hopping term from site k to site j picks up the phase factor $e^{i\theta_{jk}}$, where $\theta_{jk} = (e/\hbar)\int_{\mathbf{r}_k}^{\mathbf{r}_j} \mathbf{A}\cdot\mathbf{dl}$. In the remainder of this text, we will express the magnetic field strength (flux density) in terms of the dimensionless quantity ϕ, defined as the flux per unit cell of the lattice, expressed in units of the elementary flux quantum h/e.

In our model, we include four effects into the Hamiltonian, written as $H = H_{\mathrm{NN}} + H_{\mathrm{Z}} + H_{\mathrm{I}} + H_{\mathrm{R}}$, with

$$\begin{aligned} H_{\mathrm{NN}} &= -t\sum_{\langle j,k\rangle} e^{i\theta_{jk}} c_j^\dagger c_k, & H_{\mathrm{Z}} &= -2\pi\phi\lambda_{\mathrm{Z}}\sum_j c_j^\dagger \sigma_z c_j, \\ H_{\mathrm{I}} &= -i\,t_{\mathrm{I}}\sum_{\langle\langle j,k\rangle\rangle} e^{i\theta_{jk}} \nu_{jk} c_j^\dagger \sigma_z c_k, & H_{\mathrm{R}} &= -i\,t_{\mathrm{R}}\sum_{\langle j,k\rangle} e^{i\theta_{jk}} c_j^\dagger (\boldsymbol{\sigma}\wedge\mathbf{d}_{jk}) c_k. \end{aligned} \tag{2.1}$$

Here, $c_k = (c_{k\uparrow}, c_{k\downarrow})$ is the annihilation operator for electrons at site k. The first term H_{NN} describes hopping between two nearest-neighbour (NN) sites j and k, where t denotes the hopping amplitude. The second term H_{Z} describes the Zeeman effect, which is an on-site term that assigns different potentials to the two spin components via the Pauli matrix σ_z. Its amplitude is proportional to the magnetic flux ϕ and the coefficient λ_{Z}, which is related to the material's Landé g factor by $2\pi\phi\lambda_{\mathrm{Z}} = g\mu_{\mathrm{B}}B$, where μ_{B} is the Bohr magneton. Note that in a cold-atom emulation of this model, the parameters ϕ and λ_{Z} are tuned individually (cf. Sec. 2.6.3). The Zeeman term lifts the degeneracy by shifting the two spin-degenerate copies of the spectrum up and down by an equal amount of energy. The third term H_{I} describes the ISO coupling, which corresponds to a next-nearest-neighbour (NNN) hopping with amplitude t_{I} [43]. Here, the factor $\nu_{jk} = \pm 1$, where the sign depends on the value of $\mathbf{d}_{kl}\wedge\mathbf{d}_{lj}$, i.e., the outer product of the two bond vectors connecting site k to site j via their unique common neighbour at site l. This hopping also involves the matrix σ_z, so that the sign of the hopping amplitude is opposite for the two spin components $\uparrow$ and $\downarrow$. Thus, the two different spin species are effectively subjected to opposite local (Haldane-type [42]) magnetic flux. In absence of a magnetic field, this term opens a topologically nontrivial gap, and causes the QSH effect, characterised by so-called helical edge states, which are protected by TRS [43, 44]. The final term H_{R} is the contribution to the NN hopping due to the RSO coupling. This hopping has an amplitude t_{R}, and involves the spin matrix $\boldsymbol{\sigma}\wedge\mathbf{d}_{jk} = \sigma_x d_{jk}^y - \sigma_y d_{jk}^x$, where $\boldsymbol{\sigma} = (\sigma_x, \sigma_y)$, and $\mathbf{d}_{jk}$ is the vector connecting sites k and j. The resulting spin matrix has only off-diagonal elements, so that this hopping involves a spin flip. This term couples the two spin components, and as a consequence, σ_z is no longer a good quantum number for $t_{\mathrm{R}} \neq 0$. In practice, this means that spin states are no longer exclusively up or down, but may also point in different directions. Finally, we remark that

the model considered here preserves inversion symmetry. In particular, we disregard the effect of an additional staggered potential, which was shown to induce topological phase transitions between trivial and non-trivial phases in Refs. [43, 44]. The possible physical realisations of our model (2.1) are discussed later in Sec. 2.6.

2.3 Tools for the topological analysis

In the following sections, we will perform an analysis of the various topological phases produced by the terms in the model Hamiltonian (2.1). Before going into details, describing each term individually and their combined effects, we first present the framework and tools which we will use for this analysis. Readers who are already familiar with the notions of bulk and edge states, Chern numbers, and (spin) Hall conductivity may choose to skip this section.

2.3.1 Harper equation and the Hofstadter butterfly

We will illustrate our framework by studying the spin-degenerate model, i.e., we set $\lambda_Z = t_I = t_R = 0$ in Hamiltonian (2.1). We assume $t > 0$ throughout the whole text. The bulk band structure can be computed numerically by applying periodic boundary conditions, namely by considering a toroidal geometry. This requires to set $\phi = p/q$, where p and q are integers, in which case the system is periodic in both spatial directions. Under these conditions, and by choosing a proper gauge for the Peierls phases $e^{i\theta_{jk}}$, the system reduces to a $q \times 1$ magnetic unit cell. (See Appendix 2.A for a description of the gauge structure and its spatial periodicity.) By applying a Fourier transform and invoking Bloch's theorem, the Schrödinger equation reduces to a $4q \times 4q$ eigenvalue problem, known as the discrete Harper equation,[2]

$$(E/t)\Psi_n = \mathscr{D}_n \Psi_n + \mathscr{R}_n \Psi_{n+1} + \mathscr{R}_{n-1}^\dagger \Psi_{n-1}, \tag{2.2}$$

where $\Psi_n = (\psi_{nA\uparrow}, \psi_{nA\downarrow}, \psi_{nB\uparrow}, \psi_{nB\downarrow})$ denotes the single-particle wave function at site $n = 1, \ldots, q$, and where the 4×4 matrices $\mathscr{D}_n$ and $\mathscr{R}_n$ are given in terms of the parameters defined in Hamiltonian (2.1) (see Appendix 2.A for details). The four components of the wave function Ψ_n are due to the two sublattice (A,B) and the two spin $(\uparrow,\downarrow)$ degrees of freedom. The $4q \times 4q$ Harper problem in Eq. (2.2) is analogous to the original (spinless, square-lattice) Hofstadter problem [53], where the Harper equation involves a $q \times q$ matrix.

Solving the Harper equation (2.2) provides the bulk energy bands $E = E(k_x, k_y)$. It is instructive to evaluate the sizes of the bulk gaps as a function of the magnetic flux ϕ, which results in a diagram known as the Rammal-Hofstadter butterfly [53, 54], shown

[2] In a more general form, the Harper equation is known as an *almost Mathieu equation* in mathematical literature; see e.g., [88]. See also [53].

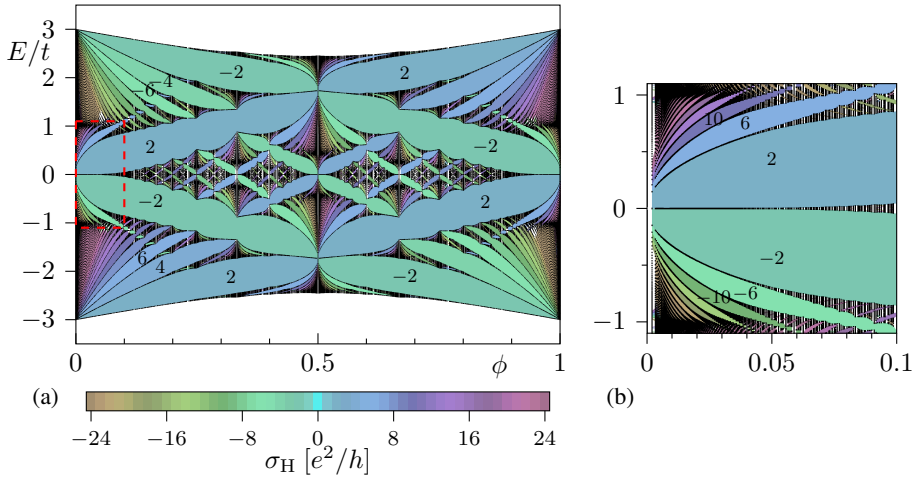

Figure 2.1: (a) Hofstadter butterfly spectrum for the spin-degenerate model, Hamiltonian (2.1) with $\lambda_Z = t_I = t_R = 0$. The bulk bands, i.e., the regions where the density of bulk states is positive, are shown in black. In the bulk gaps, the colours and numbers indicate the quantised Hall conductivity in units of e^2/h. (b) A magnification of the region indicated by the red dashed rectangle in (a) shows the low-energy, low-flux regime.

in Fig. 2.1(a). This figure may be obtained in the limit of large q, where the bands become dispersionless. The fractal structure, which is periodic in ϕ with a period of 1, is a result of the competition between two length scales: The magnetic length $l_B = \sqrt{\hbar/eB}$ and the lattice spacing. Here, ϕ parametrizes this competition, as the ratio between the area of the unit cell and that of the cyclotron orbits ($\sim l_B^2$).

2.3.2 Topological invariants

Each bulk gap in the spectrum shown in Fig. 2.1(a) may be characterised by a topological invariant, which encodes the Hall conductivity of this system when the Fermi energy lies inside this gap. The integer values of the Hall conductivity are robust against external perturbations: They remain constant as long as the bulk gaps remain open. In the following, we recall the relation between this transport coefficient and the concept of edge states and topological invariants.

Edge-state analysis

The edge-state analysis can be performed for a system featuring a boundary [89], such as a cylinder, as shown in Fig. 2.2(a). When solving the Harper equation (2.2) on a cylinder, namely by applying periodic boundary conditions along one spatial direction only, the spectrum consists of *bulk bands* and *topological edge states* [89]. Indeed, we

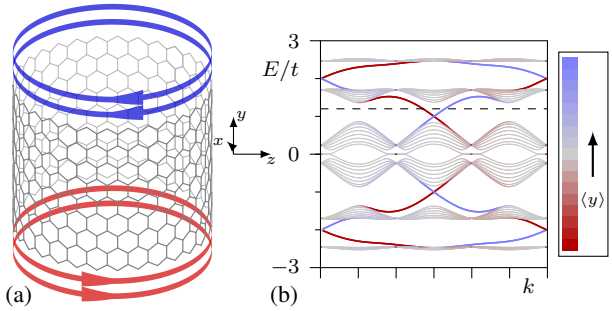

Figure 2.2: (a) The cylinder geometry representing a ribbon with periodic boundary conditions in the x direction. (b) Spectrum at $\phi = 1/3$ for the spin-degenerate model ($\lambda_Z = t_I = t_R = 0$). The colours represent the expectation value $\langle y \rangle$: Red and blue indicate edge states at the bottom and top edge, respectively, and gray represents bulk states. The spin-degenerate edge states shown in (a) correspond to those in the QH gap at the Fermi energy indicated by the dashed line in (b).

typically find a few *edge states* within the bulk gaps, some of which *cross* the gap from one bulk band to the other; see Fig. 2.2(b). Importantly, each edge state contributes e^2/h (one quantum of conductivity) to the Hall conductivity of the system. The total Hall conductivity is therefore equal to an integer number (i.e., the number of edge-state branches) times e^2/h. The topological invariance of the Hall conductivity is due to the fact that the number of edge states inside the bulk gap cannot be altered unless the gap is closed. This result can be used to derive the topological invariant associated to any of the bulk gaps, leading to the colours in the spectrum in Fig. 2.1. For this spin-degenerate model, all topological invariants are multiples of 2 because the system is twofold spin degenerate.

More precisely, in order to evaluate the Hall conductivity of a bulk gap, we count the edge states whose dispersions intersect the Fermi energy, taking into account their location and direction of propagation. The location of each state is derived by computing its expectation value $\langle y \rangle$ from the eigenstate, which provides the colouring of Fig. 2.2(b). Secondly, the direction of propagation can be obtained from the sign of its momentum derivative $\mathrm{d}E/\mathrm{d}k$, where k is the momentum parallel to the edge. Edge states with opposite directions contribute with opposite signs to the Hall current and therefore to the Hall conductivity,

$$\sigma_H = (N_R - N_L)\frac{e^2}{h}, \tag{2.3}$$

where N_L and N_R denote the number of left- and right-moving states, respectively. The Hall conductivity does not depend on the magnitude of the velocity ($\propto \mathrm{d}E/\mathrm{d}k$), but instead is given by the number of edge-state channels [90]. In this spin-degenerate model, the states are all either left- or right-moving, i.e., they are *chiral* states. The chi-

rality of the edge modes provides protection of the Hall conductivity against backscattering due to disorder in the presence of broken TRS.

Bulk topological invariants

Remarkably, the number of edge states is directly related to topological invariants, the *Chern numbers*, a quantity associated with each of the bulk bands. The Chern number is an integer topological index defined in the toroidal geometry [91, 92],

$$C_n = \frac{1}{2\pi}\int_{\mathrm{BZ}} \left(\frac{\partial \mathbf{A}^y_{n,\mathbf{k}}}{\partial k_x} - \frac{\partial \mathbf{A}^x_{n,\mathbf{k}}}{\partial k_y} \right) d\mathbf{k}, \tag{2.4}$$

where $\mathbf{A}_{n,\mathbf{k}} = i\langle u_{n,\mathbf{k}}|\boldsymbol{\nabla}_{\mathbf{k}}|u_{n,\mathbf{k}}\rangle$ is the Berry connection associated to the eigenstate $|u_{n,\mathbf{k}}\rangle$, and where BZ denotes the (toroidal) Brillouin zone. The number of edge states N_r inside the rth bulk gap, or equivalently the Hall conductivity assigned to this gap (cf. discussion above), is then equal to the sum of all the Chern numbers associated to the occupied bands [7, 63],

$$N_r = \sum_{n\in\text{occupied bands}} C_n. \tag{2.5}$$

This identity is known as the *bulk-boundary correspondence* [89, 92], as it relates the topological indices associated to the bulk bands to the number of edge excitations. This correspondence provides us with an important observation: Although the dispersions of the edge states depend on the shape of the edges (e.g., zigzag, bearded, or armchair) and on the system size, the number of edge-state branches does not: This number is a bulk property and therefore does not depend on the specific form of the edge. In the remainder of this chapter, we will study systems with zigzag and bearded edges, without any loss of generality concerning the topological properties.

In the next sections, we will characterise the topological phases by their associated Hall conductivity and edge-state structures. As described in the following, the edge states produced by the magnetic field are affected in the presence of strong perturbing terms, such as the spin-orbit couplings and Zeeman splitting. For the sake of simplicity, we will show these effects using the edge-state analysis obtained from a cylindrical geometry, rather than focusing on the analysis of the bulk topological invariants.

The Středa formula

An efficient method to compute the Hall conductivity can be formulated in terms of the normalised *integrated density of states*. Inside a bulk gap, the integrated density of states $N_\phi(E)$ is defined as the fraction of all states that lie below the gap, i.e., as $l/4q$ where l is the number of bands below the gap. The Hall conductivity is then proportional to the ϕ derivative of this quantity,

$$\sigma_{\mathrm{H}} = 4\frac{e^2}{h}\frac{\partial N}{\partial \phi}. \tag{2.6}$$

a result known as the Středa formula [93–96]. We have used this powerful formula to compute the Hall conductivity, and generate the colourful butterfly spectra presented in the remainder of this chapter.

The validity of the Středa formula is based on the following semiclassical quantisation condition: For an electron in a bulk band (or equivalently, Landau level), the area of its cyclotron orbit in reciprocal space is equal to $2\pi l_B^{-2}(l+\gamma)$ [97, 98], where l_B is the magnetic length, l is the band index and $0 \leq \gamma < 1$ is a constant that depends on the shape of the dispersion. Furthermore, electrons follow the energy contours of the dispersion, so that the area of the interior of its cyclotron orbit is equal to $N(E)A_{\mathrm{BZ}}$, where $A_{BZ} = 8\pi^2/3\sqrt{3}$ is the area of the Brillouin zone. Now let us consider a gap that exists at a flux ϕ_0, energy E_0, and with integrated density of states $N_{\phi_0}(E_0)$. We compare the area of the interior of a cyclotron orbit at flux ϕ and energy E to the one at flux ϕ_0 and energy E_0. The difference $N_\phi(E) - N_{\phi_0}(E_0)$ is proportional to $\phi - \phi_0$ due to the constant derivative $\partial N/\partial\phi$ and can also be related to the band index via the quantisation condition, written as

$$(\phi - \phi_0)\frac{\partial N}{\partial \phi} = N_\phi(E) - N_{\phi_0}(E_0) = (\phi - \phi_0)(l+\gamma).$$

Here, the second equality is the quantisation condition in terms of the flux. Hence, it follows that $\partial N/\partial\phi = l + \gamma$. The latter quantity is equal to the Hall conductivity in units of $4e^2/h$, where the factor 4 arises from the total number of bulk bands.[3] This observation completes the proof of the Středa formula, Eq. (2.6). Note that in this analysis, we have assumed that the integrated density of states varies only slowly in ϕ, so that we could approximate $N_\phi(E) \approx N_{\phi_0}(E)$. The advantage of this method is that we could pick ϕ_0 with a small denominator, where the dispersion and subsequently $N_{\phi_0}(E)$ can be computed easily.

The quantisation condition given above can also be used to approximate semiclassically the energy dependence of the thin bulk bands (Landau levels) in the spectrum close to a flux value for which the dispersion is known. For instance, in the spin-degenerate model (i.e., $t_{\mathrm{R}} = t_{\mathrm{I}} = \lambda_{\mathrm{Z}} = 0$), around $\phi = 0$ and $E = 0$, the dispersion is approximately linear around the two Dirac points [99]. The area of the cyclotron orbits is then quadratic in energy, so that the quantisation condition yields bulk-band energies that are proportional to $\sqrt{\phi}$, consistent with the observed behaviour in the Hofstadter butterfly spectrum (see Fig. 2.1). Near $E/t = \pm 3$, this dispersion has a quadratic regime (around the point Γ), thus yielding band energies linear in ϕ, also consistent with the spectrum.

[3] This factor may be compared with the fourfold degeneracy of the Landau levels for graphene in the low-field limit.

Charge and spin Hall conductivities

In the presence of terms involving the matrix σ_z in the Hamiltonian, the spin **SU**(2) symmetry is broken. If spin-flip terms (i.e., linear combinations of σ_x and σ_y) are absent, the spin in the z direction is conserved, i.e., it is a good quantum number. In this case, which happens if the ISO coupling or the Zeeman splitting is present while the RSO is not, the Hamiltonian may be decomposed into the two spin components $(\uparrow,\downarrow)$. Thus, one is able to define the component-wise Chern numbers $C_{\uparrow,n}$ and $C_{\downarrow,n}$ and Hall conductivities $\sigma_{\mathrm{H}\uparrow}$ and $\sigma_{\mathrm{H}\downarrow}$. The charge Hall conductivity of the whole system is the sum of the two component-wise conductivities, $\sigma_{\mathrm{H}} = \sigma_{\mathrm{H}\uparrow} + \sigma_{\mathrm{H}\downarrow}$, since both of them contribute equally to the Hall current. Considering their contributions to the spin current, spin-up and spin-down edge modes have opposite "spin charges" $\pm\hbar/2$. Thus, the spin Hall conductivity is equal to the difference of the two component-wise conductivities, $\sigma_{\mathrm{H}}^{\mathrm{sp}}/(e/4\pi) = (\sigma_{\mathrm{H}\uparrow} - \sigma_{\mathrm{H}\downarrow})/(e^2/h)$, where $e/4\pi$ is the elementary quantum of spin Hall conductivity.

In the spin-degenerate model discussed earlier, the two component-wise Hall conductivities are always equal, so that all spin Hall conductivities vanish. This is certainly different if the spin degeneracy is broken. For instance, in the presence of ISO, the QSH gap at zero magnetic field and at zero energy [44] is characterised by $\sigma_{\mathrm{H}\uparrow} = -\sigma_{\mathrm{H}\downarrow} = -e^2/h$. Here, the contributions to the charge Hall conductivity cancel, but the contributions to the spin Hall conductivity add up to $\sigma_{\mathrm{H}}^{\mathrm{sp}} = -2e/4\pi$.

If the Hamiltonian contains spin-flip terms, e.g., the Rashba coupling, then the spin is not conserved, and the aforementioned definition of the spin Hall conductivity is no longer valid. However, the related spin Chern numbers, which equal $C_n^{\mathrm{sp}} = C_{\uparrow,n} - C_{\downarrow,n}$ if spin is conserved, remain well-defined topological invariants, even in absence of spin conservation [100, 101].

2.4 Effects of the magnetic field

2.4.1 The spin-degenerate model: Landau Levels and the anomalous quantum Hall effect

Zooming in on the butterfly of Fig. 2.1(a) near $\phi \approx 0$, we observe that the thickness of the bands decreases in the low-flux regime [see Fig. 2.1(b)]. Thus, in this limit we can treat the bands as being infinitely thin, i.e., as Landau levels. In the low-energy regime, between the Van Hove singularities at $E/t = \pm 1$, the band structure at low flux coincides with the Landau-level spectrum known from graphene [99, 102], with energies $E \propto \pm\sqrt{2\pi l\phi}$ (where $l = 0, 1, 2, \ldots$ is the Landau-level index).

Moreover, computing the Hall conductivity in this region, we find the "anomalous" Hall-conductivity sequence $\sigma_H = 4(n+\frac{1}{2})e^2/h$ ($n \in \mathbb{Z}$), as observed in graphene [34, 35]. The breakdown of this structure around $E/t = \pm 1$ can be understood from the

large density of states near the Van Hove singularities and from the Chern numbers associated to these many bands [103]. The edge-state structures, Hall conductivity plateaus and topological aspects of spinless electrons in a honeycomb lattice subjected to a magnetic field have been thoroughly described in Ref. [103].

2.4.2 Intrinsic spin-orbit coupling

Since the seminal work of Kane and Mele [43], it is known that the ISO coupling opens a topologically nontrivial gap of size $\Delta = 6\sqrt{3}t_{\mathrm{I}}$ at zero magnetic field. This bulk gap hosts two counterpropagating edge modes per edge, with opposite spins (one Kramers pair): These *helical* edge states are related by TRS. This topological phase is known as the QSH state, and may be regarded as two opposite QH phases (i.e. each spin performs the QH effect, with opposite chirality). The system preserves TRS (due to absence of the magnetic field), which protects the QSH state against scattering processes caused by disorder. Although for any edge state a reversely propagating mode would be available to scatter to, the spin has to be flipped, and the two different ways to flip the spin interfere destructively with each other, due to a mutual phase factor of $e^{i\pi} = -1$ [104].

The combination of the ISO coupling and a magnetic field leads to the breaking of the TRS satisfied by the QSH phase. However, due to the absence of spin-flip terms in the Hamiltonian, the helical edge-state structure persists. In terms of charge and spin Hall conductivity, the resulting state is equivalent to the QSH state. As announced in the introduction of this chapter, this state is called the *weak QSH* phase [51] or *TRS broken QSH* phase [50]. From the Hofstadter butterfly in Fig. 2.3, we observe that the size of the weak QSH gap at zero energy tends to decrease if the flux is increased (but not monotonically), and closes eventually. In Fig. 2.3, in which $t_{\mathrm{I}} = 0.1\,t$, the QSH gap at $E = 0$ remains open in the range $0 \leq \phi \leq 0.2$. Here we observe the competition between the ISO coupling, which opens the (weak) QSH gap, and the magnetic field, which "tries" to destroy the weak QSH state by its TRS breaking property. Throughout the weak QSH gap, the edge states remain crossing at zero energy, which indicates that this phase is robust at least in the absence of magnetic disorder. We finally note that the spectrum remains particle-hole symmetric, as in the spinless case.

2.4.3 Zeeman effect

The Zeeman term models an on-site spin-splitting effect that is always present in real materials subjected to magnetic fields. Studying Hamiltonian (2.1) with $\lambda_{\mathrm{Z}} \neq 0$ and $t_{\mathrm{R}} = t_{\mathrm{I}} = 0$, we observe that the spin degeneracy is lifted by merely shifting the two spin states up and down in energy by $2\pi\lambda_{\mathrm{Z}}\phi$. The spectrum is otherwise left invariant. With respect to the Hofstadter butterfly represented in Fig. 2.1, this means that the spin-up and spin-down copies are "skewed" in opposite directions, as shown in Fig. 2.4. Because the lowest and highest bands of the spin-degenerate model are situated at

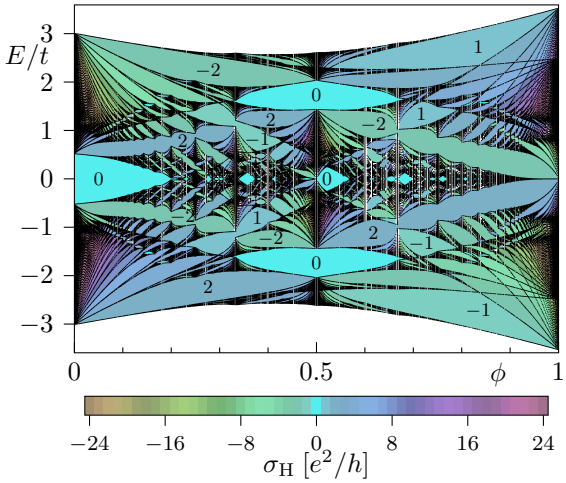

Figure 2.3: Hofstadter butterfly spectrum for the system with ISO coupling ($t_I/t = 0.1$). Although the periodicity in ϕ is 6 rather than 1 (see Appendix 2.A), we present only the range $0 \le \phi \le 1$ for the sake of comparison with the other terms.

approximately $E/t = \pm 3$, the two spin components are completely separated above a certain flux value, approximately equal to $\phi = 3/(2\pi\lambda_Z)$. Furthermore, the Zeeman shift breaks the periodicity of the butterfly spectrum along the ϕ axis.

The Zeeman-induced weak QSH phase

As we already mentioned, the spectrum of the spin-degenerate model shows Landau levels for low values of the flux (cf. Sec. 2.4.1). The Hall conductivities in the gaps are $\sigma_H/(e^2/h) = \ldots, -6, -2, 2, 6, \ldots$. If we concentrate on the bulk gaps around zero energy, we observe one and then three doubly degenerate edge states [see Fig. 2.5(a)]. When the Zeeman splitting is nonzero, the two copies of these states shift up and down, as shown in Fig. 2.5(b) for $\phi = 1/61$. Assuming that the splitting is sufficiently large, a new gap opens at zero energy, where the original band was situated. The spin-up and spin-down edge states now connect to bulk bands that have been shifted up and down, respectively. As a consequence, in the newly opened gap at zero energy, we have $N_\uparrow = -1$ and $N_\downarrow = +1$. Thus, the charge Hall conductivity vanishes, and the spin Hall conductivity is equal to $\sigma_H^{sp} = -2e/4\pi$. Based on these values, we find that this state is a weak QSH phase.

Comparing this state to the one generated by ISO [see Fig. 2.5(c)], we observe the similarity between them. In both cases, the Landau levels for the two spin components shift in opposite directions. The difference between the two terms lies in the different values of the shift: The Zeeman shift $\pm 2\pi\phi\lambda_Z$ is linear in the flux, so that it vanishes for

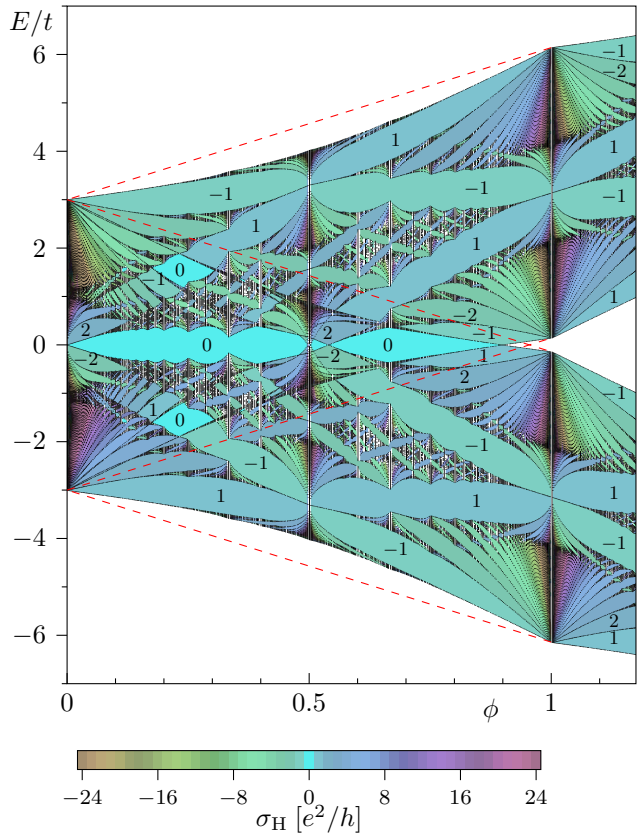

Figure 2.4: Hofstadter butterfly spectrum for the model described by Hamiltonian (2.1) with Zeeman effect, $\lambda_Z/t = 0.5$ and $t_I = t_R = 0$. The bulk bands are in black. The colours and numbers indicate the quantised Hall conductivity in units of e^2/h. The diagonal dashed lines indicate the outline of the butterfly (i.e., $E/t = \pm 3 \pm 2\pi\phi\lambda_Z$) for the two spin components.

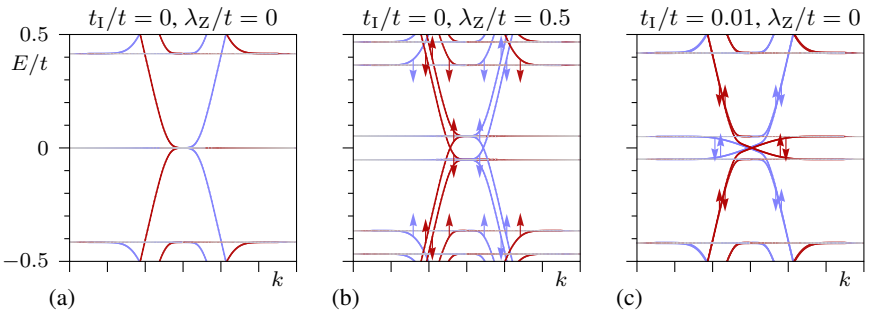

Figure 2.5: Comparison of dispersions at $\phi = 1/61$ for (a) the spin-degenerate case, (b) the system with Zeeman effect ($\lambda_Z/t = 0.5$) and (c) with ISO ($t_I/t = 0.01$). The coupling constants λ_Z and t_I have been chosen such that the (weak-QSH) gap sizes at zero energy become equal.

$\phi \to 0$, while the Landau-level shift induced by the ISO coupling equals $\pm 3\sqrt{3}t_I$ [43]. A recent study shows that a flux-independent Zeeman term (called an exchange term) may also generate the QSH state at zero magnetic field [50].

The similarity between the Zeeman and ISO terms may be understood at a formal level, in terms of the respective linearised (low-energy) Hamiltonians: The linearised Zeeman term acts as $\Psi^\dagger(\sigma_z^{\uparrow\downarrow} \otimes \mathbb{1}^{AB} \otimes \mathbb{1}^{KK'})\Psi$, where the factors indicate the proper spin, sublattice pseudospin, and valley pseudospin, respectively. On the other hand, the ISO coupling acts as $\Psi^\dagger(\sigma_z^{\uparrow\downarrow} \otimes \sigma_z^{AB} \otimes \sigma_z^{KK'})\Psi$. *A priori*, these Hamiltonians act differently on the eight-component field vector $\Psi = (\psi_{\sigma,\tau,\xi})_{\sigma=\uparrow\downarrow,\tau=AB,\xi=KK'}$. In the lowest Landau level, the four components $\psi_{\uparrow,A,K}, \psi_{\downarrow,A,K}, \psi_{\uparrow,B,K'}, \psi_{\downarrow,B,K'}$ vanish [102]. Substituting the remaining field components into the linearised Hamiltonians yields equality up to a sign,

$$\begin{aligned}\Psi^\dagger\left(\sigma_z^{\uparrow\downarrow} \otimes \mathbb{1}^{AB} \otimes \mathbb{1}^{KK'}\right)\Psi &= \psi^\dagger_{\uparrow,A,K'}\psi_{\uparrow,A,K'} - \psi^\dagger_{\downarrow,A,K'}\psi_{\downarrow,A,K'} + \psi^\dagger_{\uparrow,B,K}\psi_{\uparrow,B,K} - \psi^\dagger_{\downarrow,B,K}\psi_{\downarrow,B,K} \\ &= -\Psi^\dagger\left(\sigma_z^{\uparrow\downarrow} \otimes \sigma_z^{AB} \otimes \sigma_z^{KK'}\right)\Psi, \end{aligned} \tag{2.7}$$

which shows that the Zeeman effect and the ISO coupling act equivalently on the lowest Landau level. We remark that this reasoning is only valid at this specific Landau level: For higher Landau levels, all the eight fields are present, and the two terms become inequivalent.

The spin-imbalanced quantum Hall phases

So far, most of the studies on the QSH effect have generally concentrated on the behaviour of the system at zero energy. However, very interesting features also emerge at nonzero energies in the presence of external fields. For instance, in the low-flux regime, a Zeeman gap is formed at the $n = 1$ Landau level (at $E/t \approx 0.42$), as shown in Fig. 2.5(b). Similarly to the zero-energy gap, this gap also shows a difference between the number

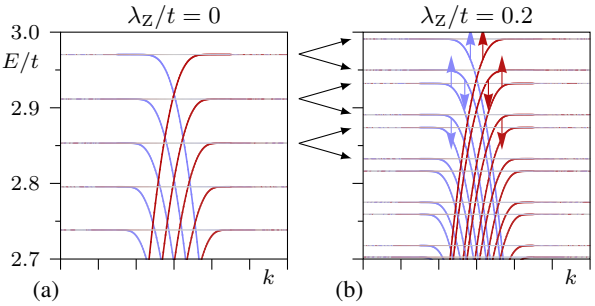

Figure 2.6: High-energy spectra for the model without spin-orbit couplings ($t_R = t_I = 0$) at $\phi = 1/61$. (a) Spectrum for the spin-degenerate model ($\lambda_Z = 0$), with quantum Hall gaps corresponding to $\sigma_H = 2,4,6,\ldots$ (in units of the conductivity quantum). (b) Spectrum with Zeeman effect ($\lambda_Z = 0.2t$), showing the spin-filtered quantum Hall state with $N_\uparrow = 1$ and $N_\downarrow = 0$. The other gaps show (alternatingly) quantum Hall phases ($N_\uparrow = N_\downarrow$) and spin-imbalanced quantum Hall phases ($|N_\uparrow| = |N_\downarrow| + 1$).

of edge states with spin up and spin down components, $N_\uparrow = 1$ and $N_\downarrow = 3$, which may be understood from the values above and below the corresponding Landau level of the spinless model. Again, the spin Hall conductivity is nonzero, $\sigma_H^{sp} = -2e/4\pi$, but the difference with the weak quantum spin Hall gap is that the charge Hall conductivity is also nonzero, $\sigma_H = 4e^2/h$, as can be deduced from Fig. 2.5(b). Furthermore, the edge states in this gap all propagate in the same direction (i.e., they are chiral), thus providing robustness against disorder. Here, we refer to this phase as the *spin-imbalanced quantum Hall phase* [51].

A special instance of the spin-imbalanced quantum Hall phase may occur if edge states of one of the spin-components are absent, i.e., either $N_\uparrow = 0$ or $N_\downarrow = 0$, in which case one speaks about the *spin-filtered quantum Hall phase*. In this state, the magnitudes of the charge Hall and spin Hall currents are therefore equal when expressed in units of their respective conductance quanta. The spin-filtered quantum Hall phase appears at high energies and low flux in the presence of Zeeman coupling, as we now explain. In the absence of Zeeman coupling, we observe equally spaced Landau levels, each of which has Chern number -2, see Fig. 2.6(a). If the Zeeman term is present, the gap that forms between the two copies of the original highest-energy Landau level exhibits a spin-filtered quantum Hall phase, characterised by the presence of edge states of only one spin component; in this case, $N_\uparrow = 1$ and $N_\downarrow = 0$, see Fig. 2.6(b). The other gaps visible in Fig. 2.6(b) are spin-imbalanced and ordinary spin-degenerate quantum Hall gaps, alternatingly. Let us mention that the spin-filtered and spin-imbalanced quantum Hall phases are ubiquitous in systems with Zeeman-split Landau levels, e.g., the quantum Hall plateaus corresponding to odd-integer filling factors in GaAs/AlGaAs

heterostructures [5], or in HgTe quantum wells, which have strong Zeeman effect and are thus ideal candidates for observation of these phases [105].

2.4.4 Rashba spin-orbit coupling

The RSO coupling differs in an essential way from the ISO coupling and the Zeeman effect, in the sense that the hopping involves a spin flip. In other words, the spin matrices involved in the Rashba hopping are off diagonal (i.e., σ_x and σ_y), whereas the other terms in the Hamiltonian involve diagonal spin matrices. This has a profound effect on the spin structure of the system: If the RSO interaction is nonzero, mixing occurs between the spin components and we find that the spin orientation of the eigenstates is generally site-dependent. The spin direction is confined to the two-dimensional plane and is perpendicular to the momentum: Aside from the out-of-plane component (z direction), the component perpendicular to the cylinder edge may also be nonzero, while the component parallel to the edge always vanishes. In other words, the helicity $(\sigma_x, \sigma_y, \sigma_z) \cdot \hbar\mathbf{k}$ of the (edge) states remains zero. This effect is caused by the nature of the Rashba coupling in the Hamiltonian (2.1), which involves the outer product of the spin vector $\boldsymbol{\sigma}$ with the bond vectors $\mathbf{d}_{jk}$, so that the spin is always perpendicular to the hopping direction. Because the edge-state spins are no longer in the up or down state, the Chern numbers for the respective spin components are no longer well-defined. Thus, the spin conductivity no longer takes quantised values. Nevertheless, the spin Chern number remains a well-defined integer-valued topological invariant [100], that can be used as a tool to distinguish between trivial and nontrivial gaps.

The second difference with the ISO coupling is that the zero-flux spectrum remains gapless and the spin degeneracy is lifted by the RSO coupling (considering $t_\mathrm{R} \neq 0$ and $t_\mathrm{I} = \lambda_\mathrm{Z} = 0$). Indeed, upon setting $t_\mathrm{R} \neq 0$, the two Dirac cones from the spinless model (at the special points K and K') are broken into four cones each: A central isotropic cone at K or K', and three anisotropic "satellite" cones around it. This effect is known as trigonal warping [106, 107]. Between the main cones and the satellite ones, there is a Van Hove singularity at low energy, which scales as $\pm(t_\mathrm{R}/t)^3$ for small t_R/t. The Berry phases associated to the main and satellite cones are $-\pi$ and π, respectively, which add up to the Berry phase 2π of the Dirac cones in the spin-degenerate model (π for each spin component).[4] For energies $|E/t| < (t_\mathrm{R}/t)^3$, the low-flux Landau-level spectrum is characterised by two different sets of Landau levels with Chern numbers 2 and 6. Outside this regime, there are only twofold-degenerate Landau levels, because the satellite cones can no longer be resolved. Around $|E/t| \approx (t_\mathrm{R}/t)^3$ there is a crossover regime where the sixfold-degenerate bands split into three, each one being twofold degenerate.

[4] For bilayer graphene, which is characterised by a Hamiltonian that is formally equivalent to $H^\mathrm{NN} + H^\mathrm{R}$, these Berry phases have been derived in Ref. [108].

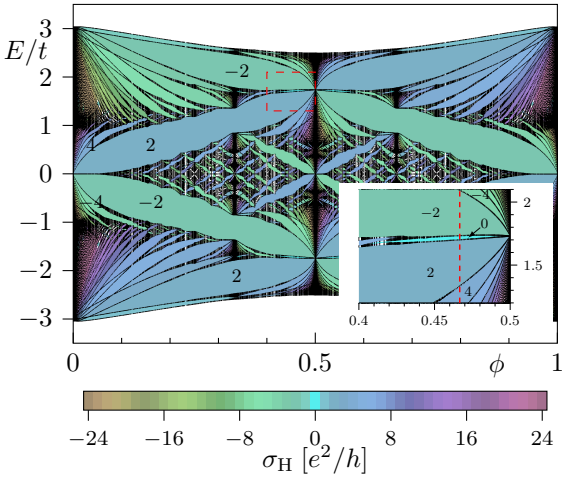

Figure 2.7: Hofstadter butterfly spectrum (with RSO coupling, $t_R/t = 0.2$). The inset shows a magnification of the region surrounded by the dashed lines. In the inset, the dashed line indicates the flux value $\phi = 7/15$.

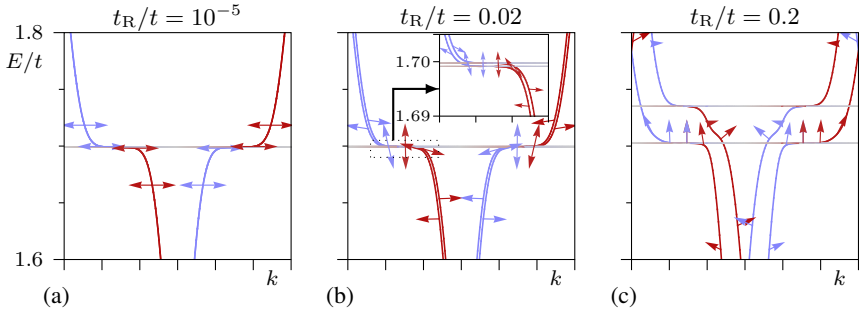

Figure 2.8: Dispersions at $\phi = 7/15$, showing the rotation of spin directions as the Rashba coupling t_R is increased.

Adding a nonzero Rashba term to the spin-degenerate model discussed in Sec. 2.3.1 will cause a spin-splitting of some bulk bands in the Hofstadter butterfly, see Fig. 2.7. In particular, at low energies, the Rashba term splits the fourfold-degenerate Landau levels into twofold-degenerate Landau levels. In the limit $\phi \to 0$, we also note that the spectrum indeed remains gapless and particle-hole symmetric. However, this is not true for other Dirac regimes in the spectrum. For instance, at $\phi = 7/15$ and $E/t \approx 1.7$ (see the inset of Fig. 2.7), the RSO coupling splits the central Landau level, and the resulting gap exhibits two counterpropagating edge modes on each edge. However, the spin Hall conductivity is undefined because the spin direction varies as a function of the Fermi energy. Nevertheless, at each energy inside the gap the spins of the two edge states are approximately equal, so that the spin current nearly vanishes. Besides, the charge Hall conductivity is exactly zero when the Fermi energy is located in this gap.

The RSO coupling has drastic effects on the edge states, as their spins no longer align perpendicularly to the sample plane, but get an additional in-plane component perpendicular to the edge. Besides, the direction of the edge-state spins depends on the Fermi energy. This observation distinguishes the Rashba effect from the Zeeman effect in a tilted field, which puts all edge-state spins in the same direction. In addition, the in-plane component is opposite for edge states at the opposite edges, whereas the perpendicular component is the same. Importantly, due to the dependence of the spin direction on the Fermi energy, the latter can be conveniently used for spin manipulations (in addition to the amplitude of the Rashba coupling itself).

We illustrate this phenomenon around the Rashba-split bulk band at $\phi = 7/15$ and $E/t \approx 1.7$. In Fig. 2.8(a), we show that in the limit of $t_R \to 0$, the eigenstates are in-plane (indicated as "left" and "right" in the figure, meaning that the spin direction is $\pm\hat{y}$). This result shows that for infinitesimal RSO coupling, it is more natural to decompose the states in terms of the eigenstates of the Pauli matrix σ_y than those of σ_z. If the Rashba coupling is then increased, the gap opens, and in the vicinity of the bulk bands, the edge states tend to rotate to the vertical direction, see Fig. 2.8(b). In addition, we observe that not all spins have the same length. This phenomenon occurs because the spins displayed in this plot represent the expectation values of the spin components (see Appendix 2.A). Since the spin direction depends on the lattice position (y coordinate), the length of this expectation value may be less than unity. In Appendix 2.B, we give a qualitative explanation for the behaviour of the edge-state spin direction.

We expect that the canting of the spins is most easily observed in gaps with a single edge state on each edge. For instance, in Ref. [51], it has been demonstrated that the RSO coupling cants the spin in a spin-filtered gap generated by the Zeeman effect. In this setting, the spin textures may be controlled at will by tuning the coupling parameters and the Fermi energy.

2.4.5 Comparison between the low-flux and "half-flux" regimes

As shown before in the low-flux limit $\phi \to 0$, the ISO coupling and the Zeeman effect affect the zero-energy modes equivalently in the sense that they both open a weak QSH gap. Indeed, it has been shown that for this mode, the ISO coupling and Zeeman effect are formally equivalent [102]. On the other hand, the RSO coupling does not open a gap at zero energy. This fact hampers the comparison of the RSO coupling to the aforementioned two terms in this energy regime.

From the Hofstadter butterfly shown in Fig. 2.1, one observes that the Landau-level structure in the low-flux, low-energy limit is not unique. In fact, similar structures appear wherever the shape of the dispersion is characterised by Dirac cones. For example, at $\phi = 1/2$ and for energies close to $E/t = \pm\sqrt{3}$, the dispersion can be approximated by a Dirac dispersion of the form $|E/t| = \sqrt{3} \pm \sqrt{\frac{3}{2}}|\mathbf{k}| - \frac{1}{4}\sqrt{3}|\mathbf{k}|^2 + \mathcal{O}(|\mathbf{k}|^3)$, where $\mathbf{k}$ is the momentum relative to the position of one of the two Dirac cones. The linear term is responsible for the square-root behaviour of the (fourfold-degenerate) Landau levels for flux values close to $\phi = 1/2$. The quadratic term causes the asymmetry of the Landau-level spectrum with respect to the energy $|E/t| = \sqrt{3}$. Furthermore, we observe that the energy $|E_{\mathrm{LL},0}/t| \approx \sqrt{3} - (\pi/3)|\phi - 1/2|$ of the central Landau level is linear in the flux rather than constant.

The approximate linear dependence of the spectrum $E(\mathbf{k})$ at $\phi = 1/2$ and $|E/t| \approx \sqrt{3}$ suggests that the Zeeman and ISO terms should behave similarly in this regime, in direct analogy to the case $\phi, E \approx 0$ discussed in Sec. 2.4.3. Although the energy of the lowest Landau level is no longer constant in ϕ, the approximation holds, thus leading to a similar behaviour with regard to the opening of the gaps, as shown in Figs. 2.9(a–d) for the flux value $\phi = 7/15$ which lies close to $\phi = 1/2$. The Zeeman effect and ISO coupling split the central Landau level at $E/t \approx 1.7$ and open up a weak QSH gap, similar to the zero mode in the low-flux regime. As discussed in Sec. 2.4.4, the RSO coupling splits the central Landau level, unlike the case for $\phi \to 0$, see Figs. 2.9(e) and (f). Although there are edge states inside the gap, it is a trivial state, because the spin Hall conductivity approximately vanishes. This comparison shows an important difference between Zeeman coupling and ISO coupling on one hand, and the Rashba coupling on the other hand: The former two create the weak QSH phase, while the latter does not. In the following section, we show that in the presence of Zeeman or ISO coupling, the Rashba coupling tends to destroy the weak QSH phases generated by the former effects.

2.5 Competition and phase transitions

After analysing the effects of the three terms H_{I}, H_{R}, and H_{Z} in Hamiltonian (2.1) independently, a natural question arises: What effects emerge when these terms are combined? Here, we study the competition featuring two terms, by tuning the ratio be-

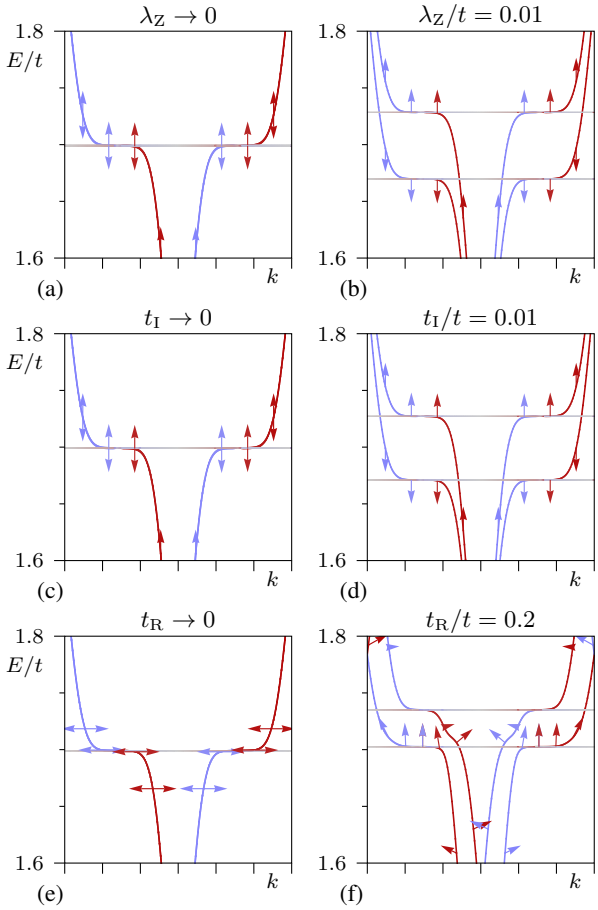

Figure 2.9: Spin splitting in an example at flux $\phi = 7/15$ and near $E/t = 1.7t$. Zeeman effect: (a) $\lambda_Z \to 0$ and (b) $\lambda_Z = 0.01t$; ISO coupling: (c) $t_I \to 0$ and (d) $t_I = 0.01t$; RSO coupling: (e) $t_R \to 0$ and (f) $t_R = 0.2t$.

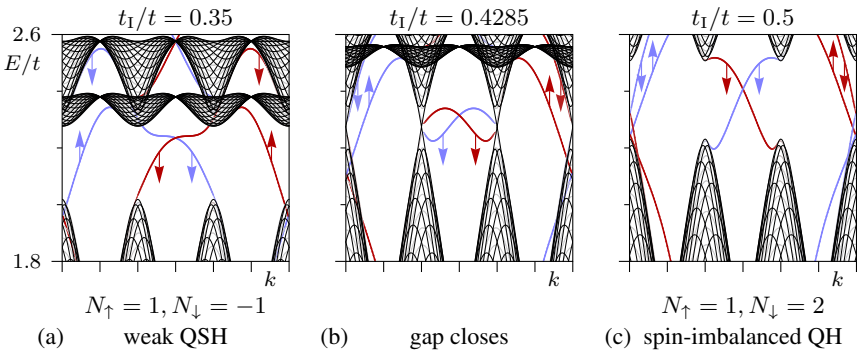

Figure 2.10: Spectra for $\phi = 1/3$, with (a) $t_I/t = 0.35$, (b) $t_I/t = 0.4285$, (c) $t_I/t = 0.5$. In (a), we observe a (weak) QSH gap, where $N_\uparrow = -N_\downarrow = 1$. (b) By increasing the ISO coupling constant, the bulk gap closes for $t_I/t \approx 0.4285$. (c) If t_I is increased further, the gap reopens, but with a different number of edge states, namely, $N_\uparrow = 1$ and $N_\downarrow = 2$, so that it enters a spin-imbalanced phase. Thus, the system undergoes a topological phase transition from a helical phase (weak QSH) to a chiral phase (spin-imbalanced QH).

tween their corresponding coupling constants. Tuning these coupling constants generally leads to opening and closing of gaps, so that the topological nature of the gaps may change. In that case, we deal with *topological phase transitions*. We recall that Kane and Mele [43] have studied the phase transition from a (time-reversal symmetric) QSH state to a trivial state, by increasing the ratio t_R/t_I. Here, we extend this study and we explore the more exotic phase transitions that occur in the presence of a magnetic field and the Zeeman effect.

2.5.1 Phase transitions driven by the ISO coupling

Let us analyse the interplay between the ISO coupling and the magnetic field by investigating a gap at a fixed flux value, in absence of the Zeeman effect and of the Rashba coupling. By tuning the value of the ISO coupling amplitude t_I, we can close the gaps and obtain different topological phases at both sides of the transition. In Fig. 2.10, we have shown the dispersions for $\phi = 1/3$, for values of t_I below, at, and above the values where the gap around $E/t = 2.3$ closes. Around this energy, there are three bulk bands: Two (overlapping) ones above and one below the gap. For values of $t_I < t_{I,0} \approx 0.4285t$, below the critical value, we observe the weak QSH phase, i.e., two counterpropagating edge modes with opposite spins on each edge, $N_\uparrow = 1$ and $N_\downarrow = -1$. The spin-down pair of edge modes connects the top and bottom bulk bands visible in this plot, and the spin-up pair connects the middle band to a lower band. For $t_I = t_{I,0}$, the gap disappears: The bulk bands touch each other in three points at $E/t \approx 2.3$, and two of these points are connected by the spin-down edge states in the middle of the figure. If the

value of t_I is increased further, a gap opens again, and a new pair of edge states (with spin down) appears. Moreover, the existing spin-down edge states have inverted their direction of propagation. Thus, for $t_I > t_{I,0}$, we have a spin-imbalanced quantum Hall state with $N_\uparrow = 1$ and $N_\downarrow = 2$. Note that only the spin-down states are modified in this phase transition, while the spin-up states remain the same.

In Ref. [51], this phase transition was investigated in the presence of a nonzero Zeeman coupling in addition to the ISO coupling. Here, we emphasise that the Zeeman effect is actually superfluous and that this transition is driven exclusively by the ISO coupling. Variation of λ_Z has no qualitative effect on the transition, but only shifts the energies of the bands and gaps. Within a large range of values for λ_Z, we obtain an identical phase transition as in Fig. 2.10. The critical value $t_{I,0}$ of the ISO strength is independent of λ_Z.

The phase transition presented here differs in a fundamental way from a crossing of Landau levels. In the latter case, the Chern numbers associated to the Landau levels do not change at the transition, and as a consequence the number of edge states inside de gap between them remains unmodified as well. For the phase transition presented here, the number of edge states does change at the transition. Consequently, this means that the Chern numbers of the bands must also change. Focusing on the spin-down edge states, we observe that $N_\downarrow = -1$ for $t_I < t_{I,0}$ and $N_\downarrow = 2$ for $t_I > t_{I,0}$, a difference of $\Delta N_\downarrow = 3$. The Chern numbers of the bands below and above the gap are 1 and 1 in the former case and -2 and 4 in the latter. The sum of these Chern numbers is unchanged, as required by the bulk-boundary correspondence, Eq. (2.5).

The question arises as to whether the difference in the number of edge states at both sides of the transition may be predicted. *A priori*, this difference cannot be predicted since it is the result of a complicated interplay of the ISO coupling and the magnetic flux. However, the difference is always a multiple of the denominator q of the flux $\phi = p/q$. This result may be understood from the fact that at a given flux value $\phi = p/q$, the Chern numbers of all the Hofstadter bands obey $C_n \equiv c \pmod q$. Here, c is the *modular multiplicative inverse* of p modulo q, defined as the unique integer c ($0 \leq c < q$) such that $cp \equiv 1 \pmod q$.[5] Consequently, the difference between two possible values of the Chern numbers is always a multiple of q, which proves the aforementioned claim. This property may also be understood from the superlattice structure: The magnetic field produces q copies of the original unit cell, and each of them reacts in the same way to the perturbation leading to the phase transition.

In Fig. 2.11, we show the phase diagram as a function of the ISO coupling t_I and the Fermi energy E_F with the flux value $\phi = 1/3$ held fixed. From this figure, we can easily read off the values of t_I and the energies E_F where the gaps close and the topological

[5] This result has been verified empirically for the spinless model. The observation that $C_n \equiv c \pmod q$ for all n implies automatically that $cp \equiv 1 \pmod q$, assuming that the Středa formula and the bulk-boundary correspondence hold. These results are valid more generally for the model described by Hamiltonian (2.1) as long as the two spin components are decoupled.

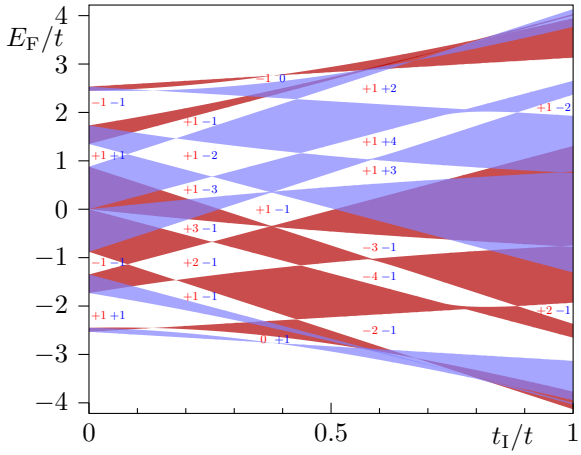

Figure 2.11: Phase diagram as a function of the ISO coupling t_I and the Fermi energy E_F for the fixed flux value $\phi = 1/3$. In the shaded regions, the system is metallic. The colours red (dark gray) and blue (light gray) distinguish the spin-up and -down components, respectively. In the white regions, the bulk is insulating, and the edges conduct. There, the pairs of numbers indicate the number of edge states $N_\uparrow$ and $N_\downarrow$ for spin up and down, respectively.

phase transitions occur. A few points must be noticed: First of all, we clearly identify the weak-QSH phase at half-filling for $t_I/t = 0.4$. The (spin-degenerate) QH phases are progressively destroyed for $t_I/t < 0.3$. For $t_I/t > 0.3$, we get spin-filtered QH [e.g., $(N_\uparrow, N_\downarrow) = (-1, 0)$], spin-imbalanced QH [e.g., $(N_\uparrow, N_\downarrow) = (+1, +2)$] and the weak QSH phase. In addition, there are also more exotic phases where the edge states are neither chiral nor helical, e.g., $(N_\uparrow, N_\downarrow) = (+1, -2)$. The spin-degenerate phases do not arise for $t_I/t > 0.3$. Secondly, the gaps are large (of the order of t) in wide regions of the parameters, which is favourable for the detection of the transitions in cold-atoms experiments. In addition, the property that the number of edge states changes by a multiple of 3 at each phase transition is clearly observed in Fig. 2.11. Finally, the energies where the phase transitions occur may be shifted by tuning the strength of the Zeeman effect. Since the spin-up and spin-down components are uncoupled, the Zeeman effect will shift all red (blue) areas in Fig. 2.11 up (down) by a fixed amount of energy. We note that the Zeeman effect alone does not induce the same type of phase transitions as the ISO coupling. The Zeeman effect can only close and open gaps between bands of different spin components, and does therefore not modify the Chern numbers of the bands, whereas the ISO coupling can also close gaps between two bands of the same spin component. Nevertheless, tuning the Zeeman coupling strength λ_Z allows one to modify the nature of the phase transitions driven by ISO coupling.

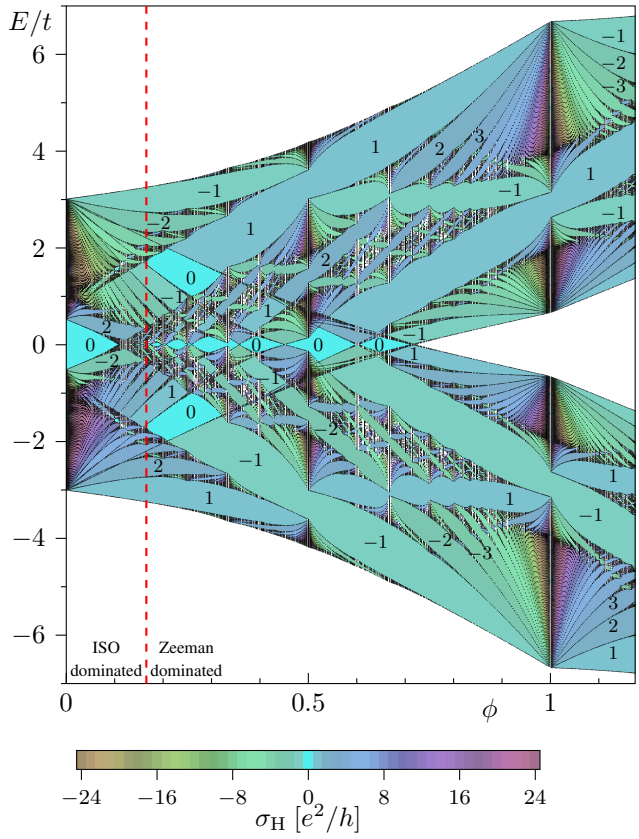

Figure 2.12: Hofstadter butterfly spectrum with ISO coupling ($t_I/t = 0.1$) and Zeeman effect (λ_Z). The vertical dashed line indicates the flux value where the two effects are comparable in strength. At this value, the crossover from the ISO-dominated (low ϕ) to the Zeeman-dominated (high ϕ) regime takes place.

2.5.2 Intrinsic spin-orbit coupling and Zeeman effect for $\phi \neq 0$

If the Zeeman effect and ISO coupling are present simultaneously, the interplay between the two terms is governed by the value of the flux ϕ, because the amplitude of the former is linear in ϕ while that of the latter is constant. Thus, in the butterfly spectrum illustrated in Fig. 2.12, we observe the ISO-dominated regime at low flux (cf. Fig. 2.3), and the Zeeman-dominated regime at high flux (cf. Fig. 2.4). The crossover between these two regimes takes place where the two terms are comparable in strength, approximately where $4\pi\phi\lambda_Z \sim 6\sqrt{3}t_I$, indicated by the vertical dashed line in Fig. 2.12 at $\phi \approx 0.165$. We remark that this crossover effect is present more generally in the situation where the Zeeman term competes with any other term with a constant amplitude:

Due to the linear ϕ dependence of the Zeeman term, it will always dominate the other one at sufficiently high values of ϕ. Naturally, this phenomenon only occurs in systems where the Zeeman splitting depends linearly on the magnetic flux ϕ. In more complicated cases, the Zeeman term may exhibit a nonlinear dependence on the applied magnetic flux due to magnetic impurities, as discussed in Ch. 3 for Mn-doped HgTe quantum wells.

Although the Zeeman effect dominates over the ISO coupling for $\phi \gg 0.165$, the effect of the ISO coupling is still visible in the high-flux spectrum: At $\phi = 1/2$ and $\phi = 1$, there are gaps at $E/t \approx 3$ (see Fig. 2.12), which are absent in the butterfly without the ISO coupling (see Fig. 2.4). We note that the dispersions around these points are of Dirac type for $t_{\mathrm{I}} = 0$, consequently, the ISO coupling opens these gaps in a way analogous to the gaps at zero flux and zero energy. However, the gaps at $\phi = 1/2$ and $\phi = 1$ are spin-filtered QH phases and not QSH, due to the subtle competition between the ISO coupling and the TRS-breaking effects.

2.5.3 Rashba spin-orbit coupling and exchange term at $\phi = 0$

In two recent works [109, 110], it has been shown that the combination of RSO and an exchange field, similar in structure to the Zeeman term, leads to chiral edge states at zero energy. In addition, the problem has been investigated for a sodium/lithium iridate model which involves NN and NNN hopping terms [111]. In the latter and more complex setup, nontrivial QH gaps appear also away from half filling. Here, we consider the combined effects of the Zeeman and Rashba couplings, away from half-filling and in the absence of ISO coupling. We demonstrate that *several* QH gaps appear in the absence of NNN hopping terms, without including any gauge field (i.e., the Peierls phases): Namely, non-trivial QH phases are produced in our model by setting $\phi = t_{\mathrm{I}} = 0$, $t_{\mathrm{R}} \neq 0$ and by applying a flux-independent Zeeman, or exchange [50, 109, 110], term

$$H_{\mathrm{ex}} = g_{\mathrm{ex}} \sum_j c_j^\dagger \sigma_z c_j, \tag{2.8}$$

which differs from H_z by the fact that the strength g_{ex} no longer depends on the flux ϕ (which we now set to zero). We stress that it is the simple association of a constant exchange term with a NN Rashba hopping term that leads to non-trivial topological phases, at half-filling but also at $E_{\mathrm{F}} \approx g_{\mathrm{ex}}$, as discussed in detail below.

When the exchange term is added to the tight-binding model with strength $0 < g_{\mathrm{ex}} < 3t$, the energy bands associated to the spin-up and spin-down components are shifted in opposite directions but overlap at half-filling. In this situation, which is illustrated in Fig. 2.13(a), the system is a semi-metal for $E_{\mathrm{F}} = \pm g_{\mathrm{ex}}$ and a metal otherwise. When the Rashba coupling is turned on, bulk gaps open not only at half-filling $E = 0$ but also at $E = \pm g_{\mathrm{ex}}$ [cf. Fig. 2.13(b)]. We have computed the edge-state structures as well as the topological indices associated to the gaps: we obtain that all these gaps are

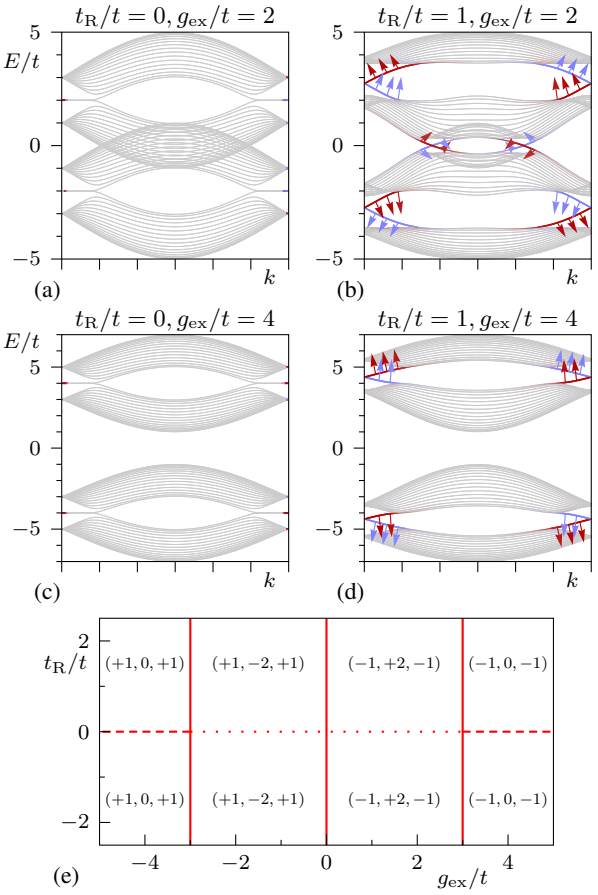

Figure 2.13: (a-d) Energy spectra $E = E(k)$ for $\phi = t_I = 0$. The Zeeman (exchange) and Rashba coupling strength are indicated. (e) Phase diagram in the parameter space defined by the coupling strengths g_{ex} and t_R. The number triplets indicate the charge Hall conductivity in the lower, middle, and upper gaps, respectively. The solid lines indicate the phase transitions for the gap at zero energy. At the dashed lines, the lower and upper gaps close and the trivial gap at zero energy remains open [as in (c)], and at the dotted lines, all three gaps close [as in (a)]. At the dashed and dotted lines, the charge Hall conductivities in the gaps do not change.

related to non-trivial QH phases. More precisely, we find that the gaps at $E = \pm g_{ex}$ host a single edge state per edge, whose spin orientation is given by $\langle \sigma_z \rangle \approx \pm 1$: these gaps correspond to spin-filtered QH phases, with equal (resp. opposite) charge (resp. spin) Hall conductivities. We observe that the spin orientation of these isolated edge states is nearly vertical, which is due to the fact that the exchange term is important in this high-energy regime. At half-filling, the bulk gap hosts two edge states per edge,

with same velocity and quasi-horizontal spin orientation. This bulk gap corresponds to a topological QH phase with $\sigma_H = 2$ and a non-trivial spin orientation. Therefore, the spin orientation of the edge states highly depends on the Fermi energy. We note that the gap openings occur for large exchange coupling, but for arbitrarily low Rashba coupling.

When the exchange strength $g_{ex} > 3t$, the energy bands associated to the spin-up and spin-down components are well separated: a trivial gap opens at half-filling, while the Dirac points are shifted to the energies $E = \pm g_{ex}$, cf. Fig. 2.13(c). In this situation, the Rashba coupling still opens two non-trivial QH phases at $E_F = \pm g_{ex}$, cf. Fig. 2.13(d). Again, these phases are characterised by spin-filtered edge states with nearly vertical spin orientation. Therefore, for sufficiently large exchange coupling, it is necessary to set the Fermi energy away from half-filling in order to detect nontrivial topological phases. This behaviour is summarised in the phase diagram of Fig. 2.13(e): For nonzero Rashba coupling t_R, the Hall conductivity at zero energy is $\sigma_H = \pm 2$ for $|g_{ex}/t| < 3$ and zero otherwise. Thus, topological phase transitions of the zero-energy gap take place at the gap closings at $g_{ex}/t = \pm 3$. The lower and upper gaps (at $E_F \approx \pm g_{ex}$) always exhibit a Hall conductivity of ± 1, where the sign depends on that of g_{ex}/t but not on that of t_R/t. Inverting the sign of g_{ex} inverts the directions of the edge currents, as well as the z component of the spins. Inverting the sign of t_R inverts the in-plane component of the spins. Continuous variation of t_R through zero changes the spin direction continuously, where the spins tend to the z direction in the limit $t_R/t \to 0$. Thus, the gap closing at $t_R = 0$ does not constitute a topological phase transition.

Let us emphasise the fact that the chiral QH phases presented here are not the consequence of the external magnetic flux (i.e., Peierls phases), since they are produced when $\phi = 0$, and solely in the presence of the exchange and Rashba terms. When $\phi \neq 0$, new QH gaps open in the system, altering the exchange-Rashba-induced phases presented in Figs. 2.13(b) and 2.13(d). This competition between QH gaps of different origins leads to complex and rich quantum phase transitions.

2.5.4 Zeeman effect and Rashba spin-orbit coupling for $\phi \neq 0$

In the low-energy regime, where the (weak) QSH phase is generated by either ISO coupling or the Zeeman effect, the additional inclusion of the Rashba coupling has several profound effects on the physics. First of all, the RSO coupling tends to decrease the size of the gap (cf. Ref. [43]), eventually completely closing it. Secondly, the combination of RSO coupling with ISO coupling and/or Zeeman effect destroys the particle-hole symmetry of the spectrum. Finally, at finite magnetic field, the RSO coupling opens up a gap (i.e., an avoided crossing) between the edge states at their crossing around zero energy. Around this crossing, the spin direction rotates from down to up (or vice versa), as illustrated in Fig. 2.14. The size of this gap is approximately linear in ϕ and in t_R (in the limit $\phi \to 0$ and $t_R \to 0$). Thus, the bulk gap is trivial in the sense that no

edge states cross it from one bulk band to the other. However, in the limit where the edge-state gap is small, one would still observe a weak QSH state. At finite temperatures, the thermal energy can "bridge" the edge-state gap, so that the charge carriers may tunnel from one edge state to another. As the edge-state gap size is increased, the backscattering is enhanced, due to the decrease in the amount of tunneling across the edge-state gap. Here, we expect that the value of the spin Hall conductivity will deviate from its quantised value $\pm 2e/4\pi$. The amount of deviation increases when the gap size increases.

Beyond the low-flux limit, a remarkable spin-manipulation process can be envisaged by combining the effects of the Rashba spin-mixing perturbation and the Zeeman splitting. As already mentioned above, the Zeeman splitting generates spin-filtered edge states in the QH gaps. In the example illustrated in Fig. 2.15 (b), a single spin-down particle propagates along the edge of the sample when $E_F \approx -2.25t$, for $\phi = 1/3$ and $\lambda_Z = 0.5t$. As shown in Fig. 2.15 (c), one can then progressively increase the Rashba coupling and control the spin orientation $\langle \sigma_\mu \rangle = \langle \Psi | \hat{\sigma}_\mu | \Psi \rangle$ of this specific and *unique* chiral edge state. This process indeed modifies the band structure, as well as the spin textures associated with the edge current, leading to a chiral Rashba phase (see Fig. 2.15): The spin components of this single edge state are now $\sigma_z = -0.5$ and $\sigma_\perp = 0.5$, where $\sigma_\perp$ is the spin component in the direction perpendicular to both the direction of propagation and the applied magnetic field. The canting of the edge-state spin is a hallmark of the competition between the Rashba term, which tends to rotate the spin direction towards the xy plane, and the Zeeman term, which tends to align the spins in the vertical direction. For $t_R = t$, a large but realistic value for a Raman-induced tunneling amplitude, this single edge state can be reached by adjusting the Fermi energy to the value $E_F \approx -3.25t$, as shown in Fig. 2.15(c). Interestingly, the spin direction of the edge states within this gap highly depends on the Fermi energy [112]. Thus, the spin direction of the edge states can be tuned by varying the filling factor. We emphasise that this effect is notably different from the constant spin orientation that would result from the Zeeman effect in a tilted magnetic field. We finally stress that the variation of t_R does not close the topological bulk gap, and therefore, its associated Chern number remains unaltered. In this sense, there is no topological phase transition involved in this manipulation of the edge-state spin.

2.6 Experimental realisations

In this section, we will discuss the several experimental approaches that allow for the observation of the topological phases and phase transitions discussed in Secs. 2.4 and 2.5. For each of them, we present the opportunities and challenges, and we discuss the range of parameters that can be probed.

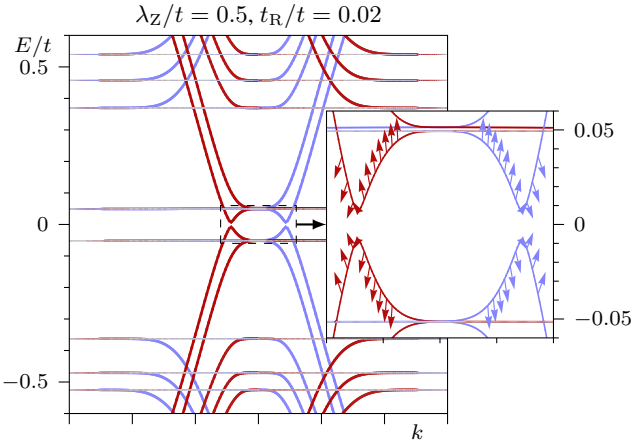

Figure 2.14: Spectrum for the system with nonzero Zeeman ($\lambda_Z/t = 0.5$) and RSO coupling ($t_R/t = 0.02$), for $\phi = 1/61$. The inset shows a zoom of the region where a gap opens between the edge states at zero energy. For comparison with the spectrum in absence of Rashba coupling, refer to Fig. 2.5(b).

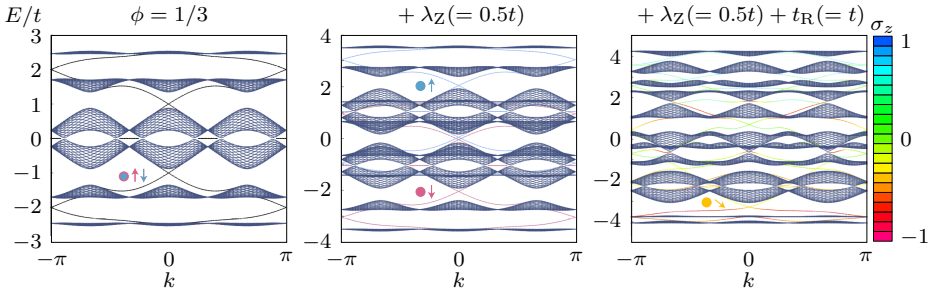

Figure 2.15: Generating a chiral Rashba phase on the edges. The energy spectrum $E = E(k)$ is represented as a function of the momentum, in a cylindrical geometry with zigzag edges. (a) Several QH phases are generated by a magnetic flux $\phi = 1/3$. When the Fermi energy lies in the gap at $E \approx -t$, a single spin-degenerate edge state propagates on each edge. (b) The inclusion of the Zeeman splitting lifts the spin degeneracy and creates spin-filtered QH phases at $E = \pm 2.25t$ and $E = \pm 3t$. At half-filling, the Zeeman splitting opens a "weak" QSH gap. (c) The addition of the Rashba term then allows for flipping the spin of the edge state to an arbitrary orientation. When the Fermi energy $E_F \approx -3.25t$, the single edge state has spin components $\sigma_z \approx -0.5$ and $\sigma_\perp \approx 0.5$ (cf. orange dot). Here, the bulk energy bands are depicted in dark blue.

2.6.1 Condensed-matter systems

Condensed-matter systems typically have a lattice spacing in the order of 1 Å, so that one flux quantum per unit cell ($\phi = 1$) corresponds to a magnetic field in the order of 10^4–10^5 T. Thus, only the low-flux limit is relevant with respect to realistic condensed-matter realisations of our model. The prime example of a two-dimensional system with a honeycomb lattice is graphene, which has received much attention both at the theoretical and experimental levels [99, 102]. In the presence of a magnetic field, graphene shows an anomalous quantum Hall effect, where the Landau-level energies [34, 35] depend on the magnetic field as $\sqrt{\phi}$, showing a radically different behaviour than in semiconductor heterostructures (e.g., GaAs/AlGaAs).

Besides, the effects of spin-orbit coupling have been extensively studied for graphene, leading to the concept of $\mathbb{Z}_2$ topological insulators [43]. However, recent analysis has shown that graphene exhibits only a very weak ISO coupling ($t_\mathrm{I}/t \sim 10^{-6}$–$10^{-5}$, where $t \sim 2.8$ meV) [46, 107], which unfortunately prevents the observation of the QSH state in this material. Nevertheless, the ISO interactions may be enhanced by putting heavy adatoms on top of the graphene surface [66], which would open up a route to build a topological heterojunction [65]. The Zeeman effect is of appreciable order of magnitude, $g \sim 2$, which corresponds to gaps of 100 K at a magnetic field of 30 T [113]. Values of the Rashba coupling as high as $t_\mathrm{R} \sim 0.1t$ have been reported for graphene on a Ni(111) substrate [114]. High values of the RSO coupling (accompanied by the spin re-orientation at the edges) may also be induced by curving graphene nanoribbons [115]. In addition, large effective pseudomagnetic fields, greater than 300 T, have been recently realised in strain-induced graphene nanobubbles [116]. In summary, the observation of the topological phases presented here remains elusive in graphene, but should not be definitively ruled out.

The QSH effect has nevertheless been observed in other two-dimensional compounds that have considerably larger values of t_I, such as Hg(Cd)Te quantum wells [47, 48], where values of the order $t_\mathrm{I} \sim$ 1–10 meV have been reported [49, 117]. Additionally, this material exhibits a strong Zeeman effect as well ($g \sim 20$) [118]. The spin-filtered QH states have already been observed in these systems at low fields [119]. Hg(Cd)Te quantum wells doped with magnetic ions (e.g., Mn) exhibit an exchange interaction leading to the quantum anomalous Hall effect at zero magnetic field [59], and to a nonlinear Zeeman effect that causes reentrant behaviour of the topological phases [105].

2.6.2 Artificial honeycomb lattices

The experimental limitation of the low flux values can be overcome by studying systems with a larger lattice spacing. Recently, several approaches have led to the engineering of artificial honeycomb lattices. First of all, arrays of quantum dots on a GaAs, arranged in a honeycomb pattern, have been engineered to simulate actual graphene

[67, 120]. The lattice spacing in these systems is of the order of 100 nm, so that high flux values ($\phi \sim 1$) are obtained already with small magnetic fields. However, this large lattice constant leads to a small hopping amplitude, which has hampered the observation of the Hofstadter butterfly until now. Patterned superlattices able to probe the Hofstadter regime with usual magnetic field intensities have been realised in the past, but for square geometries [121, 122]. To probe the physics described here, one needs a superlattice with a smaller lattice constant, grown on a substrate that could lead to the generation of a strong Rashba interaction, for example. In this case, chiral topological states could be probed also away from zero energy, as we discuss in Sec. 2.4.5.

Secondly, artificial graphene lattices have been created by manipulating CO molecules with the tip of a scanning tunneling microscope and arranging them in a triangular lattice on a Cu(111) substrate [68]. These molecules repel the electrons on the Cu surface, thus creating a honeycomb array of sites between which the electrons hop. Measurements of the density of states show that the electrons indeed exhibit a Dirac dispersion. The typical lattice constants of these systems are approximately 7 times larger than in real graphene, thus allowing for flux values ~ 50 times larger than in graphene, with reasonable magnetic fields. In addition, effective magnetic fields up to 60 T can be induced by triaxial strain of the artificial lattice. It can be speculated that by using a heavier metal as substrate, it may be possible to engineer such a lattice with strong spin-orbit coupling, leading to the QSH phase.

2.6.3 Ultracold atoms in optical lattices

Although the parameters of the Hamiltonian (2.1) can be controlled to some extent in condensed-matter systems, the possibility to engineer the physics discussed here with ultracold atoms in optical lattices is very appealing. The advantage of the ultracold-atom realisation of this model is the flexibility to control the parameters separately across a large range, compared to condensed-matter systems where these parameters are generally fixed by the material properties and the sample geometry. A second major advantage of ultracold atoms over condensed-matter systems is that the magnetic fields are produced synthetically, i.e., the Peierls phases are not due to a real magnetic field, but induced by external fields acting on atomic internal states [74]. In this way, large effective magnetic flux can be produced (i.e., $\phi \sim 1$), which allows the system to be studied beyond the low-flux limit [75]. The spin-orbit couplings can also be synthesised in optical lattices using similar methods [77–80]. Moreover, in these configurations, the Zeeman coupling can be controlled independently, as it is not related to the synthetic magnetic fields [123] (see Sec. 2.5.3, where we study the extreme situation where the effect of the Zeeman coupling is investigated in the absence of synthetic magnetic field, in which case this term is called an “exchange term”). Another important feature offered by optical-lattice setups is the possibility to control the interactions

between the particles: By exploiting Feshbach resonances [87], it is possible to reach the non-interacting regime and from there on, to include interactions in a controlled way to explore the robustness of topological order against interactions. Let us mention that these systems are usually free of disorder, although disorder can also be generated and tailored at will in optical lattices [124]. These outstanding features allow us to study the TRS broken QSH phase, namely the survival of the QSH phase in the presence of a TRS breaking perturbation [51]. Indeed, contrarily to condensed-matter experiments, the absence of (magnetic) disorder can stabilise the helical (counterpropagating) edge states even when TRS is broken. Let us also comment on the fact that all the topological phases and edge-state excitations discussed here rely on the existence of robust bulk energy gaps. Therefore, when the temperature of the system approaches the size of the topological gaps of interest, one expects the effects to be strongly affected, and eventually to disappear. For the ultracold temperatures achieved in cold-atom laboratories, the gaps of interest should typically be of the order $\Delta \sim t$, where t is the tunneling amplitude. Therefore, we anticipate that only the largest topological gaps presented in our figures should be considered from the cold-atom point of view.

The quantum phase transitions presented in this work could be equally characterised either by a change in the topological invariants associated to the bulk gaps of interest, or by the modification of the edge-state structures. Although cold atoms do not offer the possibility to directly measure transport coefficients, several methods have been proposed to detect the topological invariants related to the quantised conductivities [95, 125, 126]. These proposals are based on the fact that non-trivial band structures modify the atomic densities, leading to several signatures that can be directly seen in time-of-flight or density measurements. On the other hand, it is possible to directly probe edge-state structures using Bragg spectroscopy techniques [127–130]. In a recent work [129], it was shown that a state-dependent light probe, focused on the edge of the cloud and transferring angular momentum to the atoms, clearly identifies the presence of chiral edge states in a QH optical lattice. This method allows us to project the topological edge states on a dark background, making them visible in *in situ* density measurements. In principle, this efficient scheme could be generalised to spin-$\frac{1}{2}$ systems in order to detect and distinguish between chiral and helical edge structures.

2.7 Conclusions

We have shown an in-depth analysis of the edge-state structures generated by the combination of the ISO coupling, the RSO coupling, and the Zeeman effect, together with a uniform and perpendicular magnetic field. In Sec. 2.4, we have studied each term individually in order to pinpoint their effect on the quantum Hall states generated by the magnetic field. In the low-field limit, the ISO coupling and Zeeman effect are formally

equivalent, and give rise to the weak QSH phase. Away from zero energy, we observe spin-filtered, spin-imbalanced, and ordinary quantum Hall phases. The RSO coupling is different in the sense that it involves spin-flip terms, which causes the spin states to acquire an in-plane component. In addition, the spin direction inside the gap depends on the Fermi energy, and consequently the spin Hall conductivity of the system is ill defined. In the case of high magnetic fields, we observe Dirac-type regimes away from zero energy. Here, the Zeeman and ISO coupling open weak QSH gaps in a way analogous to the low-flux limit, whereas the RSO coupling opens a trivial gap (unlike the case at low flux, where the spectrum remains gapless). In addition, topological phase transitions driven by tuning the amplitude of the ISO coupling have been analysed in detail.

A combination of the spin-orbit terms and the Zeeman effect leads to subtle competitions, several examples of which have been discussed in Sec. 2.5. We have shown that, although the Zeeman effect and ISO coupling both give rise to the QSH phase, they do not always reinforce each other, which has been illustrated by the size of the parameter regime of the weak QSH phase in the low-flux limit. At high flux, the Zeeman effect dominates over the ISO coupling, but the effects of the latter are still well visible in the spectrum. Interestingly, a combination of the Rashba term with an exchange coupling leads to nontrivial topological phases at zero magnetic field, away from half-filling. Finally, inclusion of the Rashba coupling in the case where we have a weak QSH gap generated by the Zeeman effect opens a gap at zero energy between the edge states, which provides an illustration of the breakdown of the QSH effect in the absence of TRS and spin conservation.

This work emphasises the various topological phase transitions and edge-state structures that could be observed in a wide range of materials and quantum emulators. Although we focused our analysis on the honeycomb lattice, where the spin-orbit couplings and the magnetic field configurations are expressed by specific tunneling terms and Peierls phases, we note that our results do not rely on this specific geometry. The topological phases and the phase transitions discussed here are universal, in the sense that they only rely on the inclusion of general ingredients, which can be found or engineered in many different contexts and geometries. Indeed, this universal property can be understood in the low-energy limit, in which various (*a priori*, very different) tight-binding models actually reduce to the same (Dirac-type) equations. In general, we observe that the main ingredients needed to generate such physics are nontrivial gauge fields, which are coupled to the particles of interest (e.g., electrons in materials and atoms in optical lattices). In this work, we have aimed to emphasise the effects produced by each of these ingredients independently: We have investigated the effects of spin splitting, spin mixing, and gauge potentials leading to magnetic or Haldane-type local flux. We hope that our detailed analysis will deepen the understanding of topological insulating phases and that it will motivate further developments in this exciting and rapidly developing field.

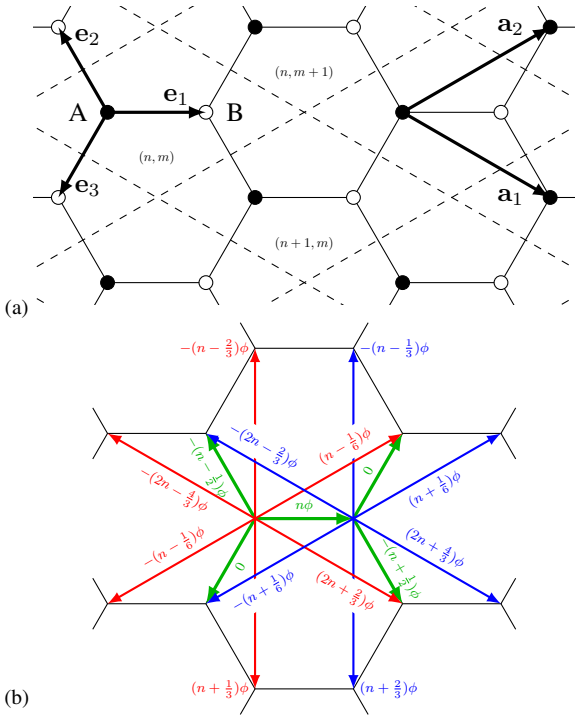

Figure 2.16: (a) The honeycomb lattice. We indicated the NN vectors $\mathbf{e}_j$ ($j = 1,2,3$) and the lattice vectors $\mathbf{a}_1$ and $\mathbf{a}_2$. The sites of the sublattices A and B are indicated with solid and open circles, respectively. The dashed lines define boundaries of the unit cells, labeled as (n,m). (b) Hopping phases $\theta_{jk}/2\pi$ for the unit cell (n,m). The phases for the NN hopping are in green. The phases for the NNN hopping are in red and blue for the sublattices A and B, respectively.

2.A Geometry and gauge

Geometrically, the honeycomb lattice is equivalent to a distorted square lattice where each unit cell has the shape of a rhombus. Since there are two inequivalent sets of sites, there are two sites per unit cell, and hence two sublattices, labeled A and B. The sites, labeled as j and k in the Hamiltonian (2.1), may be uniquely identified by two integer labels n and m for the unit cell and A or B for the sublattice: In the following, we shall write $j = (n,m,\tau)$ (where $n,m \in \mathbb{Z}$ and $\tau \in \{\mathrm{A},\mathrm{B}\}$) to uniquely identify the sites.

The coordinates of the sites are given as follows. We choose the bond vectors $\mathbf{e}_1$, $\mathbf{e}_2$ and $\mathbf{e}_3$ as displayed in Fig. 2.16(a), where their length $a \equiv 1$ is chosen as the unit of length throughout this text. Subsequently, the lattice vectors are given by $\mathbf{a}_1 = \mathbf{e}_1 - \mathbf{e}_2$ and $\mathbf{a}_2 = \mathbf{e}_1 - \mathbf{e}_3$, so that the coordinates of the sites are

$$\mathbf{r}_{n,m,\mathrm{A}} = n\mathbf{a}_1 + m\mathbf{a}_2, \qquad \mathbf{r}_{n,m,\mathrm{B}} = n\mathbf{a}_1 + m\mathbf{a}_2 + \mathbf{e}_1.$$

Furthermore, the reciprocal space is spanned by the two vectors $\mathbf{b}_1$ and $\mathbf{b}_2$, defined by $\mathbf{b}_i \cdot \mathbf{a}_j = 2\pi\delta_{ij}$. We note that the results derived in this chapter do not depend on the values of the vectors $\mathbf{e}_i$; the only effect of a change of the $\mathbf{e}_i$ is that the lattice vectors and the reciprocal lattice vectors will be different. A convenient choice for the bond vectors is $\mathbf{e}_1 = (0,0)$, $\mathbf{e}_2 = (-1,0)$ and $\mathbf{e}_3 = (0,-1)$, effectively putting both sites of the unit cell (n,m) on the coordinate (n,m).

The phases due to the magnetic field, associated with the hopping, are given in terms of the gauge potential $\mathbf{A}$ as $\theta_{jk} = (e/\hbar)\int_{\mathbf{r}_k}^{\mathbf{r}_j} \mathbf{A}\cdot\mathbf{dl}$, where the integral is over the line between sites k and j. We may employ the gauge freedom for the gauge potential to choose it in such a way that the phase θ_{jk} for two sites $j = (n,m,\tau)$ and $k = (n',m',\tau')$ (NNs or NNNs) does not depend on the unit cell index m. The hopping phases resulting from such a choice are given in Fig. 2.16(b) for hopping from the sites of the unit cell (n,m). The reader may check that the phase picked up from hopping around a loop is proportional to the area of the loop. In particular, when one considers one hexagon as the loop, the phase picked up is $2\pi\phi$, which corresponds to an enclosed flux of ϕ (in units of the flux quantum). Here, we note that the area of one hexagon is $3\sqrt{3}/2$, so that ϕ is related to the magnetic field strength B as $\phi = (3\sqrt{3}/2)eB/h$.

In addition to the gauge choice, let us furthermore assume that the flux value is a rational number, $\phi = p/q$, where p and q are coprime integers. Then, the phase assigned to each hopping is periodic in the index n with periodicity q. In other words, the unit cell of the superlattice (i.e., the lattice together with the hopping phases) is $q\times 1$ unit cells of the original lattice. With this observation, we may invoke Bloch's theorem, which states that we could write the electron wave functions $\varphi_{n,m,\tau}$ as

$$\begin{aligned}\varphi_{n,m,\mathrm{A}} &= \psi_{n\mathrm{A}} e^{i\mathbf{k}\cdot(n\mathbf{a}_1+m\mathbf{a}_2)},\\ \varphi_{n,m,\mathrm{B}} &= \psi_{n\mathrm{B}} e^{i\mathbf{k}\cdot(n\mathbf{a}_1+m\mathbf{a}_2+\mathbf{e}_1)}.\end{aligned} \tag{2.9}$$

With this ansatz, the Schrödinger equation which the fields have to satisfy reduces to a $4q$-component matrix equation: The degrees of freedom are all fields $\Psi_n = (\psi_{n\mathrm{A}\uparrow}, \psi_{n\mathrm{A}\downarrow}, \psi_{n\mathrm{B}\uparrow}, \psi_{n\mathrm{B}\downarrow})$ in the unit cell of the superlattice, so that $n = 1,\ldots,q$, and there are two sublattice and two spin components per unit cell of the original lattice. This matrix equation is then merely an eigenvalue equation of a $4q\times 4q$ matrix, known as the Harper equation [53, 131],

$$\frac{E}{t}\begin{pmatrix}\Psi_1\\ \Psi_2\\ \Psi_3\\ \vdots\\ \Psi_{q-1}\\ \Psi_q\end{pmatrix} = \begin{pmatrix}\mathscr{D}_1 & \mathscr{R}_1 & 0 & \cdots & 0 & \mathscr{R}_q^\dagger\\ \mathscr{R}_1^\dagger & \mathscr{D}_2 & \mathscr{R}_2 & \cdots & 0 & 0\\ 0 & \mathscr{R}_2^\dagger & \mathscr{D}_3 & \cdots & 0 & 0\\ \vdots & \vdots & \ddots & \ddots & \ddots & \vdots\\ 0 & 0 & 0 & \ldots & \mathscr{D}_{q-1} & \mathscr{R}_{q-1}\\ \mathscr{R}_q & 0 & 0 & \ldots & \mathscr{R}_{q-1}^\dagger & \mathscr{D}_q\end{pmatrix}\begin{pmatrix}\Psi_1\\ \Psi_2\\ \Psi_3\\ \vdots\\ \Psi_{q-1}\\ \Psi_q\end{pmatrix}. \tag{2.10}$$

Here, the 4×4 matrices $\mathscr{D}_n = \mathscr{D}_n^{(\mathrm{NN})} + \mathscr{D}_n^{(\mathrm{R})} + \mathscr{D}_n^{(\mathrm{I})} + \mathscr{D}_n^{(\mathrm{Z})}$ and $\mathscr{R}_n = \mathscr{R}_n^{(\mathrm{NN})} + \mathscr{R}_n^{(\mathrm{R})} + \mathscr{R}_n^{(\mathrm{I})}$ encode hopping between unit cells with the same index n and from unit cells with index $n+1$ to n. (Note that the Zeeman term is diagonal.) Thus, Eq. (2.10) can be written equivalently as Eq. (2.2).

The 4×4 matrices $\mathscr{D}_n$ and $\mathscr{R}_n$ may be written in terms of the sum of four contributions, that correspond to each of the terms in Hamiltonian (2.1). The contributions for the ordinary NN hopping are given by

$$\mathscr{D}_n^{(\mathrm{NN})} = \begin{pmatrix} 0 & e^{i\mathbf{k}\cdot\mathbf{e}_1}e^{2\pi i n\phi} + e^{i\mathbf{k}\cdot\mathbf{e}_3} \\ e^{-i\mathbf{k}\cdot\mathbf{e}_1}e^{-2\pi i n\phi} + e^{-i\mathbf{k}\cdot\mathbf{e}_3} & 0 \end{pmatrix} \otimes \mathbb{1}_{\mathrm{spin}}, \tag{2.11}$$

$$\mathscr{R}_n^{(\mathrm{NN})} = \begin{pmatrix} 0 & 0 \\ e^{-i\mathbf{k}\cdot\mathbf{e}_2}e^{-2\pi i(n+\frac{1}{2})\phi} & 0 \end{pmatrix} \otimes \mathbb{1}_{\mathrm{spin}}. \tag{2.12}$$

The Zeeman effect is encoded by $\mathscr{D}_n^{(\mathrm{Z})} = (2\pi\lambda_{\mathrm{Z}}\phi/t)\,\mathbb{1}_{\mathrm{AB}}\otimes\sigma_z$ and $\mathscr{R}_n^{(\mathrm{Z})} = 0$. The matrices for the ISO coupling are

$$\mathscr{D}_n^{(\mathrm{I})} = -i\frac{t_{\mathrm{I}}}{t}\times \tag{2.13}$$
$$\begin{pmatrix} -e^{-2\pi i(n-\frac{1}{6})\phi}e^{i\mathbf{k}\cdot\mathbf{f}_2} + e^{2\pi i(n-\frac{1}{6})\phi}e^{-i\mathbf{k}\cdot\mathbf{f}_2} & 0 \\ 0 & e^{-2\pi i(n+\frac{1}{6})\phi}e^{i\mathbf{k}\cdot\mathbf{f}_2} - e^{2\pi i(n+\frac{1}{6})\phi}e^{-i\mathbf{k}\cdot\mathbf{f}_2} \end{pmatrix}\otimes\sigma_z,$$

$$\mathscr{R}_n^{(\mathrm{I})} = -i\frac{t_{\mathrm{I}}}{t}\times \tag{2.14}$$
$$\begin{pmatrix} -e^{2\pi i(2n+\frac{2}{3})\phi}e^{i\mathbf{k}\cdot\mathbf{f}_3} + e^{2\pi i(n+\frac{1}{3})\phi}e^{-i\mathbf{k}\cdot\mathbf{f}_1} & 0 \\ 0 & e^{2\pi i(2n+\frac{4}{3})\phi}e^{i\mathbf{k}\cdot\mathbf{f}_3} - e^{2\pi i(n+\frac{2}{3})\phi}e^{-i\mathbf{k}\cdot\mathbf{f}_1} \end{pmatrix}\otimes\sigma_z,$$

where $\mathbf{f}_1 = \mathbf{e}_2 - \mathbf{e}_3$, $\mathbf{f}_2 = \mathbf{e}_3 - \mathbf{e}_1$, and $\mathbf{f}_3 = \mathbf{e}_1 - \mathbf{e}_2$ denote the NNN vectors. Here, the phase factors due to the flux correspond to those in Fig. 2.16(b). Due to the fact that the phases involve fractions of ϕ which are all multiples of $\frac{1}{6}$, the ϕ periodicity of the butterfly spectra is 6, rather than the periodicity of 1 which is observed in absence of the ISO coupling. Finally, for the RSO coupling, the hopping matrices are given by

$$\mathscr{D}_n^{(\mathrm{R})} = \frac{t_{\mathrm{R}}}{t}\begin{pmatrix} 0 & 0 & 0 & -a_-^{(\mathrm{R})} \\ 0 & 0 & a_+^{(\mathrm{R})} & 0 \\ 0 & a_+^{(\mathrm{R})*} & 0 & 0 \\ -a_-^{(\mathrm{R})*} & 0 & 0 & 0 \end{pmatrix}, \tag{2.15}$$

$$\mathscr{R}_n^{(\mathrm{R})} = \frac{t_{\mathrm{R}}}{t}\begin{pmatrix} 0 & 0 & 0 & 0 \\ 0 & 0 & 0 & 0 \\ 0 & b_+^{(\mathrm{R})*} & 0 & 0 \\ b_-^{(\mathrm{R})*} & 0 & 0 & 0 \end{pmatrix}, \tag{2.16}$$

where $a_\pm^{(\mathrm{R})} = e^{2\pi i n\phi}e^{i\mathbf{k}\cdot\mathbf{e}_1} + e^{\pm 2\pi i/3}e^{i\mathbf{k}\cdot\mathbf{e}_3}$ and $b_\pm^{(\mathrm{R})} = e^{-2\pi i(n+\frac{1}{2})\phi}e^{\mp 2\pi i/3}e^{i\mathbf{k}\cdot\mathbf{e}_2}$.

The solution of the Harper equation yields the dispersions of the bulk states, which are periodic over the so-called magnetic Brillouin zone, q times smaller than the original Brillouin zone. Effectively, the geometry of the system is a torus, in this case. However, to study edge states, a cylindrical geometry (as displayed in Fig. 2.2) is more convenient. The edge-state spectrum is obtained from the Harper equation similar to Eq. (2.10), but with a matrix of dimension $4w \times 4w$, where w is the width of the ribbon in unit cells, and with the blocks in the top-right and bottom-left corner replaced by zeros (i.e. $\mathscr{R}_w \equiv 0$). In this case, the dispersion depends on just one component of $\mathbf{k}$, and its periodicity is the reciprocal lattice vector.

To determine states as bulk states or edge states, we derive the density profile $|\Psi_n|^2$ as a function of the unit cell index n (or equivalently, the coordinate component y). For convenience, we choose $n = 0$ to be the center of the ribbon, so that $n = -\tilde{w}, \ldots, \tilde{w}$, where $w = 2\tilde{w} + 1$ is the width of the ribbon. The expectation value of this position, $\langle n \rangle = \sum_n n|\Psi_n|^2$ is used to distinguish edge states and bulk states. Edge states are characterised by a density profile that is sharply peaked at one edge, so that $\langle n \rangle \approx \pm\tilde{w}$. On the other hand, if the expectation value $\langle n \rangle$ is close to zero, then it means that there is a significant contribution of the density away from the edge; such a state is identified as a bulk state. In the edge state spectra of this chapter, we have used this expectation value to colour the states: Red and blue colours indicate the two opposite edges, while gray is used for the bulk states. In the same way, we use the spin expectation values $\langle \sigma_i \rangle = \sum_n \Psi_n^\dagger \sigma_i \Psi_n$ $(i = x, y, z)$ to gain information about the spin states. We note that this expectation is only reliable in the case that the spin is constant (or almost constant) where the density of the state is concentrated. This may not be the case in the presence of Rashba coupling. In the case when the spin strongly depends on position, the length of the vector $\langle \boldsymbol{\sigma} \rangle$ is less than unity.

2.B Spin direction in case of nonzero Rashba coupling

In contrast to the other terms in the Hamiltonian (2.1), the Rashba term does not preserve the spin component in the z direction. Therefore, in the presence of the Rashba coupling, the states will carry also a nonzero component in the direction perpendicular to the z direction and to the sample edges.

Examination of the spin direction of the edge states shows that it is close to the z direction where an edge state is close to a bulk band, while the spins are horizontal deep inside the bulk gaps, as is illustrated in Fig. 2.8. In order to explain this phenomenon, let us consider hopping along the edge governed by the Hamiltonian (2.1) where only NN hopping is possible (i.e., $t_\mathrm{I} = \lambda_\mathrm{Z} = 0$), either with or without spin flip,

$$H_\mathrm{NN} + H_\mathrm{R} = -\sum_{\langle j,k \rangle} \left(e^{i\theta_{jk}} c_j^\dagger \begin{pmatrix} t & t_\mathrm{R}\alpha_{jk} \\ -t_\mathrm{R}\alpha_{jk}^* & t \end{pmatrix} c_k + \mathrm{h.c.} \right), \tag{2.17}$$

where $\alpha_{jk} = id_y - d_x$ is given in terms of the hopping vector $\mathbf{d}_{jk} = (d_x, d_y)$ between sites j and k. We consider the hopping to the adjacent unit cell along the edge, which consists of the NN hopping along two differently oriented bonds. Thus, we multiply the two hopping matrices associated with these hoppings. Here, we neglect the bulk, or equivalently, we consider just a "chain" of sites. The spin eigenstates ψ of that product are then used to find the spin expectation values $\langle\psi|(\sigma_x, \sigma_y, \sigma_z)|\psi\rangle$. For a system with the zigzag edge parallel to the y axis, we obtain

$$\langle\psi|(\sigma_x, \sigma_y, \sigma_z)|\psi\rangle = \frac{1}{\sqrt{4 + \tilde{t}_R^2}} \left(\pm 2, 0, \pm \tilde{t}_R\right), \tag{2.18}$$

where $\tilde{t}_R = t_R / t$ and the signs depend on the edge state under consideration. We observe that in the limit $\tilde{t}_R \gg 2$, the spins will be in the z direction, while in the opposite limit $\tilde{t}_R \ll 2$, the spins will be in-plane. The behaviour of the spin direction of the edge states is then explained as follows. Here, we consider t as an effective hopping parameter, that incorporates also the difference between the Fermi energy and the bulk-band energy. Then, the Rashba coupling dominates over the effective hopping parameter close to the bulk bands, so that the spins are vertical, whereas in the gaps, the ordinary hopping dominates, leading to in-plane spins. Furthermore, the analysis also explains the rotation of the spin from horizontal to vertical if the Rashba coupling t_R is increased from zero to a finite value. However, in this analysis, the bulk has been neglected. Due to the fact that the edge states may extend a few unit cells into the bulk, the explanation given here is only qualitatively correct.

Chapter 3

Reentrant topological phases in Mn-doped HgTe quantum wells

Quantum wells of HgTe doped with Mn display the quantum anomalous Hall effect due to the magnetic moments of the Mn ions. In the presence of a magnetic field, these magnetic moments induce an effective nonlinear Zeeman effect, causing a non-monotonic bending of the Landau levels. As a consequence, the quantised (spin) Hall conductivity exhibits a reentrant behaviour as one increases the magnetic field. Here, we will discuss the appearance of different types of reentrant behaviour as a function of Mn concentration, well thickness, and temperature, based on the qualitative form of the Landau-level spectrum in an effective four-band model.[6]

3.1 Introduction

The study of topological states of matter has undergone a vertiginous growth since the theoretical prediction [43, 48, 132] and the experimental observation [47] of the quantum spin Hall (QSH) effect. Unlike the quantum Hall (QH) effect, which is generated by an external magnetic field, or the quantum anomalous Hall (QAH) effect, which requires time-reversal symmetry (TRS) to be spontaneously broken without applying an external magnetic field, the QSH state is characterised by TRS and is generally driven by the intrinsic spin-orbit (ISO) coupling [63]. Nevertheless, it has been recently shown that in the absence of spin-flip terms, the QSH effect survives even if the TRS is broken. This state has been dubbed a *weak QSH* state (see Ch. 2 and Refs. [51, 52]) or *TRS broken QSH* state [50], where the weakness refers to the absence of protection by TRS. Indeed, the gap and the topological Chern and spin Chern numbers associated with the topological phase remain robust if the TRS is broken by an exchange term [50] or

[6] This chapter is based on *Reentrant topological phases in Mn-doped HgTe quantum wells*, W. Beugeling, C. X. Liu, E. G. Novik, L. W. Molenkamp, and C. Morais Smith, Phys. Rev. B **85**, 195304 (2012) [105].

by an additional magnetic field [51, 101, 133], and there is a quantum phase transition to a topologically distinct or to a trivial phase only when the gap is closed [50, 51].

An interesting open question is what kind of competition could originate in systems where there is an externally applied magnetic field in addition to intrinsic magnetic moments, which on their own would lead to the QAH effect. Recently, the QAH effect has been studied thoroughly for several theoretical models of two-dimensional topological insulators, including HgTe quantum wells [59] and thin films of Bi_2Se_3 [134–136] doped with transition metal elements such as Mn, Fe, or Cr. In addition, graphene has been proposed as a candidate for the observation of this effect [50, 109, 137–139]. The influence of a magnetic field on Mn-doped HgTe quantum wells has been partially investigated in Ref. [59], with the aim of polarising the Mn magnetic moment to be eventually able to generate the QAH effect upon shutting down the magnetic field. However, here we concentrate on aspects not considered so far. Unexpectedly, in the presence of a magnetic field, the Zeeman term can also lead to the TRS broken QSH phase, even in the absence of SO coupling [51, 52, 102, 133]. Therefore it is interesting to explore the interplay between the usual Zeeman term, which is linear in the applied magnetic field, and the non-linear effect arising from the exchange coupling with the magnetic moment of the Mn atoms. In this chapter, we show that within a model with a spin-conserving Hamiltonian, the TRS broken QSH phase occurs, and that a *reentrant* behaviour is present for a certain range of parameters.

A reentrant integer QH effect was experimentally observed a few years ago in GaAs quantum wells for filling factors between $\nu = 3$ and $\nu = 4$, in the first Landau level (LL) [140]. The phenomenon was later understood to occur due to a sequence of first-order quantum phase transitions between electron-solid (Wigner crystal or bubble phases) and electron-liquid phases [141, 142], and it was grounded in the strong electron-electron interactions that dominate the physics at non-integer filling factors. Due to the self-similarity of the Hall conductance curve [30, 143], which displays a fractal behaviour, a similar phenomenon was predicted to occur also for a second-generation of composite fermions [31]. In that case, a series of reentrant plateaus would turn out to be quantised at the nearby fractional Laughlin values [144].

A second possibility is to observe reentrant integer QH effects solely due to the LL structure of the system. For instance, in Si/SiGe heterostructures, reentrant behaviour can be driven at the single-particle level by varying the in-plane magnetic field while keeping the perpendicular field fixed, as to modify the ratio between the cyclotron energy and the Zeeman splitting [145]. In these systems, the crossings of the LLs for spin up and spin down are responsible for the reentrant behaviour of the quantised Hall conductivity. For HgTe [118] and InAs/GaSb [146, 147] quantum wells, the reentrance of the Hall conductivity has been used as a practical method to prove the existence of such a LL crossing and consequently the inverted order of the bands.

In this chapter, we show that by applying a magnetic field perpendicular to a Mn-doped HgTe quantum well, the charge and spin Hall conductivities may reenter con-

comitantly, i.e., there can be a reentrance of the same topological phase, characterised by both its charge and spin topological invariants. This effect is caused by the nonmonotonic behaviour of the LL energies due to the nonlinear dependence of the Zeeman term on the externally applied magnetic field. A rich panoply of LL crossings, combined with the nonmonotonicity of the LL energies, provides us with regimes of parameters where this reentrant behaviour could be experimentally accessed. $Hg_{1-Y}Mn_YTe$ quantum wells are ideal candidates for the observation of these effects, because they have a strong ISO coupling and a large Zeeman g factor. We use the effective four-band model of Ref. [48] to compute the LL spectrum [118] together with the relevant Chern numbers in order to identify the QSH state and other QH-like states. Band structure calculations are performed for different values of the quantum-well thickness and of the Mn doping fraction to set realistic parameters for this model. We then study the LL spectra including the charge and spin Hall conductivities and determine the conditions for the observation of reentrant topological phases.

The outline of this chapter is as follows. In Sect. 3.2, we define the effective model that we use to derive our results. In Sect. 3.3, we compute the LL spectrum, explain the mechanisms that lead to the reentrant effects, and explore the parameter regimes for which they can be observed. We conclude by discussing in Sect. 3.4 the possibilities to resolve the reentrant effects in experiments.

3.2 The model

HgTe and related materials have a zinc-blende lattice structure, so that the physics of the low-energy electronic bands is well described by the eight-band Kane model [49, 148]. By using perturbation theory (see the Appendix for details), higher-energy bands are projected out in order to reduce this model to an effective four-band model [48, 49]. In this reduced model, the bands under consideration are referred to as $|E_1+\rangle, |H_1+\rangle, |E_1-\rangle, |H_1-\rangle$, in this order. Here, E and H refer to electron- and hole-like bands, respectively, and $+$ and $-$ distinguish the two members of each of the two Kramers pairs $|E_1\pm\rangle$ and $|H_1\pm\rangle$, hereafter referred to as spin components. The symmetry properties under the parity and time-reversal transformations dictate the quadratic-order Hamiltonian $H = H_0 + H_Z + H_{ex}$, with [47, 48, 118]

$$H_0 = \begin{pmatrix} h(\mathbf{k}) & 0 \\ 0 & h^*(-\mathbf{k}) \end{pmatrix}, \tag{3.1}$$

where

$$\begin{aligned} h(\mathbf{k}) &= \epsilon(\mathbf{k})\,\mathbb{1}_2 + d_\alpha(\mathbf{k})\sigma^\alpha,\ \ \epsilon(\mathbf{k}) = \mathscr{C} - \mathscr{D}(k_x^2 + k_y^2), \\ d_\alpha(\mathbf{k}) &= (\mathscr{A}\,k_x, -\mathscr{A}\,k_y, \mathscr{M}(\mathbf{k})),\ \ \mathscr{M}(\mathbf{k}) = \mathscr{M} - \mathscr{B}(k_x^2 + k_y^2). \end{aligned} \tag{3.2}$$

Here, σ^α denotes the Pauli matrices, and $\mathscr{M}$, $\mathscr{A}$, $\mathscr{B}$, $\mathscr{C}$, and $\mathscr{D}$ are parameters that depend on the material composition and on the thickness of the quantum well. In

particular, the variations of these parameters induce the topological phase transition from a regime where the electronic bands are ordered normally to a regime where the order is inverted and where the QSH effect is present [48].

The system is subjected to a perpendicular magnetic field $B\mathbf{e}_z$, which we will express in terms of the dimensionless variable ϕ, which denotes the magnetic flux per unit cell measured in units of the flux quantum h/e. With these definitions, ϕ relates to the magnetic field B and to the magnetic length l_B as $2\pi\phi = eBa^2/\hbar = a^2 l_B^{-2}$. For HgTe, with lattice constant $a = 0.646$ nm, the flux value $\phi = 10^{-3}$ corresponds to a magnetic field of $B = 9.91$ T. In the remainder of this text, we set $\mathscr{C} = 0$ for convenience, and we set $a \equiv 1$ as the unit of length, so that $\mathscr{M}$, $\mathscr{A}$, $\mathscr{B}$, and $\mathscr{D}$ all have the dimension of energy.

The materials under consideration show a large Zeeman effect, with Landé g factors of the order of 20 [118]. We therefore consider the Zeeman term in the Hamiltonian, with different g factors for electrons and holes,

$$H_Z = \mathrm{diag}(\tilde{g}_\mathrm{E}, \tilde{g}_\mathrm{H}, -\tilde{g}_\mathrm{E}, -\tilde{g}_\mathrm{H})(2\pi\phi) \tag{3.3}$$

where $\tilde{g}_{\mathrm{E(H)}} = g_{\mathrm{E(H)}}\mu_\mathrm{B}\hbar/ea^2 \approx g_{\mathrm{E(H)}} \times 91.30$ meV is a rescaled Zeeman parameter, proportional to the Bohr magneton μ_B and to the g factor $g_{\mathrm{E(H)}}$ for electrons (holes) [118].

In quantum wells of HgTe doped with Mn (with molar fraction Y, i.e., we consider $\mathrm{Hg}_{1-Y}\mathrm{Mn}_Y\mathrm{Te}$), the presence of Mn has a significant effect on the magnetic properties of the material. It has been found that for low Mn concentrations ($Y \lesssim 0.07$), the material behaves paramagnetically, so that its response to the magnetic field is nonlinear: In addition to the Zeeman effect (linear in the magnetic field strength), there is also a nonlinear contribution from the exchange interaction between Mn ions and band states. The exchange interaction term is given by [58, 149]

$$H_\mathrm{ex} = \mathrm{diag}(\chi_\mathrm{E}, \chi_\mathrm{H}, -\chi_\mathrm{E}, -\chi_\mathrm{H})B_{5/2}(\lambda_\mathrm{ex}2\pi\phi) \tag{3.4}$$

where χ_E and χ_H are the exchange energies for the electron and hole bands, respectively,

$$B_{5/2}(x) = \tfrac{6}{5}\coth(\tfrac{6}{5}x) - \tfrac{1}{5}\coth(\tfrac{1}{5}x) \tag{3.5}$$

is the Brillouin function [150],

$$\lambda_\mathrm{ex} = \frac{5}{2}\frac{g_\mathrm{Mn}\mu_\mathrm{B}\hbar/ea^2}{k_\mathrm{B}(T+T_0)} \approx \frac{5297\ \mathrm{K}}{T+T_0} \tag{3.6}$$

is an exchange parameter, with $g_\mathrm{Mn} = 2$, and $T + T_0$ is an effective temperature, where $T_0 \approx 2.6$ K [149]. Since the electron wave function $|E_1\pm\rangle$ is a linear combination of the wave functions of the Γ^6 and Γ^8 bands, the exchange energy χ_E is a linear combination of the exchange energies Δ_s and Δ_p associated with these bands, respectively. The only contribution to the hole wave function $|H_1\pm\rangle$ comes from the Γ^8 bands, so that χ_H is proportional to Δ_p [58, 59]. For a more detailed explanation, we refer the reader to the Appendix.

The energy splitting due to the exchange interactions can be considered as an effective Zeeman splitting, by virtue of the similarity between Hamiltonians (3.3) and (3.4). Here, one writes the Zeeman energy as $\tilde{g}^{\rm eff}_{\rm E(H)} 2\pi\phi$, where

$$\tilde{g}^{\rm eff}_{\rm E(H)}(\phi) = \tilde{g}_{\rm E(H)} + \frac{\chi_{\rm E(H)}}{2\pi\phi} B_{5/2}(\lambda_{\rm ex} 2\pi\phi) \tag{3.7}$$

is the effective, field-dependent g factor for the electron (hole) band. In the low-field limit ($2\pi\phi\lambda_{\rm ex} \ll 1$), the effective g factor is approximately constant, $\tilde{g}^{\rm eff}_{\rm E(H)}(\phi \to 0) = \tilde{g}_{\rm E(H)} + (7/15)\chi_{\rm E(H)}\lambda_{\rm ex}$, derived by using a linear approximation to $B_{5/2}(x)$. In the high-field limit $2\pi\phi\lambda_{\rm ex} \gg 1$, the exchange interaction energy is almost constant ($\approx \chi_{\rm E(H)}$) as a function of the field, because $B_{5/2}(x) \to 1$ for $x \to \infty$, and as a consequence, it depends also very weakly on the temperature.

3.3 Results

In order to derive the LL spectrum, we model the effect of the magnetic field $B\mathbf{e}_z$ by the Peierls substitution: In the Hamiltonian, the momentum $\hbar\mathbf{k}$ is replaced by $\hbar\mathbf{k} - e\mathbf{A}$, where $\mathbf{A}$ is the gauge potential, such that $B\mathbf{e}_z = \nabla \times \mathbf{A}$. The freedom of the gauge choice allows us to choose the symmetric gauge, $\mathbf{A} = (B/2)(-y, x, 0)$. Subsequently, we replace $k_+ = k_x + ik_y$ and $k_- = k_x - ik_y$ by the ladder operators $a^\dagger$ and a, respectively. These operators raise and lower the LL index by 1, and their prefactors are chosen such that $[a, a^\dagger] = 1$ [118]. In the model presented here, we neglect the coupling between the two spin bands which would arise in the presence of bulk-inversion asymmetry and Rashba spin-orbit coupling. By virtue of this decoupling, the two spin bands can be treated separately. Thus, the eigenvalues and eigenvectors of the Hamiltonian are given by the solutions to the equation $h_\sigma(a, a^\dagger)(|n+1\rangle, c\,|n\rangle) = E^{(i)}_{\sigma,n}(\phi)(|n+1\rangle, c\,|n\rangle)$, with the appropriate values for c. Here, the eigenvalues $E^{(i)}_{\sigma,n}(\phi)$ give the energies of the LLs, where $n = 0, 1, 2, \ldots$ is the LL index, $\sigma = +, -$ refers to the spin components, and $i = 1, 2$ distinguishes between the two solutions that exist for each spin component [118, 119]. For the Hamiltonian that includes the (effective) Zeeman effect, the resulting LL energies are given by [118, 119]

$$\begin{aligned} E^{(1,2)}_{\sigma,n} &= [-2n\mathscr{D} - \sigma\mathscr{B} + \tfrac{1}{2}\sigma\tilde{g}^{\rm eff}_+](2\pi\phi) \\ &\quad \pm \sqrt{[\mathscr{M} + (-\sigma\mathscr{D} - 2n\mathscr{B} + \tfrac{1}{2}\sigma\tilde{g}^{\rm eff}_-)(2\pi\phi)]^2 + 2n\mathscr{A}^2(2\pi\phi)} \quad (n \geq 1), \\ E_{+,0} &= \mathscr{M} - (\mathscr{D} + \mathscr{B} - \tilde{g}^{\rm eff}_{\rm E})(2\pi\phi), \qquad E_{-,0} = -\mathscr{M} - (\mathscr{D} - \mathscr{B} + \tilde{g}^{\rm eff}_{\rm H})(2\pi\phi), \end{aligned} \tag{3.8}$$

where $\tilde{g}^{\rm eff}_\pm \equiv \tilde{g}^{\rm eff}_{\rm E} \pm \tilde{g}^{\rm eff}_{\rm H}$ are the sum and the difference of the effective (field-dependent) g factors given by Eq. (3.7), including the effect of the Mn doping.

The LL spectra presented here are computed using Eq. (3.8), where the relevant parameters have been derived numerically from band structure calculations based on the

eight-band Kane model [49, 148], as explained in more detail in the Appendix. These parameters have been computed for several values of the quantum-well thickness d and Mn fraction Y. In particular, the dependence of $\mathscr{M}$ on Y has dramatic consequences: Increasing Y leads to an increase of $\mathscr{M}$, such that it drives the system from the inverted regime ($\mathscr{M} < 0$) to the topologically trivial regime ($\mathscr{M} > 0$) [49].

The charge (spin) Hall conductivity in a specific bulk gap is defined as the sum of the charge (spin) Chern numbers over all occupied LLs below it. Here, by virtue of the decoupling of the two spin components in the Hamiltonian, the charge and spin Chern numbers of each LL are equal to the sum and difference of the Chern numbers $C_{\pm,n}$ associated with each of the two components. These Chern numbers are well-defined due to the spin-conserving nature of the Hamiltonian. Thus, the charge and spin Hall conductivity expressed in units of their respective quanta, e^2/h and $e/4\pi$, are computed as

$$\sigma_{\mathrm{H}} = \sum_n (C_{+,n} + C_{-,n}), \quad \sigma_{\mathrm{H}}^{\mathrm{sp}} = \sum_n (C_{+,n} - C_{-,n}), \tag{3.9}$$

where the summation is over the occupied LLs. These values are robust, even in the absence of TRS [101]. In this model, each LL contributes a Chern number of 1, so that the analysis is simplified to merely counting the LLs. The presented values have been verified by analysis of the edge states in a ribbon geometry; see e.g. Refs. [51, 52] for the details of this alternative approach.

The absence of coupling between the two spin states has an important consequence for the QSH phase. Since the QSH state may be viewed as a combination of two independent QH effects for spin up and spin down, it persists even in the absence of time-reversal symmetry [50, 151]. Additional symmetry-breaking terms, for instance due to bulk-inversion asymmetry and Rashba spin-orbit coupling, would cause an opening of a small gap between the edge states, which allows for some backscattering in the presence of impurities [50, 51].

In Fig. 3.1(a), we have displayed the LL spectrum for an undoped ($Y = 0$) quantum well with $d = 7.5$ nm. This system is in the inverted regime, so that the spectrum displays a (weak) QSH gap, [with $(\sigma_{\mathrm{H}}, \sigma_{\mathrm{H}}^{\mathrm{sp}}) = (0,2)$], for magnetic fields up to $B =$ 7.6 T, where the LLs cross, at $\phi_{\mathrm{cross}} = \mathscr{M}/[2\pi(\mathscr{B} - \tilde{g}_+^{\mathrm{eff}}/2)]$. In addition to the (weak) QSH gap, we observe several spin-filtered [e.g., $(\sigma_{\mathrm{H}}, \sigma_{\mathrm{H}}^{\mathrm{sp}}) = (\pm 1, 1)$], spin-imbalanced [e.g., $(\sigma_{\mathrm{H}}, \sigma_{\mathrm{H}}^{\mathrm{sp}}) = (3,1)$], and ordinary [e.g., $(\sigma_{\mathrm{H}}, \sigma_{\mathrm{H}}^{\mathrm{sp}}) = (2,0)$] QH gaps, and a trivial gap [$(\sigma_{\mathrm{H}}, \sigma_{\mathrm{H}}^{\mathrm{sp}}) = (0,0)$]. The (weak) QSH gap is the only gap which exhibits a helical edge state structure; all other nontrivial gaps are chiral. Within this formalism, no other inverted gaps form besides the one at $\phi = 0$, because the involved LLs do not cross anywhere else other than at $\phi = \phi_{\mathrm{cross}}$. In contrast, a tight-binding description of a honeycomb lattice in a perpendicular magnetic field does allow for other gaps with helical edge structures at higher flux and Fermi energy values (see Ch. 2 and Refs. [51, 52]).

The LL spectrum of Fig. 3.1(a) shows two mechanisms that lead to reentrant behaviour of the Hall conductivity and spin Hall conductivity. The first mechanism is

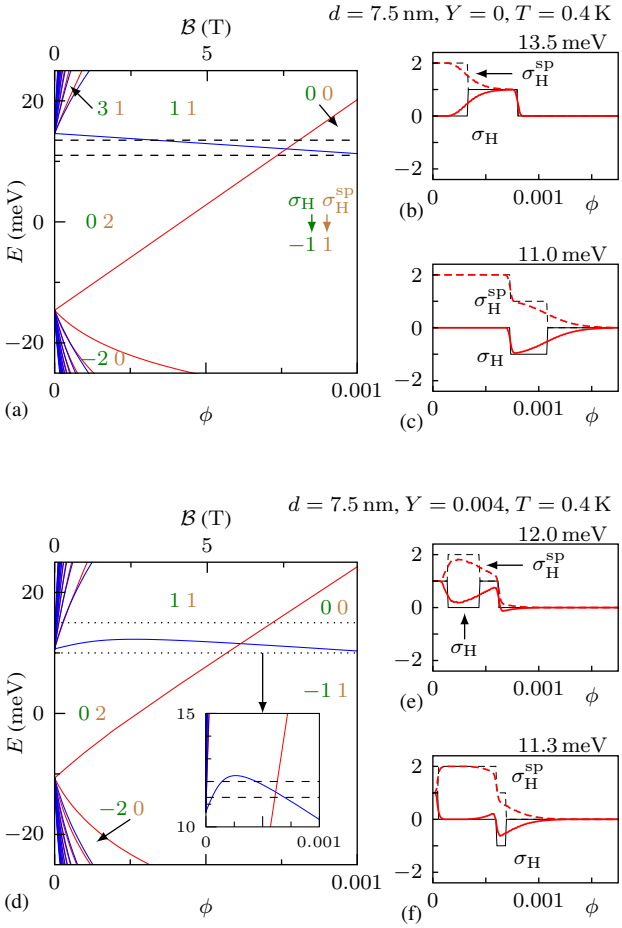

Figure 3.1: (a) LL spectrum for the quantum well with $d = 7.5$ nm without Mn doping. Red and blue curves indicate the + and − spin components, respectively. For clarity, only the LLs with $n \leq 10$ are shown. The numbers inside the gaps indicate the charge and spin Hall conductivity, σ_H and σ_H^{sp}. On the horizontal axes, the flux value ϕ and the equivalent magnetic field strength B are given. The dashed lines indicate Fermi energies where reentrant QH effect is observed. (b,c) Charge Hall (solid curves) and spin Hall (dashed curves) conductivity as a function of the flux (in terms of their respective flux quanta) for the indicated Fermi energies. The red (thick) curves indicate the effect of broadening due to disorder ($\Gamma_0 = 0.3$ meV) and temperature ($T = 0.4$ K), compared to the results without broadening (black, thin curves). (d,e,f) Equivalent plots for $d = 7.5$ nm and $Y = 0.004$. The inset in (d) is a magnification of the energy region near the LL crossing.

illustrated for a Fermi energy of 11.0 meV (lower dashed line), which lies just below the energy value at which the two lowest Landau levels (LLLs), i.e., the LLs with energies $E_{+,0}$ and $E_{-,0}$, cross. Holding the Fermi energy fixed and increasing the magnetic field, we successively traverse the weak QSH gap with $(\sigma_{\mathrm{H}}, \sigma_{\mathrm{H}}^{\mathrm{sp}}) = (0,2)$, the spin-filtered QH gap with $(\sigma_{\mathrm{H}}, \sigma_{\mathrm{H}}^{\mathrm{sp}}) = (-1,1)$, and the trivial gap, where $(\sigma_{\mathrm{H}}, \sigma_{\mathrm{H}}^{\mathrm{sp}}) = (0,0)$. Thus, the charge Hall conductivity is 0 for low and high magnetic fields, and -1 for intermediate values, which characterises a reentrance of a charge-insulating state [see Fig. 3.1(c)]. At a Fermi energy slightly above the crossing [e.g., $E = 13.5$ meV, see Fig. 3.1(b)], a similar sequence is observed, but with a different intermediate state ($\sigma_{\mathrm{H}} = +1$). In both cases, the spin Hall conductivity takes the values 2, 1, and 0, and therefore does not show reentrant behaviour. Clearly the reentrance of the Hall conductivity is caused by the structure of the spectrum around the crossing of the LLLs. To observe the reentrance of the charge Hall conductivity, it is essential that the derivatives $\mathrm{d}E/\mathrm{d}\phi$ of the two LLLs at the crossing differ in sign, which can happen only in the inverted regime. Thus, experimental observation of this type of reentrance provides proof that the HgTe quantum well can indeed be described as an inverted Dirac system [47]. One may verify that if the signs of the derivatives are equal, then the charge Hall conductivity does not reenter. Instead, we would observe reentrant spin Hall conductivity. We note that crossings of the latter type are ubiquitous for higher LLs ($n > 0$), but they are difficult to observe due to the vicinity of other LLs. However, later we will show that, under some circumstances, the crossings of the LLLs may also be of this type.

In Fig. 3.1(d), we show the effect of doping ($Y = 0.004$) on the LL spectrum. Two effects are visible. First, the size of the (weak) QSH gap has decreased, consistent with the increase of $\mathscr{M}$. Secondly, the energies $E_{\pm,0}$ of the two LLLs are no longer linear in the magnetic field. In fact, one of these LLLs shows a nonmonotonic dependence on the field. As can be observed in Fig. 3.1(d), this nonmonotonic LLL attains its maximum for a flux value less than ϕ_{cross}. Thus, if the Fermi energy is located between the energy of the crossing and that of the maximum [e.g., if $E = 12.0$ meV, see the inset of Fig. 3.1(d) and Fig. 3.1(e)], the spin-filtered QH gap reenters, and the intermediate state is the (weak) QSH gap. Thus, the system goes from a chiral, to a helical, and back to the (same) chiral phase again. This simultaneous reentrance of the charge and spin Hall conductivity should be contrasted with the reentrant behaviour around the LLL crossing, where only one of them reenters, but not both. We remark that such a sequence is possible only if the intermediate phase is the (weak) QSH phase, and consequently only if the LL involved is one of the LLLs, since the higher LLs are all monotonic. Therefore, this behaviour cannot be observed in the undoped system, where the LLL energies are linear.

As can be observed in the inset of Fig. 3.1(d), the maximum of this LLL has an energy close to that of the LL crossing. The sequence of charge and spin Hall conductivities is therefore affected by both mechanisms. We shall call this phenomenon *compound* reentrant behaviour. Above the energy of the crossing, the aforementioned

sequence (spin-filtered QH, weak QSH, spin-filtered QH) is followed by the trivial gap, so that we get an additional reentrance of the zero charge Hall conductivity. Just below the crossing energy [e.g., $E = 11.3$ meV; see Fig. 3.1(f)], the sequence of gaps is spin-filtered QH $(1,1)$, weak QSH $(0,2)$, spin-filtered QH $(-1,1)$, and trivial $(0,0)$. In this situation, the two spin-filtered QH phases are *different* gaps, unlike the sequence above the crossing. These examples show that the rich compound reentrant behaviour will appear if the crossing and the maximum of the LLLs are close to each other.

In order to be able to observe the reentrant effects in experiments, we study the qualitative structure of the LL spectrum as a function of the well width d, the doping fraction Y, and the temperature T. More specifically, for a fixed choice of parameters, we analyse whether one of the LLLs is nonmonotonic, and whether the LLLs cross. Furthermore, if the nonmonotonicity and crossing appear at the same time, we determine the relative positions of the maximum/minimum and of the crossing. For simplicity, we restrict ourselves to the structure of the two LLLs.

The bottom row of Fig. 3.2 displays five qualitatively different LLL spectra, which distinguish the regimes as given by Fig. 3.2(a)–(c). These regimes are characterised as follows. For regimes (i)–(iii), the band gap has inverted order (i.e., $\mathscr{M} < 0$), and therefore it shows the QSH phase at zero magnetic field. In regime (i), the LLLs are monotonic, so that the only mechanism that leads to reentrant effects is the crossing. In regimes (ii) and (iii) one LLL is nonmonotonic, so that we have compound reentrant behaviour. These two regimes are distinguished by the flux value of the maximum, which is smaller (ii) or greater (iii) than the flux value of the crossing. In case (iii), both LLLs are increasing at the crossing, so that we observe reentrant spin Hall conductivity, as argued before. In regimes (iv) and (v), the band gap is normally ordered (i.e., $\mathscr{M} > 0$), so that we find a trivial phase at zero magnetic field. In this situation, the LLLs do not cross, and the only mechanism that can lead to reentrant behaviour is the presence of a nonmonotonic LLL, as is the case (iv). For regime (v), both LLL are monotonic and do not cross, thus preventing any type of reentrant behaviour.

3.4 Discussion

Let us comment finally on the ability to resolve these reentrant effects, based on the range of the Fermi energies for which they are present. In order to estimate the observability, we compare this energy range to the broadening of the LLs, which will cause the change of conductivity across a LL to be smooth rather than step-like. Here, we consider a gaussian broadening with width Γ [49], which incorporates both LL broadening due to disorder and the smooth variation of the fermionic filling function at finite temperatures. The broadening due to disorder has a field-dependent width $\Gamma_{\mathrm{dis}} = \Gamma_0\sqrt{B/B_0}$, where $\Gamma_0 \sim 0.1$–2 meV and $B_0 \equiv 1$ T [49]. The thermal broadening is approximated by a gaussian with width $\Gamma_{\mathrm{th}} = \sqrt{2/3}\pi k_{\mathrm{B}} T$. In Figs. 3.1(b), (c), (e), and (f), we

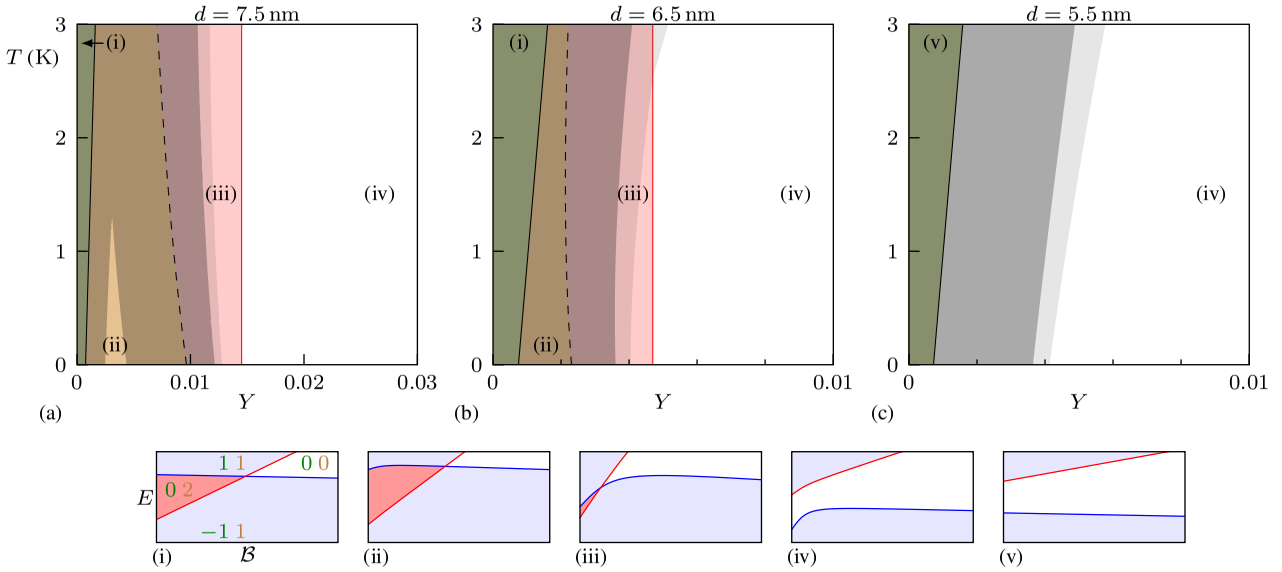

Figure 3.2: Diagram showing the possible types of reentrant behaviour, as a function of the Mn fraction Y and temperature T. In the top row, we show diagrams for (a) $d = 7.5$ nm, (b) $d = 6.5$ nm, and (c) $d = 5.5$ nm. The roman numbers correspond to different regimes in the qualitative structure of the spectrum constituted by the LLLs, displayed in the bottom row. The characteristics of the regimes (i)–(v) are explained in the text. In the top row, the different shades indicate the energy range in which the compound reentrant behaviour is present, compared to the LL broadening: Brighter colours indicate a larger range, making the effect easier to observe. The dashed line indicates the parameter values where the crossing and the maximum of the nonmonotonic LLL coincide, separating (ii) and (iii). The shading in the bottom row indicates the weak QSH (red/dark gray), spin-filtered QH (blue/light gray), and trivial (white) gaps.

illustrate the smooth transitions of the conductivities due to the combined effects of both types of broadening.

We consider the compound reentrant effects displayed in Fig. 3.2(ii) and (iii) to be well resolvable if the difference between the energies at the crossing and at the maximum exceeds twice the broadening width 2Γ. Indeed, in that case, the difference between the actual conductivity values and the quantised ones in the absence of broadening effects is $\lesssim 0.08$. However, the value of 2Γ is not a hard limit: Variations of the quantised Hall conductivity, even if they are far from the quantised values, may already be considered as a signature for a reentrant effect, for example as demonstrated in Fig. 3.1(e). In the diagrams of Fig. 3.2(a)–(c), the different shadings indicate this distance compared to Γ. In the brightest regions, the distance between the LLs is larger than 2Γ, sufficient for the reentrant effect to be observed. We find that for $\Gamma_0 = 0.3$ meV, situation (ii) is difficult to observe due to the small energy difference between the LLs, whereas the observation of (iii) is easier close to the critical doping, above which the system goes to the trivial regime (iv). For the observation of the compound reentrant effects, thicker wells are favourable because the energy range where the effects appear is larger. The simple reentrant effect due to nonmonotonicity, as in situation (iv), is generally present in a large energy regime and therefore its observation is less affected by the LL broadening.

Transport experiments with HgTe quantum wells have so far concentrated on the charge Hall conductivity of the system. For example, the reentrance of the charge Hall conductivity has been utilised to identify the possible regime of the QSH phase [118]. Observation of the simultaneous reentrant behaviour of the charge and spin Hall conductivity would also require the availability of a spin-sensitive detector, e.g., a contact consisting of a tunneling barrier and a ferromagnet [152]. However, this technique has the drawback that it only works at low fields, within the hysteresis range of the ferromagnet. Another detection mechanism could be a local magneto-optical Kerr effect (MOKE) experiment [153], although this measurement would be difficult due to the small band gap of the semiconductor. The inverse spin Hall effect may provide a way to measure the spin polarisation of the edge states [154, 155]. Nevertheless, the measurement of the charge Hall conductivity at multiple Fermi energies together with knowledge of the structure of the spectrum may provide indirect evidence for the existence of these reentrant effects.

In conclusion, we have demonstrated that the nonmonotonic behaviour of the LLs in the presence of Mn doping leads to reentrant topological phases, and that the vicinity of LL crossings leads to rich compound reentrant behaviour. Five different qualitative forms of the structure of the LLLs were shown to occur in the parameter space characterised by Mn doping, well thickness, and temperature. Furthermore, we have investigated the effects of LL broadening to estimate the ability to resolve the reentrant effects in experiments.

3.A The four-band effective model—Numerical methods

In this appendix,[7] we illustrate the used numerical method and relate it to the perturbation theory, which allows us to determine the parameters of a four-band effective model. In the Kane model, the band structure of the material consists of eight bands [148]. However, the two bands $|\Gamma^7, \pm 1/2\rangle$ are separated by approximately 1 eV from the other six bands and will be neglected here. The resulting six-band modified Kane Hamiltonian is written in the basis $|\Gamma^6, 1/2\rangle$, $|\Gamma^6, -1/2\rangle$, $|\Gamma^8, 3/2\rangle$, $|\Gamma^8, 1/2\rangle$, $|\Gamma^8, -1/2\rangle$ and $|\Gamma^8, -3/2\rangle$, which we denote as $|1\rangle$, $|2\rangle$, $|3\rangle$, $|4\rangle$, $|5\rangle$, and $|6\rangle$ for short in the following. The Hamiltonian can then be written as

$$H = H_0 + H_Z + H_{\text{ex}}, \tag{3.10}$$

where H_0 is the six-band Kane Hamiltonian [148, 156], H_Z is the linear Zeeman term, and H_{ex} is due to the exchange interaction between the Mn ions and the band states in a magnetic field B in the z direction. The Zeeman term reads

$$\begin{aligned} H_Z^{\text{c}} &= \frac{g_0}{2}\mu_{\text{B}} B \sigma_z, \\ H_Z^{\text{v}} &= \kappa' \mu_{\text{B}} B \hat{J}_z, \end{aligned} \tag{3.11}$$

for the (decoupled) conduction ($|1\rangle$ and $|2\rangle$) and valence ($|3\rangle$, $|4\rangle$, $|5\rangle$, and $|6\rangle$) band parts of the Hamiltonian. Here $\hat{J}_z$ is the angular momentum operator, g_0 is the bare Zeeman g-factor of HgTe, and κ' is a phenomenological parameter [49]. The exchange term, induced by the sp-d coupling between the Mn d level electrons and conduction or valence band electrons, has a form similar to the Zeeman term, and reads

$$\begin{aligned} H_{\text{ex}}^{\text{c}} &= -\Delta_s \sigma_z \\ H_{\text{ex}}^{\text{v}} &= -\frac{2}{3}\Delta_p \hat{J}_z \end{aligned} \tag{3.12}$$

where $\Delta_s = 0.2\ \text{eV} \times Y \langle \mathscr{S} \rangle$ and $\Delta_p = -0.3\ \text{eV} \times Y \langle \mathscr{S} \rangle$ are the coupling constants between the Mn spin $\mathscr{S}$ and the conduction band (Δ_s) or the valence band (Δ_p), respectively, and Y is the mole fraction of Mn^{2+} ions. The polarisation of the Mn spin $\mathscr{S}$ is assumed to be in the z direction. We regard the Mn spin as a classical spin and use the mean field value $\langle \mathscr{S} \rangle$ instead of $\mathscr{S}$, which yields

$$S \equiv \langle \mathscr{S} \rangle = -S_0 B_{5/2}\left(\frac{5 g_{\text{Mn}} \mu_{\text{B}} B}{2 k_{\text{B}} (T + T_0)}\right), \tag{3.13}$$

where $B_{5/2}$ is the Brillouin function as given by Eq. (3.5), $S_0 = 5/2$, $g_{\text{Mn}} = 2$, and $T_0 \approx 2.6$ K for Mn [149]. The argument of $B_{5/2}$ in this equation is equal to $\lambda_{\text{ex}} 2\pi\phi$; cf. Eqs. (3.4) and (3.6).

[7] This appendix is based on calculations performed by C. X. Liu and E. G. Novik, and is included here for completeness. Further details on this method may be found in Ref. [49].

Now, we consider the above model in a periodic superlattice grown in the z-direction with well width d and barrier width $L-d$. In the limit of large $L-d$, it becomes equivalent to a single quantum well. Due to the periodic boundary condition along the z-direction, according to Bloch's theorem, we can write the wave function as

$$\Psi_\xi = \frac{1}{2\pi} e^{i(\mathbf{k}_\parallel \cdot \mathbf{r}_\parallel + k_z z)} |U^\xi_{\mathbf{k}}(z)\rangle, \tag{3.14}$$

where $\mathbf{k} = (\mathbf{k}_\parallel, k_z) = (k_x, k_y, k_z)$ and $(\mathbf{r}_\parallel, z) = (x, y, z)$. The in-plane wave vector $\mathbf{k}_\parallel$ is a good quantum number for the system, and k_z is the superlattice wave number in the z direction, taken to be zero, because the quantum wells are effectively decoupled for large barrier thickness $L-d$. $U^\xi_{\mathbf{k}}(z)$ is a multi-component periodic wave function $U^\xi_{\mathbf{k}}(z+L) = U^\xi_{\mathbf{k}}(z)$ of the ξ-band, which is expanded in terms of a plane-wave basis as

$$|U^\xi_{\mathbf{k}}(z)\rangle = \sum_{n,\lambda} a^\xi_{n,\lambda} |n,\lambda\rangle = \sum_{n,\lambda} a^\xi_{n,\lambda} \frac{1}{\sqrt{2\pi}} e^{i(2\pi n/L)z} |\lambda\rangle, \tag{3.15}$$

where $|\lambda\rangle$ denotes the component $\lambda = 1,\ldots,6$ of the wave function, and the expansion coefficients $a^\xi_{n,\lambda}$ are functions of $\mathbf{k}_\parallel$. The eigenequation for these states is given by $\hat{H}\Psi_\xi = E_\xi \Psi_\xi$, where E_ξ depends on $\mathbf{k}_\parallel$. With the expansion (3.15), we find

$$\sum_{n',\lambda'} \langle n,\lambda|\hat{H}|n',\lambda'\rangle a^\xi_{n',\lambda'} = E_\xi a^\xi_{n,\lambda}. \tag{3.16}$$

A truncation method is applied and a finite number of basis vectors ($n = -N, -N+1, \ldots, N-1, N$) is used to solve this eigenvalue problem to obtain the coefficients $a^\xi_{n,\lambda}$. Given the fact that we are only interested in the low-energy physics, taking $N = 20$ yields a solution that is sufficiently accurate.

Next, we relate the perturbation theory to the previous numerical method. The Hamiltonian (3.10) is divided into

$$H = H_{\mathbf{k}_\parallel=0} + H^{(1)}_{\mathbf{k}_\parallel}, \tag{3.17}$$

where $H_{\mathbf{k}_\parallel=0}$ is treated as the zero-order Hamiltonian and $H^{(1)}_{\mathbf{k}_\parallel}$ as the perturbation. The wave function at the Γ point ($\mathbf{k}_\parallel = 0$) can be obtained from the numerical calculation, which is denoted as

$$|U^\xi_{\mathbf{k}=0}(z)\rangle = \sum_\lambda f_{\xi,\lambda}(z)|\lambda\rangle \tag{3.18}$$

with $f_{\xi,\lambda}(z) = \sum_n a^\xi_{n,\lambda}|n\rangle$. Only the subbands $|E_1+\rangle, |H_1+\rangle, |E_1-\rangle, |H_1-\rangle$, which are denoted as $|A\rangle, |B\rangle, |C\rangle, |D\rangle$ for short, are considered in this calculation. Using symmetry arguments, we obtain

$$\begin{aligned} |A\rangle &= f_{A,1}(z)|1\rangle + f_{A,4}(z)|4\rangle, & |B\rangle &= f_{B,3}(z)|3\rangle, \\ |C\rangle &= f_{C,2}(z)|2\rangle + f_{C,5}(z)|5\rangle, & |D\rangle &= f_{D,6}(z)|6\rangle, \end{aligned} \tag{3.19}$$

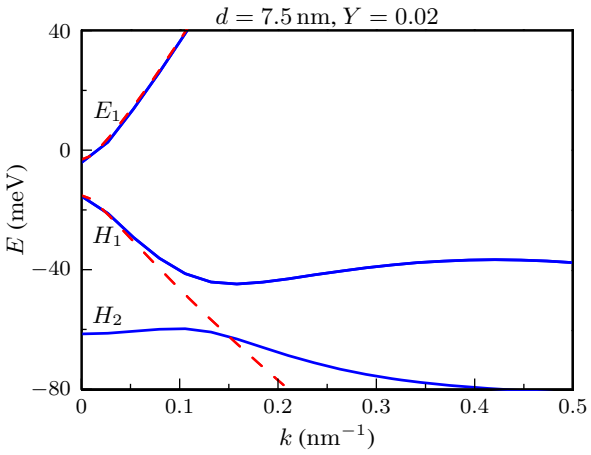

Figure 3.3: Comparison of the energy dispersion calculated from the full Hamiltonian (blue solid curves) and from the effective model (red dashed curves) for $d = 7.5$ nm and $Y = 0.02$. The two results exhibit a good overlap in the low-energy regime, which demonstrates the reliability of the effective model.

where $f_{A,1} = f_{C,2}, f_{A,4} = f_{C,5}, f_{B,3} = f_{D,6}$. Under two-dimensional spatial reflection, $f_{A,1}, f_{C,2}, f_{B,3}, f_{D,6}$ have even parity and $f_{A,4}, f_{C,5}$ have odd parity. Furthermore, in order to take into account the contribution of the other subbands in second-order perturbation theory, additional states $|E_2\pm\rangle$, $|LH\pm\rangle$, $|HH_2\pm\rangle$, and $|HH_3\pm\rangle$ (the second electron, light-hole, and second and third heavy-hole bands, respectively) are also solved numerically and can be written in a similar way [156].

With the obtained zero-order wave function, we apply the second-order perturbation formalism [156]

$$H_{m'm} = \langle m'|H|m\rangle + \sum_s \frac{1}{2}\langle m'|H^{(1)}_{\mathbf{k}_\parallel}|s\rangle\langle s|H^{(1)}_{\mathbf{k}_\parallel}|m\rangle\left(\frac{1}{E_{m'}-E_s}+\frac{1}{E_m-E_s}\right), \tag{3.20}$$

to obtain the effective model given by Eqs. (3.1)–(3.4). Here $|m\rangle, |m'\rangle$ are the states chosen from $|A\rangle$, $|B\rangle$, $|C\rangle$, and $|D\rangle$ while $|s\rangle$ is one of the intermediate states $|E_2\pm\rangle$, $|LH\pm\rangle$, $|HH_2\pm\rangle$, and $|HH_3\pm\rangle$. With this approach, we relate the parameters of the effective model (3.1)–(3.4) to the parameters of the six-band modified Kane model (3.10)–(3.12). We find that for the effective mass parameters $\mathscr{D}$ and $\mathscr{B}$ and for the effective g factor g_E, we need to take into account the second-order perturbation, while for the other parameters the first-order term is accurate enough for our purposes. As the derivation is straightforward and the expressions for the parameters are quite lengthy, we do not write them explicitly here. As an example, the exchange parameters χ_E and χ_H are

d (nm)	Y	$\mathscr{C}$ (meV)	$\mathscr{M}$ (meV)	$\mathscr{A}$ (eV)	$\mathscr{B}$ (eV)	$\mathscr{D}$ (eV)	g_{E}	g_{H}	F_1	F_4
5.5	0.00	−16.9	8.8	0.60	−1.15	−0.73	15.8	1.22	0.62	0.37
5.5	0.01	−5.8	20.0	0.62	−1.05	−0.63	14.4	1.29	0.64	0.35
5.5	0.02	5.6	31.5	0.64	−0.96	−0.55	13.2	1.36	0.66	0.33
5.5	0.03	17.4	43.3	0.66	−0.89	−0.48	12.2	1.42	0.68	0.31
6.5	0.00	−24.4	−4.9	0.58	−1.45	−1.04	20.0	1.22	0.58	0.41
6.5	0.01	−13.9	5.7	0.60	−1.30	−0.88	18.0	1.28	0.61	0.38
6.5	0.02	−3.0	16.6	0.62	−1.17	−0.75	16.3	1.35	0.63	0.36
6.5	0.03	8.4	28.0	0.65	−1.06	−0.65	14.9	1.42	0.66	0.34
7.5	0.00	−29.9	−14.6	0.55	−1.87	−1.45	24.3	1.21	0.55	0.44
7.5	0.01	−19.9	−4.6	0.58	−1.62	−1.20	21.8	1.28	0.58	0.41
7.5	0.02	−9.5	5.8	0.61	−1.42	−1.00	19.5	1.34	0.61	0.39
7.5	0.03	1.4	16.8	0.63	−1.26	−0.85	17.6	1.41	0.64	0.36

Table 3.1: Parameters for the four-band effective model [Eqs. (3.1)–(3.4)], obtained by perturbation theory from the full Kane model.

given by

$$\begin{aligned} \chi_{\mathrm{E}} B_{5/2}(\lambda_{\mathrm{ex}} 2\pi\phi) &= -(F_1\Delta_s + F_4\Delta_p/3), \\ \chi_{\mathrm{H}} B_{5/2}(\lambda_{\mathrm{ex}} 2\pi\phi) &= -\Delta_p, \end{aligned} \tag{3.21}$$

where $F_1 = \langle f_{A,1}|f_{A,1}\rangle$ and $F_4 = \langle f_{A,4}|f_{A,4}\rangle$, and $\lambda_{\mathrm{ex}} 2\pi\phi$ is the argument of $B_{5/2}$ in Eqs. (3.4) and (3.13). In Table 3.1, we show the numerical values of these parameters for several different well thicknesses and different Mn doping. In Fig. 3.3, the energy dispersion calculated from the effective model using the parameters in Table 3.1 is shown to fit well with that calculated from the full Kane model at small k. This result justifies the use of the effective model to discuss the low-energy physics, in particular in the energy range where the reentrant behaviour occurs. In this chapter, we have restricted ourselves to wells with a thickness $d < 8.1$ nm, because above this value, the H_2 band lies between the E_1 and H_1 bands, and in that case the four-band model is no longer accurate, especially in the energy regime of the valence band. Nevertheless, the mechanisms for the appearance of the reentrant effects may still be present for thicker wells.

Chapter 4

Chern-Simons theory of multicomponent quantum Hall systems

The Chern-Simons approach has been widely used to explain fractional quantum Hall states in the framework of trial wave functions. In this chapter, we generalise the concept of Chern-Simons transformations to systems with any number of components (spin or pseudospin degrees of freedom), extending earlier results for systems with one or two components. The motivation is to understand fractional quantum Hall effect in multicomponent systems such as graphene. We treat the density fluctuations by adding auxiliary gauge fields and appropriate constraints. The Hamiltonian is quadratic in these fields and hence can be treated as a harmonic oscillator Hamiltonian, with a ground state that is connected to the Halperin wave functions through the plasma analogy. We investigate conditions on the coefficients of the Chern-Simons transformation and on the filling factors under which our model is valid. Furthermore, we discuss several singular cases, associated with states with ferromagnetic properties. In addition, we include the momentum degrees of freedom to arrive at the full Hamiltonian theory. The resulting set of excitation energies satisfies Kohn's theorem, i.e., it includes the cyclotron energy. Subsequently, the microscopic operators for the densities and constraints are derived. We derive the total Hall conductivity of the system from the density operator associated to the mode at the cyclotron energy. We prove that the results generalise those of the single-component theory, and that they agree with experimental results. [8]

[8] This chapter is partially based on *Chern-Simons theory of multicomponent quantum Hall systems*, W. Beugeling, M. O. Goerbig, and C. Morais Smith, Phys. Rev. B **81**, 195303 (2010) [157].

4.1 Introduction

In understanding the fractional quantum Hall effect (FQHE), the now famous trial wave function proposed by Laughlin [9] proved to be a successful approach to describe the physics of incompressible quantum liquids at certain fractional filling factors. Laughlin's wave function is furthermore the inevitable starting point for several generalisations, such as Jain's composite-fermion proposal [10, 11], Halperin's two-component wave function [39], or more complicated wave functions describing states possessing quasi-particle excitations with non-Abelian statistics [18, 19].

A field-theoretical approach, complementary to the above-mentioned one, consists of so-called Chern-Simons theories, which formalise the idea of flux attachment that is also implicit in the trial wave functions. Chern-Simons theories have been successfully elaborated to study incompressible [16] and compressible [158] quantum liquids in one-component systems as well as two-component systems [21, 40, 41, 159–161], which comprise e.g. bilayer quantum Hall systems or single layer systems in situations where the spins are not completely polarised. Multicomponent Chern-Simons approaches have also been proposed in the study of edge excitations of the incompressible quantum Hall liquids [162]. An undeniable advantage of these Chern-Simons theories consists of their transparent insight into the exotic properties of these quantum liquids, such as their topological degeneracy, the fractional charges of their quasi-particle excitations or the statistical properties of the latter [21, 159, 160]. However, the Chern-Simons theories are usually less adapted when it comes to calculating quantities involving energy scales. Indeed, Chern-Simons transformations act on the kinetic part of the electronic Hamiltonian, whereas they leave the interaction part invariant. The kinetic part gets therefore renormalised but continues to determine the overall energy scale whereas the physical energy scale in the FQHE must be set by the electron-electron interactions.

A successful generalisation of Chern-Simons theories, that does not suffer from the problem of the correct energy scale, is the Hamiltonian theory proposed by Shankar and Murthy [23–26, 28]. This theory is a very powerful tool for the computation of physical quantities, [26, 28] and even for the description of higher-generation composite fermion states [30, 31, 163]. However, it is limited by the fact that it does not incorporate internal degrees of freedom. The success of the single-component Hamiltonian theory justifies a generalisation that can be applied to describe systems for which internal degrees of freedom (spin and/or pseudospin) are relevant. The main interest in such a generalisation stems from realistic systems with more than two internal degrees of freedom, such as graphene with its four-fold spin-valley degeneracy [99] or bilayer quantum Hall systems with non-polarised electron spins.

In this chapter, we analyse a multicomponent Chern-Simons theory within the framework of the microscopic theory by Shankar and Murthy [23–26, 28]. This approach has two main advantages over the previously proposed ones. First, it allows one

to distinguish between physically relevant Chern-Simons theories from those which are ill-defined. The basic ingredient for this distinction is the $\kappa \times \kappa$ charge matrix K, which was first introduced by Wen and Zee [21, 159, 160]. We find that matrices with negative eigenvalues need to be discarded in the study of physically relevant Chern-Simons theories because they would lead to ground-state wave functions that cannot be normalised. This structural feature of Chern-Simons theories finds its physical interpretation within Laughlin's plasma analogy [9] that indicates a tendency of the different components to undergo a phase separation and thus to form spatially inhomogeneous states. We show that zero eigenvalues of the charge matrix K, in contrast to the unphysical negative eigenvalues, find a compelling interpretation in terms of ferromagnetic quantum Hall states. Our results thus generalise previous work on two-component systems by Lopez and Fradkin [40] to an arbitrary number of components κ.

A second advantage of the present approach consists of a transparent connection between multicomponent Chern-Simons theories with trial wave functions. It has been shown, in the simpler one-component case, that treating the fluctuations of the Chern-Simons vector potential within the harmonic approximation (Gaussian model) yields Laughlin's and Jain's (unprojected) composite-fermion wave functions [28, 164]. Similarly, we obtain here, within the Gaussian model of κ-component fluctuating Chern-Simons vector potentials, multicomponent trial wave functions [165] that are generalisations of Halperin's two-component wave functions [39, 40]. Furthermore, we obtain in the same manner composite-fermion-type wave functions that may be viewed as particular multicomponent generalisations of Jain's original proposal [10, 11].

An additional motivation for this model is its role as an interacting theory for composite fermions. In order to interpret the model in this manner, one must include also the momentum degrees of freedom beyond the oscillator Hamiltonian. Within the random-phase approximation [24] at small momenta, the oscillator and momentum degrees of freedom can be decoupled. The excitation energies resulting from the decoupling procedure include the cyclotron energy, in agreement with Kohn's theorem [24]. From the microscopic density and constraint operators, one can indicate the expressions valid at all momenta [25], such that they satisfy the magnetic translation algebra. In this framework, the theory is understood in the same way as an integer or fractional QH state of composite fermions. In particular, at a fractional composite-fermion filling factor, this theory allows for an additional flux attachment leading to *second-generation* composite fermions. Such a model has been proposed to explain the FQHE at filling factor $\frac{4}{11}$, which cannot be obtained by a single flux attachment [30, 31, 163].

Another motivation to study the decoupling transformation is that the transformed density operator can be rewritten conveniently in terms of the currents. This observation provides the ability to compute the Hall currents. For single-component systems,

this computation leads to the well known Hall conductivity relation $\sigma_{\mathrm{H}} = \nu e^2/h$ in terms of the (fractional) filling factor ν [23, 24]. In the generalised theory for multicomponent systems, one obtains an identical relation for the total filling factor, but there are additional Hall conductivity values associated to other modes (e.g., the difference of the two layer filling factors in two-layer systems [40]).

This chapter is organised as follows. In Sec. 4.2, we define the Chern-Simons transformations for systems with κ components and introduce, in Sec. 4.3, extra degrees of freedom, in the form of the auxiliary gauge fields, as described by Shankar and Murthy. We subsequently diagonalise the harmonic oscillator Hamiltonian and investigate the connection of the resulting wave function with trial wave functions through the plasma analogy. In Sec. 4.4, we extend our results to the situation of singular K matrices and discuss the relation between residual symmetries and underlying ferromagnetic properties of the quantum Hall states. In Sec. 4.5, we include the momentum degrees of freedom, and we generalise the decoupling procedure used by Murthy and Shankar. We apply the results of this section to several examples. In Sec. 4.6, we discuss the transformation of the densities and the constraints, and we derive the Hall conductivities from those. Our conclusions are presented in Sec. 4.7. In the Appendices we provide extra details of our calculations and an overview of the notation.

4.2 Chern-Simons transformations

We consider a quantum Hall system with κ internal states, hereafter referred to as "components". In the simplest case of a two-dimensional electron gas at a GaAs/AlGaAs interface, one has $\kappa = 2$ for the two possible orientations of the electron spin. The case $\kappa = 4$ is relevant for bilayer quantum Hall systems, where a second pseudospin mimics the layer index, or in graphene due to its two-fold valley degeneracy, in addition to the physical spin of the electrons. Higher values of κ are rarely discussed in the literature, but may play a role in the context of multilayer systems or of bilayer graphene, where the zero-energy level consists of the $n = 0$ and $n = 1$ Landau levels [99]. The Chern-Simons transformation [10, 166] is defined by the relation between the κ original electronic fields $\psi_\alpha(\mathbf{r})$ and the κ transformed fields $\psi_\alpha^{\mathrm{CS}}(\mathbf{r})$ as

$$\psi_\alpha(\mathbf{r}) = \exp\left(-i\int \mathrm{d}^2\mathbf{r}'\theta(\mathbf{r}-\mathbf{r}')\sum_{\beta=1}^{\kappa} K_{\alpha\beta}\rho_\beta(\mathbf{r}')\right)\psi_\alpha^{\mathrm{CS}}(\mathbf{r}), \tag{4.1}$$

where $\theta(\mathbf{r}) = \arg(x+iy)$ indicates the angle between the vector $\mathbf{r} = (x, y)$ and the $\mathbf{e}_x$ direction, and $\rho_\beta(\mathbf{r}) = \psi_\beta^\dagger(\mathbf{r})\psi_\beta(\mathbf{r}) = \psi_\beta^{\mathrm{CS}\dagger}(\mathbf{r})\psi_\beta^{\mathrm{CS}}(\mathbf{r})$ is the density operator of the particles of component β. The $\kappa \times \kappa$ matrix $K_{\alpha\beta}$ encodes the topological properties of the underlying quantum liquids, such as its degeneracy, the charges of its quasi-particle excitations and the statistics of the latter [21, 159, 160]. Physically, it indicates the number of flux quanta attached to particles of component α due to the density of particles

of component β. This transformation is a *singular* transformation for the reason that $\theta(\mathbf{r}-\mathbf{r}')$ has a singularity at $\mathbf{r}'=\mathbf{r}$.

The gauge transformation is defined such that it generates the gauge potentials[9]

$$\mathbf{A}_\alpha^{\mathrm{CS}}(\mathbf{r}) = -\frac{\hbar}{e}\nabla_{\mathbf{r}}\int \mathrm{d}^2\mathbf{r}'\theta(\mathbf{r}-\mathbf{r}')\sum_\beta K_{\alpha\beta}\rho_\beta(\mathbf{r}'), \tag{4.2}$$

and such that the one-particle Hamiltonian $[-i\hbar\nabla + e\mathbf{A}(\mathbf{r})]^2/2m$ for the component α is transformed to

$$H_\alpha = \frac{1}{2m}\left[-i\hbar\nabla + e\mathbf{A}(\mathbf{r}) + e\mathbf{A}_\alpha^{\mathrm{CS}}(\mathbf{r})\right]^2.$$

Here, m is the mass of the particles, and e is the electron charge. By using $\nabla\times\nabla\theta(\mathbf{r}) = 2\pi\delta(\mathbf{r})$, we derive the corresponding magnetic fields,

$$\mathbf{B}_\alpha^{\mathrm{CS}}(\mathbf{r}) = -\frac{h}{e}\sum_\beta K_{\alpha\beta}\rho_\beta(\mathbf{r})\mathbf{e}_z.$$

Since $\mathbf{A}_\alpha^{\mathrm{CS}}$ is a gauge field, its Fourier transform $\mathbf{A}_\alpha^{\mathrm{CS}}(\mathbf{q})$ may be fixed to a convenient gauge. We choose it to be transverse, $i\mathbf{q}\cdot\mathbf{A}_\alpha^{\mathrm{CS}}(\mathbf{q}) = 0$, so that it fixes the direction of $\mathbf{A}_\alpha^{\mathrm{CS}}(\mathbf{q})$ to be $\mathbf{e}_z\times\mathbf{q}/|\mathbf{q}|$, up to a sign. For the magnitude, we use that under a Fourier transform $\mathbf{B}(\mathbf{r}) = \nabla\times\mathbf{A}(\mathbf{r})$ transforms to $\mathbf{B}(\mathbf{q}) = i\mathbf{q}\times\mathbf{A}(\mathbf{q})$, such that we obtain

$$\mathbf{A}_\alpha^{\mathrm{CS}}(\mathbf{q}) = A_\alpha^{\mathrm{CS}}(\mathbf{q})\mathbf{e}_{\mathbf{q}}^\perp = -\frac{h}{e|\mathbf{q}|}\sum_\beta K_{\alpha\beta}\rho_\beta(\mathbf{q})\mathbf{e}_{\mathbf{q}}^\perp, \tag{4.3}$$

where we define the transverse unit vector as $\mathbf{e}_{\mathbf{q}}^\perp = i\mathbf{e}_z\times\mathbf{q}/|\mathbf{q}|$.

The effective magnetic field seen by the composite particles of type α is

$$\mathbf{B}_\alpha^* = \mathbf{B} + \langle\mathbf{B}_\alpha^{\mathrm{CS}}\rangle = B\left(1-\sum_\beta K_{\alpha\beta}\nu_\beta\right)\mathbf{e}_z, \tag{4.4}$$

where ν_β are the component filling factors, given by $\nu_\beta = \frac{h}{eB}n_\beta = 2\pi l_B^2 n_\beta$ in terms of the electronic densities n_β and of the magnetic length $l_B = \sqrt{\hbar/eB}$. This result is an extension of the two-component case presented in Refs. [41, 161]. Notice that each particle type has its own effective magnetic field, and hence also its own magnetic length $l_{B_\alpha^*} = \sqrt{\hbar/eB_\alpha^*}$. The composite particle filling factors ν_α^* are expressed in terms of the electronic filling factors ν_α as [41]

$$\frac{\nu_\alpha^*}{\nu_\alpha} = \frac{l_{B_\alpha^*}^2}{l_B^2} = \frac{B}{B_\alpha^*} = \frac{1}{1-\sum_\beta K_{\alpha\beta}\nu_\beta}. \tag{4.5}$$

[9] Throughout this chapter, all sums over the component indices $(\alpha,\beta,\ldots)$ are over the values $1,\ldots,\kappa$, unless indicated otherwise.

This result generalises the one-component relation

$$\nu^* = \frac{\nu}{1-2s\nu} \qquad \leftrightarrow \qquad \nu = \frac{\nu^*}{2s\nu^*+1}, \tag{4.6}$$

in terms of the Chern-Simons charge $K = 2s$.

The statistical angle associated with the exchange of the transformed fields $\psi_\alpha^{\rm CS}$ and $\psi_\alpha^{\rm CS\dagger}$ can be derived by using their definition, Eq. (4.1), and the fact that the original fields are fermionic. Under the condition that the charge matrix $K_{\alpha\beta}$ is symmetric, which is a generalisation of the condition discussed in the two-component case [41], we obtain

$$\psi_\alpha^{\rm CS}(\mathbf{r}_1)\psi_\beta^{\rm CS}(\mathbf{r}_2) + e^{i\pi K_{\alpha\beta}}\psi_\beta^{\rm CS}(\mathbf{r}_2)\psi_\alpha^{\rm CS}(\mathbf{r}_1) = 0$$

and

$$\psi_\alpha^{\rm CS}(\mathbf{r}_1)\psi_\beta^{\rm CS\dagger}(\mathbf{r}_2) + e^{i\pi K_{\alpha\beta}}\psi_\beta^{\rm CS\dagger}(\mathbf{r}_2)\psi_\alpha^{\rm CS}(\mathbf{r}_1) = \delta_{\alpha\beta}\delta(\mathbf{r}_1-\mathbf{r}_2).$$

Thus, we have found that the statistical angles of the exchange are $\pi K_{\alpha\beta}$, i.e., proportional to the entries of the charge matrix. The parity of the diagonal elements $K_{\alpha\alpha}$ of the charge matrix K determines the statistical properties of the Chern-Simons fields $\psi_\alpha^{\rm CS}$. If they are even integers, the originally fermionic electron fields ψ_α are transformed into fermionic Chern-Simons fields. However, one may also change the statistical properties of the fields from fermions to bosons by using odd integers for the diagonal components $K_{\alpha\alpha}$. In the following sections, we mainly discuss fermionic Chern-Simons fields, in order to make a connection with the composite-fermion theory, although the main conclusions of the chapter also apply to bosonic fields.

4.3 Gaussian theory

4.3.1 Auxiliary gauge fields

The formalism proposed by Shankar and Murthy [24, 28] allows us to treat the fluctuations of the Chern-Simons vector potential via the introduction of κ real-valued transverse gauge fields $\mathbf{a}_\alpha^\circ(\mathbf{r}_{j_\alpha})$ [167]. The extended Chern-Simons Hamiltonian in first quantisation, with N_α particles of each type α, reads

$$H_{CS} = \frac{1}{2m}\sum_\alpha \sum_{j_\alpha=1}^{N_\alpha}\left[\mathbf{p}_{j_\alpha} + e\mathbf{A}_\alpha^*(\mathbf{r}_{j_\alpha}) + e\,\delta\mathbf{A}_\alpha^{\rm CS}(\mathbf{r}_{j_\alpha}) + e\,\mathbf{a}_\alpha^\circ(\mathbf{r}_{j_\alpha})\right]^2, \tag{4.7}$$

where we absorb the average value of the Chern-Simons potential (4.2) into an effective vector potential $\mathbf{A}_\alpha^*(\mathbf{r}) = \mathbf{A}(\mathbf{r}) + \langle\mathbf{A}_\alpha^{\rm CS}\rangle$. This definition yields the effective magnetic field $\nabla\times\mathbf{A}_\alpha^*(\mathbf{r}_{j_\alpha}) = \mathbf{B}_\alpha^*(\mathbf{r}_{j_\alpha})$ given in Eq. (4.4). In Fourier space, the fluctuations $\delta\mathbf{A}_\alpha^{\rm CS}(\mathbf{q})$ are transverse, similar to the gauge field itself, as given by Eq. (4.3). Here, we have

$$\delta\mathbf{A}_\alpha^{\rm CS}(\mathbf{q}) = \delta A_\alpha^{\rm CS}(\mathbf{q})\mathbf{e}_\mathbf{q}^\perp = \frac{h}{e|\mathbf{q}|}\sum_\beta K_{\alpha\beta}\,\delta\rho_\beta(\mathbf{q})\mathbf{e}_\mathbf{q}^\perp.$$

Since we have artificially added the auxiliary gauge field $\mathbf{a}^\circ_\alpha(\mathbf{r})$, we have enlarged the Hilbert space, where the physical states form only a subspace $\{|\phi_{\rm phys}\rangle\}$ characterised by

$$a^\circ_\alpha(\mathbf{q})\,|\phi_{\rm phys}\rangle = 0, \tag{4.8}$$

for all components α. In other words, the gauge field operator acting on any physical state vanishes.

Additionally, we introduce a longitudinal field $\mathbf{P}^\circ(\mathbf{q}) = iP^\circ(\mathbf{q})\mathbf{e}^{\parallel}_{\mathbf{q}}$ (with $\mathbf{e}^{\parallel}_{\mathbf{q}} \equiv \mathbf{q}/|\mathbf{q}|$), conjugate and perpendicular to the newly introduced gauge field $\mathbf{a}^\circ(\mathbf{q}) = a^\circ(\mathbf{q})\mathbf{e}^{\perp}_{\mathbf{q}}$, according to the commutation relation in Fourier space

$$[a^\circ_\alpha(\mathbf{q}), P^\circ_\beta(-\mathbf{q}')] = i\hbar\delta_{\alpha\beta}\delta_{\mathbf{q},\mathbf{q}'}.$$

Since the operator P°_α is conjugate to a°_α, it generates translations in a°_α, as may be seen from the definition

$$U = \exp\left(\frac{i}{\hbar}\sum_\alpha\sum_{\mathbf{q}'} P^\circ_\alpha(-\mathbf{q}')\delta A^{\rm CS}_\alpha(\mathbf{q}')\right),$$

which translates a°_β by the vector $-\delta A^{\rm CS}_\beta(\mathbf{q})$ as $U^\dagger a^\circ_\beta(\mathbf{q})U = a^\circ_\beta(\mathbf{q}) - \delta A^{\rm CS}_\beta(\mathbf{q})$. By using this shifting property of U, which is also valid in $\mathbf{r}$ space, and with $[\mathbf{p}_{j_\alpha}, U] = (h/eL^2)\sum_\beta K_{\alpha\beta}\mathbf{P}^\circ_\beta(\mathbf{r}_{j_\alpha})$, we may eliminate $\delta\mathbf{A}^{\rm CS}_\beta(\mathbf{q})$ from Hamiltonian (4.7), which then transforms into

$$H_{\rm CP} = U^\dagger H_{\rm CS} U = \frac{1}{2m}\sum_\alpha\sum_{j_\alpha=1}^{N_\alpha}\left[\mathbf{p}_{j_\alpha} + e\mathbf{A}^*_\alpha(\mathbf{r}_{j_\alpha}) + e\,\mathbf{a}^\circ_\alpha(\mathbf{r}_{j_\alpha}) + \frac{h}{eL^2}\sum_\beta K_{\alpha\beta}\mathbf{P}^\circ_\beta(\mathbf{r}_{j_\alpha})\right]^2,$$

while transforming the states to $\psi^{\rm CP} = U^{-1}\psi^{\rm CS}$. In these equations, L^2 is the area of the system. By transforming the states, we also transform the constraint (4.8) to

$$\left(a^\circ_\alpha(\mathbf{q}) - \delta A^{\rm CS}_\alpha(\mathbf{q})\right)|\phi_{\rm phys}\rangle = \left(a^\circ_\alpha(\mathbf{q}) - \frac{2\pi\hbar}{e|\mathbf{q}|}\sum_\beta K_{\alpha\beta}\delta\rho_\beta(\mathbf{q})\right)|\phi_{\rm phys}\rangle = 0. \tag{4.9}$$

The Hamiltonian may be decomposed into three terms, $H_{\rm CP} = H^* + H_{\rm coupl} + H_{\rm aux}$, given by

$$H^* = \frac{1}{2m}\sum_\alpha\sum_{j_\alpha=1}^{N_\alpha}\Pi^2_{j_\alpha}, \tag{4.10}$$

$$H_{\rm coupl} = \frac{1}{m}\sum_\alpha\sum_{j_\alpha=1}^{N_\alpha}\Pi_{j_\alpha}\cdot\left[e\mathbf{a}^\circ_\alpha(\mathbf{r}_{j_\alpha}) + b\sum_\beta K_{\alpha\beta}\mathbf{P}^\circ_\beta(\mathbf{r}_{j_\alpha})\right], \tag{4.11}$$

$$H_{\rm aux} = \frac{1}{2m}\sum_\alpha\sum_{j_\alpha=1}^{N_\alpha}\left[e^2 a^{\circ\,2}_\alpha(\mathbf{r}_{j_\alpha}) + b^2\sum_\beta\sum_\gamma P^\circ_\beta(\mathbf{r}_{j_\alpha})K_{\beta\alpha}K_{\alpha\gamma}P^\circ_\gamma(\mathbf{r}_{j_\alpha})\right], \tag{4.12}$$

where $\Pi_{j_\alpha} \equiv \mathbf{p}_{j_\alpha} + e\mathbf{A}^*_\alpha(\mathbf{r}_{j_\alpha})$ and $b = h/eL^2$, which has the dimensions of a magnetic field. Notice that for $H_{\rm aux}$ we have used that $\mathbf{a}^\circ_\alpha(\mathbf{q})$ and $\mathbf{P}^\circ_\beta(\mathbf{q})$ are perpendicular.

In Secs. 4.3.2–4.4, we discuss $H_{\rm aux}$ that involves the auxiliary gauge fields. The full Hamiltonian $H_{\rm CP}$, including also the other terms, is discussed in Secs. 4.5–4.6.

4.3.2 Gaussian model of the auxiliary gauge fields

In this section we will analyse H_{aux} in detail. By observing that $\sum_{j_\alpha}\delta(\mathbf{r}-\mathbf{r}_{j_\alpha})=\rho_\alpha(\mathbf{r})=n_\alpha+\delta\rho_\alpha(\mathbf{r})$, we can rewrite Eq. (4.12) as

$$H_{\text{aux}}=\frac{1}{2m}\sum_\alpha\int \mathrm{d}^2\mathbf{r}\,\rho_\alpha(\mathbf{r})\left(e^2 {a_\alpha^\circ}^2(\mathbf{r})+b^2\sum_\beta\sum_\gamma P_\beta^\circ(\mathbf{r})K_{\beta\alpha}K_{\alpha\gamma}P_\gamma^\circ(\mathbf{r})\right).$$

Up to this point, all equations are exact. Now, we approximate H_{aux} by assuming that the density fluctuations $\delta\rho_\alpha$ are small with respect to the average densities n_α. Since the resulting Hamiltonian becomes quadratic, this approximation is called the *harmonic approximation*. We should keep in mind that this approximation breaks down if the fluctuations are not small with respect to the average densities. In particular, the approximation is certainly invalid if one of the average densities is zero. We therefore assume that none of the average densities n_α vanishes. However, in the case of a singular charge matrix K, a redefinition of the filling factors might lift this problem, as will be discussed in more detail in Sec. 4.4. The Hamiltonian H_{aux} in Fourier space is approximated by

$$H_{\text{osc}}=\sum_{\mathbf{q}}\sum_\alpha\frac{n_\alpha L^2}{2m}\left(e^2 a_\alpha^\circ(-\mathbf{q})a_\alpha^\circ(\mathbf{q})+b^2\sum_\beta\sum_\gamma P_\beta^\circ(-\mathbf{q})K_{\beta\alpha}K_{\alpha\gamma}P_\gamma^\circ(\mathbf{q})\right), \tag{4.13}$$

where we note that $a^\circ(-\mathbf{q})=(a^\circ(\mathbf{q}))^\dagger$ and $P^\circ(-\mathbf{q})=[P^\circ(\mathbf{q})]^\dagger$. Because the Hamiltonian (4.13) is quadratic in the gauge fields a_α° and its conjugate fields P_α°, it is possible to write it in terms of ladder operators. However, due to the appearance of the matrices K in the term with P°'s, it is a nontrivial task to define suitable ladder operators $\mathscr{A}_\alpha(\mathbf{q})$ such that the commutators between them are of the form $[\mathscr{A}_\alpha(\mathbf{q}),\mathscr{A}_\beta^\dagger(\mathbf{q}')]=\delta_{\alpha\beta}\delta_{\mathbf{q},\mathbf{q}'}$.

In order to diagonalise the Hamiltonian, we define $N=\mathrm{diag}(\{\nu_\alpha\})$ as the dimensionless diagonal matrix of filling factors, $N_{\alpha\beta}=\nu_\alpha\delta_{\alpha\beta}$, and also write the fields and their conjugates as vectors in the component space, $a^\circ=(a_1^\circ,\ldots,a_\kappa^\circ)$ and $P^\circ=(P_1^\circ,\ldots,P_\kappa^\circ)$. We omit the $\mathbf{q}$ dependence for a while. In this concise notation, the oscillator Hamiltonian can be written as

$$H_{\text{osc}}=\frac{L^2}{2m}\frac{eB}{h}\left[e^2 a^{\circ\dagger}N a^\circ+b^2 P^{\circ\dagger}K^\dagger NK P^\circ\right]. \tag{4.14}$$

The prefactor can also be written as $L^2\omega_{\text{c}}/2h$, where $\omega_{\text{c}}=eB/m$ is the cyclotron frequency. We recall that the matrix K is real and symmetric, so that $K^\dagger=K$. We perform the diagonalisation in two steps. First, we define $a'=\sqrt{N}a^\circ$ and $P'=\sqrt{N^{-1}}P^\circ$, so that the Hamiltonian becomes

$$H_{\text{osc}}=\frac{L^2\omega_{\text{c}}}{2h}\left[e^2 a'^\dagger a'+b^2 P'^\dagger\sqrt{N}KNK\sqrt{N}P'\right].$$

The matrix between the P''s is the square of the matrix $E\equiv\sqrt{N}K\sqrt{N}$, which is real and symmetric. Therefore, it can be diagonalised in terms of a diagonal matrix D and an

orthogonal matrix C, such that $E = C^{-1}DC$. The matrix D has the eigenvalues λ_α of E on its diagonal, and C^{T} contains the corresponding eigenvectors as columns. The ability to choose C as an orthogonal matrix (i.e., $C^{-1} = C^{\mathrm{T}}$) is provided by the property that the matrix E is symmetric, so that the eigenvectors can be chosen such that they form an orthonormal basis. Having found the diagonalisation $E = C^{\mathrm{T}}DC$, we define

$$\overline{a} = C\,a' = C\sqrt{N}a^\circ, \quad \overline{P} = C\,P' = C\sqrt{N^{-1}}P^\circ, \tag{4.15}$$

so that the Hamiltonian becomes

$$H_{\mathrm{osc}} = \frac{L^2\omega_{\mathrm{c}}}{2h}\left[e^2\overline{a}^\dagger\overline{a} + b^2\overline{P}^\dagger D^2\overline{P}\right] \tag{4.16a}$$

$$= \frac{L^2\omega_{\mathrm{c}}}{2h}\sum_\alpha\left[e^2\overline{a}_\alpha^\dagger\overline{a}_\alpha + b^2\overline{P}_\alpha^\dagger\lambda_\alpha^2\overline{P}_\alpha\right], \tag{4.16b}$$

written in matrix form and in components, respectively. For the derivation we have used that $\sum_\alpha \overline{a}_\alpha^\dagger\overline{a}_\alpha = \overline{a}^\dagger\overline{a} = a'^\dagger a'$ by virtue of the orthogonality of C, $\sum_\gamma C_{\alpha\gamma}C_{\beta\gamma} = \sum_\gamma C_{\alpha\gamma}C^{\mathrm{T}}_{\gamma\beta} = \delta_{\alpha\beta}$. For this transformation to be well defined, it is required that $\nu_\beta \neq 0$ for all components β, which we already assumed in order for the harmonic approximation to be valid. The definition is such that the commutator between $\overline{a}$ and $\overline{P}$ is given by

$$[\overline{a}_\alpha(\mathbf{q}), \overline{P}_\beta(-\mathbf{q}')] = i\hbar\delta_{\alpha\beta}\delta_{\mathbf{q},\mathbf{q}'}, \tag{4.17}$$

which holds also by virtue of the orthogonality of C.

By setting $P^\circ_\alpha = -i\hbar\frac{\partial}{\partial a^\circ_\alpha}$ and consequently $\overline{P}_\alpha = -i\hbar\frac{\partial}{\partial\overline{a}_\alpha}$, we can derive that

$$\chi_{\mathrm{osc}} = \exp\left(-\frac{e}{2\hbar b}\sum_{\mathbf{q}}\sum_\alpha\overline{a}_\alpha(-\mathbf{q})\xi_\alpha\overline{a}_\alpha(\mathbf{q})\right) \tag{4.18}$$

is a ground state of the Hamiltonian (4.16) if we set $\xi_\alpha = |\lambda_\alpha|^{-1}$. Evidently, ξ_α is only well defined if the matrix E is nonsingular, i.e., if none of its eigenvalues is zero. Moreover, the eigenvalues appearing in the eigenstate are actually not the eigenvalues of E itself, but the square roots of the eigenvalues of $E^2 = \sqrt{N}KNK\sqrt{N}$, namely $\sqrt{\lambda_\alpha^2} = |\lambda_\alpha|$. The ground state (4.18) can then be written in matrix form as

$$\chi_{\mathrm{osc}} = \exp\left(-\frac{e}{2\hbar b}\overline{a}^\dagger D^{-1}\overline{a}\right) = \exp\left(-\frac{e}{2\hbar b}a^{\circ\dagger}K^{-1}a^\circ\right) \tag{4.19}$$

where we used $\overline{a}^\dagger D^{-1}\overline{a} = a^{\circ\dagger}K^{-1}a^\circ$ in order to write the ground state in terms of the original auxiliary gauge fields a°. Notice that, had we chosen the negative square roots $-\sqrt{\lambda_\alpha^2}$ for the eigenvalues of E, the ground-state wave function (4.19) could not be normalised. Negative eigenvalues are indeed unphysical because they would lead to an instability of the electron liquid, the components of which phase-separate, as may

be seen within the plasma picture of the FQHE [168]. It is therefore important, for the structure of the Chern-Simons theory to be well defined, to discard negative eigenvalues λ_α. This is namely the case for the analysis presented in Sec. 4.3.3, where we assume a positive definite K. The case of zero eigenvalues is treated separately in Sec. 4.4.

Acting with Hamiltonian (4.16) on the ground state (4.18) gives its energy eigenvalues

$$\sum_\alpha \frac{L^2\omega_c}{2h}\hbar eb|\lambda_\alpha| = \frac{\hbar\omega_c}{2}\sum_\alpha|\lambda_\alpha| = \frac{\hbar}{2}\sum_\alpha\omega_\alpha,$$

where $\omega_\alpha = |\lambda_\alpha|\omega_c$ are the characteristic frequencies, given in terms of the eigenvalues λ_α and the cyclotron frequency ω_c.

At this point, we define the ladder operators as

$$\begin{aligned}\mathscr{A}_\alpha(\mathbf{q}) &= \frac{L}{\sqrt{4\pi\hbar^2\lambda_\alpha}}\Big(e\overline{a}_\alpha(\mathbf{q}) + ib\lambda_\alpha\overline{P}_\alpha(\mathbf{q})\Big),\\ \mathscr{A}^\dagger_\alpha(\mathbf{q}) &= \frac{L}{\sqrt{4\pi\hbar^2\lambda_\alpha}}\Big(e\overline{a}_\alpha(-\mathbf{q}) - ib\lambda_\alpha\overline{P}_\alpha(-\mathbf{q})\Big),\end{aligned} \tag{4.20}$$

still under the assumption that the eigenvalues λ_α are positive. The commutator of the rescaled ladder operators becomes $[\mathscr{A}_\alpha(\mathbf{q}),\mathscr{A}^\dagger_\beta(\mathbf{q}')] = \delta_{\alpha\beta}\delta_{\mathbf{q},\mathbf{q}'}$, so that $\mathscr{A}^\dagger_\alpha(\mathbf{q})\mathscr{A}_\alpha(\mathbf{q})$ is the number operator for the oscillator states in the component α of the diagonalised basis. The Hamiltonian can be conveniently written in terms of the ladder operators as

$$H_{\rm osc} = \sum_{\mathbf{q}}\sum_\alpha \hbar\omega_\alpha\big(\mathscr{A}^\dagger_\alpha(\mathbf{q})\mathscr{A}_\alpha(\mathbf{q}) + \tfrac{1}{2}\big). \tag{4.21}$$

This result also proves that the "ground state" (4.18) is indeed the lowest-energy state.

Notice that the energies $\hbar\omega_\alpha$ play the role of *quasi-particle gaps* in the Chern-Simons theory, and the ground state is well defined for $\det(K) \neq 0$ [21]. Zero-energy gaps are obtained if one of the eigenvalues $\lambda_\alpha = 0$, i.e., when the matrix K is singular, $\det(K) = \det(E) = 0$. Contrary to what one may naively expect, this situation is not in contradiction with an incompressible quantum liquid, where all (collective) charge modes must be gapped. As we discuss in more detail in Sec. 4.4, the zero-gap modes associated with $\lambda_\alpha = 0$ reveal ferromagnetic properties of the underlying state [165], which in the presence of interactions evolve into spin-wave modes while keeping the charge modes gapped.

4.3.3 Connection with trial wave functions

In order to obtain the wave functions corresponding to the ground state (4.19), we may rewrite it in terms of the density fluctuations $\delta\rho_\alpha(\mathbf{q})$, using the constraint (4.9). Once again, it is more convenient to do the computation in matrix notation. The constraint

is then given by $a^\circ = (h/e|\mathbf{q}|)K(\delta\rho)$ for physical states, with $(\delta\rho) = (\delta\rho_1, \ldots, \delta\rho_\kappa)$ the vector of the density fluctuations. Hence, we find

$$\chi_{\rm osc} = \exp\left(-\frac{1}{2}(\delta\rho)^\dagger \frac{2\pi L^2}{|\mathbf{q}|^2} K(\delta\rho)\right). \tag{4.22}$$

Notice that, written in terms of density fluctuations, the ground-state wave function is no longer confronted with the problem of zero-eigenvalues of E (or K) because it is the matrix K, and not its inverse K^{-1}, which appears here.

As shown in Ref. [164], we may relate the expression (4.22) to the plasma picture proposed by Laughlin in his original publication [9]. In this picture, we regard $|\chi_{\rm osc}|^2$ as the Boltzmann weight $\exp(-\beta\mathscr{H})$ of the plasma Hamiltonian $\mathscr{H}$, where one sets $\beta = 2$ (Ref. [168]). Then $\mathscr{H}$ can be identified as the Hamiltonian of particles interacting due to the Coulomb potential in two dimensions, $-\log|\mathbf{r}|$, which equals $2\pi L^2/|\mathbf{q}|^2$ in momentum space. As discussed in Appendix 4.A, the wave function that we obtain is

$$\psi(\{z_{j_\alpha}\}) = \prod_\alpha \prod_{\substack{j_\alpha, k_\alpha \\ j_\alpha < k_\alpha}} (z_{j_\alpha} - z_{k_\alpha})^{K_{\alpha\alpha}} \prod_{\substack{\alpha,\beta \\ \alpha<\beta}} \prod_{j_\alpha, k_\beta} (z_{j_\alpha} - z_{k_\beta})^{K_{\alpha\beta}} \times \exp\left(-\sum_{\alpha,\beta} \nu_\alpha K_{\alpha\beta} \sum_{k_\beta} \frac{|z_{k_\beta}|^2}{4l_B^2}\right) \phi_{\{\nu_\alpha^*\}}(\{z_{j_\alpha}\}), \tag{4.23}$$

where we write $z = x - iy$. This wave function is a product of the oscillator function and the wave function $\phi_{\{\nu_\alpha^*\}}(\{z_{j_\alpha}\})$, which encodes the residual degrees of freedom for particles in the reduced field $\mathbf{B}_\alpha$, i.e., at the effective filling factors ν_α^* given by Eq. (4.5). Quite generally, one may describe the same system in the framework of different Chern-Simons theories, according to how much flux is absorbed in the transformation by the matrix $K_{\alpha\beta}$. It is often convenient, if possible, to choose the Chern-Simons transformation such that the residual wave function is factorisable into single-component wave functions $\tilde{\phi}_{\nu_\alpha^*}$,

$$\phi_{\{\nu_\alpha^*\}}(\{z_{j_\alpha}\}) = \prod_{\alpha=1}^{\kappa} \tilde{\phi}_{\nu_\alpha^*}(\{z_{j_\alpha}\}), \tag{4.24}$$

so that each component may be treated independently after the transformation. Notice, however, that this aim may be in conflict with the above-mentioned condition of positive eigenvalues of the charge matrix $K_{\alpha\beta}$, namely in the context of symmetric states with ferromagnetic properties that we discuss in Sec. 4.4.2.

The simplest state of a factorisable residual wave function according to Eq. (4.24) consists of a product of states at an effective filling factor $\nu_\alpha^* = 1$ for each component, each of which involves a Slater determinant, in the form

$$\tilde{\phi}_{\nu_\alpha^*=1}(\{z_{j_\alpha}\}) = \prod_{j_\alpha < k_\alpha} (z_{j_\alpha} - z_{k_\alpha}) \exp\left(-\sum_{k_\alpha} \frac{|z_{k_\alpha}|^2}{4l_{B_\alpha^*}^2}\right). \tag{4.25}$$

Such a state would then correspond to a Halperin wave function that is described by an exponent matrix $M_{\alpha\beta} = K_{\alpha\beta} + \delta_{\alpha\beta}$. In order to have a fermionic wave function, the elements $K_{\alpha\alpha}$ must naturally be even integers, and we thus have a Chern-Simons theory that transforms fermions into (composite) fermions. Alternatively, one may have chosen the bosonic version of the Chern-Simons theory, in which case the diagonal elements of the matrix $K_{\alpha\beta} = M_{\alpha\beta}$ would be odd. The same state [Eq. (4.23)] would then be described as a product of the oscillator wave function $\chi_{\rm osc}$, which absorbs all the flux, and a *bosonic* wave function for zero net magnetic field $B^*_\alpha = 0$, for all components, $\phi_{\{B^*_\alpha=0\}}(\{z_{j_\alpha}\}) = 1$.

Until now, we have discussed states that may be described in terms of generalised κ-component Halperin wave functions [165], where the residual wave function $\phi_{\{\nu^*_\alpha\}}(\{z_{j_\alpha}\})$ is itself a (typically simpler) Halperin wave function described by a "residual" exponent matrix $M^*_{\alpha\beta}$ such that $M_{\alpha\beta} = K_{\alpha\beta} + M^*_{\alpha\beta}$ (see also Appendix 4.A). Notice, however, that the Chern-Simons theory discussed above may also provide us with another class of factorisable trial wave functions if we replace the Slater determinants (4.25) for the effective filling factors $\nu^*_\alpha = 1$ by Slater determinants for p_α completely filled composite-fermion levels $\phi^{(\alpha)}_{p_\alpha}(\{z_{j_\alpha}\})$ in each component. The resulting wave function Eq. (4.23) is related to the κ-component Halperin wave function in the same manner as Jain's one-component composite-fermion [10, 11] to Laughlin's wave function [9]. Naturally, the proposed Slater determinants contain non-analytic components in the polynomial, and, in the same manner as for Jain's wave functions, one needs to project the resulting wave function to the subspace of analytic functions in order to satisfy the lowest-Landau-level condition.

Ultimately, the theory may be generalised to the case where the ν^*_α's can take any fractional value, as to allow the multicomponent generalisation of higher-generation FQHE states. An example of the latter in one component is the $\nu = \frac{4}{11}$ state, which can be understood as a second generation FQHE state [30, 31, 33, 163, 169].

4.4 Singular transformations

The analysis in the previous section demonstrates that a Chern-Simons transformation with a nonsingular charge matrix is already interesting in itself. However, transformations with singular charge matrices play an important role in the study of states with (partial) ferromagnetic order, since these states are described by singular exponent matrices [165]. In this section, we investigate the consequences of the symmetry properties of the exponent matrices M and M^* and the charge matrix K for the results of the previous section.

4.4.1 Conditions on the ranks of the matrices

Without performing the diagonalisation of the oscillator Hamiltonian, it is already possible to give some conditions on the exponent matrices and the charge matrix. Consider a state that is described by a singular exponent matrix M. As a consequence, not all filling factors are defined separately. Suppose furthermore that the electronic and composite-fermion filling factors are given by $\sum_\beta M_{\alpha\beta}\nu_\beta = 1$ and $\sum_\beta M^*_{\alpha\beta}\nu^*_\beta = 1$, respectively, with $M = M^* + K$. We note that Eq. (4.5) has to be satisfied simultaneously, which does not necessarily follow from the other conditions.[10] From the fact that M, M^* and K are required to be nonnegative definite, it follows that also K and M^* are singular. More specifically, it follows that the null spaces of M^* and K may be of higher dimension than that of M. As a consequence, the dimension of the null space of the exponent matrix is either increased or kept invariant by the Chern-Simons transformation. In other words, if before applying the Chern-Simons transformation the theory involves a certain number of independent combinations of filling factors, then the number of independent combinations after the transformation is either the same or lower. In terms of the ranks of the matrices, which is equal to their size minus the dimension of the null space (i.e., $\dim\ker M + \operatorname{rank} M = \kappa$), we find that the ranks of K and M^* must both be smaller than or equal to the rank of M.

For the case that $\operatorname{rank} M^* < \operatorname{rank} M$, which is not ruled out by the above discussion, some problems may arise. In this case, Eq. (4.5) fixes the filling factors ν^*_α to be confined to a subspace of the space of all solutions of $\sum_\beta M^*_{\alpha\beta}\nu^*_\beta = 1$. For example, if $M = \left(\begin{smallmatrix} 3 & 1 \\ 1 & 3 \end{smallmatrix}\right)$ and $K = \left(\begin{smallmatrix} 2 & 0 \\ 0 & 2 \end{smallmatrix}\right)$, we have $M^* = \left(\begin{smallmatrix} 1 & 1 \\ 1 & 1 \end{smallmatrix}\right)$, so that, based on the exponent matrices, the electronic and composite-fermion filling factors are given by $(\nu_1, \nu_2) = (\frac{1}{4}, \frac{1}{4})$ and $\nu^*_1 + \nu^*_2 = 1$, respectively. However, based on Eq. (4.5), the composite-fermion filling factors are fixed at $(\nu^*_1, \nu^*_2) = (\frac{1}{2}, \frac{1}{2})$. Therefore, the matrix M^* does not appropriately describe the possible composite-fermion filling factors of the system. We would expect that this leads to problematic results, if we would use the Chern-Simons approach to obtain a separation between high-energy and low-energy degrees of freedom. For this reason, we will only analyse the case that M and M^* share their ranks. We stress that there is no problem in using a singular charge matrix K if M and M^* are both nonsingular.

4.4.2 The oscillator Hamiltonian

Here, we discuss how the singularity of the matrix K affects the analysis that we used to study the harmonic oscillator. Apart from the zero modes in the harmonic oscillator, we must also take into account that the number of independent constraints [Eq. (4.9)] is reduced, since these also involve the matrix K. Indeed, the number of independent constraints is given by the rank r of the matrix K, whereas the number of zero modes

[10] The given conditions are satisfied simultaneously if M^* is a block-diagonal matrix where the entries within each block are equal to each other, which includes most physically interesting cases.

is $\kappa - r$. Before we derive the fully general results, we find it instructive to illustrate the procedure first with a simple example.

We consider a two-component system, where we choose the charge matrix of the Chern-Simons transformation to be the singular matrix $K = \left(\begin{smallmatrix} 2 & 2 \\ 2 & 2 \end{smallmatrix}\right)$. The eigenvalues of K are 4 and 0, and the respective eigenvectors are $(1,1)/\sqrt{2}$ and $(1,-1)/\sqrt{2}$. We can write the constraints in components as

$$0 = \left[a^\circ_\alpha(\mathbf{q}) - \frac{h}{e|\mathbf{q}|}\big(2\,\delta\rho_1(\mathbf{q}) + 2\,\delta\rho_2(\mathbf{q})\big)\right] |\phi_{\text{phys}}\rangle\,,$$

for $\alpha = 1,2$. The two components a°_1 and a°_2 of the gauge field satisfy the same constraint, so that they are fixed to the fluctuations of the total density $\delta\rho_1 + \delta\rho_2$. On the other hand, the difference of density fluctuations $\delta\rho_1 - \delta\rho_2$ (associated with the zero eigenvalue) is absent, implying that one may have zero-energy fluctuations that lower the particle number in one component while increasing that in the other component. Eventually such a reorganisation of the particles on the two components may even completely polarise the system, with $\nu_1 = \nu$ and $\nu_2 = 0$. Inversely this means that in the case of a singular matrix K, we may always choose both filling factors nonzero or even equal, i.e., N nonsingular, such as to render the harmonic approximation Eq. (4.13) valid.

We now turn to the harmonic oscillator Hamiltonian. We write $N = \text{diag}(\nu_1, \nu_2)$, where $\nu_{1,2}$ are the electronic filling factors. For this example, we compute

$$E = \sqrt{N}K\sqrt{N} = 2\begin{pmatrix} \nu_1 & \sqrt{\nu_1\nu_2} \\ \sqrt{\nu_1\nu_2} & \nu_2 \end{pmatrix}.$$

This matrix is diagonalised as $C^{\mathrm{T}}DC$, where $D = \text{diag}(\lambda_1, \lambda_2)$ is the diagonal matrix with the eigenvalues $\lambda_1 = 2(\nu_1 + \nu_2)$ and $\lambda_2 = 0$. The corresponding eigenvectors are proportional to $(\sqrt{\nu_1}, \sqrt{\nu_2})$ and $(-\sqrt{\nu_2}, \sqrt{\nu_1})$, respectively. The diagonalised Hamiltonian is given by Eq. (4.16b), where $\alpha = 1,2$ and

$$\begin{pmatrix} \overline{a}_1 \\ \overline{a}_2 \end{pmatrix} = \frac{1}{\sqrt{\nu_1+\nu_2}}\begin{pmatrix} \nu_1 a^\circ_1 + \nu_2 a^\circ_2 \\ \sqrt{\nu_1\nu_2}\,(-a^\circ_1 + a^\circ_2) \end{pmatrix}, \qquad \begin{pmatrix} \overline{P}_1 \\ \overline{P}_2 \end{pmatrix} = \frac{1}{\sqrt{\nu_1+\nu_2}}\begin{pmatrix} P^\circ_1 + P^\circ_2 \\ -\sqrt{\frac{\nu_2}{\nu_1}}\,P^\circ_1 + \sqrt{\frac{\nu_1}{\nu_2}}\,P^\circ_2 \end{pmatrix}.$$

We note that $\overline{P}_2$ is not present in the Hamiltonian since the term $\overline{P}_2^\dagger \lambda_2^2 \overline{P}_2$ vanishes due to $\lambda_2 = 0$. The term $\overline{a}_2^\dagger \overline{a}_2$ also vanishes, since $\overline{a}_2 = 0$, due to the constraint $a^\circ_1 = a^\circ_2$. In the end, we obtain a harmonic oscillator Hamiltonian with only one coordinate $(\overline{a}_1)$ and one momentum $(\overline{P}_1)$ component.

The Hamiltonian restricted to this single coordinate has a ground state $\chi_{\text{osc},1} = \exp[-(e/2\hbar b)\overline{a}^\dagger \widehat{D}\,\overline{a}]$, where we define $\widehat{D} = \text{diag}(\frac{1}{2}(\nu_1+\nu_2)^{-1}, 0)$. We note that $\chi_{\text{osc},1}$ only involves $\overline{a}_1$, but not $\overline{a}_2$. Transforming back to the coordinates (a°_1, a°_2) and imposing the constraints $a^\circ_1 = a^\circ_2 = (h/e|\mathbf{q}|)\big(2\,\delta\rho_1 + 2\,\delta\rho_2\big)$, we obtain

$$\chi_{\text{osc},1} = \exp\left(-\frac{1}{2}(\delta\rho_1 + \delta\rho_2)^\dagger \frac{2\pi L^2}{|\mathbf{q}|^2}(2)\,(\delta\rho_1 + \delta\rho_2)\right),$$

where the notation (2) is to point out that it should be interpreted as a matrix. At this point, we observe that $(\delta\rho_1 + \delta\rho_2)^\dagger(2)(\delta\rho_1 + \delta\rho_2)$ is exactly equal to $(\delta\rho_1, \delta\rho_2)^\dagger K(\delta\rho_1, \delta\rho_2)$. This means that in this example Eq. (4.22) is valid without change, and the other results concerning the Halperin wave functions hold as well, as we have already mentioned in the discussion of the general oscillator function (4.22). We remark that the linear combination of filling factors $\nu_1 - \nu_2$ is not present at all in the diagonalised theory.

Another important point is that we can make the connection with ferromagnetic Laughlin states in two-component systems [168]. For instance, the exponent matrix $M = \left(\begin{smallmatrix} 3 & 3 \\ 3 & 3 \end{smallmatrix}\right)$ defines a state for which the total filling factor is $\nu_1 + \nu_2 = \frac{1}{3}$, but the separate filling factors are not defined, since the exponent matrix is singular [168]. Using the Chern-Simons transformation of the example above, we may understand this state in terms of a composite-fermion theory with exponent matrix $M^* = \left(\begin{smallmatrix} 1 & 1 \\ 1 & 1 \end{smallmatrix}\right)$. This state has total composite-fermion filling factor $\nu_1^* + \nu_2^* = 1$, and again the separate filling factors are undefined. We remark that although the intermediate steps in the procedure contain the separate filling factors ν_1 and ν_2, the results are completely independent of $\nu_1 - \nu_2$.

In contrast to the ferromagnetic Laughlin state discussed in the preceding paragraph, we may also discuss the two-component state at total filling factor $\nu = \frac{2}{5}$, described by the matrix $M = \left(\begin{smallmatrix} 3 & 2 \\ 2 & 3 \end{smallmatrix}\right)$ and the reduced exponent matrix $M^* = \left(\begin{smallmatrix} 1 & 0 \\ 0 & 1 \end{smallmatrix}\right)$. Although the Chern-Simons transformation is described by a singular charge matrix K and does therefore not impose a constraint on the relative particle distribution on the two components, the constraint is imposed by M^*, $\nu_1^* = \nu_2^* = 1$. The state thus described is then a spin-unpolarised state, as one could have also expected from the original exponent matrix M.

The reasoning given for the example above can be readily generalised to any situation in which K is singular. Here, we assume that the rank r of the matrix K is smaller than the number of components κ. As argued in Appendix 4.B, the ground state can be decomposed as a product of the usual ground state (4.19) restricted to the r independent components, $\chi_{\mathrm{osc},r}$ and the degenerate part $\tilde{\chi}$ [see Eqs. (4.144) and (4.145)]. Moreover, Eq. (4.22) remains valid even in the singular case, despite the fact that the original derivation involves the inverse of K. Hence, the Halperin connection in Sec. 4.3.3 is valid in the singular case without modification.

The equivalence of the decomposition (4.144) for the κ-component oscillator wave function may be interpreted in a straightforward physical manner. Indeed, the decomposition indicates that, in the case of a charge matrix K of rank r, the "reduced" r-component wave function corresponds to an r-component Halperin wave function with gapped oscillator frequencies ω_α. The other factor $\tilde{\chi}$ in Eq. (4.144) corresponds to the $\kappa - r$ zero eigenvalues of the matrix K with an associated space spanned by the oscillator components $\overline{a}_\alpha$, with $\alpha = r+1, \ldots, \kappa$. The ground-state manifold comprises therefore any possible combination of these components $\overline{a}_\alpha$, and a particular choice

spontaneously breaks the residual ground-state symmetry, which may be related to the ferromagnetic properties of the Halperin state, and $\tilde{\chi}$ may then be interpreted as the ferromagnetic part of the wave function.

In order to see this particular point, consider the r constraints to fix the filling factors of the first $r-1$ components. The last constraint then imposes simply the *sum* of the fillings of all other components $\alpha = r,\ldots,\kappa$. This is naturally a simplified assumption, because the r constraints do not in general fix particular components, but the dependencies may be more complicated.[11] One is then free to distribute the involved particles over these components in a quantum mechanical manner. All different distributions define the ground-state manifold. Schematically, this may be formalised with the help of a wave function

$$\tilde{\chi} = u_r\,|\alpha = r\rangle + u_{r+1}\,|\alpha = r+1\rangle + \ldots + u_\kappa\,|\alpha = \kappa\rangle\,,$$

where the complex amplitudes u_α are subject to a normalisation condition, which plays the role of the last constraint. These complex amplitudes may be viewed as the components of a $\mathrm{CP}^{\kappa-r}$ field.[12] The ground-state manifold may then be described by spatially constant $\mathrm{CP}^{\kappa-r}$ fields with a global $\mathbf{SU}(\kappa-r+1)$ symmetry, which is precisely the symmetry group that describes the ferromagnetic properties of the oscillator wave function. In summary, this argument shows that, in the case of a Chern-Simons transformation with a matrix K of rank r, one may decompose an arbitrary oscillator wave function into a product of a reduced r-component Halperin wave function and a $\mathbf{SU}(\kappa-r+1)$-symmetric ferromagnetic part. Naturally, this symmetry may be further reduced if the components of the Chern-Simons field fix further filling factors.

We finally mention that the spontaneous breaking of the $\mathbf{SU}(\kappa-r+1)$ symmetry yields Goldstone modes, which are physical (pseudo)spin waves. On the level of the Gaussian model, these Goldstone modes are dispersionless and remain at zero energy. This is no longer the case if one takes into account interactions between the particles associated with the different components. One may indeed treat rather easily a density-density interaction within the present model. This interaction may be translated, via the constraints (4.9), into an interaction between the oscillator fields, which one can then diagonalise within the Gaussian model. Notice that these fields are coupled to the Π_α [see Eq. (4.11)], which describe the low-energy electronic degrees of freedom. A discussion of collective Goldstone-type modes is therefore more involved and requires a decoupling of the oscillator and the electronic degrees of freedom. However, the Chern-Simons analysis within the Gaussian model yields valuable insight into

[11] Other continuous subgroups of $\mathbf{SU}(\kappa)$ may appear as well as symmetry groups. These include product groups like $\mathbf{SU}(2)\times\mathbf{SU}(2)$, which is relevant for four-component systems with two $\mathbf{SU}(2)$ symmetries of a different origin, such as spin and pseudospin.

[12] The $\kappa-r+1$ complex components u_α, $\alpha = r,\ldots,\kappa$ may indeed be viewed as an element of the complex projective space $\mathrm{CP}^{\kappa-r}$ in which one identifies all elements that differ only by a global (complex) factor c, $(u_r,\ldots,u_\kappa) \equiv (cu_r,\ldots,cu_\kappa)$.

the ferromagnetic properties of the states, which are governed by symmetry, as well as into the number of their Goldstone modes.

4.5 Decoupling of the full Hamiltonian

The harmonic oscillator Hamiltonian on its own does not have a physical eigenvalue spectrum. Kohn's theorem [170] predicts that the physical spectrum must contain at least one mode at the cyclotron frequency ω_c. Since this mode is not present in the spectrum of the harmonic oscillator, this spectrum cannot be physical. This result is not surprising, because in the previous model we have omitted the two terms H^* and H_{coupl} [Eqs. (4.10) and (4.11), respectively], which contain also the momentum degrees of freedom. In this section, we will compute the eigenvalue spectrum of the full Hamiltonian, $H = H^* + H_{\text{coupl}} + H_{\text{osc}}$.

For pedagogical reasons, we will first focus on the Hamiltonian of one-component systems, reviewing the procedure proposed by Murthy and Shankar [24]. However, we perform their analysis in a slightly different way, such that is generalised more easily to the multicomponent case. The review of the decoupling procedure in the single-component case will provide us an insight into how it works. Then, we will generalise this procedure step by step to systems with multiple components.

4.5.1 Review: One-component systems

Hamiltonian in random-phase approximation

Let us first rewrite the momentum operators Π_j, as defined in Eq. (4.10), in a different way. After defining $\Pi_j^{\pm} = \Pi_j^x \pm i\,\Pi_j^y$, we can compute that

$$H^* = \frac{1}{2m}\sum_j \Pi_j \cdot \Pi_j = \frac{1}{2m}\sum_j \tfrac{1}{2}(\Pi_j^+\Pi_j^- + \Pi_j^-\Pi_j^+) = \frac{1}{2m}\sum_j (\Pi_j^+\Pi_j^- + \tfrac{1}{2}[\Pi_j^-, \Pi_j^+]),$$

where the commutator is given by $[\Pi_j^-, \Pi_k^+] = 2eB^*\hbar\delta_{j,k}$. Next, we define[13]

$$c(\mathbf{q}) = \frac{1}{L}\sum_j \hat{q}_+ \Pi_j^- e^{-i\mathbf{q}\cdot\mathbf{r}_j}, \qquad c^\dagger(\mathbf{q}) = \frac{1}{L}\sum_j \hat{q}_- \Pi_j^+ e^{i\mathbf{q}\cdot\mathbf{r}_j}, \tag{4.26}$$

where $\hat{q}_\pm = (q_x \pm i\,q_y)/|\mathbf{q}|$. Using this definition, we compute

$$\sum_{\mathbf{q}} c^\dagger(\mathbf{q})c(\mathbf{q}) = \frac{1}{L^2}\sum_{\mathbf{q}}\sum_{j,k} \Pi_j^+\Pi_k^- e^{i\mathbf{q}\cdot\mathbf{r}_j} e^{-i\mathbf{q}\cdot\mathbf{r}_k}. \tag{4.27}$$

[13] Some authors, e.g., Shankar and Murthy in Refs. [23, 24], use a different sign convention. Therefore, the expressions in this work and in Refs. [23, 24] may show sign differences, but the conclusions remain compatible.

At this point, we use the *random-phase approximation* (RPA) [24, 28], which implies that

$$\sum_j e^{i(\mathbf{q}-\mathbf{q}')\cdot\mathbf{r}_j} \approx \delta_{\mathbf{q},\mathbf{q}'} nL^2 \quad \text{and} \quad \sum_{\mathbf{q}} e^{i\mathbf{q}\cdot(\mathbf{r}_j-\mathbf{r}_k)} \approx \delta_{j,k} nL^2, \tag{4.28}$$

where n is the electronic density, and nL^2 is the total number of electrons. Within this approximation, $\sum_{\mathbf{q}} c^\dagger(\mathbf{q})c(\mathbf{q}) = n\sum_j \Pi_j^+\Pi_j^-$, which can be used to rewrite the effective-field Hamiltonian H^* to

$$H^*_{\mathrm{RPA}} = \frac{1}{2mn}\sum_{\mathbf{q}} c^\dagger(\mathbf{q})c(\mathbf{q}) + \sum_j \frac{\hbar e B^*}{2m}. \tag{4.29}$$

The last term is just a constant energy offset, that we will neglect for the time being.

The oscillator Hamiltonian is given by $H_{\mathrm{osc}} = \hbar\omega\sum_{\mathbf{q}} \mathscr{A}^\dagger(\mathbf{q})\mathscr{A}(\mathbf{q})$ (up to a constant energy offset). Here, $\mathscr{A}$ and $\mathscr{A}^\dagger$ are the ladder operators of the oscillator,

$$\begin{aligned} \mathscr{A}(\mathbf{q}) &= \frac{L}{\sqrt{4\pi\hbar^2 K}}\big(e\,a^\circ(\mathbf{q}) + ibKP^\circ(\mathbf{q})\big), \\ \mathscr{A}^\dagger(\mathbf{q}) &= \frac{L}{\sqrt{4\pi\hbar^2 K}}\big(e\,a^\circ(-\mathbf{q}) - ibKP^\circ(-\mathbf{q})\big), \end{aligned} \tag{4.30}$$

where a° and P° are now single-component vectors. These are derived from Eq. (4.20), together with the definitions $\overline{a} = \sqrt{\nu}\,a^\circ$ and $\overline{P} = \sqrt{\nu^{-1}}P^\circ$ in Eqs. (4.15), and from the fact that $E = \sqrt{N}K\sqrt{N}$ is in this case a 1×1 matrix with the single eigenvalue $\lambda = \nu K$, where K is the charge of the Chern-Simons transformation. The eigenfrequency of the oscillator is $\omega = \lambda\omega_{\mathrm{c}} = \nu K\omega_{\mathrm{c}}$.

The coupling Hamiltonian (4.11) can be rewritten as

$$H_{\mathrm{coupl}} = \frac{\sqrt{4\pi\hbar^2 K}}{2m}\sum_{\mathbf{q}}\big(c^\dagger(\mathbf{q})\mathscr{A}(\mathbf{q}) + \mathscr{A}^\dagger(\mathbf{q})c(\mathbf{q})\big). \tag{4.31}$$

For a detailed proof, we refer the reader to Appendix 4.C. We can rewrite the prefactor of the coupling Hamiltonian conveniently by defining

$$\theta = \frac{1}{2\hbar n\sqrt{\pi K}} = \theta_0\frac{1}{\nu\sqrt{K}}, \tag{4.32}$$

with

$$\theta_0 = \frac{\sqrt{\pi}}{eB} = \frac{l_B^2\sqrt{\pi}}{\hbar}, \tag{4.33}$$

which yields $\sqrt{4\pi\hbar^2 K}/2m = (\hbar/m)\sqrt{\pi K} = \hbar\omega\theta$. Moreover, we can compute

$$\hbar\omega\theta^2 = \frac{1}{2m}\frac{2\pi\hbar}{eB}\frac{1}{\nu} = \frac{1}{2mn}, \tag{4.34}$$

which is exactly the prefactor of the first term of H^*_{RPA} in Eq. (4.29).

With these observations, we combine the three terms H^*_{RPA}, H_{osc} and H_{coupl} into

$$H_{\mathrm{RPA}} \equiv \hbar\omega\theta^2 \sum_{\mathbf{q}} c^\dagger(\mathbf{q})c(\mathbf{q}) + \hbar\omega \sum_{\mathbf{q}} \mathscr{A}^\dagger(\mathbf{q})\mathscr{A}(\mathbf{q}) + \hbar\omega\theta \sum_{\mathbf{q}} \big(c^\dagger(\mathbf{q})\mathscr{A}(\mathbf{q}) + \mathscr{A}^\dagger(\mathbf{q})c(\mathbf{q})\big),$$

which can be written conveniently in matrix form as

$$H_{\mathrm{RPA}} = \hbar \sum_{\mathbf{q}} \begin{pmatrix} c^\dagger(\mathbf{q}) & \mathscr{A}^\dagger(\mathbf{q}) \end{pmatrix} \begin{pmatrix} \omega\theta^2 & \omega\theta \\ \omega\theta & \omega \end{pmatrix} \begin{pmatrix} c(\mathbf{q}) \\ \mathscr{A}(\mathbf{q}) \end{pmatrix}. \tag{4.35}$$

Diagonalisation

The Hamiltonian in matrix form can be used to redefine the operators c and $\mathscr{A}$ so that the coupling term disappears. This is nothing more than diagonalisation of the matrix. Before we perform the diagonalisation, we use rescaled forms c' and $\mathscr{A}'$ of the operators c and $\mathscr{A}$, so that their commutators become of equal magnitude. In other words, the operators c' and $\mathscr{A}'$ are defined such that the commutators $[c'(\mathbf{q}), c'^\dagger(\mathbf{q}')]$ and $[\mathscr{A}'(\mathbf{q}), \mathscr{A}'^\dagger(\mathbf{q}')]$ become equal. Because $[\mathscr{A}(\mathbf{q}), \mathscr{A}^\dagger(\mathbf{q}')] = \delta_{\mathbf{q},\mathbf{q}'}$, let us define $\mathscr{A}' = \mathscr{A}$. In order to obtain the scale factor for the operators $[c'(\mathbf{q}), c'^\dagger(\mathbf{q}')]$, we can compute

$$[c(\mathbf{q}), c^\dagger(\mathbf{q}')] = \frac{1}{L^2} \sum_{j,k} \hat{q}_- \hat{q}'_+ e^{i(\mathbf{q}'\cdot\mathbf{r}_k - \mathbf{q}\cdot\mathbf{r}_j)} [\Pi^+_j, \Pi^-_k] \approx 2eB^*\hbar n \delta_{\mathbf{q},\mathbf{q}'}, \tag{4.36}$$

where $\approx$ indicates that we are using the RPA, thereby neglecting terms of order $\mathscr{O}(\mathbf{q})$. The commutators $[c(\mathbf{q}), c(\mathbf{q}')]$ and $[c^\dagger(\mathbf{q}), c^\dagger(\mathbf{q}')]$ vanish up to this order. Due to the neglect of terms of higher order, our analysis is only a reasonable approximation in the limit of small $\mathbf{q}$. We set $c' = (\theta/\mu)c$, where μ is determined by the requirement that $[c'(\mathbf{q}), c'^\dagger(\mathbf{q}')] = \delta_{\mathbf{q},\mathbf{q}'}$, so that the condition

$$\mu^2 = 2eB^*\hbar n\theta^2 = \frac{1}{\nu^* K} \tag{4.37}$$

follows from Eq. (4.36).

In terms of the rescaled fields c' and $\mathscr{A}'$, the Hamiltonian reads

$$H_{\mathrm{RPA}} = \hbar\omega \sum_{\mathbf{q}} \begin{pmatrix} c'^\dagger(\mathbf{q}) & \mathscr{A}'^\dagger(\mathbf{q}) \end{pmatrix} \begin{pmatrix} \mu^2 & \mu \\ \mu & 1 \end{pmatrix} \begin{pmatrix} c'(\mathbf{q}) \\ \mathscr{A}'(\mathbf{q}) \end{pmatrix}. \tag{4.38}$$

The *Hamiltonian matrix* $H'_{\mathrm{mat}} = \left(\begin{smallmatrix} \mu^2 & \mu \\ \mu & 1 \end{smallmatrix}\right)$ in this equation is diagonalised by the (normalised) eigenvectors

$$\frac{1}{\sqrt{1+\mu^2}} \begin{pmatrix} 1 \\ -\mu \end{pmatrix} \quad \text{and} \quad \frac{1}{\sqrt{1+\mu^2}} \begin{pmatrix} \mu \\ 1 \end{pmatrix},$$

with corresponding eigenvalues 0 and $1+\mu^2$, respectively. In other words, we can write $H'_{\mathrm{mat}} = S^{\mathrm{T}} \tilde{H}_{\mathrm{mat}} S$, with

$$S^{\mathrm{T}} = \frac{1}{\sqrt{1+\mu^2}} \begin{pmatrix} 1 & \mu \\ -\mu & 1 \end{pmatrix} \quad \text{and} \quad \tilde{H}_{\mathrm{mat}} = \begin{pmatrix} 0 & 0 \\ 0 & 1+\mu^2 \end{pmatrix}. \tag{4.39}$$

We define $(\tilde{c}', \tilde{\mathscr{A}}') = S(c', \mathscr{A}')$, which is nothing more than a rotation in the $(c', \mathscr{A}')$ plane, since the matrix S is just an element of **SO**(2); the rotation angle u satisfies $\sin u = \mu/\sqrt{1+\mu^2}$ and $\cos u = 1/\sqrt{1+\mu^2}$. This observation shows that our reasoning is equivalent to the one in Ref. [24], where the decoupling procedure is understood in terms of a rotation.

The diagonalised Hamiltonian is given by

$$\begin{aligned} H_{\mathrm{RPA}} &= \hbar\omega \sum_{\mathbf{q}} \begin{pmatrix} \tilde{c}'^{\dagger}(\mathbf{q}) & \tilde{\mathscr{A}}'^{\dagger}(\mathbf{q}) \end{pmatrix} \begin{pmatrix} 0 & 0 \\ 0 & 1+\mu^2 \end{pmatrix} \begin{pmatrix} \tilde{c}'(\mathbf{q}) \\ \tilde{\mathscr{A}}'(\mathbf{q}) \end{pmatrix} \\ &= \hbar\omega(1+\mu^2) \sum_{\mathbf{q}} \tilde{\mathscr{A}}'^{\dagger}(\mathbf{q}) \tilde{\mathscr{A}}'(\mathbf{q}). \end{aligned} \tag{4.40}$$

The operators $\tilde{c}'$ and $\tilde{c}'^{\dagger}$ are completely absent from this Hamiltonian, which means that in the RPA, the diagonalised momentum operators do not contribute to the Hamiltonian. By using $\mu^2 = 1/\nu^* K$ [Eq. (4.37)] and relation (4.5) (which implies $\nu^* = \nu/(1 - K\nu)$ in the single component case), we derive that the eigenfrequency associated to the mode $\tilde{\mathscr{A}}'(\mathbf{q})$ is given by

$$\omega(1+\mu^2) = \omega \frac{\nu^* K + 1}{\nu^* K} = \omega \frac{1}{\nu K} = \omega_{\mathrm{c}}. \tag{4.41}$$

Hence the oscillator frequency is equal to the cyclotron frequency ω_{c}, which agrees [28] with Kohn's theorem [170]. To summarise the result, the RPA Hamiltonian can be concisely written as

$$H_{\mathrm{RPA}} = \hbar\omega_{\mathrm{c}} \sum_{\mathbf{q}} \tilde{\mathscr{A}}^{\dagger}(\mathbf{q}) \tilde{\mathscr{A}}(\mathbf{q}), \tag{4.42}$$

in which we have set $\tilde{\mathscr{A}}(\mathbf{q}) \equiv \tilde{\mathscr{A}}'(\mathbf{q})$.

There are two energy offsets that we have neglected so far: The constant term $\sum_{\mathbf{q}} \hbar\omega/2$ from the oscillator Hamiltonian, and the term $\sum_j \hbar e B^*/2m$ from H^*. Summing both contributions, we obtain

$$H_{\mathrm{const}} \equiv \sum_{\mathbf{q}} \frac{\hbar}{2}\omega + \sum_j \frac{\hbar e B^*}{2m} = \sum_{\mathbf{q}} \frac{\hbar}{2}\omega_{\mathrm{c}} \nu K + \sum_j \frac{\hbar e B}{2m}(1 - \nu K) = nL^2 \frac{\hbar\omega_{\mathrm{c}}}{2},$$

using Eq. (4.5) to rewrite B^* in terms of B. Here, we have assumed that the sums over j and over q contain the same number of terms, namely, the number of particles nL^2. In other words, we set the number of oscillators to be equal to the number of particles [23, 25]. As a result, the constant energy contribution per particle is $\hbar\omega_{\mathrm{c}}/2$. Adding these contributions to the diagonalised Hamiltonian H_{RPA} of Eq. (4.42) yields

$$H_{\mathrm{RPA}} + H_{\mathrm{const}} = \hbar\omega_{\mathrm{c}} \sum_{\mathbf{q}} \big(\tilde{\mathscr{A}}^{\dagger}(\mathbf{q}) \tilde{\mathscr{A}}(\mathbf{q}) + \tfrac{1}{2} \big). \tag{4.43}$$

Hence, the total contribution of the zero energy is $\hbar/2$ times the eigenfrequency of the transformed oscillators. This feature was also present for the oscillator Hamiltonian by

itself, although for a different frequency. Remarkably, adding the terms H^* and H_{coupl} to the oscillator Hamiltonian and subsequently diagonalising it, effectively rescales the eigenfrequency and the zero energy by the same factor.

In this analysis, we have neglected the errors due to the RPA. On one hand, we have neglected the difference

$$H_{\text{non-RPA}} = \frac{1}{2mnL^2} \sum_{\mathbf{q}} \sum_{j,k} \Pi_j^+ \Pi_k^- e^{i\mathbf{q}\cdot\mathbf{r}_j} e^{-i\mathbf{q}\cdot\mathbf{r}_k} - \frac{1}{2mn} \sum_{\mathbf{q}} c^\dagger(\mathbf{q}) c(\mathbf{q}),$$

and on the other hand, the $\mathcal{O}(q)$ terms from the approximation of $[c, c^\dagger]$ in Eq. (4.36). An estimation of these errors lies outside the scope of this work.

4.5.2 Multicomponent systems

It is possible to generalise the previous analysis to multicomponent systems, although we shall see that some steps become more complicated because we will have to use matrices instead of single numbers. To avoid more difficulties, we shall assume the matrix K (and subsequently E and D) to be invertible and positive definite. The case where K is singular is discussed at the end of this section.

Hamiltonian in random-phase approximation

As with the one-component case, we first write the RPA Hamiltonian in a matrix from, analogous to Eq. (4.35). We define $\Pi^\pm_{\alpha,j_\alpha} = \Pi^x_{\alpha,j_\alpha} \pm i\,\Pi^y_{\alpha,j_\alpha}$, which satisfy $[\Pi^-_{\alpha,j_\alpha}, \Pi^+_{\beta,k_\beta}] = 2eB^*_\alpha \hbar \delta_{\alpha,\beta}\delta_{j_\alpha,k_\beta}$, and subsequently

$$c_\alpha(\mathbf{q}) = \frac{1}{L} \sum_{j_\alpha=1}^{N_\alpha} \hat{q}_+ \Pi^-_{\alpha,j_\alpha} e^{-i\mathbf{q}\cdot\mathbf{r}_{j_\alpha}} \quad \text{and} \quad c^\dagger_\alpha(\mathbf{q}) = \frac{1}{L} \sum_{j_\alpha=1}^{N_\alpha} \hat{q}_- \Pi^+_{\alpha,j_\alpha} e^{i\mathbf{q}\cdot\mathbf{r}_{j_\alpha}}. \tag{4.44}$$

Using the derivation of Sec. 4.5.1 for each component separately eventually yields

$$H^*_{\text{RPA}} = \sum_\alpha \left(\frac{1}{2mn_\alpha} \sum_{\mathbf{q}} c^\dagger_\alpha(\mathbf{q}) c_\alpha(\mathbf{q}) + \sum_{j_\alpha=1}^{N_\alpha} \frac{\hbar e B^*_\alpha}{2m} \right). \tag{4.45}$$

Again, we will neglect the constant terms for the moment.

The oscillator Hamiltonian is given by

$$H_{\text{osc}} = \sum_{\mathbf{q}} \sum_\alpha \hbar\omega_\alpha \mathscr{A}^\dagger_\alpha(\mathbf{q}) \mathscr{A}_\alpha(\mathbf{q}),$$

according to Eq. (4.21), up to a constant energy. We remark that it is written in terms of the diagonalised ladder operators $\mathscr{A}_\alpha$ and $\mathscr{A}^\dagger_\alpha$ as defined in Eq. (4.20), while the original form before diagonalisation Eq. (4.13) is given in terms of non-diagonalised operators.

This also holds for the coupling Hamiltonian (4.11). For the latter, it is convenient to define the operators

$$\begin{aligned}\mathscr{A}^\circ_\alpha(\mathbf{q}) &= \frac{L}{\sqrt{4\pi\hbar^2}}\left(e\,a^\circ_\alpha(\mathbf{q}) + ib\sum_\beta K_{\alpha\beta}P^\circ_\beta(\mathbf{q})\right),\\ \mathscr{A}^{\circ\dagger}_\alpha(\mathbf{q}) &= \frac{L}{\sqrt{4\pi\hbar^2}}\left(e\,a^\circ_\alpha(-\mathbf{q}) - ib\sum_\beta K_{\alpha\beta}P^\circ_\beta(-\mathbf{q})\right).\end{aligned} \tag{4.46}$$

These operators are not ladder operators, since the commutator $[\mathscr{A}^\circ_\alpha(\mathbf{q}),\mathscr{A}^{\circ\dagger}_\beta(\mathbf{q}')]$ is not proportional to $\delta_{\alpha\beta}\delta_{\mathbf{q},\mathbf{q}'}$. We use these operators to rewrite the coupling Hamiltonian (4.11): If we apply the result (4.31), which we have proved in Appendix 4.C, to each component, we obtain

$$H_{\text{coupl}} = \frac{\sqrt{4\pi\hbar^2}}{2m}\sum_\alpha\sum_{\mathbf{q}}\big(c^\dagger_\alpha(\mathbf{q})\mathscr{A}^\circ_\alpha(\mathbf{q}) + \mathscr{A}^{\circ\dagger}_\alpha(\mathbf{q})c_\alpha(\mathbf{q})\big). \tag{4.47}$$

In order to write also the coupling term in terms of the $\mathscr{A}_\alpha$ and $\mathscr{A}^\dagger_\alpha$ rather than the $\mathscr{A}^\circ_\alpha$ and $\mathscr{A}^{\circ\dagger}_\alpha$, we express the former in terms of the latter. Equation (4.20) may be written concisely as

$$\mathscr{A} = \frac{L}{\sqrt{4\pi\hbar^2}}\sqrt{D^{-1}}\big(e\,\overline{a} + ibD\,\overline{P}\big),$$

where we recall that D is the diagonal matrix of eigenvalues of $E = \sqrt{N}K\sqrt{N}$. Then we rewrite this expression using Eqs. (4.15) in terms of a° and P°, as

$$\begin{aligned}\mathscr{A} &= \frac{L}{\sqrt{4\pi\hbar^2}}\Big(e\sqrt{D^{-1}}C\sqrt{N}a^\circ + ib\sqrt{D}\,C\sqrt{N^{-1}}P^\circ\Big)\\ &= \frac{L}{\sqrt{4\pi\hbar^2}}\sqrt{D^{-1}}C\sqrt{N}\Big(e\,a^\circ + ib\sqrt{N^{-1}}C^{-1}\sqrt{D}\sqrt{D}\,C\sqrt{N^{-1}}P^\circ\Big)\\ &= \frac{L}{\sqrt{4\pi\hbar^2}}\sqrt{D^{-1}}C\sqrt{N}\Big(e\,a^\circ + ibK\,P^\circ\Big) = \sqrt{D^{-1}}C\sqrt{N}\mathscr{A}^\circ,\end{aligned}$$

using that $C^{-1}DC = E = \sqrt{N}K\sqrt{N}$. Thus, we obtain

$$\mathscr{A}^\circ = \sqrt{N^{-1}}C^{\mathrm{T}}\sqrt{D}\,\mathscr{A} \quad\text{and}\quad \mathscr{A}^{\circ\dagger} = \mathscr{A}^\dagger\sqrt{D}\,C\sqrt{N^{-1}}, \tag{4.48}$$

which we substitute into the coupling Hamiltonian (4.47), which is then converted to

$$H_{\text{coupl}} = \frac{\sqrt{4\pi\hbar^2}}{2m}\sum_{\mathbf{q}}\Big(c^\dagger(\mathbf{q})\sqrt{N^{-1}}C^{\mathrm{T}}\sqrt{D}\,\mathscr{A}(\mathbf{q}) + \mathscr{A}^\dagger(\mathbf{q})\sqrt{D}\,C\sqrt{N^{-1}}c(\mathbf{q})\Big). \tag{4.49}$$

By taking together H^*_{RPA}, H_{osc}, and H_{coupl}, given by Eqs. (4.29), (4.13), and (4.49), respectively, we obtain the full Hamiltonian (up to some constant energy offset),

$$\begin{aligned}H_{\text{RPA}} = \frac{1}{2m}\frac{2\pi\hbar}{eB}\sum_{\mathbf{q}}c^\dagger(\mathbf{q})N^{-1}c(\mathbf{q}) + \hbar\omega_{\text{c}}\sum_{\mathbf{q}}\mathscr{A}^\dagger(\mathbf{q})D\mathscr{A}(\mathbf{q})\\ + \frac{\sqrt{4\pi\hbar^2}}{2m}\sum_{\mathbf{q}}\Big(c^\dagger(\mathbf{q})\sqrt{N^{-1}}C^{\mathrm{T}}\sqrt{D}\,\mathscr{A}(\mathbf{q}) + \mathscr{A}^\dagger(\mathbf{q})\sqrt{D}\,C\sqrt{N^{-1}}c(\mathbf{q})\Big).\end{aligned}$$

In order to make the connection with the RPA Hamiltonian (4.35) for one component, we define the matrices $\Omega = \omega_c D$ and $\Theta = \theta_0 \sqrt{D^{-1}} C \sqrt{N^{-1}}$, with $\theta_0 = \sqrt{\pi}/eB$ as in Eq. (4.33) as generalisations of ω and θ, respectively. Then we can write the coupling term as

$$\frac{\sqrt{4\pi\hbar^2}}{2m\omega_c\theta_0} \sum_{\mathbf{q}} \Big(c^\dagger(\mathbf{q}) \Theta^{\mathrm{T}} \Omega \mathscr{A}(\mathbf{q}) + \mathscr{A}^\dagger(\mathbf{q}) \Omega \Theta c(\mathbf{q}) \Big),$$

where $\sqrt{4\pi\hbar^2}/2m\omega_c\theta_0 = 2\hbar\sqrt{\pi}/2eB\theta_0 = \hbar$. Moreover, we can compute that

$$\hbar \Theta^{\mathrm{T}} \Omega \Theta = \hbar \theta_0^2 \omega_c \Big(\sqrt{N^{-1}} C^{\mathrm{T}} \sqrt{D^{-1}} \Big) D \Big(\sqrt{D^{-1}} C \sqrt{N^{-1}} \Big) = \hbar \frac{\pi}{(eB)^2} \frac{eB}{m} N^{-1} = \frac{2\pi\hbar}{2m\,eB} N^{-1}, \tag{4.50}$$

where we used $C^{\mathrm{T}} C = \mathbb{1}$ in the second step. Hence, the full Hamiltonian reads

$$\begin{aligned} H_{\mathrm{RPA}} &= \hbar \sum_{\mathbf{q}} \Big[c^\dagger(\mathbf{q}) \Theta^{\mathrm{T}} \Omega \Theta c(\mathbf{q}) + \mathscr{A}^\dagger(\mathbf{q}) \Omega \mathscr{A}(\mathbf{q}) + c^\dagger(\mathbf{q}) \Theta^{\mathrm{T}} \Omega \mathscr{A}(\mathbf{q}) + \mathscr{A}^\dagger(\mathbf{q}) \Omega \Theta c(\mathbf{q}) \Big] \\ &= \hbar \sum_{\mathbf{q}} \begin{pmatrix} c^\dagger(\mathbf{q}) & \mathscr{A}^\dagger(\mathbf{q}) \end{pmatrix} \begin{pmatrix} \Theta^{\mathrm{T}} \Omega \Theta & \Theta^{\mathrm{T}} \Omega \\ \Omega \Theta & \Omega \end{pmatrix} \begin{pmatrix} c(\mathbf{q}) \\ \mathscr{A}(\mathbf{q}) \end{pmatrix}, \end{aligned} \tag{4.51}$$

which clearly generalises Eq. (4.35).

Diagonalisation

We again rescale c and $c^\dagger$ so that the commutator of the transformed quantities is of unit magnitude, as is also the case with the commutator of $\mathscr{A}$ and $\mathscr{A}^\dagger$. We first write the commutator (in RPA)

$$[c_\alpha(\mathbf{q}), c_\beta^\dagger(\mathbf{q}')] \approx 2eB_\alpha^* \hbar\, n_\alpha \delta_{\alpha\beta} \delta_{\mathbf{q},\mathbf{q}'} = 2eB\hbar \left(1 - \sum_\gamma K_{\alpha\gamma} \nu_\gamma \right) \frac{eB}{h} \nu_\alpha \delta_{\alpha\beta} \delta_{\mathbf{q},\mathbf{q}'},$$

where we used $\nu_\alpha = (h/eB) n_\alpha$, and B_α^* expressed in terms of B according to Eq. (4.5). Defining the diagonal matrix R as

$$R_{\alpha\beta} = \left(1 - \sum_\gamma K_{\alpha\gamma} \nu_\gamma \right) \delta_{\alpha\beta} = \frac{\nu_\alpha}{\nu_\alpha^*} \delta_{\alpha\beta}, \tag{4.52}$$

we can write $[c_\alpha(\mathbf{q}), c_\beta^\dagger(\mathbf{q}')] = [(eB)^2/\pi] R_{\alpha\beta} \nu_\beta = \theta_0^{-2} (RN)_{\alpha\beta}$. Then, we define

$$c' = \theta_0 \sqrt{(RN)^{-1}}\, c, \tag{4.53}$$

or in components $c'_\alpha = \theta_0 (RN)^{-1/2}_{\alpha\alpha} c_\alpha$, so that $[c'_\alpha(\mathbf{q}), c'^\dagger_\beta(\mathbf{q}')] = \delta_{\alpha\beta}\delta_{\mathbf{q},\mathbf{q}'}$. Here, we note that the (diagonal) matrix $\theta_0 \sqrt{(RN)^{-1}}$ plays the same role as θ/μ, defined by Eqs. (4.32) and (4.37), for single-component systems. For consistency of notation, we define $\mathscr{A}' = \mathscr{A}$.

The Hamiltonian in terms of the rescaled fields $(c', \mathscr{A}')$ is therefore

$$H_{\mathrm{RPA}} = \hbar \sum_{\mathbf{q}} \begin{pmatrix} c'^{\dagger}(\mathbf{q}) & \mathscr{A}'^{\dagger}(\mathbf{q}) \end{pmatrix} \begin{pmatrix} \frac{1}{\theta_0^2}\sqrt{RN}\Theta^{\mathrm{T}}\Omega\Theta\sqrt{RN} & \frac{1}{\theta_0}\sqrt{RN}\Theta^{\mathrm{T}}\Omega \\ \frac{1}{\theta_0}\Omega\Theta\sqrt{RN} & \Omega \end{pmatrix} \begin{pmatrix} c'(\mathbf{q}) \\ \mathscr{A}'(\mathbf{q}) \end{pmatrix}$$
$$\equiv \hbar\omega_{\mathrm{c}} \sum_{\mathbf{q}} \begin{pmatrix} c'^{\dagger}(\mathbf{q}) & \mathscr{A}'^{\dagger}(\mathbf{q}) \end{pmatrix} H'_{\mathrm{mat}} \begin{pmatrix} c'(\mathbf{q}) \\ \mathscr{A}'(\mathbf{q}) \end{pmatrix}, \tag{4.54}$$

where

$$H'_{\mathrm{mat}} = \begin{pmatrix} R & \sqrt{R}C^{\mathrm{T}}\sqrt{D} \\ \sqrt{D}C\sqrt{R} & D \end{pmatrix} \tag{4.55}$$

is the *Hamiltonian matrix*, consisting of $2\kappa \times 2\kappa$ dimensionless entries. The four $\kappa \times \kappa$ blocks will be called *quadrants* in the following. The diagonal quadrants are both diagonal $\kappa \times \kappa$ matrices. The off-diagonal quadrants are each other's transpose, which proves that H'_{mat} is a symmetric matrix. From Eq. (4.54) it is clear that the eigenenergies of the Hamiltonian are given by $\hbar\omega_{\mathrm{c}}$ times the eigenvalues of H'_{mat}.

Now, we proceed with the diagonalisation of the Hamiltonian matrix H'_{mat}. First of all, already from the form of Eq. (4.51) it is visible that the Hamiltonian matrix is singular. Indeed, the vectors

$$v_\alpha = \begin{pmatrix} \mathbf{e}_\alpha \\ -\sqrt{D^{-1}}C\sqrt{R}\mathbf{e}_\alpha \end{pmatrix}, \tag{4.56}$$

with $\mathbf{e}_\alpha$ ($\alpha = 1, \ldots, \kappa$) being the ($\kappa$-dimensional) unit vectors, are eigenvectors of H'_{mat} with eigenvalue 0. This means that the Hamiltonian matrix has at least κ zero eigenvalues. These eigenvalues and their corresponding eigenvectors are associated with the transformed fields $\tilde{c}'_\alpha, \tilde{c}'^{\dagger}_\alpha$, which subsequently do not appear in the diagonalised Hamiltonian. This behaviour is similar to what we have seen for the one-component case.

The other κ eigenvalues and eigenvectors can be identified as follows. Define the 2κ-component vector

$$w_\alpha = \begin{pmatrix} \sqrt{RN}\tilde{\mathbf{g}}_\alpha \\ \sqrt{D}C\sqrt{N}\tilde{\mathbf{g}}_\alpha \end{pmatrix}, \tag{4.57}$$

where $\tilde{\mathbf{g}}_\alpha$ is a κ-component vector, the properties of which will be derived later. Multiplying H'_{mat} by the vector w_α yields

$$H'_{\mathrm{mat}} w_\alpha = \begin{pmatrix} R^{3/2}\sqrt{N}\tilde{\mathbf{g}}_\alpha + \sqrt{R}C^{\mathrm{T}}DC\sqrt{N}\tilde{\mathbf{g}}_\alpha \\ \sqrt{D}CR\sqrt{N}\tilde{\mathbf{g}}_\alpha + D^{3/2}C\sqrt{N}\tilde{\mathbf{g}}_\alpha \end{pmatrix}.$$

Now we use that $C^{\mathrm{T}}DC = E = \sqrt{N}K\sqrt{N}$ or equivalently $DC = CE = C\sqrt{N}K\sqrt{N}$. Then, the previous expression can be rewritten as

$$H'_{\mathrm{mat}} w_\alpha = \begin{pmatrix} R^{3/2}\sqrt{N}\tilde{\mathbf{g}}_\alpha + \sqrt{R}\sqrt{N}KN\tilde{\mathbf{g}}_\alpha \\ \sqrt{D}CR\sqrt{N}\tilde{\mathbf{g}}_\alpha + \sqrt{D}C\sqrt{N}KN\tilde{\mathbf{g}}_\alpha \end{pmatrix} = \begin{pmatrix} \sqrt{RN}\big(R+KN\big)\tilde{\mathbf{g}}_\alpha \\ \sqrt{D}C\sqrt{N}\big(R+KN\big)\tilde{\mathbf{g}}_\alpha \end{pmatrix}, \tag{4.58}$$

where we have used that D, R and N are diagonal so that commute with each other. Hence, w_α is an eigenvector of $H'_{\rm mat}$ if $\tilde{\mathbf{g}}_\alpha$ is an eigenvector of the matrix $R+KN$. Indeed, if $(R+KN)\tilde{\mathbf{g}}_\alpha = \mu_\alpha \tilde{\mathbf{g}_\alpha}$, then $H'_{\rm mat} w_\alpha = \mu_\alpha w_\alpha$. In other words, κ of the eigenvectors of $H'_{\rm mat}$ are constructed using the eigenvectors of $R+KN$, and the corresponding eigenvalues coincide.

The vector $\mathbf{1} = (1,\ldots,1) = \sum_\alpha \mathbf{e}_\alpha$ plays a special role here. This vector is always an eigenvector of $R+KN$, with eigenvalue equal to 1. Indeed, by the definition of R in Eq. (4.52), we have $(R\mathbf{1})_\alpha = 1 - \sum_\gamma K_{\alpha\gamma}\nu_\gamma$, and moreover, $(KN\mathbf{1})_\alpha = \sum_\gamma K_{\alpha\gamma}\nu_\gamma$, so that $(R+KN)\mathbf{1} = \mathbf{1}$. Consequently, the 2κ-component vector

$$w_1 = \begin{pmatrix} \sqrt{RN}\mathbf{1} \\ \sqrt{D}C\sqrt{N}\mathbf{1} \end{pmatrix} \tag{4.59}$$

is always an eigenvector of $H'_{\rm mat}$, with eigenvalue 1. Therefore, the Hamiltonian (4.54) has the cyclotron energy $\hbar\omega_{\rm c}$ as one of its energy eigenvalues, which is a requirement for Kohn's theorem [170] to be satisfied. The presence of other eigenvalues unequal to 1 does not contradict Kohn's theorem, which only states that *at least one* mode with the cyclotron energy must be present.

For some purposes it is more convenient to write the eigenvectors of $H'_{\rm mat}$ in terms of the eigenvectors $\mathbf{g}_\alpha$ of $R+\sqrt{N}K\sqrt{N} = R+E$. Since this matrix is symmetric, it is possible to find an orthonormal basis of its eigenvectors. In other words, there is an orthogonal matrix G and diagonal matrix F such that $R+E = G^{\rm T}FG$. The columns of $G^{\rm T}$ are the normalised eigenvectors $\mathbf{g}_\alpha$, and the diagonal elements of F are the corresponding eigenvalues μ_α. The eigenvalues of $R+E$ are equal to those of $R+KN$, and their eigenvectors ($\mathbf{g}_\alpha$ and $\tilde{\mathbf{g}}_\alpha$, respectively) relate as $\mathbf{g}_\alpha = \sqrt{N}\tilde{\mathbf{g}}_\alpha$. In terms of the eigenvectors of $R+E$, the eigenvectors w_α as defined by Eq. (4.57) can also be written as

$$w_\alpha = \begin{pmatrix} \sqrt{R}\mathbf{g}_\alpha \\ \sqrt{D}C\mathbf{g}_\alpha \end{pmatrix}. \tag{4.60}$$

This is an important result since it shows that the problem of diagonalisation of the $2\kappa\times 2\kappa$ matrix $H'_{\rm mat}$ is reduced to diagonalisation of the $\kappa\times\kappa$ matrix $R+E$.

From the property that $H'_{\rm mat}$ is symmetric, it is possible to find an orthonormal basis of eigenvectors. It is straightforward to prove that the zero-eigenvalue eigenvectors ν_α given by Eq. (4.56) are perpendicular to the vectors w_β. The orthogonality of the w_α is a direct consequence of the orthonormality of the $\mathbf{g}_\alpha$. We have

$$w_\alpha^{\rm T} w_\beta = \mathbf{g}_\alpha^{\rm T} R\mathbf{g}_\beta + \mathbf{g}_\alpha^{\rm T} C^{\rm T}\sqrt{D}\sqrt{D}C\mathbf{g}_\beta = \mathbf{g}_\alpha^{\rm T}(R+E)\mathbf{g}_\beta = \mathbf{g}_\alpha^{\rm T}\mu_\beta\mathbf{g}_\beta = \mu_\alpha\delta_{\alpha\beta}, \tag{4.61}$$

employing the fact that $\mathbf{g}_\beta$ is an eigenvector of $R+E$ with eigenvalue μ_β, and that the vectors $\mathbf{g}_\beta$ form an orthonormal basis.[14] Note however that the eigenvectors ν_α of $H'_{\rm mat}$

[14] If the $\mathbf{g}_\beta$ are not normalised, we would instead find $w_\alpha^{\rm T} w_\beta = \mu_\alpha\delta_{\alpha\beta}|\mathbf{g}_\alpha|^2$.

for the zero eigenvalue given by Eq. (4.56) are not orthogonal among themselves. Nevertheless, defining an orthonormal basis for the span of the vectors is possible, but there is *a priori* no preferred way to do this. Interestingly, the physical quantities that we may compute, such as the Hall conductivities and the quasiparticle charges, do not depend on how this basis is chosen. We will discuss this issue in more detail in Sec. 4.6.2.

Analogous to the single-component case, we assign the labels $\tilde{c}'_\alpha$ to the normalised eigenvectors corresponding to the zero eigenvalues (i.e., the v_α) and $\tilde{\mathscr{A}}_\alpha = \tilde{\mathscr{A}}'_\alpha$ to the normalised eigenvectors with nonzero eigenvalues (the w_α). Then the Hamiltonian can be written conveniently as

$$H_{\mathrm{RPA}} = \sum_{\mathbf{q}} \sum_{\alpha} \hbar\omega_{\mathrm{c}} \mu_\alpha \tilde{\mathscr{A}}^\dagger_\alpha(\mathbf{q}) \tilde{\mathscr{A}}_\alpha(\mathbf{q}), \tag{4.62}$$

with μ_α being the eigenvalues of $R+E$ as described before. Like in the one-component case, the operators $\tilde{c}'_\alpha$ are absent from the RPA Hamiltonian. As a consequence, the choice of a basis for the span of the $\tilde{c}'_\alpha$ (i.e., the κ-dimensional eigenspace belonging to the zero eigenvalues) has no effect on the Hamiltonian. Moreover, the cyclotron energy is always present among the eigenvalues of the Hamiltonian, in line with Kohn's theorem [170]. These observations clearly indicate that Eq. (4.62) is therefore a generalisation of Eq. (4.42).

The trace of the Hamiltonian matrix

An interesting quantity to study is the sum of eigenvalues of H'_{mat}, in other words, its trace. From Eq. (4.55) it follows that the $\operatorname{tr} H'_{\mathrm{mat}} = \operatorname{tr} R + \operatorname{tr} D = \operatorname{tr} R + \operatorname{tr} E$. The trace of R is given by

$$\operatorname{tr} R = \sum_\alpha R_{\alpha\alpha} = \sum_\alpha \left(1 - \sum_\gamma K_{\alpha\gamma}\nu_\gamma\right) = \kappa - \sum_{\alpha,\gamma} K_{\alpha\gamma}\nu_\gamma. \tag{4.63}$$

By the cyclicity property of the trace, we find $\operatorname{tr} E = \operatorname{tr}\sqrt{N}K\sqrt{N} = \operatorname{tr} KN$. Substituting the definition that N is the diagonal matrix of the filling factors ν_α proves that $\operatorname{tr} D = \operatorname{tr} KN = \sum_\alpha K_{\alpha\alpha}\nu_\alpha$. Together with Eq. (4.63), this yields

$$\operatorname{tr} H'_{\mathrm{mat}} = \operatorname{tr} R + \operatorname{tr} E = \kappa - \sum_{\alpha,\gamma} K_{\alpha\gamma}\nu_\gamma + \sum_\alpha K_{\alpha\alpha}\nu_\alpha = \kappa - \sum_\alpha \sum_{\gamma\neq\alpha} K_{\alpha\gamma}\nu_\gamma. \tag{4.64}$$

The trace of D cancels the diagonal part of the sum on the right hand side of Eq. (4.63), so that only the contribution for the off-diagonal part remains. Hence we may state that having positive off-diagonal elements in the Chern-Simons matrix K reduces the sum of the eigenvalues of the Hamiltonian matrix.

This trace formula is very useful for two-component systems. Since there are only two nonzero eigenvalues, of which one is equal to 1, the other can be computed directly

from the trace formula. For example, let $M = \left(\begin{smallmatrix} m & n \\ n & m \end{smallmatrix}\right)$ while $M^* = \left(\begin{smallmatrix} 1 & 0 \\ 0 & 1 \end{smallmatrix}\right)$, and $K = M - M^*$, with associated filling factors $\nu_1 = \nu_2 = 1/(m+n)$ and $\nu_1^* = \nu_2^* = 1$. We compute the energies to be $\hbar\omega_c$ and

$$\hbar\omega_c \left(1 - \sum_\alpha \sum_{\gamma\neq\alpha} K_{\alpha\gamma}\nu_\gamma\right) = \hbar\omega_c \frac{m-n}{m+n},$$

where the latter result was derived using the trace formula, without explicit diagonalisation. These energies agree with those given in Refs. [171, 172].

The trace of the Hamiltonian matrix is also related to the zero-point energy per particle. As with the one-component case, we have neglected two constant contributions. First, we have the contribution from the oscillator Hamiltonian, for which the zero-point energy is $\sum_\alpha \sum_{\mathbf{q}} \frac{1}{2}\hbar\omega_c\lambda_\alpha$, where λ_α are the eigenvalues of E. Secondly, we neglected the difference

$$\frac{1}{2ml_B^2}\sum_\alpha\sum_{\mathbf{q}} c_\alpha^\dagger(\mathbf{q}) N_{\alpha\alpha}^{-1} c_\alpha(\mathbf{q}) - \frac{1}{2m}\sum_\alpha\sum_{j_\alpha}\Pi_{\alpha,j_\alpha}\cdot\Pi_{\alpha,j_\alpha}$$

in the derivation of H^*_{RPA}. Using the commutator $[c_\alpha(\mathbf{q}), c_\alpha^\dagger(\mathbf{q})] = \theta_0^{-2}(RN)_{\alpha\alpha}$, we compute that this difference is equal to

$$\frac{1}{2ml_B^2}\frac{1}{2\theta_0}\sum_\alpha\sum_{\mathbf{q}} R_{\alpha\alpha} = \frac{\hbar}{2}\omega_c\sum_\alpha\sum_{\mathbf{q}} R_{\alpha\alpha},$$

in RPA. These two neglected constant contributions are then simply $\frac{1}{2}\hbar\omega_c\sum_{\mathbf{q}}\mathrm{tr}\,D$ and $\frac{1}{2}\hbar\omega_c\sum_{\mathbf{q}}\mathrm{tr}\,R$, respectively. They add up to $\frac{1}{2}\hbar\omega_c\sum_{\mathbf{q}}\mathrm{tr}\,H'_{\mathrm{mat}}$. Writing the trace of H'_{mat} as the sum of its eigenvalues, which is equal to $\sum_\alpha\mu_\alpha$, we can write the full RPA Hamiltonian including the zero-point energy as

$$H_{\mathrm{RPA}} + H_{\mathrm{const}} = \sum_{\mathbf{q}}\sum_\alpha \hbar\omega_c\mu_\alpha\left(\tilde{\mathscr{A}}_\alpha^\dagger(\mathbf{q})\tilde{\mathscr{A}}_\alpha(\mathbf{q}) + \tfrac{1}{2}\right). \tag{4.65}$$

which may be compared to the single-component analogue (4.43). Since the sum over $\mathbf{q}$ has as many terms as there are degrees of freedom (i.e., particles) in the system, we derive that the average zero-point energy per particle is $\frac{1}{2}\hbar\omega_c\,\mathrm{tr}\,H'_{\mathrm{mat}}$. This agrees with the single-component result, since in that case $\mathrm{tr}\,H'_{\mathrm{mat}} = 1$.

Single-component case as special case

We now show that the results for one-component system described in Sec. 4.5.1 is a special case of the results derived from the results of Sec. 4.5.2. We first make the connection between the Hamiltonians. For one component, the Hamiltonian is given by Eq. (4.54) with the 2×2 Hamiltonian matrix

$$H'_{\mathrm{mat}} = \begin{pmatrix} \nu/\nu^* & \sqrt{\nu/\nu^*}\sqrt{\nu K} \\ \sqrt{\nu/\nu^*}\sqrt{\nu K} & \nu K \end{pmatrix}.$$

Here, we have used that $R = 1 - \nu K = \nu/\nu^*$ and $D = \nu K$. With the identities $\omega_c = \omega/\nu K$ and $\mu^2 = 1/\nu^* K$ this result yields the one-component Hamiltonian (4.38). Moreover, the two eigenvectors of the Hamiltonian matrix, given by Eqs. (4.56) and (4.59) are proportional to $(1, -\mu)$ and $(\mu, 1)$, respectively, as discussed in Sec. 4.5.1. The trace formula (4.64) holds trivially in the case of one component: The matrix K has no off-diagonal elements, so the sum of the eigenvalues is simply equal to $\kappa = 1$. This is in agreement with the two eigenvalues of the Hamiltonian matrix being equal to 0 and 1.

Decomposable systems

In many cases, some off-diagonal elements of the Chern-Simons matrix and the exponent matrix may be zero, so that the system "decouples" into multiple systems with a smaller number of components than the full system. For instance, for a system with 2 pseudospin and 2 proper spin internal degrees of freedom, we might imagine Chern-Simons transformations which mix for instance only the spin components, but leave the pseudospin alone, or vice versa. A system is decomposable if we can define multiple *sectors* (sets of components), such that for indices α and β in different sectors, the entries $K_{\alpha\beta}$ of the charge matrix and $M_{\alpha\beta}$ of the exponent matrix are zero.

For simplicity, we assume that the components are ordered such that the sectors are ranges of subsequent components. Otherwise we have to do a permutation of the components first. The assumption means that K can be written in *block form*,

$$K = \begin{pmatrix} K_1 & 0 & \dots & 0 \\ 0 & K_2 & \dots & 0 \\ \vdots & \vdots & \ddots & \vdots \\ 0 & 0 & \dots & K_s \end{pmatrix}, \tag{4.66}$$

where K_a ($a = 1, \dots, s$) are square symmetric matrices along the diagonal. The number of components in each sector a is denoted by κ_a, i.e. K_a is a $\kappa_a \times \kappa_a$ matrix. The number of sectors is denoted by s, and the total number of components is $\kappa = \sum_{a=1}^{s} \kappa_a$. We furthermore assume that the exponent matrix M can be written in the same block form, i.e., with the same sectors as K.

It is not difficult to see that the diagonalisation procedure in Sec. 4.3.2 can be performed for each sector independently. The harmonic oscillator Hamiltonian can then be written as the sum of the harmonic oscillator Hamiltonians of each sector. In other words, the matrix $E = \sqrt{N}K\sqrt{N}$ has the same block form as K and M. The ground state of the full oscillator Hamiltonian is then the product of the ground states of the Hamiltonian of each sector. This observation may be used to simplify the problem of diagonalising the oscillator Hamiltonian by splitting it into several smaller diagonalisation problems. As a consequence, the orthogonal matrix C can also be written in the same block form as K. Each of the blocks of C is itself an orthogonal matrix.

By virtue of the block form of C, the off-diagonal quadrants of the Hamiltonian matrix of Eq. (4.55) also have this block form. The diagonal quadrants of H'_{mat} are diagonal, so that each quadrant has the same block form. Hence, the diagonalisation of H'_{mat} reduces to the diagonalisation of the Hamiltonian matrix in each of the sectors. Each sector a has $2\kappa_a$ eigenvalues, of which κ_a are zero. The corresponding eigenvectors are given by Eq. (4.56) with the component α in the sector a. In addition, for each sector, this matrix has at least one eigenvalue equal to 1, associated to the eigenvectors

$$w_{a1} = \begin{pmatrix} \sqrt{RN}\,\mathbf{1}_a \\ \sqrt{D}C\sqrt{N}\,\mathbf{1}_a \end{pmatrix},$$

defined by Eq. (4.60) with $\tilde{\mathbf{g}}_\alpha = \mathbf{1}_a \equiv \sum_{\alpha\in(a)} \mathbf{e}_\alpha$ the vector with ones for all components in the sector a and zeros elsewhere, which is an eigenvector of $R + KN$ with eigenvalue equal to 1.[15] This result proves that Kohn's theorem applies to each sector separately.

Since the matrix $R + KN$ has the same block form as K, this feature is also extensible to the remaining eigenvectors of $R + KN$. Given that the block $(R + KN)_a$ (the $\kappa_a \times \kappa_a$ matrix consisting only of the rows and columns belonging to sector a) has an eigenvector $\tilde{\mathbf{g}}_{a\alpha}$, then the vector $\tilde{\mathbf{g}}_\alpha$, consisting of the components of $\tilde{\mathbf{g}}_{a\alpha}$ in sector a and zero components elsewhere, is an eigenvector of the full matrix $R + E$. In other words, we may diagonalise each of the blocks separately.

As a consequence, the trace formula (4.64) can also be applied to each sector separately, by which we mean that for each sector a the sum of associated eigenvalues of either $R + E$ or H'_{mat} is equal to

$$\sum_{\alpha\in(a)} R_{\alpha\alpha} + D_{\alpha\alpha} = \kappa_a - \sum_{\alpha,\gamma\in(a)} K_{\alpha\gamma}\nu_\gamma + \sum_{\alpha\in(a)} K_{\alpha\alpha}\nu_\alpha = \kappa_a - \sum_{\alpha\in(a)} \sum_{\substack{\gamma\in(a)\\ \gamma\neq\alpha}} K_{\alpha\gamma}\nu_\gamma,$$

which denotes the partial trace of H'_{mat}, in which we sum only over the diagonal elements of the sector a. These results are very useful for determining the eigenvalues and eigenvectors of the Hamiltonian matrix, especially if the blocks are small. If there are only 1×1 or 2×2 blocks, then all eigenvalues can be computed easily. Each 1×1 block contributes the eigenvalues $0, 1$, and each 2×2 block contributes the eigenvalues $0, 0, 1$ and a fourth eigenvalue which can be computed using the trace formula. If K is diagonal, we may view it as a matrix with κ 1×1 blocks. In that case we find that the eigenvalues of the Hamiltonian matrix are 0 and 1, both with multiplicity κ. This is also the result that we would have expected based on Kohn's theorem, by treating diagonal transformations as κ independent one-component Chern-Simons transformations. We will treat some examples exhibiting this feature in Sec. 4.5.3.

[15] We compute $(R\,\mathbf{1}_a)_\alpha = 1 - \sum_{\gamma\in(a)} K_{\alpha\gamma}\nu_\gamma$, which vanishes for α outside sector a, since for α and γ in different sectors we assumed that $K_{\alpha\gamma} = 0$. We also have $(KN\,\mathbf{1}_a)_\alpha = \sum_{\gamma\in(a)} K_{\alpha\gamma}\nu_\gamma$, which is also zero for α outside sector a. Then, we prove that $(R\,\mathbf{1}_a)_\alpha + (KN\,\mathbf{1}_a)_\alpha$ is equal to 1 for α in sector a and 0 otherwise. This is exactly the same as the component α of $\mathbf{1}_a$, so that $(R + KN)\,\mathbf{1}_a = \mathbf{1}_a$.

Decoupling of the Hamiltonian in the singular case

The previous analysis was performed under the assumptions that the matrix K is nonsingular and that the filling factors are uniquely defined. However, there are many interesting cases violating these assumptions, like the two-component (mmm) Halperin state. In Sec. 4.4, we have proved that the oscillator formalism may be extended to the case of singular K by replacing the inverse of K by its pseudoinverse. Moreover, the fact that the filling factors are not uniquely determined does not lead to problems. Here, we may replace the inverses of D by their pseudoinverses in the derivation of the Hamiltonian matrix in Eq. (4.55). Then, this matrix may be diagonalised as in the nonsingular case. However, due to the appearance of $\sqrt{D^{-1}}$ in Eq. (4.56), this expression cannot be used to define the eigenvectors of H'_{mat} with eigenvalue 0. Instead, the eigenvectors with zero eigenvalue are given by

$$v_\alpha = \begin{pmatrix} \sqrt{R^{-1}} C^{\mathrm{T}} \sqrt{D}\, \mathbf{e}_\alpha \\ -\mathbf{e}_\alpha \end{pmatrix}. \tag{4.67}$$

In the nonsingular case, this expression defines an alternative basis [with respect to the one defined by Eq. (4.56)] for the zero-eigenvalue eigenspace. Equations (4.57) and (4.60) for the eigenvectors for the nonzero eigenvalues are valid without modification. The latter observation shows that the diagonalisation of the Hamiltonian still reduces to the diagonalisation of the matrix $R+E$ or $R+KN$.

The eigenvalues of $R+KN$ can be computed without more difficulty than in the nonsingular case. However, in the singular case, some of the filling factors ν_α may not be uniquely determined, but only subject to a number of mutual dependencies. Then the matrix $R+KN$ may depend explicitly on the separate filling factors. Therefore, the eigenvalues of H'_{mat} generally depend on the filling factors as well. On the other hand, since these eigenvalues are connected to physical quantities, they must not depend on any undetermined parameter in the system. Whether or not the latter condition is satisfied depends on the form of the dependencies between the filling factors, which in turn depend on the matrices K and M^*.

Fortunately, this physical requirement is satisfied if M^* and K are both proportional to the $\kappa \times \kappa$ matrix of only ones, i.e.,

$$M^* = m \begin{pmatrix} 1 & \cdots & 1 \\ \vdots & & \vdots \\ 1 & \cdots & 1 \end{pmatrix}, \qquad K = k \begin{pmatrix} 1 & \cdots & 1 \\ \vdots & & \vdots \\ 1 & \cdots & 1 \end{pmatrix}.$$

Indeed, in this situation, the eigenvalues of the Hamiltonian matrix are κ copies of 0, a single 1, and $\kappa - 1$ copies of $1 - k\nu_{\mathrm{T}}$, where $\nu_{\mathrm{T}} = 1/(m^* + k)$ is the (constant) total filling factor of the system. If the matrices $M*$ and K can be decomposed into blocks of this form (see the previous subsection), then the requirement is satisfied as well, and the eigenvalues of the Hamiltonian matrix will then be independent on the separate filling

factors. These examples have in common that the dependencies between the filling factors are given by equations of the form

$$\nu_{\alpha_1} + \nu_{\alpha_2} + \ldots + \nu_{\alpha_j} = \text{const.} \tag{4.68}$$

From a physical perspective, dependencies of a form different than Eq. (4.68) cannot appear due to the requirement that the total number of electrons (or equivalently, total filling factor) is conserved. In other words, one particle of a certain component can be exchanged only for exactly one particle of a different component. A counterexample (for $\kappa = 3$), where the matrix K is singular but not equal to a constant times the matrix of ones is given by

$$K = \begin{pmatrix} 4 & 2 & 0 \\ 2 & 2 & 2 \\ 0 & 2 & 4 \end{pmatrix}, \qquad M^* = \begin{pmatrix} 1 & 1 & 1 \\ 1 & 1 & 1 \\ 1 & 1 & 1 \end{pmatrix},$$

which leads to the equations $\nu_1+\nu_2+\nu_3 = \frac{1}{3}$ and $\nu_1 = \nu_3$, the latter of which is not of the form in Eq. (4.68). Here, $\operatorname{tr} H'_{\text{mat}} = \operatorname{tr}(R + KN) = \frac{5}{3} + 4\nu_1$, which is explicitly dependent on ν_1. This proves that at least one of the eigenvalues depends on ν_1. This example shows that if Eq. (4.68) is not satisfied, then the eigenvalues may depend on the filling factors, which is an unphysical situation. Although here the total filling factor seems to be conserved, an exchange of a particle 2 with a particle of another component violates the conservation of total particle number, due the condition $\nu_1 = \nu_3$, which means a particle of component 2 can only be exchanged for two particles (one of component 1 and one of component 3). In the following, we will avoid this unphysical situation by assuming that all dependencies of the filling factor are of the form (4.68).

4.5.3 Examples

Since after the diagonalisation of the full Hamiltonian we find physical eigenvalues, we will elaborate some examples with physical significance. We will discuss and compare the results for examples of systems with 1, 2, and 4 components.

First, we investigate the two-component example discussed before. Given $M^* = \left(\begin{smallmatrix} 1 & 0 \\ 0 & 1 \end{smallmatrix}\right)$ and $K = \left(\begin{smallmatrix} m-1 & n \\ n & m-1 \end{smallmatrix}\right)$, the matrix $R + E$ has the eigenvalues $\mu_1 = 1$ and $\mu_2 = (m-n)/(m+n)$. The eigenvector belonging to the eigenvalue 1 is $\mathbf{g}_1 = (1,1)/\sqrt{2}$, as expected. This mode is always present at the cyclotron energy, and is called the *in-phase* mode [40], since all components contribute to it with the same amount. The other mode is the so-called *out-of-phase* mode, with the corresponding eigenvector equal to $\mathbf{g}_2 = (1,-1)/\sqrt{2}$, which is perpendicular to the eigenvector of the in-phase mode.

Secondly, we investigate the results of adding an **SU**(2) symmetry to a Laughlin state. Physically speaking, we compare a spin-polarised and a spin-symmetric state at the same filling factor. To reach this aim, we analyse the Laughlin $\nu = 1/m$ state and the Halperin (mmm) state ($\nu_\uparrow + \nu_\downarrow = 1/m$). Starting with the latter, with $M^* = \left(\begin{smallmatrix} 1 & 1 \\ 1 & 1 \end{smallmatrix}\right)$

and $K = \left(\begin{smallmatrix} m-1 & m-1 \\ m-1 & m-1 \end{smallmatrix}\right)$, we find that the nonzero eigenvalues of the Hamiltonian matrix are $\mu_1 = 1$ and $\mu_2 = 1/m$. The eigenvectors of $R+E$ are proportional to $(\sqrt{\nu_\uparrow}, \sqrt{\nu_\downarrow})$ and $(-\sqrt{\nu_\downarrow}, \sqrt{\nu_\uparrow})$, corresponding to the in-phase and out-of-phase modes, respectively. In the case of equal filling factors, these eigenvectors are equal to those of the in-phase and out-of-phase modes in the non-**SU**(2)-symmetric case. If the modes are expressed in terms of eigenvectors of $R + KN$ instead, then the in-phase mode becomes proportional to $(1,1)$ for all filling factors, while the out-of-phase mode still depends on the filling factors.

The in-phase mode corresponds to the single mode of the Laughlin state, while the out-of-phase mode is only present in the two-component case, because the latter is related to spin degrees of freedom which are absent in the single-component case. Although this idea looks quite trivial when comparing two-component states with one-component states, it becomes more interesting for systems with more components. In order to demonstrate this mechanism, we will show a comparison between a four-component and a two-component state further on.

The study of our model for four components is relevant for systems that contain two pseudospin and two (proper) spin degrees of freedom, as is the case for bilayers with the real spin included. The four-component case is particularly interesting, since it allows for a partial symmetry as well as the full symmetry: Instead of the full symmetry **SU**(4), it is possible to have a partial symmetry in either the spin ($\mathbf{SU}(2)_{\mathrm{sp}}$) or in the pseudospin ($\mathbf{SU}(2)_{\psi\mathrm{sp}}$), or in spin and pseudospin separately ($\mathbf{SU}(2)_{\mathrm{sp}} \times \mathbf{SU}(2)_{\psi\mathrm{sp}}$). We label the four components by $1\uparrow, 1\downarrow, 2\uparrow, 2\downarrow$, where $1,2$ label the pseudospin and $\uparrow,\downarrow$ the spin components. In this basis, we use the specific form

$$K = \begin{pmatrix} k_+ & k_- & k'_+ & k'_- \\ k_- & k_+ & k'_- & k'_+ \\ k'_+ & k'_- & k_+ & k_- \\ k'_- & k'_+ & k_- & k_+ \end{pmatrix} \tag{4.69}$$

of the charge matrix, where k_+, k_-, k'_+, k'_- are integer coefficients. Following the results of Sec. 4.4.1, we will assume that this matrix is nonnegative definite, which translates into the conditions

$$\begin{aligned} k_+ + k_- + k'_+ + k'_- &\geq 0, \\ k_+ + k_- - k'_+ - k'_- &\geq 0, \\ k_+ - k_- - k'_+ + k'_- &\geq 0, \\ k_+ - k_- + k'_+ - k'_- &\geq 0. \end{aligned} \tag{4.70}$$

Furthermore, assuming that all components are equally filled, $\nu_{1\uparrow} = \nu_{1\downarrow} = \nu_{2\uparrow} = \nu_{2\downarrow} \equiv$

ν_0, we compute that the eigenvalues and eigenvectors of $R + KN$ are given by

$$\begin{aligned} \mu_1 &= 1, & \tilde{\mathbf{g}}_1 &= \tfrac{1}{2}(1,1,1,1), \\ \mu_2 &= 1 - 2(k'_+ + k'_-)\nu_0, & \tilde{\mathbf{g}}_2 &= \tfrac{1}{2}(1,1,-1,-1), \\ \mu_3 &= 1 - 2(k_- + k'_-)\nu_0, & \tilde{\mathbf{g}}_3 &= \tfrac{1}{2}(1,-1,1,-1), \\ \mu_4 &= 1 - 2(k_- + k'_+)\nu_0, & \tilde{\mathbf{g}}_4 &= \tfrac{1}{2}(1,-1,-1,1). \end{aligned} \tag{4.71}$$

Besides the fully-in-phase mode $\tilde{\mathbf{g}}_1$ at the cyclotron energy, we now also have the mode $\tilde{\mathbf{g}}_2$ where the spin is in phase and the pseudospin is out of phase, the mode $\tilde{\mathbf{g}}_3$ where the spin is out of phase and the pseudospin is in phase, and the mode $\tilde{\mathbf{g}}_4$ where both spin and pseudospin are out of phase.

We will demonstrate this behaviour with a specific example, for which the total filling factor is $4\nu_0 = \frac{4}{9}$, which is mentioned in Ref. [173] in the context of **SU**(4) states in graphene. We start with the choice $\nu^*_{1\uparrow} = \nu^*_{1\downarrow} = \nu^*_{2\uparrow} = \nu^*_{2\downarrow} = 1$, or, in other words, we take M^* to be equal to the 4×4 identity matrix. Given these assumptions and the matrix equation $\sum_\beta M_{\alpha\beta}\nu_\beta = 1$ (where $M = K + M^*$), we find that the possible choices of the charge matrix must satisfy $1 + k_+ + k_- + k'_+ + k'_- = 1/\nu_0 = 9$ together with the conditions (4.70). In the following, we limit ourselves to the case $k_+ \geq k_- \geq k'_+ \geq k'_- \geq 0$.

In Sec. Sec. 4.3.3, we have observed that larger coefficients in the exponent matrix lead to larger exponents in the Halperin wave function. In the plasma analogy, larger exponents correspond to larger repulsive interactions between the corresponding components [168]. With our assumptions, this correspondence means physically that the interaction of an electron of a certain component with another electron of the same component is the strongest, followed by the interaction between electrons in the same layer, but with a different spin. Interactions between electrons in different layers are even weaker, and those with different spins are the weakest in the case $k'_+ \geq k'_-$. This is the most relevant physical situation in a bilayer system. In order to apply this analysis also to other situations, one may perform permutations of the off-diagonal coefficients k_-, k'_+, and k'_-.

In Table 4.1 we list all possible choices of coefficients under the aforementioned conditions, and we give the eigenvalues of $R+E$ for each of them. Several observations can be made. For $(k_+, k_-, k'_+, k'_-) = (8,0,0,0)$, the matrices K and M are both diagonal, so that all components decouple. In other words, the system may be treated as four separate one-component systems. Applying Kohn's theorem to each of the components, we find that all eigenvalues of $R + E$ must be equal to 1. This is in accordance with the result in Table 4.1, by the observation that the basis of the single-component eigenvectors (i.e., the unit vectors of four components) is the same as the basis of the eigenvectors given by Eq. (4.71).

In the same manner, only the pseudospin components may be decoupled. This happens for $(k_+, k_-, k'_+, k'_-) = (6,2,0,0)$ and $(k_+, k_-, k'_+, k'_-) = (4,4,0,0)$. In those cases, the system may be treated as two separate layers; both are two-component systems.

k_+	k_-	k'_+	k'_-	$\dim\ker K$	μ_1	μ_2	μ_3	μ_4
8	0	0	0	0	1	1	1	1
6	2	0	0	0	1	1	$\frac{5}{9}$	$\frac{5}{9}$
6	1	1	0	0	1	$\frac{7}{9}$	$\frac{7}{9}$	$\frac{5}{9}$
4	4	0	0	2	1	1	$\frac{1}{9}$	$\frac{1}{9}$
4	3	1	0	1	1	$\frac{7}{9}$	$\frac{1}{3}$	$\frac{1}{9}$
4	2	2	0	1	1	$\frac{5}{9}$	$\frac{5}{9}$	$\frac{1}{9}$
4	2	1	1	0	1	$\frac{5}{9}$	$\frac{1}{3}$	$\frac{1}{3}$
2	2	2	2	3	1	$\frac{1}{9}$	$\frac{1}{9}$	$\frac{1}{9}$

Table 4.1: Eigenvalues of the four-component system with total filling factor $\frac{4}{9}$, with M^* equal to the identity matrix, and K given by Eq. (4.69). We assume $k_+ \geq k_- \geq k'_+ \geq k'_- \geq 0$. The "co-rank" of K, $\dim\ker K \equiv \kappa - \operatorname{rank} K$ denotes the number of zero eigenvalues of K, or equivalently, the number of conditions in Eq. (4.70) that become equalities. The eigenvalues μ_α and the corresponding eigenvectors are listed in the same order as in Eq. (4.71).

Since Kohn's theorem applies to both layers, both pseudospin components have one eigenvalue equal to 1. The two modes at the cyclotron energy have the spin components in phase, while the pseudospin components can be either in-phase or out-of-phase. (The cyclotron modes can be described equivalently as linear combinations of the pseudospin-decoupled modes, $(1,1,0,0)/\sqrt{2}$ and $(0,0,1,1)/\sqrt{2}$). The modes with the spin out of phase ($\tilde{\mathbf{g}}_3$ and $\tilde{\mathbf{g}}_4$) have equal eigenvalues, by virtue of $k'_- = k'_+$. We note that the eigenvalues of the spin-out-of-phase modes are equal to those of the two-component system in the state $(m,m,n) = (k_+ + 1, k_+ + 1, k_-)$, which shows that we may indeed treat the system as if the pseudospin components were decoupled. This example demonstrates the results derived in Sec. 4.5.2 for decomposable systems. For the fully symmetric charge matrix, $(k_+, k_-, k'_+, k'_-) = (2,2,2,2)$, the three out-of-phase modes have equal eigenvalues.

4.6 Densities and constraints

The decoupling transformation described in the previous section affects also the density operator $\rho(\mathbf{q}) = L^{-2}\sum_j e^{-i\mathbf{q}\cdot\mathbf{r}_j}$ (where $\mathbf{r}_j$ are the coordinates of the electrons), an essential quantity in the formulation of the theory of the fractional quantum Hall effect. This quantity satisfies the magnetic translation (or Girvin-MacDonald-Platzman [174]) algebra. Thus, in order to formulate the Hamiltonian theory of the composite fermions, one needs to compute how this operator transforms under the decoupling transformation presented in the previous section. For single-component systems, the transformations of the density and constraint operators have been computed by Murthy and Shankar in Ref. [24]. In this description, the transformation is computed

in linear order in the momentum. However, the algebra for the approximate transformed operators does not close. Shankar [25] realised that the resulting expressions should be considered as the low-order terms in the expansion of two exponentials, which can be interpreted as density operators for the electron guiding center and for a pseudovortex (the latter of which is does not appear in the Hamiltonian). A linear combination of this operators gives the composite-fermion density operator, necessary to compute the form factors in the resulting theory.

This result motivates the need to formulate a similar theory for multicomponent systems. However, this theory is more involved than the single-component version, since the decoupling transformation also involves a mixing of different components, rather than only a rotation between the operators $\tilde{c}(\mathbf{q})$ and $\tilde{\mathscr{A}}(\mathbf{q})$. This mixing complicates the extension of the linearised transformed density and constraint operators to an all-momentum theory. However, another motivation to derive the approximate expressions is that they can be rewritten in terms of current operators, from which one can derive the response to the application of an external electric potential. This response is the Hall conductivity of the system. In this section, we generalise this derivation to multicomponent systems in order to find the Hall conductivity. Although a full derivation as for the single-component theory in Ref. [24] is not required, we do present a generalised version of this theory because it serves as the basis for the all-momentum Hamiltonian theory, possibly to be formulated in a future work. As with the previous section, we first review the single-component derivation of Ref. [24] to present the framework that we generalise.

4.6.1 Review: One component

Transformation of full density

In order to obtain the density $\rho(\mathbf{q})$ in terms of the oscillators, we will follow an analogous procedure as the one presented by Murthy and Shankar in Ref. [24]. Let us first define the action of the transformation S, which is an $\mathbf{SO}(2)$ rotation in the space $(c', \mathscr{A}')$. Recalling that S, given by Eqs. (4.39), is just an $\mathbf{SO}(2)$ rotation, we can write its generator (in operator form) as

$$S_0 = \sum_{\mathbf{q}} \left(c'^{\dagger}(\mathbf{q}) \mathscr{A}'(\mathbf{q}) - \mathscr{A}'^{\dagger}(\mathbf{q}) c'(\mathbf{q}) \right).$$

For a given operator Z, let us define its image $Z(u)$ under a rotation with angle u, as

$$Z(u) = e^{-iuS_0} Z(0) e^{iuS_0} \qquad (Z(0) \equiv Z).$$

The identity

$$\frac{\mathrm{d}}{\mathrm{d}u} \left(e^{-iuS_0} Z(0) e^{iuS_0} \right)|_{u=0} = i e^{-iuS_0} [Z(0), S_0] e^{iuS_0}|_{u=0} = [Z(0), S_0]$$

shows that the commutator $[Z(0), S_0]$ determines how Z transforms under infinitesimal rotations.

Now, we investigate how the full density operator

$$\rho(\mathbf{q}) = L^{-2}\sum_j e^{-i\mathbf{q}\cdot\mathbf{r}_j} \tag{4.72}$$

transforms under the rotation S in the $(c', \mathscr{A}')$ plane. The density $\rho(\mathbf{q})$ represents a physical quantity, so that it is invariant under this transformation; the result of the transformation is the same quantity, but represented in a different basis. To compute the transformation rules for $\rho(\mathbf{q})$, we compute the commutator

$$\begin{aligned}[\rho(\mathbf{q}), c(\mathbf{q}')] &= \sum_{j,k}\left[L^{-2}e^{-i\mathbf{q}\cdot\mathbf{r}_j}, L^{-1}\hat{q}'_+\Pi^-_k e^{-i\mathbf{q}'\cdot\mathbf{r}_k}\right] = \frac{1}{L^3}\sum_{j,k}\hat{q}'_+\hbar|\mathbf{q}|\hat{q}_-\delta_{jk}e^{-i\mathbf{q}\cdot\mathbf{r}_j}e^{-i\mathbf{q}'\cdot\mathbf{r}_k} \\ &= \frac{1}{L^3}\sum_j \hat{q}'_+\hbar|\mathbf{q}|\hat{q}_- e^{-i(\mathbf{q}+\mathbf{q}')\cdot\mathbf{r}_j} \approx -\hbar|\mathbf{q}|nL^{-1}\delta_{\mathbf{q},-\mathbf{q}'},\end{aligned} \tag{4.73}$$

where we have used the RPA [Eq. (4.28)] and we recall that $\hat{q}_\pm = (q_x \pm iq_y)/|\mathbf{q}|$. Here we have also used the identity

$$[e^{-i\mathbf{q}\cdot\mathbf{r}_j}, \Pi^-_k] = \hbar q_-\delta_{jk}e^{-i\mathbf{q}\cdot\mathbf{r}_j} = \hbar|\mathbf{q}|\hat{q}_-\delta_{jk}e^{-i\mathbf{q}\cdot\mathbf{r}_j},$$

which follows from

$$\begin{aligned}[e^{-i\mathbf{q}\cdot\mathbf{r}_j}, \Pi^\mu_k] &= \sum_\nu \frac{\partial}{\partial r^\nu_j}(e^{-i\mathbf{q}\cdot\mathbf{r}_j})[r^\nu_j, p^\mu_k + eA^{*\mu}_k] = \sum_\nu(-iq^\nu)e^{-i\mathbf{q}\cdot\mathbf{r}_j}(i\hbar\delta_{jk}\delta^{\mu\nu}) \\ &= \hbar\mathbf{q}^\mu\delta_{jk}e^{-i\mathbf{q}\cdot\mathbf{r}_j},\end{aligned}$$

where the superscripts μ and ν denote spatial indices (x, y). Analogously, we derive

$$[\rho(\mathbf{q}), c^\dagger(\mathbf{q}')] = \hbar|\mathbf{q}|nL^{-1}\delta_{\mathbf{q},\mathbf{q}'}, \tag{4.74}$$

(in RPA). Moreover, $\rho(\mathbf{q})$ commutes with the oscillators $\mathscr{A}(\mathbf{q})$ and $\mathscr{A}^\dagger(\mathbf{q})$. Then, we derive the commutator of $\rho(\mathbf{q})$ with the generator S_0,

$$\begin{aligned}[\rho(\mathbf{q}), S_0] &= \sum_{\mathbf{q}'}\Big([\rho(\mathbf{q}), c'^\dagger(\mathbf{q}')]\mathscr{A}'(\mathbf{q}') - \mathscr{A}'^\dagger(\mathbf{q}')[\rho(\mathbf{q}), c'(\mathbf{q}')]\Big) \\ &= \frac{\hbar|\mathbf{q}|n\theta}{L\mu}\big(\mathscr{A}'(\mathbf{q}) + \mathscr{A}'^\dagger(-\mathbf{q})\big),\end{aligned}$$

where we recall that $c' = (\theta/\mu)\,c$. On the other hand, we have

$$\begin{aligned}[c'(\mathbf{q}) + c'^\dagger(-\mathbf{q}), S_0] &= \sum_{\mathbf{q}'}\Big([c'(\mathbf{q}), c'^\dagger(\mathbf{q}')]\mathscr{A}'(\mathbf{q}') - \mathscr{A}'^\dagger(\mathbf{q}')[c'^\dagger(-\mathbf{q}), c'(\mathbf{q}')]\Big) \\ &= \mathscr{A}'(\mathbf{q}) + \mathscr{A}'^\dagger(-\mathbf{q}),\end{aligned}$$

by which we observe that

$$\rho'(\mathbf{q}) \equiv \frac{L\mu}{\hbar|\mathbf{q}|n\theta}\rho(\mathbf{q}) \tag{4.75}$$

transforms in the same way as $c'(\mathbf{q}) + c'^{\dagger}(-\mathbf{q})$ does. Thus,

$$\rho(\mathbf{q},u) - \rho'(\mathbf{q},0) = \big(c'(\mathbf{q},u) + c'^{\dagger}(-\mathbf{q},u)\big) - \big(c'(\mathbf{q},0) + c'^{\dagger}(-\mathbf{q},0)\big). \tag{4.76}$$

In the following, let us write the result of the transformation as

$$\begin{pmatrix}\tilde{c}'\\ \tilde{\mathscr{A}}'\end{pmatrix} = S\begin{pmatrix}c'\\ \mathscr{A}'\end{pmatrix} = \frac{1}{\sqrt{1+\mu^2}}\begin{pmatrix}1 & -\mu\\ \mu & 1\end{pmatrix}\begin{pmatrix}c'\\ \mathscr{A}'\end{pmatrix}, \tag{4.77}$$

Therefore, the transformed quantity $\tilde{\rho}'(\mathbf{q}) \equiv \rho'(\mathbf{q},u)$ satisfies the equation

$$\tilde{\rho}'(\mathbf{q}) - \rho'(\mathbf{q}) = \big(\tilde{c}'(\mathbf{q}) + \tilde{c}'^{\dagger}(-\mathbf{q})\big) - \big(c'(\mathbf{q}) + c'^{\dagger}(-\mathbf{q})\big). \tag{4.78}$$

We write this quantity in terms of the transformed operators $\tilde{c}$ and $\tilde{\mathscr{A}}$, and their conjugates. With $c' = (\tilde{c}' + \mu\tilde{\mathscr{A}}')/\sqrt{1+\mu^2}$, we obtain

$$\begin{aligned}\tilde{\rho}'(\mathbf{q}) - \rho'(\mathbf{q}) &= \big(\tilde{c}'(\mathbf{q}) + \tilde{c}'^{\dagger}(-\mathbf{q})\big) - \frac{1}{\sqrt{1+\mu^2}}\Big[\big(\tilde{c}'(\mathbf{q}) + \tilde{c}'^{\dagger}(-\mathbf{q})\big) + \mu\big(\tilde{\mathscr{A}}'(\mathbf{q}) + \tilde{\mathscr{A}}'^{\dagger}(-\mathbf{q})\big)\Big]\\ &= -\frac{1}{\sqrt{1+\mu^2}}\Big[\Big(1-\sqrt{1+\mu^2}\Big)\big(\tilde{c}'(\mathbf{q}) + \tilde{c}'^{\dagger}(-\mathbf{q})\big) + \mu\big(\tilde{\mathscr{A}}'(\mathbf{q}) + \tilde{\mathscr{A}}'^{\dagger}(-\mathbf{q})\big)\Big].\end{aligned} \tag{4.79}$$

Now, we undo the rescaling of the densities and operators, as set by Eq. (4.75), by $c' = (\theta/\mu)c$, and by $\mathscr{A}' = \mathscr{A}$, with similar relations for the transformed quantities ($\tilde{\rho}$, $\tilde{c}$, and $\tilde{\mathscr{A}}$). Then, we find

$$\begin{aligned}\tilde{\rho}(\mathbf{q}) - \rho(\mathbf{q}) &= -\frac{\hbar|\mathbf{q}|n\theta}{L\mu}\frac{1}{\sqrt{1+\mu^2}}\left[\Big(1-\sqrt{1+\mu^2}\Big)\frac{\theta}{\mu}\big(\tilde{c}(\mathbf{q}) + \tilde{c}^{\dagger}(-\mathbf{q})\big) + \mu\big(\tilde{\mathscr{A}}(\mathbf{q}) + \tilde{\mathscr{A}}^{\dagger}(-\mathbf{q})\big)\right]\\ &= -\frac{\hbar|\mathbf{q}|n}{L}\left[\left(\frac{1}{\sqrt{1+\mu^2}} - 1\right)\frac{\theta^2}{\mu^2}\big(\tilde{c}(\mathbf{q}) + \tilde{c}^{\dagger}(-\mathbf{q})\big) + \frac{\theta}{\sqrt{1+\mu^2}}\big(\tilde{\mathscr{A}}(\mathbf{q}) + \tilde{\mathscr{A}}^{\dagger}(-\mathbf{q})\big)\right].\end{aligned} \tag{4.80}$$

We substitute the identities

$$\frac{\mu^2}{\theta^2} = 2eB^*\hbar n = 2eB(1-\nu K)\hbar n, \tag{4.81}$$

$$\hbar n\theta = \frac{1}{2\sqrt{\pi K}}, \tag{4.82}$$

$$1+\mu^2 = \frac{1}{\nu K}, \tag{4.83}$$

which follow from the definitions Eqs. (4.32) and (4.37), into Eq. (4.80), and we obtain

$$\begin{aligned}\rho(\mathbf{q}) &= \tilde{\rho}(\mathbf{q}) + \frac{|\mathbf{q}|}{2LeB(1-\nu K)}\left(\sqrt{\nu K}-1\right)\left(\tilde{c}(\mathbf{q})+\tilde{c}^{\dagger}(-\mathbf{q})\right) + \frac{|\mathbf{q}|\sqrt{\nu K}}{2L\sqrt{\pi K}}\left(\tilde{\mathscr{A}}(\mathbf{q})+\tilde{\mathscr{A}}^{\dagger}(-\mathbf{q})\right)\\ &= \tilde{\rho}(\mathbf{q}) - \frac{|\mathbf{q}|}{2LeB(1+\sqrt{\nu K})}\left(\tilde{c}(\mathbf{q})+\tilde{c}^{\dagger}(-\mathbf{q})\right) + \frac{|\mathbf{q}|\sqrt{\nu K}}{2L\sqrt{\pi K}}\left(\tilde{\mathscr{A}}(\mathbf{q})+\tilde{\mathscr{A}}^{\dagger}(-\mathbf{q})\right).\end{aligned}$$

At this point, we rewrite

$$\tilde{\rho}(\mathbf{q}) = \sum_j e^{-i\mathbf{q}\cdot\mathbf{r}_j}, \tag{4.84}$$

$$|\mathbf{q}|\left(\tilde{c}(\mathbf{q})+\tilde{c}^{\dagger}(-\mathbf{q})\right) = -2iL^{-1}\sum_j(\mathbf{q}\wedge\Pi_j)e^{-i\mathbf{q}\cdot\mathbf{r}_j}, \tag{4.85}$$

where the notation $\mathbf{q}\wedge\tilde{\Pi}_j$ stands for $q_x\tilde{\Pi}_j^y - q_y\tilde{\Pi}_j^x$. Here, we note that these identities are similar to the ones in the "untransformed" setting, since the represent physical quantities, the values of which are unaffected by the transformation. Substituting Eqs. (4.84) and (4.85), we obtain

$$\tilde{\rho}(\mathbf{q}) = \bar{\rho}(\mathbf{q}) + \rho_{\mathrm{osc}}(\mathbf{q}), \tag{4.86a}$$

with

$$\bar{\rho}(\mathbf{q}) = \frac{1}{L^2}\sum_j\left[1+\frac{il_B^2}{\hbar(1+\sqrt{\nu K})}(\mathbf{q}\wedge\Pi_j)\right]e^{-i\mathbf{q}\cdot\mathbf{r}_j} \tag{4.86b}$$

and

$$\rho_{\mathrm{osc}}(\mathbf{q}) = \frac{|\mathbf{q}|\sqrt{\nu K}}{2L\sqrt{\pi K}}\left(\tilde{\mathscr{A}}(\mathbf{q})+\tilde{\mathscr{A}}^{\dagger}(-\mathbf{q})\right), \tag{4.86c}$$

which agrees with the result found by Shankar and Murthy [23, 24]. The transformed density is given as the sum of two terms $\bar{\rho}(\mathbf{q})+\rho_{\mathrm{osc}}(\mathbf{q})$, where $\bar{\rho}(\mathbf{q})$ is the term containing the momentum operators $\tilde{\Pi}_j$, and $\rho_{\mathrm{osc}}(\mathbf{q})$ is the term involving the ladder operators $\tilde{\mathscr{A}}(\mathbf{q})$ and $\tilde{\mathscr{A}}^{\dagger}(-\mathbf{q})$. We observe that the difference between $\bar{\rho}(\mathbf{q})$ and $\rho(\mathbf{q})$ is of the form $e^{-i\mathbf{q}\cdot\tilde{\mathbf{r}}_j}$ multiplied by an expression *linear* in $\mathbf{q}$.

Transformation of the constraint

We treat the transformation of the constraint (4.9), which we write as $\chi(\mathbf{q})\,|\phi_{\mathrm{phys}}\rangle = 0$, in the same fashion as the density operator. The constraint operator $\chi(\mathbf{q})$ is given by

$$\chi(\mathbf{q}) = \delta\rho(\mathbf{q}) - \frac{e|\mathbf{q}|}{2\pi\hbar K}a^{\circ}(\mathbf{q}). \tag{4.87}$$

For clarity, we switch to the notation

$$\chi'(\mathbf{q}) \equiv \frac{L\mu}{\hbar|\mathbf{q}|n\theta}\chi(\mathbf{q}) = \delta\rho'(\mathbf{q}) - \frac{L}{2n\pi\hbar^2 K}\frac{\mu}{\theta}e\,a^\circ(\mathbf{q}), \tag{4.88}$$

analogous to Eq. (4.75). The second term on the right-hand side is equal to

$$\frac{L}{2n\pi\hbar^2 K}\frac{\mu}{\theta}e\,a^\circ(\mathbf{q}) = \frac{L}{2n\pi\hbar^2 K}\frac{\mu}{\theta}\frac{1}{2}\frac{\sqrt{4\pi\hbar^2 K}}{L}\big(\mathscr{A}(\mathbf{q}) + \mathscr{A}^\dagger(-\mathbf{q})\big) = \mu\big(\mathscr{A}(\mathbf{q}) + \mathscr{A}^\dagger(-\mathbf{q})\big),$$

where we used the identity $2n\pi\hbar^2 K\theta = \sqrt{\pi\hbar^2 K}$, which follows from Eq. (4.82), and we have written a° in terms of $\mathscr{A}$ and $\mathscr{A}^\dagger$ by virtue of Eqs. (4.30). Furthermore, we recall that $\mathscr{A}' = \mathscr{A}$, so that we may write the constraint as

$$\chi'(\mathbf{q}) = \delta\rho'(\mathbf{q}) - \mu\big(\mathscr{A}'(\mathbf{q}) + \mathscr{A}'^\dagger(-\mathbf{q})\big). \tag{4.89}$$

Next, we write the constraint in terms of the transformed quantities $\delta\tilde{\rho}$, $\tilde{c}$ and $\tilde{\mathscr{A}}$. We may write the $\delta\rho'(\mathbf{q})$ on the right-hand side of Eq. (4.89) in terms of its transformed version $\delta\tilde{\rho}'(\mathbf{q})$ by using Eq. (4.79), thereby noting that $\delta\rho(\mathbf{q}) = \rho(\mathbf{q})$ and similarly $\delta\tilde{\rho}(\mathbf{q}) = \tilde{\rho}(\mathbf{q})$ for all nonzero $\mathbf{q}$.[16] The second term on the right-hand side of Eq. (4.89) can be rewritten as

$$\mu\big(\mathscr{A}'(\mathbf{q}) + \mathscr{A}'^\dagger(-\mathbf{q})\big) = \frac{\mu}{\sqrt{1+\mu^2}}\Big[\big(\tilde{\mathscr{A}}'(\mathbf{q}) + \tilde{\mathscr{A}}'^\dagger(-\mathbf{q})\big) - \mu\big(\tilde{c}'(\mathbf{q}) + \tilde{c}'^\dagger(-\mathbf{q})\big)\Big],$$

in terms of transformed operators $\tilde{c}'$ and $\tilde{\mathscr{A}}'$. Then, we find that the constraint (4.89) is written in terms of the transformed quantities as

$$\begin{aligned}\chi'(\mathbf{q}) = \delta\tilde{\rho}'(\mathbf{q}) &+ \frac{1}{\sqrt{1+\mu^2}}\Big[\Big(1-\sqrt{1+\mu^2}\Big)\big(\tilde{c}'(\mathbf{q}) + \tilde{c}'^\dagger(-\mathbf{q})\big) + \mu\big(\tilde{\mathscr{A}}'(\mathbf{q}) + \tilde{\mathscr{A}}'^\dagger(-\mathbf{q})\big)\Big] \\ &- \frac{\mu}{\sqrt{1+\mu^2}}\Big[\big(\tilde{\mathscr{A}}'(\mathbf{q}) + \tilde{\mathscr{A}}'^\dagger(-\mathbf{q})\big) - \mu\big(\tilde{c}'(\mathbf{q}) + \tilde{c}'^\dagger(-\mathbf{q})\big)\Big].\end{aligned}$$

The oscillator terms cancel, so that we are left with

$$\chi'(\mathbf{q}) = \delta\tilde{\rho}'(\mathbf{q}) - \Big(1-\sqrt{1+\mu^2}\Big)\big(\tilde{c}'(\mathbf{q}) + \tilde{c}'^\dagger(-\mathbf{q})\big) = \delta\tilde{\rho}'(\mathbf{q}) - \left(1-\frac{1}{\sqrt{\nu K}}\right)\big(\tilde{c}'(\mathbf{q}) + \tilde{c}'^\dagger(-\mathbf{q})\big). \tag{4.90}$$

Undoing the rescaling of $\chi(\mathbf{q})$ defined in Eq. (4.88), we obtain

$$\chi(\mathbf{q}) = \delta\tilde{\rho}(\mathbf{q}) - \frac{\hbar|\mathbf{q}|n\theta}{L\mu}\frac{\theta}{\mu}\left(1-\frac{1}{\sqrt{\nu K}}\right)\big(\tilde{c}(\mathbf{q}) + \tilde{c}^\dagger(-\mathbf{q})\big),$$

recalling that $c' = (\theta/\mu)c$ and $1+\mu^2 = 1/\nu K$. Using Eq. (4.81), we proceed in the same way as for the transformed density, which yields

$$\chi(\mathbf{q}) = \delta\tilde{\rho}(\mathbf{q}) + \frac{|\mathbf{q}|}{2LeB\sqrt{\nu K}(1+\sqrt{\nu K})}\big(\tilde{c}(\mathbf{q}) + \tilde{c}^\dagger(-\mathbf{q})\big).$$

[16] For $\mathbf{q} = 0$, we have $\delta\rho(\mathbf{q}) = 0$ and $|\mathbf{q}|a^\circ(\mathbf{q}) = 0$, so that $\chi'(0) = 0$ automatically.

By employing the identities (4.84) and (4.85), we find

$$\chi(\mathbf{q}) = \frac{1}{L^2}\sum_j \left[1 - \frac{i l_B^2}{\hbar\sqrt{\nu K}(1+\sqrt{\nu K})}(\mathbf{q}\wedge\Pi_j)\right] e^{-i\mathbf{q}\cdot\mathbf{r}_j}. \tag{4.91}$$

There are no oscillators $\tilde{\mathscr{A}}$ and $\tilde{\mathscr{A}}^\dagger$ present in the transformed constraint. This is what we desire, since the decoupling of the Hamiltonian is of no use if the constraint still couples the c's and $\mathscr{A}$'s [23, 24]. Our result agrees with Refs. [23–25], up to a sign that is caused by our different definition of c and $c^\dagger$ (see footnote on page 81).

From Eq. (4.89), we note that the constraint $\chi'(\mathbf{q})$ transforms in the same way as $(c' + c'^\dagger) - \mu(\mathscr{A}' + \mathscr{A}'^\dagger)$. The latter expression is equal to $\sqrt{1+\mu^2}(\tilde{c}' + \tilde{c}'^\dagger)$, which is independent of the transformed oscillators $\tilde{\mathscr{A}}'$ and $\tilde{\mathscr{A}}'^\dagger$.

The results at this stage [Eqs. (4.86) and (4.91)] have been used by Shankar [25] to propose the all-momentum extension. Since this all-momentum theory lies beyond the scope of this thesis, we do not review it here.

Currents and conductivity

The RPA Hamiltonian can be rewritten conveniently in terms of the current density $\mathbf{J}$, which is defined in terms of the Hamiltonian (4.35) as

$$J_\sigma(\mathbf{q}) = \frac{1}{L^2}\frac{\delta H_{\mathrm{RPA}}}{\delta A_\sigma(\mathbf{q})} \qquad (\sigma = x, y),$$

where $A_\sigma(\mathbf{q})$ are the components of the vector potential of the external magnetic field $\mathbf{B}$. The factor $1/L^2$ is due to the fact that the current density is defined as the derivative of the Hamiltonian density with respect to the vector potential, while H_{RPA} is the Hamiltonian of the entire system. It is convenient to write the currents in complex notation by defining $J_\pm = J_x \pm i J_y$, so that

$$J_\pm(\mathbf{q}) = \frac{2}{L^2}\frac{\delta H_{\mathrm{RPA}}}{\delta A_\mp(\mathbf{q})}, \tag{4.92}$$

where $A_\pm(\mathbf{q}) = A_x(\mathbf{q}) \pm i A_y(\mathbf{q})$.

We will now write the currents in terms of $\mathscr{A}(\mathbf{q})$ and $c(\mathbf{q})$. The operator $\mathscr{A}(\mathbf{q})$ depends only on the auxiliary gauge fields (the operators a, P, and their hermitian conjugates), so that

$$\frac{\delta\mathscr{A}(\mathbf{q}')}{\delta A_\pm(\mathbf{q})} = 0.$$

On the other hand, we have

$$\frac{\delta c(\mathbf{q}')}{\delta A_\pm(\mathbf{q})} = \sum_j \frac{\delta A_{j,\pm}}{\delta A_\pm(\mathbf{q})}\frac{\delta c(\mathbf{q}')}{\delta A_{j,\pm}} = \sum_j e^{i\mathbf{q}\cdot\mathbf{r}_j}\frac{\delta}{\delta A_{j,\pm}}\left(\frac{1}{L}\sum_k \hat{q}'_+\Pi_k^- e^{-i\mathbf{q}'\cdot\mathbf{r}_k}\right),$$

where we use the definition (4.26) for $c(\mathbf{q}')$, and we have written $A_{j,-} = A_-(\mathbf{r}_j)$. We recall that $\Pi_k^- = p_{k,-} + e\,A_{k,-} + e\langle A_{\mathrm{CS},k,-}\rangle$, so that we obtain

$$\frac{\delta c(\mathbf{q}')}{\delta A_-(\mathbf{q})} = \frac{e}{L}\sum_j \hat{q}'_+ e^{i(\mathbf{q}-\mathbf{q}')\cdot\mathbf{r}_j} = enL\hat{q}'_+\delta_{\mathbf{q},\mathbf{q}'}$$

using that $\sum_j e^{i(\mathbf{q}-\mathbf{q}')\cdot\mathbf{r}_j} = nL^2\delta_{\mathbf{q},\mathbf{q}'}$, where nL^2 is the total number of particles. Since Π_k^- does not depend on $A_{k,+}$, we find

$$\frac{\delta c(\mathbf{q}')}{\delta A_+(\mathbf{q})} = 0.$$

We proceed in a similar way for the derivatives of $c^\dagger(\mathbf{q})$. The results are

$$\frac{\delta c^\dagger(\mathbf{q}')}{\delta A_+(\mathbf{q})} = \frac{e}{L}\sum_j \hat{q}'_- e^{i(\mathbf{q}+\mathbf{q}')\cdot\mathbf{r}_j} = enL\hat{q}'_-\delta_{\mathbf{q}+\mathbf{q}',0} = -enL\hat{q}_-\delta_{\mathbf{q},-\mathbf{q}'}$$

and

$$\frac{\delta c^\dagger(\mathbf{q}')}{\delta A_-(\mathbf{q})} = 0.$$

In the computation of $J_-(\mathbf{q})$, we observe that $c^\dagger(\mathbf{q})$ is the only quantity in the RPA Hamiltonian Eq. (4.35) with a nontrivial derivative with respect to $A_+(\mathbf{q})$. We therefore derive

$$\begin{aligned} J_-(\mathbf{q}) &= \frac{2}{L^2}\left(\hbar\omega\theta^2\sum_{\mathbf{q}'}\frac{\delta c^\dagger(\mathbf{q}')}{\delta A_+(\mathbf{q})}c(\mathbf{q}') + \hbar\omega\theta\sum_{\mathbf{q}'}\frac{\delta c^\dagger(\mathbf{q}')}{\delta A_+(\mathbf{q})}\mathscr{A}(\mathbf{q}')\right) \\ &= \frac{2\hbar\omega\theta}{L^2}\sum_{\mathbf{q}'}(-enL\hat{q}_-\delta_{\mathbf{q},-\mathbf{q}'})\big[\theta\, c(\mathbf{q}') + \mathscr{A}(\mathbf{q}')\big]. \end{aligned}$$

We can rewrite this into a more convenient form by recalling that $\hbar\omega\theta^2 = 1/2mn$ [from Eq. (4.34)], so that we obtain

$$J_-(\mathbf{q}) = -\frac{e}{mL\theta}\hat{q}_-\big(\theta\, c(-\mathbf{q}) + \mathscr{A}(-\mathbf{q})\big).$$

With $c' = (\theta/\mu)c$ and $\mathscr{A}' = \mathscr{A}$, we can write $\theta\, c(-\mathbf{q}) + \mathscr{A}(-\mathbf{q}) = \mu\, c'(-\mathbf{q}) + \mathscr{A}'(-\mathbf{q})$. In view of Eq. (4.39), this linear combination is exactly the transformed ladder operator $\tilde{\mathscr{A}}'(-\mathbf{q})$, up to a factor. Hence, we can write

$$J_-(\mathbf{q}) = -\frac{e}{mL\theta}\sqrt{1+\mu^2}\,\hat{q}_-\tilde{\mathscr{A}}'(-\mathbf{q}) = -\frac{e}{mL\theta\sqrt{\nu K}}\hat{q}_-\tilde{\mathscr{A}}(-\mathbf{q}) = -\frac{e}{L}\omega_{\mathrm{c}}\frac{\sqrt{\nu}}{\sqrt{\pi}}\hat{q}_-\tilde{\mathscr{A}}(-\mathbf{q}), \tag{4.93}$$

by using Eqs. (4.83) and (4.32). The current $J_+(\mathbf{q})$ can be determined in a similar manner, or by noting that $J_+(\mathbf{q})$ is the complex conjugate of $J_-(-\mathbf{q})$,

$$J_+(\mathbf{q}) = \frac{e}{mL\theta\sqrt{\nu K}}\hat{q}_+\tilde{\mathscr{A}}^\dagger(\mathbf{q}) = \frac{e}{L}\omega_{\mathrm{c}}\frac{\sqrt{\nu}}{\sqrt{\pi}}\hat{q}_+\tilde{\mathscr{A}}^\dagger(\mathbf{q}). \tag{4.94}$$

Equations (4.93) and (4.94) show that the ladder operators after the final diagonalisation procedure are just proportional to the currents of the RPA Hamiltonian. The diagonalised version of this Hamiltonian, $H_{\rm RPA} = \hbar\omega_{\rm c}\sum_{\mathbf{q}}\tilde{\mathscr{A}}^{\dagger}(\mathbf{q})\tilde{\mathscr{A}}(\mathbf{q})$, can be written in terms of the currents as

$$H_{\rm RPA} = \hbar\omega_{\rm c}\sum_{\mathbf{q}}\left(\frac{L\sqrt{\pi}}{e\omega_{\rm c}\sqrt{\nu}}\right)^2 J_+(\mathbf{q})J_-(-\mathbf{q}) = \frac{\pi\hbar L^2}{e^2\omega_{\rm c}}\sum_{\mathbf{q}} J_+(\mathbf{q})\,\nu^{-1}J_-(-\mathbf{q}), \tag{4.95}$$

or equivalently

$$H_{\rm RPA} = \frac{\pi\hbar L^2}{e^2\omega_{\rm c}}\sum_{\mathbf{q}}\nu^{-1}\big(J_x(\mathbf{q})J_x(-\mathbf{q}) + J_y(\mathbf{q})J_y(-\mathbf{q})\big). \tag{4.96}$$

The oscillator part $\rho_{\rm osc}(\mathbf{q})$ of the density in Eqs. (4.86) can also be rewritten conveniently in terms of the current. Using Eqs. (4.93) and (4.94), we find

$$\rho_{\rm osc}(\mathbf{q}) = \frac{|\mathbf{q}|\sqrt{\nu}}{2L\sqrt{\pi}}\big(\tilde{\mathscr{A}}(\mathbf{q}) + \tilde{\mathscr{A}}^{\dagger}(-\mathbf{q})\big) = \frac{|\mathbf{q}|}{2e\omega_{\rm c}}\big(\hat{q}_+J_-(-\mathbf{q}) - \hat{q}_-J_+(-\mathbf{q})\big).$$

Because $|\mathbf{q}|\hat{q}_\pm = q_\pm = q_x \pm i\,q_y$ and $J_\pm = J_x \pm iJ_y$, this expression is equal to

$$\rho_{\rm osc}(\mathbf{q}) = \frac{1}{e\omega_{\rm c}}\big(i\,q_yJ_x(-\mathbf{q}) - i\,q_xJ_y(-\mathbf{q})\big) = -\frac{i}{e\omega_{\rm c}}\mathbf{q}\wedge\mathbf{J}(-\mathbf{q}). \tag{4.97}$$

We may derive the Hall conductivity by coupling this oscillator term [Eq. (4.97)] to an external electric potential $\Phi_{\rm ext}$ [24], described by

$$H_{\rm ext} = -eL^2\sum_{\mathbf{q}}\Phi_{\rm ext}(\mathbf{q})\rho_{\rm osc}(\mathbf{q}) = -\frac{L^2}{2\omega_{\rm c}}\sum_{\mathbf{q}}\big(\Phi_{\rm ext}(\mathbf{q})q_-^*J_-(-\mathbf{q}) + \Phi_{\rm ext}(-\mathbf{q})q_-J_-^{\dagger}(-\mathbf{q})\big),$$

writing $q_+ = q_-^*$ and $J_+(\mathbf{q}) = J_-^{\dagger}(-\mathbf{q})$. We add this term to the RPA Hamiltonian (4.95),

$$H_{\rm RPA} + H_{\rm ext} = \frac{\pi\hbar L^2}{e^2\omega_{\rm c}\nu}\sum_{\mathbf{q}}J_-^{\dagger}(-\mathbf{q})J_-(-\mathbf{q}) - \frac{L^2}{2\omega_{\rm c}}\sum_{\mathbf{q}}\big(\Phi_{\rm ext}(\mathbf{q})q_-^*J_-(-\mathbf{q}) + \Phi_{\rm ext}(-\mathbf{q})q_-J_-^{\dagger}(-\mathbf{q})\big).$$

In order to obtain the average current $\langle J_-(-\mathbf{q})\rangle$ and its hermitian conjugate, we complete the squares in this Hamiltonian, i.e., we write $H_{\rm RPA} + H_{\rm ext}$ as

$$H_{\rm RPA} + H_{\rm ext} = \frac{\pi\hbar L^2}{e^2\omega_{\rm c}}\sum_{\mathbf{q}}\big(J_-(-\mathbf{q}) - \langle J_-(-\mathbf{q})\rangle\big)^{\dagger}\big(J_-(-\mathbf{q}) - \langle J_-(-\mathbf{q})\rangle\big) + \text{const},$$

where we neglected a constant term, quadratic in $\langle J_-(-\mathbf{q})\rangle$. Then we obtain

$$\langle J_-(-\mathbf{q})\rangle = \frac{e^2\nu}{2\pi\hbar}q_-\Phi_{\rm ext}(-\mathbf{q}) \quad\text{and}\quad \langle J_-^{\dagger}(-\mathbf{q})\rangle = \frac{e^2\nu}{2\pi\hbar}q_-^*\Phi_{\rm ext}(\mathbf{q}).$$

The external electric field is related to the potential as $\mathbf{E}(\mathbf{q}) = -i\mathbf{q}\Phi_{\text{ext}}(\mathbf{q})$. Writing $E_\pm = E_x \pm iE_y$, we find

$$\langle J_-(\mathbf{q})\rangle = -\frac{e^2\nu}{2\pi\hbar} q_- \Phi_{\text{ext}}(\mathbf{q}) = -\frac{e^2\nu}{h} iE_-(\mathbf{q}) \tag{4.98a}$$

and

$$\langle J_+(\mathbf{q})\rangle = \frac{e^2\nu}{2\pi\hbar} q_+ \Phi_{\text{ext}}(\mathbf{q}) = \frac{e^2\nu}{h} iE_+(\mathbf{q}). \tag{4.98b}$$

The conductivity tensor is defined by

$$\begin{pmatrix} J_x \\ J_y \end{pmatrix} = \begin{pmatrix} \sigma_{xx} & -\sigma_{xy} \\ \sigma_{xy} & \sigma_{xx} \end{pmatrix} \begin{pmatrix} E_x \\ E_y \end{pmatrix}, \tag{4.99}$$

where σ_{xx} and σ_{xy} denote the *longitudinal* and *transverse* (or *Hall*) *conductivity*, respectively. In the complex basis, the conductivities are given by $J_\pm = \sigma_\pm E_\pm$, where $\sigma_\pm = \sigma_{xx} \pm i\sigma_{xy}$. Hence, from Eqs. (4.98) we read off that $\sigma_\pm = \pm ie^2\nu/h$, so that the Hall conductivity is

$$\sigma_{xy} = \frac{e^2\nu}{2\pi\hbar} = \frac{e^2}{h}\nu, \tag{4.100}$$

equal to the filling factor times the conductivity quantum e^2/h [24]. This result is in agreement with measurements of the Hall conductivity for fractional quantum Hall states, both in the lowest Landau level ($\nu \leq 1$) [4, 8, 175–178] and in higher Landau levels ($\nu > 1$) [179, 180].

4.6.2 Multicomponent systems

Density transformation

As in the one-component case, we will compute the density in terms of the transformed density and the transformed operators. Again, the transformation in the $(c', \mathscr{A}')$ space can be regarded as a rotation, but in the multicomponent case it is generated by multiple generators

$$\begin{aligned} S^{(c\mathscr{A})}_{\beta\gamma} &= \sum_{\mathbf{q}} \big(c'^\dagger_\beta(\mathbf{q}) \mathscr{A}'_\gamma(\mathbf{q}) - \mathscr{A}'^\dagger_\gamma(\mathbf{q}) c'_\beta(\mathbf{q}) \big), \\ S^{(\mathscr{A}\mathscr{A})}_{\beta\gamma} &= \sum_{\mathbf{q}} \big(\mathscr{A}'^\dagger_\beta(\mathbf{q}) \mathscr{A}'_\gamma(\mathbf{q}) - \mathscr{A}'^\dagger_\gamma(\mathbf{q}) \mathscr{A}'_\beta(\mathbf{q}) \big), \\ S^{(cc)}_{\beta\gamma} &= \sum_{\mathbf{q}} \big(c'^\dagger_\beta(\mathbf{q}) c'_\gamma(\mathbf{q}) - c'^\dagger_\gamma(\mathbf{q}) c'_\beta(\mathbf{q}) \big). \end{aligned}$$

In order to compute the commutators of the full density of component α,

$$\rho_\alpha(\mathbf{q}) = L^{-2} \sum_{j_\alpha=1}^{N_\alpha} e^{-i\mathbf{q}\cdot\mathbf{r}_{j_\alpha}} \tag{4.101}$$

with the generators of the rotation, we compute the commutators of $\rho_\alpha(\mathbf{q})$ with $c_\beta(\mathbf{q}')$ and $c_\beta^\dagger(\mathbf{q}')$ first:

$$[\rho_\alpha(\mathbf{q}), c_\beta(\mathbf{q}')] = -\hbar|\mathbf{q}|n_\alpha L^{-1}\delta_{\alpha\beta}\delta_{\mathbf{q},-\mathbf{q}'},$$
$$[\rho_\alpha(\mathbf{q}), c_\beta^\dagger(\mathbf{q}')] = \hbar|\mathbf{q}|n_\alpha L^{-1}\delta_{\alpha\beta}\delta_{\mathbf{q},\mathbf{q}'},$$

in RPA, similar to Eqs. (4.73) and (4.74). Now, we recall that $c'_\alpha = \theta_0\sqrt{(RN)^{-1}_{\alpha\alpha}}\,c_\alpha$ [Eq. (4.53)], so that

$$[\rho_\alpha(\mathbf{q}), S^{(c\mathscr{A})}_{\beta\gamma}] = -\hbar\theta_0\sqrt{(RN)^{-1}_{\alpha\alpha}}\,|\mathbf{q}|n_\alpha L^{-1}\delta_{\alpha\beta}\big(\mathscr{A}'_\gamma(\mathbf{q}) + \mathscr{A}'^\dagger_\gamma(-\mathbf{q})\big),$$
$$[\rho_\alpha(\mathbf{q}), S^{(\mathscr{A}\mathscr{A})}_{\beta\gamma}] = 0,$$
$$[\rho_\alpha(\mathbf{q}), S^{(cc)}_{\beta\gamma}] = -\hbar\theta_0\sqrt{(RN)^{-1}_{\alpha\alpha}}\,|\mathbf{q}|n_\alpha L^{-1}\big(\delta_{\alpha\beta}c'_\gamma(\mathbf{q}) - \delta_{\alpha\gamma}c'_\beta(\mathbf{q}) + \delta_{\alpha\beta}c'^\dagger_\gamma(-\mathbf{q}) - \delta_{\alpha\gamma}c'^\dagger_\beta(-\mathbf{q})\big).$$

Furthermore, we have

$$[c'_\alpha(\mathbf{q}) + c'^\dagger_\alpha(-\mathbf{q}), S^{(c\mathscr{A})}_{\beta\gamma}] = \delta_{\alpha\beta}\big(\mathscr{A}'_\gamma(\mathbf{q}) + \mathscr{A}'^\dagger_\gamma(-\mathbf{q})\big),$$
$$[c'_\alpha(\mathbf{q}) + c'^\dagger_\alpha(-\mathbf{q}), S^{(\mathscr{A}\mathscr{A})}_{\beta\gamma}] = 0,$$
$$[c'_\alpha(\mathbf{q}) + c'^\dagger_\alpha(-\mathbf{q}), S^{(cc)}_{\beta\gamma}] = \delta_{\alpha\beta}c'_\gamma(\mathbf{q}) - \delta_{\alpha\gamma}c'_\beta(\mathbf{q}) + \delta_{\alpha\beta}c'^\dagger_\gamma(-\mathbf{q}) - \delta_{\alpha\gamma}c_\beta{}'^\dagger(-\mathbf{q}).$$

Thus, $\rho_\alpha(\mathbf{q})$ has the same transformation rules as $\hbar\theta_0\sqrt{(RN)^{-1}_{\alpha\alpha}}\,|\mathbf{q}|n_\alpha L^{-1}[c'_\alpha(\mathbf{q}) + c'^\dagger_\alpha(-\mathbf{q})]$. We subsequently define

$$\rho'_\alpha(\mathbf{q}) = \frac{L\sqrt{(RN)_{\alpha\alpha}}}{\theta_0\hbar|\mathbf{q}|n_\alpha}\rho_\alpha(\mathbf{q}), \tag{4.102}$$

which transforms infinitesimally in the same way as $c'_\alpha(\mathbf{q}) + c'^\dagger_\alpha(-\mathbf{q})$. Recalling that $\theta_0 = l_B^2\sqrt{\pi}/\hbar$ [Eq. (4.33)] and $n_\alpha = \nu_\alpha/2\pi l_B^2$, we can write Eq. (4.102) concisely in matrix notation as

$$\rho'(\mathbf{q}) = \frac{2L\sqrt{\pi}}{|\mathbf{q}|}\sqrt{RN^{-1}}\,\rho(\mathbf{q}). \tag{4.103}$$

The full transformation in the $(c', \mathscr{A}')$ space is given by the orthogonal $2\kappa \times 2\kappa$ matrix S which follows from the diagonalisation of the Hamiltonian matrix H'_{mat}, i.e. S is such that $H'_{\text{mat}} = S^{\mathrm{T}}\tilde{H}_{\text{mat}}S$. We define the four $\kappa \times \kappa$ matrices T, U, V, and W such that

$$S = \begin{pmatrix} T & U \\ V & W \end{pmatrix} \quad \text{and} \quad \tilde{H}_{\text{mat}} = \begin{pmatrix} 0 & 0 \\ 0 & F \end{pmatrix}, \tag{4.104}$$

where F is the diagonal matrix of the nonzero eigenvalues of H'_{mat}. In Appendix 4.D we establish the relations between the matrices T, U, V, and W, and their relations

to the four quadrants of the Hamiltonian matrix. In the appendix, we find that T and U are not fixed. On the other hand, V and W are fixed, up to a permutation of the eigenvectors $\mathbf{g}_\alpha$. The transformation of $(c', \mathscr{A}')$ is then given by $(\tilde{c}', \tilde{\mathscr{A}}') = S(c', \mathscr{A}') = (Tc' + U\mathscr{A}', Vc' + W\mathscr{A}')$, and the inverse is given by $(c', \mathscr{A}') = S^{-1}(\tilde{c}', \tilde{\mathscr{A}}') = (T^{\mathrm{T}}\tilde{c}' + V^{\mathrm{T}}\tilde{\mathscr{A}}', U^{\mathrm{T}}\tilde{c}' + W^{\mathrm{T}}\tilde{\mathscr{A}}')$, by virtue of $S^{-1} = S^{\mathrm{T}}$.

We now return to the transformations of the densities. We have defined $\rho'_\alpha(\mathbf{q})$ such that it transforms in the same way as $c'_\alpha(\mathbf{q}) + c'^\dagger_\alpha(-\mathbf{q})$. For a single component this is expressed in Eq. (4.76), which is also valid for the case of multiple components if we interpret it as a matrix equation, thereby replacing $c'^\dagger$ and $\mathscr{A}'^\dagger$ by $c'^\ddagger$ and $\mathscr{A}'^\ddagger$, respectively, which denote the column vectors $(c'^\dagger_1, \ldots, c'^\dagger_\kappa)$ and $(\mathscr{A}'^\dagger_1, \ldots, \mathscr{A}'^\dagger_\kappa)$, respectively.[17] Writing the original fields c' (under S^{-1}) explicitly in terms of the transformed fields $\tilde{c}'$ and $\tilde{\mathscr{A}}'$, we obtain

$$\begin{aligned}\tilde{\rho}'(\mathbf{q}) - \rho'(\mathbf{q}) &= \big(\tilde{c}'(\mathbf{q}) + \tilde{c}'^\ddagger(-\mathbf{q})\big) - \big(c(\mathbf{q}) + c^\ddagger(-\mathbf{q})\big) \\ &= \big(\tilde{c}'(\mathbf{q}) + \tilde{c}'^\ddagger(-\mathbf{q})\big) - T^{\mathrm{T}}\big(\tilde{c}'(\mathbf{q}) + \tilde{c}'^\ddagger(-\mathbf{q})\big) - V^{\mathrm{T}}\big(\tilde{\mathscr{A}}'(\mathbf{q}) + \tilde{\mathscr{A}}'^\ddagger(-\mathbf{q})\big) \\ &= (\mathbb{1} - T^{\mathrm{T}})\big(\tilde{c}'(\mathbf{q}) + \tilde{c}'^\ddagger(-\mathbf{q})\big) - V^{\mathrm{T}}\big(\tilde{\mathscr{A}}'(\mathbf{q}) + \tilde{\mathscr{A}}'^\ddagger(-\mathbf{q})\big). \end{aligned} \tag{4.105}$$

The aim is to express $\rho'(\mathbf{q})$ in terms of the transformed quantities $\tilde{\rho}'(\mathbf{q})$, $\tilde{\mathscr{A}}'(\mathbf{q}) + \tilde{\mathscr{A}}'^\ddagger(\mathbf{q})$, and $\tilde{c}'(\mathbf{q}) + \tilde{c}'^\ddagger(\mathbf{q})$. By rearranging terms, we obtain

$$\rho'(\mathbf{q}) = \tilde{\rho}'(\mathbf{q}) + (T^{\mathrm{T}} - \mathbb{1})\big(\tilde{c}'(\mathbf{q}) + \tilde{c}'^\ddagger(-\mathbf{q})\big) + V^{\mathrm{T}}\big(\tilde{\mathscr{A}}'(\mathbf{q}) + \tilde{\mathscr{A}}'^\ddagger(-\mathbf{q})\big), \tag{4.106}$$

where the right-hand side now contains transformed quantities only.

The next step is to undo the rescaling to the primed quantities, given by Eq. (4.103) for ρ and $\tilde{\rho}$, and Eq. (4.53) for c and $c^\ddagger$. We have to take into account that the transformed quantities scale differently than the original ones. We define $\check{\rho}$, $\check{\tilde{\rho}}$ and $\check{\tilde{c}} + \check{\tilde{c}}^\ddagger$ by

$$\check{\rho}(\mathbf{q}) = G\sqrt{N^{-1}}\rho(\mathbf{q}), \tag{4.107a}$$

$$\check{\tilde{\rho}}(\mathbf{q}) = G\sqrt{N^{-1}}\tilde{\rho}(\mathbf{q}), \tag{4.107b}$$

$$\check{\tilde{c}}(\mathbf{q}) + \check{\tilde{c}}^\ddagger(\mathbf{q}) = G\sqrt{N^{-1}}\big(\tilde{c}(\mathbf{q}) + \tilde{c}^\ddagger(-\mathbf{q})\big). \tag{4.107c}$$

This definition is just a change of basis to the basis of the eigenvectors of the matrix $R + KN$. Indeed, the columns of the matrix $\sqrt{N}G^{\mathrm{T}} = \big(G\sqrt{N^{-1}}\big)^{-1}$ are the eigenvectors $\tilde{\mathbf{g}}_\alpha$ of $R + KN$, as given by the reasoning in Sec. 4.5.2. Together with Eq. (4.103) for ρ and $\tilde{\rho}$, and Eq. (4.53) for c and $c^\ddagger$, the definitions (4.107) may be rewritten in terms of

[17] We introduce this notation here, because strictly speaking, writing $c'(\mathbf{q}) + c'^\dagger(-\mathbf{q})$ makes no sense, since c' is a column vector and $c'^\dagger$ is a row vector. Therefore we will adopt the notation $c'^\ddagger$ for the column vector with components $c'^\dagger_\alpha$. We note that if c' is transformed by left-multiplication by a real matrix that acts only on the component indices α, then $c'^\ddagger$ is also left-multiplied by the same matrix.

the primed quantities as

$$\check{\rho}(\mathbf{q}) = \frac{|\mathbf{q}|}{2L\sqrt{\pi}} G\sqrt{R^{-1}}\rho'(\mathbf{q}), \tag{4.108a}$$

$$\check{\tilde{\rho}}(\mathbf{q}) = \frac{|\mathbf{q}|}{2L\sqrt{\pi}} G\sqrt{R^{-1}}\tilde{\rho}'(\mathbf{q}), \tag{4.108b}$$

$$\check{c}(\mathbf{q}) + \check{c}^{\ddagger}(-\mathbf{q}) = \theta_0^{-1} G\sqrt{R}\big(\tilde{c}'(\mathbf{q}) + \tilde{c}'^{\ddagger}(-\mathbf{q})\big), \tag{4.108c}$$

with θ_0 as in Eq. (4.33). Left-multiplying both sides of Eq. (4.106) by $|\mathbf{q}|/(2L\sqrt{\pi})$ and using definitions (4.108), we obtain

$$\check{\rho}(\mathbf{q}) = \check{\tilde{\rho}}(\mathbf{q}) + \check{\rho}_{\mathrm{osc}}(\mathbf{q}), \tag{4.109a}$$

with

$$\check{\tilde{\rho}}(\mathbf{q}) = \check{\tilde{\rho}}(\mathbf{q}) + \frac{|\mathbf{q}|}{2LeB}\Gamma\big(\check{c}(\mathbf{q}) + \check{c}^{\ddagger}(-\mathbf{q})\big) \tag{4.109b}$$

and

$$\check{\rho}_{\mathrm{osc}}(\mathbf{q}) = \frac{|\mathbf{q}|}{2L\sqrt{\pi}}\sqrt{F^{-1}}(\tilde{\mathscr{A}}(\mathbf{q}) + \tilde{\mathscr{A}}^{\ddagger}(-\mathbf{q})\big), \tag{4.109c}$$

where we used that $V^{\mathrm{T}} = \sqrt{R}\,G^{\mathrm{T}}\sqrt{F^{-1}}$ from Eq. (4.154), and we have defined the matrix Γ as

$$\Gamma = G\sqrt{R^{-1}}(T^{\mathrm{T}} - \mathbb{1})\sqrt{R^{-1}}G^{\mathrm{T}}. \tag{4.110}$$

In Eqs. (4.109), we have split the density into a low-energy part $\check{\tilde{\rho}}(\mathbf{q})$ involving the momentum operators and a high-energy part $\check{\rho}_{\mathrm{osc}}(\mathbf{q})$ involving the oscillators, like we have done in the single-component case.

To illustrate the analogy with the one-component case, we will write the low-energy part in components, using

$$\check{\tilde{\rho}}_\alpha(\mathbf{q}) = \frac{1}{L^2}\sum_\beta\sum_j G_{\alpha\beta}\sqrt{\nu_\beta^{-1}}\epsilon_{\beta,j}e^{-i\mathbf{q}\cdot\mathbf{r}_j} \tag{4.111}$$

$$|\mathbf{q}|\big(\check{c}_\alpha(\mathbf{q}) + \check{c}_\alpha^{\dagger}(-\mathbf{q})\big) = -2iL^{-1}\sum_\beta\sum_j G_{\alpha\beta}\sqrt{\nu_\beta^{-1}}(\mathbf{q}\wedge\Pi_{\beta,j})\epsilon_{\beta,j}e^{-i\mathbf{q}\cdot\mathbf{r}_j}, \tag{4.112}$$

where we define the ϵ *symbol* by setting $\epsilon_{\beta,j} = 1$ if particle j is of type β and $\epsilon_{\beta,j} = 0$ otherwise. Equation (4.112) is the multicomponent generalisation of Eq. (4.85). The low-energy part of the density Eq. (4.109b) written out in components is

$$\check{\tilde{\rho}}_\alpha(\mathbf{q}) = \frac{1}{L^2}\sum_{\beta,\gamma}\sum_j\left[\delta_{\alpha\beta} - \frac{il_B^2}{\hbar}\Gamma_{\alpha\beta}(\mathbf{q}\wedge\Pi_{\gamma,j})\right]G_{\beta\gamma}\sqrt{\nu_\gamma^{-1}}\epsilon_{\gamma,j}e^{-i\mathbf{q}\cdot\mathbf{r}_j}. \tag{4.113}$$

In order to make the connection with the single-component case, we observe that in that case we may replace $G\to 1$, $T^{\mathrm{T}}\to\sqrt{\nu K}$ and $R\to 1-\nu K$, so that $\Gamma\to -(\sqrt{\nu K}+1)^{-1}$. We recall that $\check{\tilde{\rho}}_\alpha = (G\sqrt{N^{-1}}\tilde{\rho})_\alpha \to \sqrt{\nu^{-1}}\rho$. With these observations, (4.113) reduces to (4.86b), as desired.

Gauge invariance

It is important to notice that the expression for $\check{\rho}$ involves only the matrix T, but not W. On the other hand, from Eq. (4.148) (see Appendix 4.D) it follows that the Hamiltonian matrix does not involve T, but only W, which is related to the fact that the eigenvalues associated with $\tilde{c}'$ and $\tilde{c}'^{\dagger}$ are zero and hence these drop out of the diagonalised Hamiltonian. As discussed in Appendix 4.D, the transformations (4.155) change T, but leave all the given conditions (Eqs. (4.147) and (4.151)) invariant. Changing T according to these transformations is equivalent to selecting a different orthonormal basis for the null eigenspace of H'_{mat} (i.e., the $\tilde{c}'_\alpha$). However, physical quantities may not depend on the choice of the matrix T. In other words, the transformations on T define a gauge invariance, and physical quantities must be gauge invariant.

The density $\check{\rho}(\mathbf{q})$ is not invariant under the transformations (4.155), because the matrix Γ explicitly depends on T (i.e., Γ is not invariant under these transformations). In other words, $\check{\rho}(\mathbf{q})$ depends on the specific choice of the basis for the $\tilde{c}'_\alpha$, and therefore it cannot represent a physical quantity. However, when the result Eq. (4.113) would be extended to an expression valid at all momenta analogous to Shankar's extension [25], we expect that the commutators $[\check{\rho}_\alpha(\mathbf{q}), \check{\rho}_\beta(\mathbf{q}')]$ of the density operators will be gauge invariant. These commutators are therefore expected to describe the physics.

On the other hand, the oscillator density $\check{\rho}_{\mathrm{osc}}(\mathbf{q})$ [Eq. (4.109c)] involves only the matrix F (i.e., the eigenvalues of $R+E$) and there is no dependence on T, so that it is invariant under the transformations (4.155). This invariance is related to the fact that the oscillator density does not involve the low-energy degrees of freedom (the operators $\tilde{c}'$ and $\tilde{c}'_\dagger$), but only the high-energy degrees of freedom $\tilde{\mathscr{A}}(\mathbf{q})$ and $\tilde{\mathscr{A}}^\dagger(\mathbf{q})$. The latter are determined by the matrix W, which is fixed, so that there is no freedom in choosing a basis for them. The invariance of $\check{\rho}_{\mathrm{osc}}(\mathbf{q})$ suggests that it may be connected to a physical quantity. Indeed, as we will see in Sec. 4.6.2, the oscillator density $\check{\rho}_{\mathrm{osc}}(\mathbf{q})$ is related to the Hall conductivity, clearly a physical observable.

Transformation of the constraint

We continue with the constraint (4.9), which we write in the form $\chi_\alpha(\mathbf{q})\,|\phi_{\mathrm{phys}}\rangle = 0$, with

$$\chi_\alpha(\mathbf{q}) = \delta\rho_\alpha(\mathbf{q}) - \frac{e|\mathbf{q}|}{2\pi\hbar}\sum_\beta (K^{-1})_{\alpha\beta}\, a^\circ_\beta(\mathbf{q}).$$

Now we switch to matrix notation again, i.e., we write $\chi = (\chi_1, \ldots, \chi_\kappa)$. We rescale the constraint similar to the one-component case [Eq. (4.88)],

$$\chi'(\mathbf{q}) = \frac{2L\sqrt{\pi}}{|\mathbf{q}|}\sqrt{RN^{-1}}\,\chi(\mathbf{q}). \tag{4.114}$$

By using Eq. (4.46), we can rewrite $\chi'(\mathbf{q})$ as

$$\chi'(\mathbf{q}) = \delta\rho'(\mathbf{q}) - \frac{2L\sqrt{\pi}}{|\mathbf{q}|}\frac{|\mathbf{q}|}{2\pi\hbar}\frac{1}{2}\frac{\sqrt{4\pi\hbar^2}}{L}\sqrt{RN^{-1}}K^{-1}\big(\mathscr{A}^{\circ}(\mathbf{q}) + \mathscr{A}^{\circ\ddagger}(-\mathbf{q})\big).$$

Expressing $\mathscr{A}^{\circ}$ and $\mathscr{A}^{\circ\ddagger}$ in terms of $\mathscr{A}$ and $\mathscr{A}^{\ddagger}$ according to Eq. (4.48), we obtain

$$\chi'(\mathbf{q}) = \delta\rho'(\mathbf{q}) - \sqrt{R}\sqrt{N^{-1}}K^{-1}\sqrt{N^{-1}}C^{\mathrm{T}}\sqrt{D}\big(\mathscr{A}(\mathbf{q}) + \mathscr{A}^{\ddagger}(-\mathbf{q})\big).$$

We recall that $\sqrt{N^{-1}}K^{-1}\sqrt{N^{-1}} = E^{-1} = C^{\mathrm{T}}D^{-1}C$, so that we obtain

$$\chi'(\mathbf{q}) = \delta\rho'(\mathbf{q}) - \sqrt{R}C^{\mathrm{T}}\sqrt{D^{-1}}\big(\mathscr{A}(\mathbf{q}) + \mathscr{A}^{\ddagger}(-\mathbf{q})\big) = \delta\rho'(\mathbf{q}) - Q^{\mathrm{T}}\big(\mathscr{A}'(\mathbf{q}) + \mathscr{A}'^{\ddagger}(-\mathbf{q})\big), \quad (4.115)$$

with Q given by Eq. (4.152), and with $\mathscr{A}' = \mathscr{A}$. Now, we write $\mathscr{A}'$ and $\mathscr{A}'^{\dagger}$ in terms of the transformed operators $\tilde{c}'$, $\tilde{\mathscr{A}}'$, and their hermitian conjugates. Moreover, we express $\delta\rho'(\mathbf{q})$ in terms of $\delta\tilde{\rho}'(\mathbf{q})$ by using (4.105) together with the observation that $\delta\tilde{\rho}'(\mathbf{q}) - \delta\rho'(\mathbf{q}) = \tilde{\rho}'(\mathbf{q}) - \rho'(\mathbf{q})$ for $\mathbf{q} \neq 0$, analogous to the one-component case discussed in Sec. 4.6.1. Then the constraint can be written as

$$\begin{aligned}\chi'(\mathbf{q}) = \delta\tilde{\rho}'(\mathbf{q}) - (\mathbb{1} - T^{\mathrm{T}})\big(\tilde{c}'(\mathbf{q}) + \tilde{c}'^{\ddagger}(-\mathbf{q})\big) + V^{\mathrm{T}}\big(\tilde{\mathscr{A}}'(\mathbf{q}) + \tilde{\mathscr{A}}'^{\ddagger}(-\mathbf{q})\big) \\ - Q^{\mathrm{T}}\big[U^{\mathrm{T}}\big(\tilde{c}'(\mathbf{q}) + \tilde{c}'^{\ddagger}(-\mathbf{q})\big) + W^{\mathrm{T}}\big(\tilde{\mathscr{A}}'(\mathbf{q}) + \tilde{\mathscr{A}}'^{\ddagger}(-\mathbf{q})\big)\big]. \quad (4.116)\end{aligned}$$

Using the relations $U = -TQ^{\mathrm{T}}$ and $V = WQ$, as given by Eq. (4.151), we see that the term with $\mathscr{A}'(\mathbf{q}) + \mathscr{A}'^{\ddagger}(-\mathbf{q})$ vanishes, while the remaining terms are

$$\begin{aligned}\tilde{\chi}'(\mathbf{q}) &= \delta\tilde{\rho}'(\mathbf{q}) - (-Q^{\mathrm{T}}QT^{\mathrm{T}} - T^{\mathrm{T}} + \mathbb{1})\big(\tilde{c}'(\mathbf{q}) + \tilde{c}'^{\ddagger}(-\mathbf{q})\big) \\ &= \delta\tilde{\rho}'(\mathbf{q}) - \big(\mathbb{1} - (\mathbb{1} + Q^{\mathrm{T}}Q)T^{\mathrm{T}}\big)\big(\tilde{c}'(\mathbf{q}) + \tilde{c}'^{\ddagger}(-\mathbf{q})\big).\end{aligned}$$

By virtue of Eq. (4.153a), we have $\mathbb{1} + Q^{\mathrm{T}}Q = (T^{\mathrm{T}}T)^{-1} = T^{-1}(T^{\mathrm{T}})^{-1}$, so that

$$\chi'(\mathbf{q}) = \delta\tilde{\rho}'(\mathbf{q}) - (\mathbb{1} - T^{-1})\big(\tilde{c}'(\mathbf{q}) + \tilde{c}'^{\ddagger}(-\mathbf{q})\big).$$

It is clear that this equation generalises the one-component analogue (4.90).

With the relations (4.108) and the definition

$$\check{\chi}(\mathbf{q}) = \frac{|\mathbf{q}|}{2L\sqrt{\pi}}G\sqrt{R^{-1}}\chi'(\mathbf{q}), \quad (4.117)$$

we find

$$\check{\chi}(\mathbf{q}) = \delta\tilde{\rho}(\mathbf{q}) - \frac{|\mathbf{q}|}{2eBL}\Delta\big(\tilde{c}(\mathbf{q}) + \tilde{c}^{\ddagger}(-\mathbf{q})\big), \quad (4.118)$$

where the matrix Δ is given by

$$\Delta = G\sqrt{R^{-1}}(\mathbb{1} - T^{-1})\sqrt{R^{-1}}G^{\mathrm{T}}. \quad (4.119)$$

Using Eqs. (4.112) and (4.111), we find that

$$\check{\chi}_{\alpha}(\mathbf{q}) = \frac{1}{L^2}\sum_{\beta,\gamma}\sum_{j}\left[\delta_{\alpha\beta} + \frac{il_B^2}{\hbar}\Delta_{\alpha\beta}(\mathbf{q}\wedge\Pi_{\gamma,j})\right]G_{\beta\gamma}\sqrt{\nu_{\gamma}^{-1}}\epsilon_{\gamma,j}e^{-i\mathbf{q}\cdot\mathbf{r}_j}, \quad (4.120)$$

analogous to Eq. (4.113). We may prove that Eq. (4.120) reduces to Eq. (4.91) in the case of one component.

Currents and conductivity

In line with the deduction of the Hall conductivity as derivatives of the Hamiltonian for the single-component case, we will show here that this procedure generalises to the multicomponent case. As before, we start by computing the derivatives of c_α and $c_\alpha^\dagger$ with respect to the vector potentials $A_\pm(\mathbf{q})$. Application of the chain rule,

$$\frac{\delta c_\alpha(\mathbf{q}')}{\delta A_\pm(\mathbf{q})} = \sum_\beta \sum_{k_\beta=1}^{N_\beta} \frac{\delta A_{k_\beta,\pm}}{\delta A_\pm(\mathbf{q})} \frac{\delta c_\alpha(\mathbf{q}')}{\delta A_{k_\beta,\pm}},$$

yields

$$\frac{\delta c_\alpha(\mathbf{q}')}{\delta A_-(\mathbf{q})} = e n_\alpha L \delta_{\mathbf{q},\mathbf{q}'} \hat{q}_+ \quad \text{and} \quad \frac{\delta c_\alpha(\mathbf{q}')}{\delta A_+(\mathbf{q})} = 0,$$

where we have used $\sum_{j_\alpha} e^{i(\mathbf{q}-\mathbf{q}')\cdot\mathbf{r}_{j_\alpha}} = n_\alpha L^2 \delta_{\mathbf{q},\mathbf{q}'}$, where $n_\alpha L^2$ is the number of particles of component α. We also find

$$\frac{\delta c_\alpha^\dagger(\mathbf{q}')}{\delta A_+(\mathbf{q})} = -e n_\alpha L \delta_{\mathbf{q},-\mathbf{q}'} \hat{q}_- \quad \text{and} \quad \frac{\delta c_\alpha^\dagger(\mathbf{q}')}{\delta A_-(\mathbf{q})} = 0.$$

In order to determine $J_-(\mathbf{q})$, we derive the Hamiltonian (4.51) with respect to $A_+(\mathbf{q})$. Using that only the terms containing $c_\alpha^\dagger(\mathbf{q}')$ have a nontrivial derivative, we obtain

$$\begin{aligned} J_-(\mathbf{q}) &= \frac{2}{L^2} \frac{\delta H_{\mathrm{RPA}}}{\delta A_+(\mathbf{q})} \\ &= \frac{2\hbar}{L^2} \sum_{\mathbf{q}'} \sum_{\alpha,\beta} \left(\frac{\delta c_\alpha^\dagger(\mathbf{q}')}{\delta A_+(\mathbf{q})} (\Theta^{\mathrm{T}} \Omega \Theta)_{\alpha\beta} c_\beta(\mathbf{q}') + \frac{\delta c_\alpha^\dagger(\mathbf{q}')}{\delta A_+(\mathbf{q})} (\Theta^{\mathrm{T}} \Omega)_{\alpha\beta} \mathscr{A}_\beta(\mathbf{q}') \right). \end{aligned}$$

Substituting the derivative of $c_\alpha^\dagger(\mathbf{q}')$, we get

$$J_-(\mathbf{q}) = \frac{2\hbar}{L^2} \sum_{\mathbf{q}'} \sum_{\alpha,\beta} (-e n_\alpha L \delta_{\mathbf{q},-\mathbf{q}'} \hat{q}_-) \big((\Theta^{\mathrm{T}} \Omega \Theta)_{\alpha\beta} c_\beta(\mathbf{q}') + (\Theta^{\mathrm{T}} \Omega)_{\alpha\beta} \mathscr{A}_\beta(\mathbf{q}') \big).$$

We recall that the matrix $\Theta^{\mathrm{T}} \Omega \Theta$ is proportional to N^{-1} according to Eq. (4.50). We also rewrite $n_\alpha = \nu_\alpha / 2\pi l_B^2$. These observations yield

$$\begin{aligned} J_-(\mathbf{q}) &= -\frac{2e}{L} \frac{2\pi\hbar}{2m\,eB} \frac{1}{2\pi l_B^2} \sum_\alpha \hat{q}_- N_{\alpha\alpha}^{-1} \nu_\alpha \left(c_\alpha(-\mathbf{q}) + \sum_\beta (\Theta^{-1})_{\alpha\beta} \mathscr{A}_\beta(-\mathbf{q}) \right) \\ &= -\frac{e}{mL} \sum_\alpha \hat{q}_- \left(c_\alpha(-\mathbf{q}) + \sum_\beta (\Theta^{-1})_{\alpha\beta} \mathscr{A}_\beta(-\mathbf{q}) \right). \end{aligned}$$

We can decompose the current as $J_-(\mathbf{q}) = \sum_\alpha J_{\alpha,-}(\mathbf{q})$ with

$$J_{\alpha,-}(\mathbf{q}) = -\frac{e}{mL} \hat{q}_- \left(c_\alpha(-\mathbf{q}) + \sum_\beta (\Theta^{-1})_{\alpha\beta} \mathscr{A}_\beta(-\mathbf{q}) \right).$$

The currents $J_{\alpha,-}$ can also be obtained directly by taking the derivative of the Hamiltonian with respect to $A_{\alpha,+} \equiv \sum_{j_\alpha} e^{i\mathbf{q}\cdot\mathbf{r}_{j_\alpha}} A_+(\mathbf{q})$.

In the expression for $J_{\alpha,-}(\mathbf{q})$, we find a linear combination of $c(-\mathbf{q})$ and $\mathscr{A}(-\mathbf{q})$. In analogy with the one-component case, we attempt to connect this linear combination to the transformed ladder operator $\tilde{\mathscr{A}}(-\mathbf{q})$. In the multicomponent case, this linear combination is the α component of

$$c(-\mathbf{q}) + \Theta^{-1}\mathscr{A}(-\mathbf{q}) = c(-\mathbf{q}) + \frac{1}{\theta_0}\sqrt{N}C^{\mathrm{T}}\sqrt{D}\mathscr{A}(-\mathbf{q}).$$

Performing the rescaling $c' = \theta_0\sqrt{(RN)^{-1}}c$ according to Eq. (4.53), we find that

$$\begin{aligned} J_{\alpha,-}(\mathbf{q}) &= -\frac{e}{mL\theta_0}\hat{q}_-\big(\sqrt{RN}\,c'(-\mathbf{q}) + \sqrt{N}C^{\mathrm{T}}\sqrt{D}\mathscr{A}'(-\mathbf{q})\big)_\alpha \\ &= -\frac{e}{mL\theta_0}\hat{q}_-\big[\sqrt{N}C^{\mathrm{T}}\sqrt{D}\big(\sqrt{D^{-1}}C\sqrt{R}\,c'(-\mathbf{q}) + \mathscr{A}'(-\mathbf{q})\big)\big]_\alpha. \end{aligned}$$

Let us compare this expression to the α component of $\tilde{\mathscr{A}}(-\mathbf{q}) = \tilde{\mathscr{A}}'(-\mathbf{q})$. The result of the rotation in $(c', \mathscr{A}')$ space is

$$\tilde{\mathscr{A}}'(-\mathbf{q}) = V\,\tilde{c}'(-\mathbf{q}) + W\,\tilde{\mathscr{A}}'(-\mathbf{q}) = W\big(Q\,\tilde{c}'(-\mathbf{q}) + \tilde{\mathscr{A}}'(-\mathbf{q})\big),$$

where we used $V = WQ$, with $Q = \sqrt{D^{-1}}C\sqrt{R}$, as given by Eqs. (4.151) and (4.152). This shows that we can write $\sqrt{D^{-1}}C\sqrt{R}\,c'(-\mathbf{q}) + \mathscr{A}'(-\mathbf{q})$ in the expression for $J_{\alpha,-}(\mathbf{q})$ as $W^{-1}\tilde{\mathscr{A}}'(-\mathbf{q})$. We therefore obtain

$$J_{\alpha,-}(\mathbf{q}) = -\frac{e}{mL\theta_0}\hat{q}_-\big(\sqrt{N}C^{\mathrm{T}}\sqrt{D}\,W^{-1}\tilde{\mathscr{A}}'(-\mathbf{q})\big)_\alpha = -\frac{e}{mL\theta_0}\hat{q}_-\big(\sqrt{N}G^{\mathrm{T}}\sqrt{F}\tilde{\mathscr{A}}(-\mathbf{q})\big)_\alpha, \tag{4.121}$$

rewriting W^{-1} using Eq. (4.154). Here again, G and F are the orthogonal and diagonal matrices, respectively, obtained from the diagonalisation of $R+E$. By noting that $\Theta^{-1} = \theta_0^{-1}\sqrt{N}C^{\mathrm{T}}\sqrt{D}$, we can also write the current as

$$J_{\alpha,-}(\mathbf{q}) = -\frac{e}{mL}\hat{q}_-\big(\Theta^{-1}\,W^{-1}\tilde{\mathscr{A}}'(-\mathbf{q})\big)_\alpha,$$

which is similar to the one-component analogue, in particular the first form mentioned in Eq. (4.93): The one-component quantities $1/\theta$ and $\sqrt{1+\mu^2}$ have been replaced by the matrices Θ^{-1} and W^{-1}, respectively. The currents $J_{\alpha,+}(\mathbf{q})$ can be derived in the same manner or by the fact that they are the hermitian conjugates of $J_{\alpha,-}(-\mathbf{q})$:

$$J_{\alpha,+}(\mathbf{q}) = \frac{e}{mL\theta_0}\hat{q}_+\big(\tilde{\mathscr{A}}^\dagger(\mathbf{q})\sqrt{F}G\sqrt{N}\big)_\alpha = \frac{e}{mL}\hat{q}_+\big(\tilde{\mathscr{A}}^\dagger(\mathbf{q})(W^{-1})^{\mathrm{T}}(\Theta^{-1})^{\mathrm{T}}\big)_\alpha. \tag{4.122}$$

With Eqs. (4.121) and (4.122), we can rewrite the diagonalised Hamiltonian in a very convenient form. Recalling that $F = \mathrm{diag}(\{\mu_\alpha\}$, we write the diagonalised RPA Hamiltonian [Eq. (4.62)] as

$$H_{\mathrm{RPA}} = \hbar\omega_{\mathrm{c}}\sum_{\mathbf{q}}\tilde{\mathscr{A}}^\dagger(\mathbf{q})F\tilde{\mathscr{A}}(\mathbf{q}) = \hbar\omega_{\mathrm{c}}\sum_{\alpha}\sum_{\mathbf{q}}\tilde{\mathscr{A}}_\alpha^\dagger(\mathbf{q})F_{\alpha\alpha}\tilde{\mathscr{A}}_\alpha(\mathbf{q}). \tag{4.123}$$

In this expression, we rewrite the ladder operators $\mathscr{A}_\alpha(\mathbf{q})$ and $\mathscr{A}_\alpha^\dagger(\mathbf{q})$ in terms of $J_{\alpha,-}(-\mathbf{q})$ and $J_{\alpha,+}(\mathbf{q})$, respectively. We then obtain

$$H_{\mathrm{RPA}} = \hbar\omega_{\mathrm{c}}\left(\frac{mL}{e}\right)^2 \sum_\alpha \sum_{\beta,\gamma} \sum_{\mathbf{q}} J_{\beta,+}(\mathbf{q})\big(\sqrt{N^{-1}}G^{\mathrm{T}}\sqrt{F^{-1}}\big)_{\beta\alpha} F_{\alpha\alpha}\big(\sqrt{F^{-1}}G\sqrt{N^{-1}}\big)_{\alpha\gamma} J_{\gamma,-}(-\mathbf{q}).$$

Simplification of the matrix between the current operators to N^{-1} yields

$$H_{\mathrm{RPA}} = \frac{\hbar\omega_{\mathrm{c}} m^2 L^2}{e^2}\theta_0^2 \sum_\alpha \sum_{\mathbf{q}} J_{\alpha,+}(\mathbf{q}) N^{-1}_{\alpha\alpha} J_{\alpha,-}(-\mathbf{q}) \;= \frac{\pi\hbar L^2}{e^2\omega_{\mathrm{c}}} \sum_\alpha \sum_{\mathbf{q}} J_{\alpha,+}(\mathbf{q})\, \nu_\alpha^{-1} J_{\alpha,-}(-\mathbf{q}), \tag{4.124}$$

where we have used Eq. (4.33) and $\omega_{\mathrm{c}} = eB/m$. It is clear that the Hamiltonian written in this form generalises the one-component formula (4.95).

Some expressions in the above reasoning become more elegant if we define the currents in the eigenvector basis as

$$\check{J}_\pm = G\sqrt{N^{-1}} J_{\beta,\pm}, \tag{4.125}$$

or in components,

$$\check{J}_{\alpha,\pm} = \sum_\beta G_{\alpha\beta}\nu_\beta^{-1/2} J_{\beta,\pm}. \tag{4.126}$$

With this definition, Eqs. (4.121) and (4.122) reduce to

$$\check{J}_{\alpha,-}(\mathbf{q}) = -\frac{e}{mL\theta_0}\hat{q}_-\sqrt{\mu_\alpha}\tilde{\mathscr{A}}_\alpha(-\mathbf{q}) \quad \text{and} \quad \check{J}_{\alpha,+}(\mathbf{q}) = \frac{e}{mL\theta_0}\hat{q}_+\sqrt{\mu_\alpha}\tilde{\mathscr{A}}_\alpha^\dagger(\mathbf{q}),$$

where μ_α are the entries of the diagonal matrix F. Then it is straightforward to derive from Eq. (4.123) the RPA Hamiltonian in terms of the currents $\check{J}_{\alpha,-}$ and $\check{J}_{\alpha,+}$ as

$$H_{\mathrm{RPA}} = \frac{\pi\hbar L^2}{e^2\omega_{\mathrm{c}}} \sum_\alpha \sum_{\mathbf{q}} \check{J}_{\alpha,+}(\mathbf{q})\check{J}_{\alpha,-}(-\mathbf{q}). \tag{4.127}$$

This expression can also be derived directly from Eq. (4.124).

Also the oscillator part $\check{\rho}_{\mathrm{osc},\alpha}$ of the transformed density in Eq. (4.109c) can be written in terms of the currents given by Eq. (4.125), as

$$\check{\rho}_{\mathrm{osc},\alpha}(\mathbf{q}) = \frac{|\mathbf{q}|m\theta_0}{2e\sqrt{\pi}}\mu_\alpha^{-1}\big(\hat{q}_+\check{J}_{\alpha,-}(-\mathbf{q}) - \hat{q}_-\check{J}_{\alpha,+}(-\mathbf{q})\big). \tag{4.128}$$

The oscillator density in the original basis and the eigenvector basis relate as $\check{\rho}_{\mathrm{osc}}(\mathbf{q}) = G\sqrt{N^{-1}}\rho_{\mathrm{osc}}(\mathbf{q})$, so that $\rho_{\mathrm{osc}}(\mathbf{q})$ can be written in terms of the original currents as

$$\rho_{\mathrm{osc},\alpha}(\mathbf{q}) = \frac{|\mathbf{q}|m\theta_0}{2e\sqrt{\pi}}\sum_\beta\big(\sqrt{N}G^{\mathrm{T}}F^{-1}G\sqrt{N^{-1}}\big)_{\alpha\beta}\big(\hat{q}_+\check{J}_{\beta,-}(-\mathbf{q}) - \hat{q}_-\check{J}_{\beta,+}(-\mathbf{q})\big). \tag{4.129}$$

The matrix $\sqrt{N}G^{\mathrm{T}}F^{-1}G\sqrt{N^{-1}}$ can be simplified using $G^{\mathrm{T}}FG = R + E$, as defined in Sec. 4.5.2. Hence, $G^{\mathrm{T}}F^{-1}G = (R+E)^{-1}$, where $E = \sqrt{N}K\sqrt{N}$, so that we obtain

$$\sqrt{N}G^{\mathrm{T}}F^{-1}G\sqrt{N^{-1}} = \sqrt{N}(R+E)^{-1}\sqrt{N^{-1}} = (R+NK)^{-1}.$$

Substituting this equality into Eq. (4.129), we arrive at

$$\begin{aligned}\rho_{\mathrm{osc},\alpha}(\mathbf{q}) &= \frac{|\mathbf{q}|m\theta_0}{2e\sqrt{\pi}}\sum_\beta\big((R+NK)^{-1}\big)_{\alpha\beta}\big(\hat{q}_+J_{-,\beta}(-\mathbf{q}) - \hat{q}_-J_{+,\beta}(-\mathbf{q})\big)\\ &= -\frac{i}{e\omega_{\mathrm{c}}}\sum_\beta\big((R+NK)^{-1}\big)_{\alpha\beta}\big(\mathbf{q}\wedge\mathbf{J}_\beta(-\mathbf{q})\big).\end{aligned} \tag{4.130}$$

Of special interest is the sum of oscillator parts, $\sum_\alpha \rho_{\mathrm{osc},\alpha}(\mathbf{q})$. This sum may be evaluated by computing the inner product of the vector $\mathbf{1} = (1,\ldots,1)$ with the vector $(\rho_{\mathrm{osc},1}, \ldots, \rho_{\mathrm{osc},\kappa})$. This computation involves the matrix multiplication $\mathbf{1}^{\mathrm{T}}(R+NK)^{-1}$, which can also be written as the transpose of $(R+KN)^{-1}\mathbf{1}$. From the discussion of the eigenvector of H'_{mat} with eigenvalue 1, we recall that $R+KN$ leaves the vector $\mathbf{1}$ invariant, i.e., $(R+KN)\mathbf{1} = \mathbf{1}$. Hence, the same must be valid for the inverse, i.e., $(R+KN)^{-1}\mathbf{1} = \mathbf{1}$, so that $\mathbf{1}^{\mathrm{T}}(R+NK)^{-1} = \mathbf{1}^{\mathrm{T}}$. Then we obtain the result

$$\begin{aligned}\sum_\alpha\rho_{\mathrm{osc},\alpha}(\mathbf{q}) &= -\frac{i}{e\omega_{\mathrm{c}}}\sum_{\alpha,\beta}\mathbf{1}_\alpha\big((R^{-1}+NK)^{-1}\big)_{\alpha\beta}\big(\mathbf{q}\wedge\mathbf{J}_\beta(-\mathbf{q})\big)\\ &= -\frac{i}{e\omega_{\mathrm{c}}}\sum_\beta\mathbf{1}_\beta\big(\mathbf{q}\wedge\mathbf{J}_\beta(-\mathbf{q})\big) = -\frac{i}{e\omega_{\mathrm{c}}}\sum_\beta\mathbf{q}\wedge\mathbf{J}_\beta(-\mathbf{q}) = -\frac{i}{e\omega_{\mathrm{c}}}\mathbf{q}\wedge\mathbf{J}_{\mathrm{T}}(-\mathbf{q}),\end{aligned} \tag{4.131}$$

where $\mathbf{J}_{\mathrm{T}}(-\mathbf{q}) = \sum_\beta\mathbf{J}_\beta(-\mathbf{q})$ is the total current. The analogy with the one-component case, Eq. (4.97), is obvious.

The eigenvectors $\tilde{\mathbf{g}}_\alpha$ of $R+KN$, discussed in Sec. 4.5.2, also play a special role here. The eigenvalue equation involving $\tilde{\mathbf{g}}_\alpha$ implies that $\tilde{\mathbf{g}}_\alpha^{\mathrm{T}}(R+NK)^{-1} = \tilde{\mathbf{g}}_\alpha^{\mathrm{T}}\mu_\alpha^{-1}$, where μ_α is the eigenvalue of $R+KN$ associated with the eigenvector $\tilde{\mathbf{g}}_\alpha$. Hence, we find

$$\begin{aligned}\sum_\beta(\tilde{\mathbf{g}}_\alpha)_\beta\rho_{\mathrm{osc},\beta}(\mathbf{q}) &= -\frac{i}{e\omega_{\mathrm{c}}}\sum_{\beta,\gamma}(\tilde{\mathbf{g}}_\alpha)_\beta\big((R^{-1}+NK)^{-1}\big)_{\beta\gamma}\big(\mathbf{q}\wedge\mathbf{J}_\gamma(-\mathbf{q})\big)\\ &= -\frac{i}{e\omega_{\mathrm{c}}}\sum_\beta(\tilde{\mathbf{g}}_\alpha)_\beta\big(\mathbf{q}\wedge\mathbf{J}_\beta(-\mathbf{q})\big).\end{aligned} \tag{4.132}$$

Since $\mathbf{1}$ is an eigenvector of $R+KN$ with eigenvalue 1, Eq. (4.131) is a special case of Eq. (4.132).

In order to obtain the conductivities, we couple the oscillator part of the density to an external electric potential, like in the single-component case. However, for multiple components, each component has its own potential $\Phi_\alpha(\mathbf{q})$, which we couple to $\rho_{\mathrm{osc},\alpha}(\mathbf{q})$, which yields the coupling term

$$H_{\mathrm{ext}} = \frac{-eL^2}{2\omega_{\mathrm{c}}}\sum_\alpha\sum_{\mathbf{q}}\Phi_\alpha(\mathbf{q})\rho_{\mathrm{osc},\alpha}(\mathbf{q})$$

in the Hamiltonian. For clarity, we study the coupling in matrix notation, i.e., we define $\Phi(\mathbf{q}) = \big(\Phi_1(\mathbf{q}),\ldots,\Phi_\kappa(\mathbf{q})\big)$ and similar expressions for the currents. Moreover, we write $J_{+,\alpha}(\mathbf{q}) = J^\dagger_{-,\alpha}(-\mathbf{q})$ and $\Phi^\dagger_\alpha(\mathbf{q}) = -\Phi_\alpha(-\mathbf{q})$ for all α. In this notation, the coupling between the potential and $\rho_{\rm osc}$ is given by

$$H_{\rm ext} = -\frac{L^2}{2\omega_{\rm c}}\sum_{\mathbf{q}}\big(\Phi^\dagger(-\mathbf{q})q_-^*(R^{-1}+NK)^{-1}J_-(-\mathbf{q})J_-^\dagger(-\mathbf{q})(R^{-1}+KN)^{-1}q_-\Phi(-\mathbf{q})\big),$$

and the original Hamiltonian (4.124) is written as

$$H_{\rm RPA} = \frac{\pi\hbar L^2}{e^2\omega_{\rm c}}\sum_{\mathbf{q}} J_-^\dagger(-\mathbf{q})\,N^{-1}J_-(-\mathbf{q}).$$

As in the single-component case, we add these terms together, and we "complete the squares". For convenience, we use $\sqrt{N^{-1}}J_-(\mathbf{q})$ and its hermitian conjugate as the variables for which we compute the averages. Writing $(R+NK)^{-1} = \sqrt{N}(R+E)^{-1}\sqrt{N^{-1}}$, we obtain the vector-valued equations

$$\langle\sqrt{N^{-1}}J_-(-\mathbf{q})\rangle = \frac{e^2}{2\pi\hbar}q_-(R+E)^{-1}\sqrt{N}\Phi(-\mathbf{q}),$$

and

$$\langle J_-^\dagger(-\mathbf{q})\sqrt{N^{-1}}\rangle = \frac{e^2}{2\pi\hbar}q_-^*\Phi^\dagger(-\mathbf{q})\sqrt{N}(R+E)^{-1}.$$

From these expressions, we derive the currents

$$\langle J_-(\mathbf{q})\rangle = -\frac{e^2}{h}q_-\sqrt{N}(R+E)^{-1}\sqrt{N}\Phi(\mathbf{q}) = -\frac{e^2}{h}q_-(R+NK)^{-1}N\Phi(\mathbf{q}) \tag{4.133}$$

and

$$\langle J_+(\mathbf{q})\rangle = \frac{e^2}{h}q_+\Phi^\dagger(-\mathbf{q})\sqrt{N}(R+E)^{-1}\sqrt{N} = \frac{e^2}{h}q_+\Phi^\dagger(-\mathbf{q})N(R+KN)^{-1}. \tag{4.134}$$

Similar to the one-component case, we derive the conductivity by recalling that the electric fields are given by $\mathbf{E}_\alpha = -i\mathbf{q}\Phi_\alpha(\mathbf{q})$. In the multicomponent case, the definition of the conductivity tensor is

$$\begin{pmatrix}J_{\alpha,x}\\ J_{\alpha,y}\end{pmatrix} = \sum_\beta\begin{pmatrix}(\sigma_{xx})_{\alpha\beta} & -(\sigma_{xy})_{\alpha\beta}\\ (\sigma_{xy})_{\alpha\beta} & (\sigma_{xx})_{\alpha\beta}\end{pmatrix}\begin{pmatrix}E_{\beta,x}\\ E_{\beta,y}\end{pmatrix}, \tag{4.135}$$

which generalises the single-component conductivity tensor of Eq. (4.99). In complex form, the conductivities are given by $J_{\alpha,\pm} = \sum_\beta(\sigma_\pm)_{\alpha\beta}E_{\beta,\pm}$, with $(\sigma_\pm)_{\alpha\beta} = (\sigma_{xx})_{\alpha\beta} \pm$

$i(\sigma_{xy})_{\alpha\beta}$. Writing the currents (4.133) and (4.134) in components and in complex form, as

$$\langle J_{\pm,\alpha}(\mathbf{q})\rangle = \pm i\frac{e^2}{h}\sum_\beta \big[(R+NK)^{-1}N\big]_{\alpha\beta}E_{\pm,\beta}(\mathbf{q}),$$

we obtain the Hall conductivities

$$(\sigma_{xy})_{\alpha\beta} = \frac{e^2}{h}\big[(R+NK)^{-1}N\big]_{\alpha\beta} = \frac{e^2}{h}\big[\sqrt{N}(R+E)^{-1}\sqrt{N}\big]_{\alpha\beta} \tag{4.136}$$

The latter form shows that the matrix of Hall conductivities is proportional to $\sqrt{N}(R+E)^{-1}\sqrt{N} = (RN^{-1}+K)^{-1}$, a symmetric matrix. As a consequence of the invariance of the oscillator density under the transformations (4.155) acting on T, discussed in Sec. 4.6.2, the currents and conductivities are invariant as well, as should be the case for any physical quantity. We remark that Eq. (4.136) agrees with two-component results derived by Lopez and Fradkin [40].

The eigenvectors $\tilde{\mathbf{g}}_\alpha$ of $R+KN$ also play a special role with respect to the Hall conductivities. Indeed, left-multiplication by $\tilde{\mathbf{g}}_\alpha^{\mathrm{T}}$ yields

$$\sum_\beta (\tilde{\mathbf{g}}_\alpha)_\beta(\sigma_{xy})_{\beta\gamma} = \frac{e^2}{h}\mu_\alpha^{-1}(\tilde{\mathbf{g}}_\alpha)_\gamma \nu_\gamma. \tag{4.137}$$

In particular, left-multiplication of the currents by the eigenvector $\tilde{\mathbf{g}}_\alpha = \mathbf{1}$ (with eigenvalue $\mu_\alpha = 1$) yields the total Hall current

$$\langle J_{\mathrm{T}}^y(\mathbf{q})\rangle \equiv \sum_\alpha \langle J_\alpha^y(\mathbf{q})\rangle = \sum_\alpha\sum_\beta (\sigma_{xy})_{\alpha\beta}E_\beta^x(\mathbf{q}) = \frac{e^2}{h}\sum_\beta \nu_\beta E_\beta^x(\mathbf{q}). \tag{4.138}$$

where we used $\sum_\beta(\sigma_{xy})_{\beta\gamma} = \nu_\gamma e^2/h$, which follows from Eq. (4.137). Hence, if the electric fields of all components are equal, then the total Hall current is proportional to the conductivity quantum e^2/h times the total filling factor, which is equivalent to the familiar relation for single component systems, Eq. (4.100). This behaviour has been seen in experiments with bilayer systems [181, 182] and triple-layer systems [183–185]. Systems of this type have also been studied theoretically in the framework of a Chern-Simons theory [186, 187]. The results are also relevant for systems with other pseudospin degrees of freedom (e.g., valley pseudospin), such as graphene [37, 38] and silicon-based structures [188, 189].

At this point, it might be instructive to apply the results to the two-component Halperin state (mmn). As discussed before in Sec. 4.5.3, the eigenvectors of $R+KN$ are given by $(1,1)/\sqrt{2}$ and $(1,-1)/\sqrt{2}$, corresponding to the in-phase mode and out-of-phase mode. In view of the discussion above, we define the in-phase and the out-of-phase current by

$$\mathbf{J}_{\mathrm{i}}(\mathbf{q}) = \mathbf{J}_\uparrow(\mathbf{q}) + \mathbf{J}_\downarrow(\mathbf{q}) \quad \text{and} \quad \mathbf{J}_{\mathrm{o}}(\mathbf{q}) = \mathbf{J}_\uparrow(\mathbf{q}) - \mathbf{J}_\downarrow(\mathbf{q}),$$

respectively, where the components are indicated by ↑ and ↓. The in-phase current, or total current, is equal to

$$\langle J_{\rm i}^y\rangle = \frac{e^2}{h}\sum_\beta \nu_\beta E_\beta^x = \frac{e^2}{h}(\nu_\uparrow E_\uparrow^x + \nu_\downarrow E_\downarrow^x) = \frac{e^2}{h}(\tfrac{1}{2}\nu_{\rm T})(E_\uparrow^x + E_\downarrow^x), \tag{4.139}$$

where $\nu_{\rm T} = \nu_\uparrow + \nu_\downarrow = 2/(m+n)$ is the total filling factor. If the electric fields of both components are equal, $E_\uparrow^x = E_\downarrow^x = E_0^x$, then we find $\langle J_{\rm i}^x\rangle = (e^2/h)\nu_{\rm T}E_0^x$. In other words, if the electric fields are equal for both components, then we find the same Hall conductivity as we would find for a single-component system with filling factor equal to $\nu_{\rm T}$.

For the out-of-phase current, we compute

$$\langle J_{\rm o}^y\rangle = \begin{pmatrix}1 & -1\end{pmatrix}\begin{pmatrix}\langle J_\uparrow^y\rangle \\ \langle J_\downarrow^y\rangle\end{pmatrix} = \begin{pmatrix}1 & -1\end{pmatrix}\sigma_{xy}\begin{pmatrix}E_{\uparrow,x} \\ E_{\downarrow,x}\end{pmatrix}.$$

Substituting the matrix $\sigma_{xy} = (e^2/h)(R+NK)^{-1}N$, and using that $(1,-1)$ is an eigenvector of $R+KN$ with eigenvalue $\mu_2 = (m-n)/(m+n)$, we find

$$\langle J_{\rm o}^y\rangle = \frac{e^2}{h}\mu_2^{-1}\begin{pmatrix}1 & -1\end{pmatrix}\begin{pmatrix}\nu_\uparrow E_\uparrow^x \\ \nu_\downarrow E_\downarrow^x\end{pmatrix} = \frac{e^2}{h}\frac{1}{m-n}(E_\uparrow^x - E_\downarrow^x).$$

We remark that in the case of equal electric fields, the out-of-phase current is absent. In the case of opposite electric fields, $E_\uparrow^x = -E_\downarrow^x = E_0^x$, the total current vanishes and the out-of-phase current is equal to $\langle J_{\rm o}^y\rangle = 2(m-n)^{-1}(e^2/h)E_0^x$. This situation could be reached by counterflow experiments in bilayers (see e.g. Refs. [190–192] for counterflow experiments at $\nu_{\rm T} = 1$).

For the **SU**(2)-symmetric (mmm) state, with $M = \left(\begin{smallmatrix}1 & 1\\ 1 & 1\end{smallmatrix}\right)$ and $\nu_\uparrow + \nu_\downarrow = 1/m$, we have found (in Sec. 4.5.3) that the eigenvectors of $R+KN$ are proportional to $(1,1)$ and $(\nu_\uparrow^{-1}, -\nu_\downarrow^{-1})$, with eigenvalues 1 and $1/m$, respectively. We therefore define the in-phase and the out-of-phase current as

$$\mathbf{J}_{\rm i}(\mathbf{q}) = \mathbf{J}_\uparrow(\mathbf{q}) + \mathbf{J}_\downarrow(\mathbf{q}) \quad \text{and} \quad \mathbf{J}_{\rm o}(\mathbf{q}) = \frac{\mathbf{J}_\uparrow(\mathbf{q})}{\nu_\uparrow} - \frac{\mathbf{J}_\downarrow(\mathbf{q})}{\nu_\downarrow},$$

respectively. Using the same reasoning as above, we find that the total current satisfies

$$\langle J_{\rm i}^y\rangle = \frac{e^2}{h}(\tfrac{1}{2}\nu_{\rm T})(E_\uparrow^x + E_\downarrow^x),$$

which is the same as Eq. (4.139) for the (mmn) state, but now with $\nu_{\rm T} = 1/m$. The out-of-phase current is given by

$$\langle J_{\rm o}^y\rangle = \frac{e^2}{h}\mu_2^{-1}\begin{pmatrix}\nu_\uparrow^{-1} & -\nu_\downarrow^{-1}\end{pmatrix}\begin{pmatrix}\nu_\uparrow E_\uparrow^x \\ \nu_\downarrow E_\downarrow^x\end{pmatrix} = \frac{e^2}{h}m(E_\uparrow^x - E_\downarrow^x).$$

From the definition of $\mathbf{J}_o$, we observe that generally $\mathbf{J}_\uparrow$ and $\mathbf{J}_\downarrow$ depend on the filling factors. However, in order to have a fully symmetric system, also the currents and the electric fields of both components have to be equal. In that case, the out-of-phase current vanishes, and the in-phase (or total) current satisfies $\langle J_i^x \rangle = (e^2/h)\nu_T E_0^x$, where $E_0^y = E_\uparrow^x = E_\downarrow^x$. This result shows that from the point of view of the conductivity, we may treat an **SU**(2)-symmetric two component system at total filling factor ν_T as if it were a single-component system at filling factor ν_T. As expected, the presence of **SU**(2) spin degrees of freedom has no effect on the conductivity.

Strictly speaking, one may object against this result, because some parts in the derivation in this section cannot be performed with a singular matrix K, since they involve the inverse D^{-1} which does not exist. However, the results for the nonsingular case do not involve inverses of any matrix which becomes singular if K is singular. For example, the definitions of the currents, Eqs. (4.121) and (4.122), remain valid if K is singular. Thus, the results, in particular the one for the Hall conductivity [Eq. (4.136)] are valid without modification.

4.7 Conclusions

In conclusion, we have studied a microscopic Chern-Simons approach to general multicomponent quantum Hall systems (with κ components). Beyond the mean-field approximation, which yields a renormalisation of the magnetic field that depends on the average particle densities for each component, their fluctuations are taken into account within a Gaussian model of auxiliary gauge fields. These gauge fields, introduced by Shankar and Murthy in the framework of the Hamiltonian theory of the FQHE [23–26, 28], are indeed connected via constraints to the component density fluctuations.

The analysis of the Gaussian model —although it may be viewed as a first step in the discussion of a more complete Hamiltonian theory for multicomponent quantum Hall systems— already yields valuable insight into the structure and the correctness of the Chern-Simons theory, which is characterised by a symmetric $\kappa \times \kappa$ charge matrix K [159, 160]. Most saliently, one needs to discard charge matrices with negative eigenvalues because the associated Chern-Simons theories yield oscillator ground-state wave functions that are not normalised. This is in line with physical insight obtained from a multicomponent version of Laughlin's plasma picture [9] according to which charge matrices with negative eigenvalues yield inhomogeneous ground states where the components phase-separate [168].

Whereas singular charge matrices, with zero eigenvalues, had originally been discussed by Lopez and Fradkin [40] only for the **SU**(2)-symmetric case, we have argued here that the associated Chern-Simons theories reflect underlying ferromagnetic states in a more general setting. Indeed, we have shown that the density fluctuations of the κ components are then determined by only $r < \kappa$ constraints, such that $\kappa - r$ particular

combinations of the component densities may be chosen freely in the ground-state manifold, which is thus described by the $\mathbf{SU}(\kappa - r + 1)$ group. This symmetry is spontaneously broken by a particular ferromagnetic state, which can be described by $\kappa - r$ different Goldstone modes that may be viewed as generalised spin waves. Our results encompass the particular $\mathbf{SU}(2)$ case of two-component Chern-Simons theories discussed in the literature [21, 40, 41, 159–161].

We emphasise moreover that the analysis of the microscopic multicomponent Chern-Simons theory within the Gaussian approximation heuristically yields trial wave functions for multicomponent quantum Hall systems that may be further studied numerically. As an example, we have discussed generalised κ-component Halperin wave functions that play a similarly central role as Laughlin's wave functions do in one-component quantum Hall systems. Beyond these generalised Halperin wave functions, we have briefly discussed a second class of states, where the residual wave function that is not encoded in the Chern-Simons oscillator part χ_{osc} is a product of Slater determinants of p_α completely filled (α-component) composite-fermion levels. This construction is reminiscent of Jain's generalisation of one-component Laughlin wave functions to filling factors $\nu = p/(2sp+1)$ [10, 11, 16].

Within the oscillator framework, the energy $\hbar\omega_{\mathrm{c}}$ is generally not present among the eigenvalues. Hence Kohn's theorem, which states that the eigenvalue $\hbar\omega_{\mathrm{c}}$ must be present, implies that the spectrum of this Hamiltonian is unphysical. This result is not very surprising, because the electronic degrees of freedom, in the form of the momentum operators $p + e\langle A^*\rangle$ associated with the average gauge fields, have been neglected in this analysis. Therefore, the electronic degrees of freedom have to be included in order to obtain the physical eigenvalues. For the single-component case, this procedure has been described by Shankar and Murthy [23–26, 28]. The full Hamiltonian, which includes both the ladder operators of the oscillator Hamiltonian and the electronic momentum operators, is studied in the RPA. Here, we have shown that in the multicomponent version of the decoupling procedure the eigenvalue $\hbar\omega_{\mathrm{c}}$ is recovered, among other eigenvalues, so that Kohn's theorem holds and the spectrum is considered to be physical in this sense.

In this multicomponent theory, the eigenvector $\mathbf{1}$ associated to the energy $\hbar\omega_{\mathrm{c}}$ indicates that every component of the system contributes equally to this mode; it is therefore called the *in-phase* mode. The other eigenvectors are associated with modes where components are out of phase. For instance, in a two-component system where both components have equal filling factors, the second eigenvector of $R + K\,N$ is proportional to $(1, -1)$; the corresponding mode is therefore called the *out-of-phase* mode. In Sec. 4.5.3, we have demonstrated several properties of the eigenvalues and the modes by giving examples of states in two- and four-component systems.

The final part of this chapter deals with the densities and the constraints in terms of the diagonalised operators. For the single-component case, these results eventually lead to a connection between this microscopic theory, valid at low momenta, to

a theory valid at all momenta [26]. By a coupling between the oscillator part of the density and an electric potential, one is able to derive the Hall conductivity. In Sec. 4.6, we have generalised the method of Murthy and Shankar to multicomponent systems. For the conductivities, we have found that the eigenvectors of the Hamiltonian matrix also play an important role here. In particular, the vector **1** is connected to the total Hall conductivity, which is shown to be equal to e^2/h times the total filling factor ν_{T}. This is equal to the familiar value for single-component systems. In other words, this proves that the presence of internal degrees of freedom does not affect the value of the Hall conductivity for fractional quantum Hall states. This behaviour has been observed experimentally in multicomponent systems, like bilayer [181, 182] and trilayer [183–185] systems, graphene [37, 38], and silicon-based structures [188, 189]. In addition to the total Hall conductivity, our approach also gives conductivities related to other linear combinations of components, e.g., the difference (out-of-phase mode) in the two-component case.

4.A Multicomponent plasma analogy

The single-component plasma analogy proposed by Laughlin [9] is readily generalised to the multicomponent case. Here, we use the ground state

$$\chi_{\mathrm{osc}} = \exp\left(-\frac{1}{2}\sum_{\mathbf{q}}\sum_{\beta,\gamma}\delta\rho_\beta(-\mathbf{q})\frac{2\pi L^2}{|\mathbf{q}|^2}K_{\beta\gamma}\delta\rho_\gamma(\mathbf{q})\right), \tag{4.140}$$

which is Eq. (4.22) written out in components. Recalling that $2\pi L^2/|\mathbf{q}|^2$ is the Fourier transform of $-\log|\mathbf{r}|$, we perform an inverse Fourier transformation and we substitute the density fluctuations $\delta\rho_\alpha(\mathbf{r}) = \sum_{j_\alpha}\delta(\mathbf{r}-\mathbf{r}_{j_\alpha}) - n_\alpha$. Then, we can rewrite χ_{osc} as

$$\chi_{\mathrm{osc}} = \exp\left[\frac{1}{2}\sum_{\alpha,\beta}K_{\alpha\beta}\int \mathrm{d}^2\mathbf{r}\mathrm{d}^2\mathbf{r}'\left(\sum_{j_\alpha=1}^{N_\alpha}\delta(\mathbf{r}-\mathbf{r}_{j_\alpha}) - n_\alpha\right)\log|\mathbf{r}-\mathbf{r}'|\left(\sum_{k_\beta=1}^{N_\beta}\delta(\mathbf{r}'-\mathbf{r}_{k_\beta}) - n_\beta\right)\right].$$

By evaluating the integrals, one finds

$$\chi_{\mathrm{osc}} = \mathrm{const}\cdot\prod_{\alpha,\beta}\prod_{\substack{j_\alpha,k_\beta\\ j_\alpha\neq k_\beta}}|\mathbf{r}_{j_\alpha}-\mathbf{r}_{k_\beta}|^{K_{\alpha\beta}/2}\exp\left(-\frac{\pi}{2}\sum_{\alpha,\beta}n_\alpha K_{\alpha\beta}\sum_{k_\beta}|\mathbf{r}_{k_\beta}|^2\right).$$

Using that $\nu_\alpha = 2\pi l_B^2 n_\alpha$, and changing to complex notation, with $z = x - iy$,[18] we can explicitly write this expression as

$$\chi_{\mathrm{osc}} = \mathrm{const}\cdot\prod_{\alpha}\prod_{\substack{j_\alpha,k_\alpha\\ j_\alpha<k_\alpha}}|z_{j_\alpha}-z_{k_\alpha}|^{K_{\alpha\alpha}}\prod_{\substack{\alpha,\beta\\ \alpha<\beta}}\prod_{j_\alpha,k_\beta}|z_{j_\alpha}-z_{k_\beta}|^{K_{\alpha\beta}}\exp\left(-\sum_{\alpha,\beta}\nu_\alpha K_{\alpha\beta}\sum_{k_\beta}\frac{|z_{k_\beta}|^2}{4l_B^2}\right).$$

[18] This counterintuitive definition is used in order to have analytic lowest Landau level wave functions. This is due to the negative charge $-e$ of the electrons, for which the basic Hamiltonians are defined. Therefore, one has $\theta(\mathbf{r}) = \arg(x+iy) = \arg z^* = -\arg(z)$.

The Jastrow-type products in this expression only contain distances between the particles, i.e., only the moduli $|z_{j_\alpha} - z_{k_\beta}|$. Phase factors of the form

$$[(z_{j_\alpha} - z_{k_\beta})/|z_{j_\alpha} - z_{k_\beta}|]^{K_{\alpha\beta}} = \exp[iK_{\alpha\beta}\arg(z_{j_\alpha} - z_{k_\beta})] = \exp[-iK_{\alpha\beta}\theta(\mathbf{r}_{j_\alpha} - \mathbf{r}_{k_\beta})]$$

are obtained from substitution of the full density $\rho_\alpha(\mathbf{r}) = \sum_{j_\alpha}\delta(\mathbf{r} - \mathbf{r}_{j_\alpha})$ into the Chern-Simons transformation (4.1). Applying this transformation to χ_{osc}, we obtain the product of the latter with the phase factors,

$$\psi(\{z_{j_\alpha}\}) = \prod_\alpha \prod_{\substack{j_\alpha,k_\alpha \\ j_\alpha<k_\alpha}} (z_{j_\alpha} - z_{k_\alpha})^{K_{\alpha\alpha}} \prod_{\substack{\alpha,\beta \\ \alpha<\beta}} \prod_{j_\alpha,k_\beta} (z_{j_\alpha} - z_{k_\beta})^{K_{\alpha\beta}} \times \exp\left(-\sum_{\alpha,\beta}\nu_\alpha K_{\alpha\beta}\sum_{k_\beta}\frac{|z_{k_\beta}|^2}{4l_B^2}\right)\phi_{\{\nu_\alpha^*\}}(\{z_{j_\alpha}\}), \quad (4.141)$$

where $\phi_{\{\nu_\alpha^*\}}$ denotes the composite-particle wave function for filling factors ν_α^*, which will be investigated in the following. The magnetic lengths appearing in $\phi_{\{\nu_\alpha^*\}}(\{z_{j_\alpha}\})$ are the reduced magnetic lengths $l_{B_\alpha^*}$ given by Eq. (4.5).

As an example, we consider the situation in which ν_α^* can be determined by an exponent matrix M^* [159, 160, 165, 168], such that $\phi_{\{\nu_\alpha^*\}}$ is the Halperin wave function

$$\phi_{\{\nu_\alpha^*\}}(\{z_{j_\alpha}\}) = \prod_\alpha \prod_{\substack{j_\alpha,k_\alpha \\ j_\alpha<k_\alpha}} (z_{j_\alpha} - z_{k_\alpha})^{M^*_{\alpha\alpha}} \prod_{\substack{\alpha,\beta \\ \alpha<\beta}} \prod_{j_\alpha,k_\beta} (z_{j_\alpha} - z_{k_\beta})^{M^*_{\alpha\beta}} \exp\left(-\sum_\alpha\sum_{k_\alpha}\frac{|z_{k_\alpha}|^2}{4l_{B_\alpha^*}^2}\right). \quad (4.142)$$

Combining Eqs. (4.141) and (4.142), we obtain the full electronic wave function,

$$\psi(\{z_{j_\alpha}\}) = \prod_\alpha \prod_{\substack{j_\alpha,k_\alpha \\ j_\alpha<k_\alpha}} (z_{j_\alpha} - z_{k_\alpha})^{K_{\alpha\alpha}+M^*_{\alpha\alpha}} \prod_{\substack{\alpha,\beta \\ \alpha<\beta}} \prod_{j_\alpha,k_\beta} (z_{j_\alpha} - z_{k_\beta})^{K_{\alpha\beta}+M^*_{\alpha\beta}} \exp\left(-\sum_\alpha\sum_{k_\alpha}\frac{|z_{k_\alpha}|^2}{4l_B^2}\right), \quad (4.143)$$

which is the Halperin wave function for the exponent matrix $M_{\alpha\beta} = M^*_{\alpha\beta} + K_{\alpha\beta}$ [165]. Here, we have expressed the effective magnetic lengths in the exponential of Eq. (4.142) in terms of the original one, as $1/l_{B_\alpha^*}^2 = (1 - \sum_\beta K_{\alpha\beta}\nu_\beta)/l_B^2$, by virtue of Eq. (4.5).

4.B Ground state in the singular case

The reasoning given for the two-component example in Sec. 4.4.2 can be extended to any number of components. Suppose that the charge matrix K (being a $\kappa\times\kappa$ symmetric nonnegative definite matrix) is of rank r, which means that it has r independent rows or columns. In particular, there are $\kappa - r$ rows or columns that can be written as a linear combination of the other r independent rows or columns. This also means that the dimension of the null space, or equivalently, the multiplicity of zero eigenvalues is equal to $\kappa - r$.

Since the constraints [Eq. (4.9)] are expressed as a linear relation involving the matrix K, there are only r independent constraints. Hence, the vector $a^\circ = (a_1^\circ, \ldots, a_\kappa^\circ)$ lives only in an r-dimensional subspace; $\kappa - r$ of its components can be written as a linear combination of the other r.

Now we analyse the Hamiltonian (4.13). Since we have assumed that the matrix of densities N is nonsingular (i.e., all filling factors are nonzero, as required for the harmonic approximation to be valid), the rank of $E = \sqrt{N}K\sqrt{N}$ is equal to the rank of K. This means that E has r positive eigenvalues and $\kappa - r$ zero eigenvalues, just as the matrix K. We diagonalise E as usual in terms of a diagonal matrix D and an orthogonal matrix C such that $E = C^{\mathrm{T}} D C$. Note that the order of the eigenvalues on the diagonal of D (and simultaneously the order of the rows of C) may be chosen at will, so that we may choose for simplicity $D = \mathrm{diag}(\lambda_1, \ldots, \lambda_r, 0, \ldots, 0)$, where $\lambda_1, \ldots, \lambda_r$ are the positive eigenvalues of E. In the diagonalised Hamiltonian (4.16), the components $\overline{P}_{r+1}, \ldots, \overline{P}_\kappa$ are absent since they are multiplied with the zero eigenvalues of D. We still have κ components of $\overline{a}$ in the Hamiltonian, but we should remember that only r of them are independent.

The diagonalised Hamiltonian contains r nonzero eigenvalues, which depend on the filling factors ν_α. However, some variations in the filling factors will leave the eigenvalues, and hence the diagonalised Hamiltonian, invariant, namely, those satisfying the equation

$$0 = (\nabla \lambda_\beta) \cdot \delta\nu = \sum_\alpha \frac{\partial \lambda_\beta}{\partial \nu_\alpha} \delta\nu_\alpha \quad \text{for all } \beta.$$

In other words, the desired variations are the vectors in the null space of the gradient matrix $(\nabla\lambda)$ of the eigenvalues, which is defined as the matrix of derivatives of λ, with respect to ν, $(\nabla\lambda)_{\beta\alpha} = \partial\lambda_\beta/\partial\nu_\alpha$. Since $\kappa - r$ of the eigenvalues λ_β are zero, the rank of the gradient matrix is at most r, and this consequently means that we can find at least $\kappa - r$ independent variations in the filling factors which leave the eigenvalues invariant.

In the example discussed in Sec. 4.4.2, we observed that $\nu_1 - \nu_2$ does not appear in the diagonalised Hamiltonian. In order to demonstrate the procedure sketched in the preceding paragraph, we compute the gradients of the eigenvalues 0 and $2(\nu_1+\nu_2)$. Obviously, in this example the gradient matrix is $(\nabla\lambda) = \left(\begin{smallmatrix} 0 & 0 \\ 2 & 2 \end{smallmatrix}\right)$ and its null space is spanned by the single vector $(1, -1)$. Since this vector is independent of the filling factors ν_1 and ν_2, we can state that all eigenvalues, and hence the diagonalised Hamiltonian, are invariant under the transformation $\{\nu_1 \to \nu_1 + \delta\nu, \nu_2 \to \nu_2 - \delta\nu\}$. This means that the linear combination $\nu_1 - \nu_2$ is completely absent from the Hamiltonian, as argued earlier. We remark that the variation that leaves the Hamiltonian invariant need not always be constant in the filling factors ν_α. However, for physically relevant systems, the variations are constant, describing particle exchange among different components.

We now return to the diagonalised Hamiltonian, and try to find the lowest-energy states, in the same way as we have done for the example in Sec. 4.4.2. For the moment, we do not impose the constraints, thus regarding all components $\overline{a}_\alpha$ as independent.

Only the first r components $\overline{a}_{\tilde{\alpha}}$ ($\tilde{\alpha}=1,\ldots,r$) have a corresponding momentum operator $\overline{P}_{\tilde{\alpha}}$ in the Hamiltonian, while the other $\kappa-r$ components do not. This means that the resulting states are degenerate in the coordinates $\overline{a}_{r+1},\ldots,\overline{a}_{\kappa}$. Thus, we may write the lowest-energy states as

$$\chi_{\mathrm{osc}}(\overline{a}_1,\ldots,\overline{a}_\kappa)=\chi_{\mathrm{osc},r}(\overline{a}_1,\ldots,\overline{a}_r)\,\tilde{\chi}(\overline{a}_{r+1},\ldots,\overline{a}_\kappa), \tag{4.144}$$

where $\tilde{\chi}$ is the degenerate part of the wave function (further discussed in Sec. 4.4.2), and

$$\chi_{\mathrm{osc},r}(\overline{a}_1,\ldots,\overline{a}_r)=\exp\left(-\frac{e}{2\hbar b}\sum_{\tilde{\alpha}=1}^{r}\overline{a}_{\tilde{\alpha}}^{\dagger}\lambda_{\tilde{\alpha}}^{-1}\overline{a}_{\tilde{\alpha}}\right) \tag{4.145}$$

is the nondegenerate part. Notice that the components associated with the zero eigenvalues of the matrix E do not contribute. By the observation that the pseudoinverse [193, 194] of $D=\mathrm{diag}(\lambda_1,\ldots,\lambda_r,0,\ldots,0)$ is equal to $\widehat{D}=\mathrm{diag}(\lambda_1^{-1},\ldots,\lambda_r^{-1},0,\ldots,0)$, we may also rewrite $\chi_{\mathrm{osc},r}$ as

$$\chi_{\mathrm{osc},r}=\exp\left(-\frac{e}{2\hbar b}\overline{a}^{\dagger}\widehat{D}\,\overline{a}\right)=\exp\left(-\frac{e}{2\hbar b}a^{\circ\dagger}\widehat{K}a^{\circ}\right),$$

where we used that $\overline{a}^{\dagger}\widehat{D}\,\overline{a}=a^{\circ\dagger}\widehat{K}a^{\circ}$. This result is nothing else than Eq. (4.19) with the inverses of D and K replaced by the pseudoinverses. Substituting the density fluctuations $\delta\rho_\alpha$ for the gauge fields a_α° using the constraint Eq. (4.9) yields exactly Eq. (4.22) by virtue of the property of $\widehat{K}$ that $K\widehat{K}K=K$. This result is exactly equal to the steps we followed before, but only with K^{-1} replaced by $\widehat{K}$. Therefore, the ground state Eq. (4.22) found for the case of strictly positive eigenvalues is also valid if there are zero eigenvalues. All subsequent steps concerning the connection to the trial wave functions remain valid as well.

4.C The coupling Hamiltonian

In this appendix we will prove expression (4.31) for the coupling Hamiltonian, starting from the one-component version of Eq. (4.11),

$$H_{\mathrm{coupl}}=\frac{1}{m}\sum_{j=1}^{N}\Pi_j\cdot\left(e\,\mathbf{a}^{\circ}(\mathbf{r}_j)+bK\mathbf{P}^{\circ}(\mathbf{r}_j)\right). \tag{4.146}$$

We first convert the fields $\mathbf{a}^{\circ}(\mathbf{r}_j)$ and $\mathbf{P}^{\circ}(\mathbf{r}_j)$ to their counterparts in Fourier space, and subsequently we recall that $\mathbf{a}^{\circ}(\mathbf{q})=a^{\circ}(\mathbf{q})\mathbf{e}_{\mathbf{q}}^{\perp}$ and $\mathbf{P}^{\circ}(\mathbf{q})=iP^{\circ}(\mathbf{q})\mathbf{e}_{\mathbf{q}}^{\parallel}$. This yields

$$H_{\mathrm{coupl}}=\frac{1}{m}\sum_{\mathbf{q}}\sum_{j=1}^{N}e^{i\mathbf{q}\cdot\mathbf{r}_j}\Pi_j\cdot\left(e\,a^{\circ}(\mathbf{q})\mathbf{e}_{\mathbf{q}}^{\perp}+ibKP^{\circ}(\mathbf{q})\mathbf{e}_{\mathbf{q}}^{\parallel}\right).$$

We now write the vectors explicitly in their x and y components. We recall that $\Pi_j^{\pm}$ has been defined as $\Pi_j^x \pm i\Pi_j^y$ so that $\Pi_j^x = (\Pi_j^+ + \Pi_j^-)/2$ and $\Pi_j^y = (\Pi_j^+ - \Pi_j^-)/2i$. Moreover, we recall the definitions $\mathbf{e}_{\mathbf{q}}^{\parallel} = (q_x, q_y)/|\mathbf{q}|$ and $\mathbf{e}_{\mathbf{q}}^{\perp} = i(-q_y, q_x)/|\mathbf{q}|$. Hence we may write

$$H_{\text{coupl}} = \frac{1}{m}\sum_{\mathbf{q}}\sum_{j=1}^{N}\frac{e^{i\mathbf{q}\cdot\mathbf{r}_j}}{2|\mathbf{q}|}\begin{pmatrix}\Pi_j^+ + \Pi_j^- \\ (\Pi_j^+ - \Pi_j^-)/i\end{pmatrix}\cdot\begin{pmatrix}e\,a^\circ(\mathbf{q})(-iq_y) + ibKP^\circ(\mathbf{q})q_x \\ e\,a^\circ(\mathbf{q})(iq_x) + ibKP^\circ(\mathbf{q})q_y\end{pmatrix}.$$

Computing the inner product explicitly and gathering terms, we obtain

$$H_{\text{coupl}} = \frac{1}{2m}\sum_{\mathbf{q}}\sum_{j=1}^{N} e^{i\mathbf{q}\cdot\mathbf{r}_j}\Big(e\,a^\circ(\mathbf{q})\hat{q}_-\Pi_j^+ - e\,a^\circ(\mathbf{q})\hat{q}_+\Pi_j^- + bKP^\circ(\mathbf{q})i\hat{q}_-\Pi_j^+ + bKP^\circ(\mathbf{q})i\hat{q}_+\Pi_j^-\Big).$$

Here, we used the notation $\hat{q}_\pm = (q_x \pm i\,q_y)/|\mathbf{q}|$. For the second and fourth term, we substitute $\mathbf{q} \to -\mathbf{q}$, so that

$$H_{\text{coupl}} = \frac{1}{2m}\sum_{\mathbf{q}}\sum_{j=1}^{N}\Big[e^{i\mathbf{q}\cdot\mathbf{r}_j}\Big(e\,a^\circ(\mathbf{q}) + ibKP^\circ(\mathbf{q})\Big)\hat{q}_-\Pi_j^+ + e^{-i\mathbf{q}\cdot\mathbf{r}_j}\Big(e\,a^\circ(-\mathbf{q}) - ibKP^\circ(-\mathbf{q})\Big)\hat{q}_+\Pi_j^-\Big].$$

With the definitions of $c(\mathbf{q})$ and $c^\dagger(\mathbf{q})$ [Eq. (4.26)], and of the ladder operators $\mathscr{A}(\mathbf{q})$ and $\mathscr{A}^\dagger(\mathbf{q})$ [Eq. (4.30)], we immediately observe that

$$H_{\text{coupl}} = \frac{\sqrt{4\pi\hbar^2 K}}{2m}\big(c^\dagger(\mathbf{q})\mathscr{A}(\mathbf{q}) + \mathscr{A}^\dagger(\mathbf{q})c(\mathbf{q})\big),$$

which is identical to Eq. (4.31) that we wished to prove.

4.D Diagonalisation of the Hamiltonian matrix

The Hamiltonian matrix H'_{mat} can be diagonalised abstractly by a diagonal matrix $\tilde{H}_{\text{mat}}$ and an orthogonal matrix S, such that $H'_{\text{mat}} = S^{\mathrm{T}}\tilde{H}_{\text{mat}}S$. We write the resulting matrices as

$$S = \begin{pmatrix}T & U\\ V & W\end{pmatrix} \quad\text{and}\quad \tilde{H}_{\text{mat}} = \begin{pmatrix}0 & 0\\ 0 & F\end{pmatrix},$$

where F is the diagonal matrix of the nonzero eigenvalues of H'_{mat}, and T, U, V, and W are four $\kappa\times\kappa$ matrices. In the following, we will investigate how they are related.

The condition that S is orthogonal, $S^{\mathrm{T}}S = \mathbb{1}_{2\kappa\times 2\kappa}$ and $SS^{\mathrm{T}} = \mathbb{1}_{2\kappa\times 2\kappa}$, yields the following conditions on the matrices T, U, V, and W:

$$\begin{cases} T^{\mathrm{T}}T + V^{\mathrm{T}}V = \mathbb{1}, \\ U^{\mathrm{T}}U + W^{\mathrm{T}}W = \mathbb{1}, \\ T^{\mathrm{T}}U + V^{\mathrm{T}}W = 0. \end{cases} \qquad \begin{cases} TT^{\mathrm{T}} + UU^{\mathrm{T}} = \mathbb{1}, \\ VV^{\mathrm{T}} + WW^{\mathrm{T}} = \mathbb{1}, \\ TV^{\mathrm{T}} + UW^{\mathrm{T}} = 0. \end{cases} \tag{4.147}$$

Moreover, the fact that S diagonalises H'_{mat} according to $H'_{\mathrm{mat}} = S^{\mathrm{T}} \tilde{H}_{\mathrm{mat}} S$ gives the conditions

$$\begin{aligned} V^{\mathrm{T}} F V &= R, \\ W^{\mathrm{T}} F W &= D, \\ W^{\mathrm{T}} F V &= \sqrt{D} C \sqrt{R}, \end{aligned} \tag{4.148}$$

with H'_{mat} given by Eq. (4.55).

Knowing the eigenvectors with zero eigenvalue from Eq. (4.56), it is possible to specify a relation between T and U. By virtue of the diagonalisation of H'_{mat}, the first κ columns of the matrix S^{T} form a basis of eigenvectors for the eigenspace corresponding to the eigenvalue 0. We can put the eigenvectors v_α from Eq. (4.56) side by side, writing a $2\kappa \times \kappa$ matrix equal to

$$\begin{pmatrix} \mathbb{1} \\ -\sqrt{D^{-1}} C \sqrt{R} \end{pmatrix}. \tag{4.149}$$

However, this specifies only one particular basis for the eigenspace with eigenvalue 0. An arbitrary basis is spanned by κ independent linear combinations $v'_\beta = \sum_\alpha t_{\beta\alpha} v_\alpha$ of the vectors v_α. Here, the coefficients $t_{\beta\alpha}$ form a nonsingular $\kappa \times \kappa$ matrix. We now suppose that this nonsingular matrix is T^{T}, so that the new basis of eigenvectors is given by right multiplication by T^{T} of both $\kappa \times \kappa$ matrices in Eq. (4.149). The result is equal to the first κ columns of S^{T}, i.e.

$$\begin{pmatrix} T^{\mathrm{T}} \\ -\sqrt{D^{-1}} C \sqrt{R}\, T^{\mathrm{T}} \end{pmatrix} = \begin{pmatrix} T^{\mathrm{T}} \\ U^{\mathrm{T}} \end{pmatrix}, \tag{4.150}$$

so that we find the condition $U = -T\sqrt{R} C^{\mathrm{T}} \sqrt{D^{-1}}$.

We can derive a similar condition for V and W. Given the eigenvalue equation $S H'_{\mathrm{mat}} = \tilde{H}_{\mathrm{mat}} S$, we derive $V R + W\sqrt{D} C \sqrt{R} = F V$ and $V\sqrt{R} C^{\mathrm{T}} \sqrt{D} + W D = F W$. By right-multiplying both sides of the latter equation with $\sqrt{D^{-1}} C \sqrt{R}$, its left hand side becomes equal to the left hand side of the other equation. Subsequently combining them yields

$$F W \sqrt{D^{-1}} C \sqrt{R} = V R + W \sqrt{D} C \sqrt{R} = F V.$$

Since F is nonsingular, we obtain $V = W\sqrt{D^{-1}} C \sqrt{R}$. Summarising, we may write the relations between T and U and between V and W as

$$U = -T Q^{\mathrm{T}} \quad \text{and} \quad V = W Q, \tag{4.151}$$

respectively, where we have defined

$$Q = \sqrt{D^{-1}} C \sqrt{R}. \tag{4.152}$$

At this point, we use the orthogonality conditions (4.147) to derive more conditions on T and W. From $T^{\mathrm{T}} U + V^{\mathrm{T}} W = 0$ we obtain $T^{\mathrm{T}} T Q^{\mathrm{T}} = Q^{\mathrm{T}} W^{\mathrm{T}} W$, with Q as defined

in Eq. (4.152). Then $T^{\mathrm{T}}T + V^{\mathrm{T}}V = \mathbb{1}$ and $U^{\mathrm{T}}U + W^{\mathrm{T}}W = \mathbb{1}$ yield the conditions $T^{\mathrm{T}}T + T^{\mathrm{T}}TQ^{\mathrm{T}}Q = \mathbb{1}$ and $QQ^{\mathrm{T}}W^{\mathrm{T}}W + W^{\mathrm{T}}W = \mathbb{1}$, respectively. It follows that T and W must satisfy

$$T^{\mathrm{T}}T = (\mathbb{1} + Q^{\mathrm{T}}Q)^{-1} = \left(\mathbb{1} + \sqrt{R}C^{\mathrm{T}}D^{-1}C\sqrt{R}\right)^{-1}, \tag{4.153a}$$

$$W^{\mathrm{T}}W = (\mathbb{1} + QQ^{\mathrm{T}})^{-1} = \left(\mathbb{1} + \sqrt{D^{-1}}CRC^{\mathrm{T}}\sqrt{D^{-1}}\right)^{-1}. \tag{4.153b}$$

Since the eigenvectors of H'_{mat} with nonzero eigenvalues are known, expressions for V and W may be given in terms of the eigenvectors and eigenvalues of $R+E$. Unlike T and U, these expressions are unique (up to permutations), since the eigenspaces belonging to the nonzero eigenvalues are generally nondegenerate. In Sec. 4.5.2 we derived that the eigenvalues of H'_{mat} are the eigenvalues of $R+E$, and the corresponding eigenvectors of H'_{mat} can be written as $(\sqrt{R}\mathbf{g}_\alpha, \sqrt{D}C\mathbf{g}_\alpha)$, as in Eq. (4.60). Since $R+E$ is a symmetric matrix, we may define an orthonormal basis of eigenvectors $\mathbf{g}_\alpha$. We define G to be the orthogonal matrix such that the normalised eigenvectors $\mathbf{g}_\alpha$ are the columns of its transpose G^{T}. Then G diagonalises $R+E$ as $R+E = G^{\mathrm{T}}FG$, where we recall that F is the diagonal matrix of eigenvalues. With the same reasoning as used above to connect T^{T} and U^{T} to the eigenvectors v_α, we find that the columns of $\begin{pmatrix} V^{\mathrm{T}} \\ W^{\mathrm{T}} \end{pmatrix}$ are multiples of the vectors $\begin{pmatrix} \sqrt{R}\mathbf{g}_\alpha \\ \sqrt{D}C\mathbf{g}_\alpha \end{pmatrix}$. Let us write the columns of $\begin{pmatrix} V^{\mathrm{T}} \\ W^{\mathrm{T}} \end{pmatrix}$ as $r_\alpha \begin{pmatrix} \sqrt{R}\mathbf{g}_\alpha \\ \sqrt{D}C\mathbf{g}_\alpha \end{pmatrix}$. The orthonormality of these eigenvectors is expressed either by $VV^{\mathrm{T}} + WW^{\mathrm{T}}$ or by Eq. (4.61). From the latter it follows that we must set $r_\alpha = 1/\sqrt{\mu_\alpha}$. Writing the eigenvectors side by side, we find that W and V are determined by

$$W^{\mathrm{T}} = \sqrt{D}CG^{\mathrm{T}}\sqrt{F^{-1}}, \quad \text{and} \quad V^{\mathrm{T}} = \sqrt{R}G^{\mathrm{T}}\sqrt{F^{-1}}, \tag{4.154}$$

using that G^{T} has $\mathbf{g}_\alpha$ as its columns, and that F is the diagonal matrix with entries μ_α. These definitions are consistent with $V^{\mathrm{T}} = Q^{\mathrm{T}}W^{\mathrm{T}}$ and with all other aforementioned conditions involving V and/or W.

On the other hand, the matrix T (and along with it U) is not fixed. It can be shown that the two transformations

$$T \to XT \tag{4.155a}$$

and

$$T \to T(\mathbb{1} + Q^{\mathrm{T}}Q)^{1/2}X(\mathbb{1} + Q^{\mathrm{T}}Q)^{-1/2}, \tag{4.155b}$$

with X an arbitrary orthogonal matrix, leave all conditions invariant. For some purposes, it is convenient to choose T in a particular way. For physical quantities, a specific gauge choice is not necessary since they are gauge invariant. However, it may prove convenient to specify a relation between T and W, the latter of which is fixed. Let us give one example of such a relation, where T satisfies all given conditions. For

this example, let us write the polar decomposition of Q as $Q = Q^{\mathrm{U}}\sqrt{Q^{\mathrm{T}}Q}$. Here, $\sqrt{Q^{\mathrm{T}}Q}$ is a positive definite matrix, and $Q^{\mathrm{U}} \equiv Q(Q^{\mathrm{T}}Q)^{-1/2}$ is an orthogonal matrix. We also have $Q = \sqrt{QQ^{\mathrm{T}}}Q^{\mathrm{U}}$, with the same Q^{U}.[19] Then it follows that $Q^{\mathrm{U}} f(Q^{\mathrm{T}}Q) = f(QQ^{\mathrm{T}})Q^{\mathrm{U}}$ for any function f that can be expanded as a power series in its argument. Choose $T = Q^{\mathrm{UT}}WQ^{\mathrm{U}}$. Using the properties of Q^{U} we can show that all conditions on T and $U = -TQ^{\mathrm{T}}$ are satisfied.

There is an additional argument in favour of this particular choice of T, which involves the computation of the logarithm of S, i.e., the matrix $\log S$ that is defined by $\exp(\log S) = S$. Since S is orthogonal, the eigenvalues of S are complex numbers of unit length. Therefore, the eigenvalues of $\log S$ are purely imaginary. Moreover, the orthogonality of S implies that $\log S$ is antihermitian, $(\log S)^\dagger = -\log S$. For our choice $T = Q^{\mathrm{UT}}WQ^{\mathrm{U}}$, we find[20] that $\log S$ is real, and hence also antisymmetric. We may write

$$\log S = \begin{pmatrix} Y & -Z \\ Z^{\mathrm{T}} & \tilde{Y} \end{pmatrix},$$

where Y and $\tilde{Y}$ are antisymmetric matrices, and Z is arbitrary. In addition, we find that Y and $\tilde{Y}$ have the same set of eigenvalues for this specific choice of T. In other words, we may write $Y = \Xi^\dagger(i\Phi)\Xi$ and $\tilde{Y} = \tilde{\Xi}^\dagger(i\Phi)\tilde{\Xi}$, where Φ is a real diagonal traceless[21] matrix, and Ξ and $\tilde{\Xi}$ are unitary matrices, with $\Xi\tilde{\Xi}^\dagger$ real, and Z is arbitrary. Remark that for $\kappa = 2$, the quadrants Y and $\tilde{Y}$ are both proportional to $\left(\begin{smallmatrix} 0 & -1 \\ 1 & 0 \end{smallmatrix}\right)$. Since their eigenvalues are equal, we must have $Y = \pm\tilde{Y}$. Then Φ is a (real) multiple of $\left(\begin{smallmatrix} 1 & 0 \\ 0 & -1 \end{smallmatrix}\right)$. Recalling that $\log S$ defines the generators of the $O(2n)$ rotation S, we observe that the generators Y in the $c^\dagger c$ sector (upper left quadrant of $\log S$) have the same "strength" as the generators $\tilde{Y}$ in the $\mathscr{A}^\dagger\mathscr{A}$ sector (lower right quadrant of $\log S$). This indicates that $T = Q^{\mathrm{UT}}WQ^{\mathrm{U}}$ is in this sense a "natural" choice. Summarising, this choice, together with the relations linking U to T and V to W, leads to

$$S = \begin{pmatrix} T & U \\ V & W \end{pmatrix} = \begin{pmatrix} Q^{\mathrm{UT}}WQ^{\mathrm{U}} & -Q^{\mathrm{UT}}W\sqrt{QQ^{\mathrm{T}}} \\ W\sqrt{QQ^{\mathrm{T}}}Q^{\mathrm{U}} & W \end{pmatrix}.$$

At this point it might be instructive to compare the results in this appendix to the one-component case. Recall that for one component, we have $R = 1 - \nu K$ and $D = \nu K$. The matrix S is given by Eq. (4.39), so that we have $T = W = 1/\sqrt{1+\mu^2}$. Since $\nu K = 1/(1+\mu^2)$, we derive that $Q = (1-\nu K)/\nu K = \mu$. Then $(\mathbb{1} + Q^{\mathrm{T}}Q)^{-1} = 1/(1+\mu^2)$, which is indeed equal to $T^{\mathrm{T}}T$ and $W^{\mathrm{T}}W$. This shows that one might think about the matrix $Q = \sqrt{D^{-1}}C\sqrt{R}$ as being the multicomponent generalisation of μ.

[19] Proof: Assume that $Q = Q^{\mathrm{U}}\sqrt{Q^{\mathrm{T}}Q}$. Then we can write $QQ^{\mathrm{T}} = Q^{\mathrm{U}}(Q^{\mathrm{T}}Q)^{1/2}(Q^{\mathrm{T}}Q)^{1/2}Q^{\mathrm{UT}}$. Now, insert $Q^{\mathrm{UT}}Q^{\mathrm{U}}$ in the middle to obtain $QQ^{\mathrm{T}} = Q^{\mathrm{U}}(Q^{\mathrm{T}}Q)^{1/2}Q^{\mathrm{UT}}Q^{\mathrm{U}}(Q^{\mathrm{T}}Q)^{1/2}Q^{\mathrm{UT}}$. It follows that $(QQ^{\mathrm{T}})^{1/2} = Q^{\mathrm{U}}(Q^{\mathrm{T}}Q)^{1/2}Q^{\mathrm{UT}}$. Multiplying on the right by Q^{U} gives the desired equation.

[20] This observation and the following were made by several numerical trials with $\kappa = 2, 3, 4$.

[21] For each entry ϕ_α in the matrix Φ, there is also an entry equal to $-\phi_\alpha$.

4.D.1 Singular case

In Sec. 4.5.2, we proved that in the case that K is singular, Eq. (4.56) is invalid since the inverse of D does not exist. As a consequence, Eqs. (4.149) and (4.150) are invalid as well. From Eq. (4.67), we derive that we have to replace Eq. (4.150) by

$$\begin{pmatrix} -\sqrt{R^{-1}}\,C^{\mathrm{T}}\sqrt{D}\,U^{\mathrm{T}} \\ U^{\mathrm{T}} \end{pmatrix} = \begin{pmatrix} T^{\mathrm{T}} \\ U^{\mathrm{T}} \end{pmatrix}, \tag{4.156}$$

which is also valid in the nonsingular case. Equations (4.154) defining V and W remain valid in the singular case.

Also the definition of Q [Eq. (4.152)] contains an inverse of D, so that it is invalid in the singular case. However,

$$Q^{-1} = \sqrt{R^{-1}}\,C^{\mathrm{T}}\sqrt{D} \tag{4.157}$$

does exist in the singular case. In this case, Q^{-1} cannot be regarded as the inverse of a matrix Q, but it has to be treated as a matrix formally defined by Eq. (4.157). Then we must also replace Eq. (4.151) by

$$T = -U\,(Q^{-1})^{\mathrm{T}} \quad \text{and} \quad W = V\,Q^{-1}. \tag{4.158}$$

In the same way as before, we also derive

$$\begin{aligned} T^{\mathrm{T}}T &= Q^{-1}\big(\mathbb{1} + (Q^{-1})^{\mathrm{T}}Q^{-1}\big)^{-1}(Q^{-1})^{\mathrm{T}} \\ &= \sqrt{R^{-1}}\,C^{\mathrm{T}}\sqrt{D}\big(\mathbb{1} + \sqrt{D}\,CR^{-1}C^{\mathrm{T}}\sqrt{D}\big)^{-1}\sqrt{D}\,C\sqrt{R^{-1}}, \qquad (4.159a) \\ W^{\mathrm{T}}W &= (Q^{-1})^{\mathrm{T}}\big(\mathbb{1} + Q^{-1}(Q^{-1})^{\mathrm{T}}\big)^{-1}Q^{-1} = \sqrt{D}\,C(R + C^{\mathrm{T}}DC)^{-1}C^{\mathrm{T}}\sqrt{D}, \qquad (4.159b) \end{aligned}$$

which replaces Eqs. (4.153) in the singular case, and which is equivalent to Eqs. (4.153) in the nonsingular case (i.e., when Q exists). We remark that U and V have full rank (i.e., are invertible), while the ranks of T and W equal the rank of K. Consequently, the inverses of T and W do not exist if K is singular.

4.E Index of notations

$\mathbf{1} = (1,\ldots,1)$	κ-component vector with all components equal to 1	
$\mathbb{1}$	identity matrix	
$\mathbf{A}$	magnetic gauge field	
$\mathscr{A}(\mathbf{q})$, $\mathscr{A}_\alpha(\mathbf{q})$	ladder operators	Eq. (4.20)
$\mathbf{A}_\alpha^{\mathrm{CS}}$	Chern-Simons gauge field	Eq. (4.2)
$\mathbf{A}^*$	average gauge field	Eq. (4.7)
a_α	auxiliary gauge field	Sec. 4.3.1
$b = h/eL^2$		Sec. 4.3.1
$\mathbf{B} = B\mathbf{e}_z$	magnetic field	

C	orthogonal matrix in diagonalisation of E	Sec. 4.3.2
$c(\mathbf{q})$, $c_\alpha(\mathbf{q})$	momentum operators	Eqs. (4.26), (4.44)
$c'_\alpha(\mathbf{q})$		Eq. (4.53)
D	diagonal matrix of eigenvalues of E	Sec. 4.3.2
$\Delta = G\sqrt{R^{-1}}(\mathbb{1} - T^{-1})\sqrt{R^{-1}}G^{\mathrm{T}}$		Eq. (4.119)
$E = \sqrt{N}K\sqrt{N}$		
e	electron charge	
F	diagonal matrix of eigenvalues of $R+E$	Sec. 4.5.2
G	orthogonal matrix in diagonalisation of $R+E$	Sec. 4.5.2
$\mathbf{g}_\alpha$	eigenvectors of $R+E$	Sec. 4.5.2
$\tilde{\mathbf{g}}_\alpha$	eigenvectors of $R+KN$	Sec. 4.5.2
$\Gamma = G\sqrt{R^{-1}}(T^{\mathrm{T}} - \mathbb{1})\sqrt{R^{-1}}G^{\mathrm{T}}$		Eq. (4.110)
$\mathbf{J}$, $\mathbf{J}_\alpha$, $\mathbf{J}_{\mathrm{T}}$	currents	Secs. 4.6.1, 4.6.2
K	Chern-Simons charge matrix	
κ	number of components	
L^2	area of the system	
λ_α	eigenvalues of E	Sec. 4.3.2
$l_B = \sqrt{\hbar/eB}$	magnetic length	
m	electron mass	
M^*	exponent matrix of the composite-fermion system	
μ_α	eigenvalues of $R+E$	Sec. 4.5.2
N	diagonal matrix of filling factors	
$n_{\mathrm{T}} = \nu_{\mathrm{T}}/2\pi l_B^2$	total density	
$N_{\mathrm{T}} = n_{\mathrm{T}}L^2$	total number of particles	
ν_α	filling factors	
$\nu_{\mathrm{T}} = \sum_\alpha \nu_\alpha$	total filling factor	
ν^*_α	composite fermion filling factors	
$\omega_\alpha = \omega_{\mathrm{c}}\lambda_\alpha$	oscillator frequencies	Sec. 4.3.2
$\omega_{\mathrm{c}} = eB/m$	cyclotron frequency	
P_α	conjugate of auxiliary gauge field a_α	Sec. 4.3.1
$\Pi_{\alpha,j}$	momentum operator	
$\Pi^{\pm}_{\alpha,j} = \Pi^x_{\alpha,j} \pm i\Pi^y_{\alpha,j}$		
$\hat{q}_\pm = (q_x \pm i\,q_y)/\lvert\mathbf{q}\rvert$		
$Q = \sqrt{D^{-1}}C\sqrt{R}$		Eq. (4.152)
$R = \mathrm{diag}(1 - K\nu) = \mathrm{diag}(\{\nu_\alpha/\nu^*_\alpha\})$		Eq. (4.52)
S	$2\kappa \times 2\kappa$ orthogonal matrix in diagonalisation of H'_{mat}	
T, U, V, W	$\kappa \times \kappa$ submatrices of S	App. 4.D
$\Theta = \theta_0\sqrt{D}\,C\sqrt{N}$		Sec. 4.5.2
$\theta_0 = \sqrt{\pi}/eB = l_B^2\sqrt{\pi}/\hbar$		Eq. (4.33)
$\wedge\mathbf{q} = (q_y, -q_x)$		
$\mathbf{q} \wedge \mathbf{q}' = (q_x q'_y - q_y q'_x)$		

Chapter 5

Conclusion and outlook

In this thesis, we have investigated topological phases in two-dimensional systems from different perspectives. The systems studied have in common that they exhibit multiple internal degrees of freedom, i.e., spin and/or pseudospin.

In Chapter 2, we have studied how a tight-binding model of a honeycomb lattice in a perpendicular magnetic field with spin-orbit couplings and the Zeeman effect leads to many different topological phases, characterised by the number of edge states in the bulk gaps and by their spins. In this Chapter, we have shown that the quantum spin Hall state, which is usually considered in a time-reversal symmetric setting, persists in the presence of a magnetic field; we have called this state the *weak quantum spin Hall* phase. In the latter case, the edge states are not protected by time-reversal symmetry, but if there is no coupling between the two spin components, i.e., if there is no Rashba spin-orbit coupling and if there are no magnetic impurities, then the two spin components can be treated as two uncoupled quantum Hall systems, which provide robust chiral edge states. This phenomenon also leads to a change in the character of the topological invariant: In the time-reversal symmetric case, the topological invariant lives in $\mathbb{Z}_2$, while the two uncoupled quantum Hall states lead to a $\mathbb{Z} \times \mathbb{Z}$ topological invariant. Thus, in the latter case, it is possible to find gaps with nonzero charge and spin Hall conductivity, reminiscent of both the quantum Hall and the quantum spin Hall effect. In addition, we have found that in the low-energy, low-flux limit the Zeeman term produces the weak quantum spin Hall phase in the same manner as the intrinsic spin-orbit coupling.

In this framework, the combination of the magnetic field, the intrinsic spin-orbit coupling, and the Zeeman effect leads to a rich interplay between the quantum phases. At a fixed magnetic flux value, modifying the amplitude of the intrinsic spin-orbit coupling leads to many bulk-gap closures. Where the bulk gaps close, the Chern numbers of the touching bulk bands may change, accompanied by a change of the number of edge states in the gap that closes. The change of Chern numbers is mostly unpredictable, as the system is subject to a subtle interplay of effects. However, the

sum of the Chern numbers of the involved bands is always invariant, and the change is a multiple of q, the denominator of the rational flux value $\phi = p/q$. We have explained this feature from the multiplicity q of the touching points inside the Brillouin zone.

The Rashba spin-orbit is different from the other terms in the model Hamiltonian, because it couples the spin components. In the presence of this coupling, one can no longer distinguish spin up and spin down states, since the spin is no longer a conserved quantum number. Instead, the spin direction on the edges gains an additional component in the plane of the sample perpendicular to the edge. This spin direction is no longer a topological invariant: The direction of the edge-state spin varies when the Fermi energy is modified, even when staying within one bulk gap. We have shown that variation of the Fermi energy provides an interesting tool to rotate the edge-state spin at will. In this aspect, we note that these edge states differ fundamentally from those generated by the Zeeman effect in a tilted magnetic field. Finally, in this chapter we have also demonstrated that a weak Rashba coupling indeed destroys the weak quantum spin Hall state: The edge states become gapped, and the system goes into a topologically trivial phase.

In Chapter 3, we have presented a phenomenological model of HgTe quantum wells, where topological phases of the same nature are observed due to the simultaneous presence of the magnetic field and of spin-orbit coupling. This system, unlike the one in Chapter 2, is treated within a low-energy approximation. We have studied the Landau-level spectra, consisting of bands which have Chern number ± 1, rather than bands which can have any Chern number as it is the case for Dirac systems in the presence of a rational flux.

In HgTe quantum wells doped with Mn ions, the magnetisation due to these ions modifies the band structure and the response to the magnetic field. This modified response leads to a bending of the Landau levels, and therefore to a reentrant behaviour of charge and/or spin Hall conductivity. In addition to this mechanism, also Landau-level crossings may be responsible for reentrant effects. We have investigated the regimes in parameter space (doping fraction, quantum-well thickness and temperature) where the different reentrant effects occur. Moreover, we have estimated the experimental conditions to observe these reentrant effects, by studying the energy ranges in which they appear, taking into account broadening of the Landau levels by disorder and by temperature (effectively, due to a smearing of the fermionic occupation function).

Chapter 4 describes the extension of the Hamiltonian theory for flux attachment in quantum Hall systems with internal degrees of freedom. In this theory, we study trial wave functions similar to those proposed by Laughlin [9], Jain [10, 11], and Halperin [39]. These theories provide an approximate, but very powerful method to understand the physics of these highly correlated electron systems. In this chapter, we have generalised the theory by Shankar and Murthy to multi-component systems, motivated

by the many systems of this type, e.g. multilayer heterostructures and graphene. In this framework, the (even) number of attached flux quanta k is replaced by the matrix K. When we only treat the oscillator degrees of freedom in this theory, Laughlin's plasma analogy remains valid, even when the system is in a "symmetric state", where the flux-attachment matrix K and the exponent matrices are singular. If in addition to the oscillators we include also the momentum degrees of freedom, then Kohn's theorem (stating that there must be a mode at the cyclotron energy $\hbar\omega_c$) remains valid in the multi-component case. We have identified these Kohn modes as being associated with the total particle density. The other modes usually have a lower energy, and are typically the so-called out-of-phase modes. We have also presented the generalisation of the coupling between the oscillator part of the transformed density operator and the electric field, which allows us to compute the Hall conductivities associated with the aforementioned modes.

It remains to be emphasised that although the systems discussed are very specific, the topological phases they exhibit are present in a very general setting, as may be understood from the classification of topological states (the tenfold way [60, 61]) discussed earlier. Other lattices showing the same type of topological phases and phase transitions include the Lieb lattice, the kagome lattice, and the T_3 lattice [195, 196]. An additional route is to include real next-nearest neighbour hopping to the tight-binding model, in addition to the imaginary next-nearest-neighbour hopping such as the intrinsic spin-orbit coupling. It can be shown that this type of hopping may induce topological phase transitions in the Lieb lattice and the kagome lattice at zero magnetic field, and in the honeycomb lattice only with nonzero magnetic field [197].

The systems discussed in this thesis have in common that they are (effectively) non-interacting. Even in the case of the fractional quantum Hall effect discussed in Chapter 4, the interacting system is described in terms of a noninteracting theory, namely the integer quantum Hall effect. In this aspect, an interesting question arises: Could we find interacting theories associated to any one of the (non-interacting) topologically nontrivial theories in the tenfold way? The fractional quantum Hall effect is known to be related to the integer quantum Hall effect through the flux attachment. One may speculate that also for the other symmetry classes with nontrivial homotopy groups similar interacting theories exist. In particular, one may raise the question whether arguments similar to the flux attachment give rise to a *fractional quantum spin Hall effect*. Recently, there have been proposals for the generalisation of the notion of the topological invariant to interacting systems in two and four dimensions [198]. It has also been shown that interactions can have a profound effect on the group structure of the invariants: In a model of Majorana chains, the $\mathbb{Z}$ invariant in the non-interacting model breaks down to $\mathbb{Z}_8$ when interactions are included [199, 200]. Currently, it is an open question whether a classification for interacting theories is possible. It might be speculated that the generalisation of the flux attachment and trial wave functions may lead to new topological phases with possibly exotic topological

invariants. Although a full classification of interaction-driven topological phases might be elusive, the argument of flux attachments could provide valuable insight into their structure.

Bibliography

[1] K. von Klitzing, G. Dorda, and M. Pepper, Phys. Rev. Lett. **45**, 494 (1980).

[2] E. H. Hall, Amer. J. Math. **2**, 287 (1879).

[3] K. von Klitzing, Rev. Mod. Phys. **58**, 519 (1986).

[4] D. C. Tsui, H. L. Stormer, and A. C. Gossard, Phys. Rev. Lett. **48**, 1559 (1982).

[5] S. Das Sarma and A. Pinczuk, *Perspectives in Quantum Hall Effects: Novel Quantum Liquids in Low-Dimensional Semiconductor Structures* (John Wiley & Sons, 2008).

[6] Z. F. Ezawa, *Quantum Hall effects: Field theoretical approach and related topics* (World Scientific, 2000).

[7] D. J. Thouless, M. Kohmoto, M. P. Nightingale, and M. den Nijs, Phys. Rev. Lett. **49**, 405 (1982).

[8] D. C. Tsui, H. L. Störmer, J. C. M. Hwang, J. S. Brooks, and M. J. Naughton, Phys. Rev. B **28**, 2274 (1983).

[9] R. B. Laughlin, Phys. Rev. Lett. **50**, 1395 (1983).

[10] J. K. Jain, Phys. Rev. Lett. **63**, 199 (1989).

[11] J. K. Jain, Phys. Rev. B **41**, 7653 (1990).

[12] J. K. Jain and R. K. Kamilla, in *Composite Fermions*, edited by O. G. Heinonen (World Scientific, Singapore/River Edge, NJ, 1998) pp. 1–90.

[13] J. K. Jain and R. K. Kamilla, Phys. Rev. B **55**, R4895 (1997).

[14] K. Park, N. Meskini, and J. K. Jain, J. Phys.: Cond. Mat. **11**, 7283 (1999).

[15] R. H. Morf, N. d'Ambrumenil, and S. Das Sarma, Phys. Rev. B **66**, 075408 (2002).

[16] A. Lopez and E. Fradkin, Phys. Rev. B **44**, 5246 (1991).

[17] A. Lopez and E. Fradkin, in *Composite Fermions*, edited by O. G. Heinonen (World Scientific, Singapore/River Edge, NJ, 1998) pp. 192–253.

[18] G. Moore and N. Read, Nucl. Phys. B **360**, 362 (1991).

[19] N. Read and E. Rezayi, Phys. Rev. B **59**, 8084 (1999).

[20] C. Nayak, S. H. Simon, A. Stern, M. Freedman, and S. Das Sarma, Rev. Mod. Phys. **80**, 1083 (2008).

[21] X. G. Wen and A. Zee, Phys. Rev. B **44**, 274 (1991).

[22] A. Lopez and E. Fradkin, Phys. Rev. B **47**, 7080 (1993).

[23] R. Shankar and G. Murthy, Phys. Rev. Lett. **79**, 4437 (1997).

[24] G. Murthy and R. Shankar, in *Composite Fermions*, edited by O. G. Heinonen (World Scientific, Singapore/River Edge, NJ, 1998) pp. 254–306.

[25] R. Shankar, Phys. Rev. Lett. **83**, 2382 (1999).

[26] R. Shankar, Phys. Rev. B **63**, 085322 (2001).

[27] G. Murthy, Phys. Rev. B **64**, 195310 (2001).

[28] G. Murthy and R. Shankar, Rev. Mod. Phys. **75**, 1101 (2003).

[29] W. Pan, H. L. Stormer, D. C. Tsui, L. N. Pfeiffer, K. W. Baldwin, and K. W. West, Phys. Rev. Lett. **90**, 016801 (2003).

[30] M. O. Goerbig, P. Lederer, and C. Morais Smith, Europhys. Lett. **68**, 72 (2004).

[31] M. O. Goerbig, P. Lederer, and C. Morais Smith, Phys. Rev. B **69**, 155324 (2004).

[32] S. S. Mandal and J. K. Jain, Phys. Rev. B **66**, 155302 (2002).

[33] C.-C. Chang and J. K. Jain, Phys. Rev. Lett. **92**, 196806 (2004).

[34] Y. Zhang, Y.-W. Tan, H. L. Stormer, and P. Kim, Nature **438**, 201 (2005).

[35] K. S. Novoselov, A. K. Geim, S. V. Morozov, D. Jiang, M. I. Katsnelson, I. V. Grigorieva, S. V. Dubonos, and A. A. Firsov, Nature **438**, 197 (2005).

[36] K. S. Novoselov, Z. Jiang, Y. Zhang, S. V. Morozov, H. L. Stormer, U. Zeitler, J. C. Maan, G. S. Boebinger, P. Kim, and A. K. Geim, Science **315**, 1379 (2007).

[37] X. Du, I. Skachko, F. Duerr, A. Luican, and E. Y. Andrei, Nature **462**, 192 (2009).

[38] K. I. Bolotin, F. Ghahari, M. D. Shulman, H. L. Stormer, and P. Kim, Nature **462**, 196 (2009).

[39] B. I. Halperin, Helv. Phys. Acta **56**, 75 (1983).

[40] A. Lopez and E. Fradkin, Phys. Rev. B **51**, 4347 (1995).

[41] R. Rajaraman, Phys. Rev. B **56**, 6788 (1997).

[42] F. D. M. Haldane, Phys. Rev. Lett. **61**, 2015 (1988).

[43] C. L. Kane and E. J. Mele, Phys. Rev. Lett. **95**, 146802 (2005).

[44] C. L. Kane and E. J. Mele, Phys. Rev. Lett. **95**, 226801 (2005).

[45] X.-L. Qi and S.-C. Zhang, Physics Today **63**, 33 (2010).

[46] J. C. Boettger and S. B. Trickey, Phys. Rev. B **75**, 121402 (2007).

[47] M. König, S. Wiedmann, C. Brüne, A. Roth, H. Buhmann, L. W. Molenkamp, X.-L. Qi, and S.-C. Zhang, Science **318**, 766 (2007).

[48] B. A. Bernevig, T. L. Hughes, and S.-C. Zhang, Science **314**, 1757 (2006).

[49] E. G. Novik, A. Pfeuffer-Jeschke, T. Jungwirth, V. Latussek, C. R. Becker, G. Landwehr, H. Buhmann, and L. W. Molenkamp, Phys. Rev. B **72**, 035321 (2005).

[50] Y. Yang, Z. Xu, L. Sheng, B. Wang, D. Y. Xing, and D. N. Sheng, Phys. Rev. Lett. **107**, 066602 (2011).

[51] N. Goldman, W. Beugeling, and C. Morais Smith, EPL **97**, 23003 (2012).

[52] W. Beugeling, N. Goldman, and C. Morais Smith, Phys. Rev. B **86**, 075118 (2012).

[53] D. R. Hofstadter, Phys. Rev. B **14**, 2239 (1976).

[54] R. Rammal, J. Phys. (Paris) **46**, 1345 (1985).

[55] A. L. Clough and E. H. Hall, Proc. Amer. Acad. A. Sci. **28**, 189 (1892).

[56] N. A. Sinitsyn, J. Phys. Cond. Mat. **20**, 023201 (2008).

[57] X.-L. Qi, Y.-S. Wu, and S.-C. Zhang, Phys. Rev. B **74**, 085308 (2006).

[58] J. K. Furdyna, J. Appl. Phys. **64**, R29 (1988).

[59] C.-X. Liu, X.-L. Qi, X. Dai, Z. Fang, and S.-C. Zhang, Phys. Rev. Lett. **101**, 146802 (2008).

[60] A. Kitaev, AIP Conf. Proc. **1134**, 22 (2009).

[61] S. Ryu, A. P. Schnyder, A. Furusaki, and A. W. W. Ludwig, New J. Phys. **12**, 065010 (2010).

[62] X.-L. Qi, T. L. Hughes, and S.-C. Zhang, Phys. Rev. B **78**, 195424 (2008).

[63] M. Z. Hasan and C. L. Kane, Rev. Mod. Phys. **82**, 3045 (2010).

[64] X.-L. Qi and S.-C. Zhang, Rev. Mod. Phys. **83**, 1057 (2011).

[65] O. Shevtsov, P. Carmier, C. Petitjean, C. Groth, D. Carpentier, and X. Waintal, Phys. Rev. X **2**, 031004 (2012).

[66] C. Weeks, J. Hu, J. Alicea, M. Franz, and R. Wu, Phys. Rev. X **1**, 021001 (2011).

[67] A. Singha, M. Gibertini, B. Karmakar, S. Yuan, M. Polini, G. Vignale, M. I. Katsnelson, A. Pinczuk, L. N. Pfeiffer, K. W. West, and V. Pellegrini, Science **332**, 1176 (2011).

[68] K. K. Gomes, W. Mar, W. Ko, F. Guinea, and H. C. Manoharan, Nature **483**, 306 (2012).

[69] P. Soltan-Panahi, J. Struck, P. Hauke, A. Bick, W. Plenkers, G. Meineke, C. Becker, P. Windpassinger, M. Lewenstein, and K. Sengstock, Nature Phys. **7**, 434 (2011).

[70] L. Tarruell, D. Greif, T. Uehlinger, G. Jotzu, and T. Esslinger, Nature **483**, 302 (2012).

[71] K. L. Lee, B. Grémaud, R. Han, B.-G. Englert, and C. Miniatura, Phys. Rev. A **80**, 043411 (2009).

[72] Y.-J. Lin, R. L. Compton, K. Jiménez-García, J. V. Porto, and I. B. Spielman, Nature **462**, 628 (2009).

[73] Y.-J. Lin, K. Jiménez-García, and I. B. Spielman, Nature **471**, 83 (2011).

[74] J. Dalibard, F. Gerbier, G. Juzeliūnas, and P. Öhberg, Rev. Mod. Phys. **83**, 1523 (2011).

[75] M. Aidelsburger, M. Atala, S. Nascimbène, S. Trotzky, Y.-A. Chen, and I. Bloch, Phys. Rev. Lett. **107**, 255301 (2011).

[76] N. R. Cooper, Phys. Rev. Lett. **106**, 175301 (2011).

[77] N. Goldman, I. Satija, P. Nikolic, A. Bermudez, M. A. Martin-Delgado, M. Lewenstein, and I. B. Spielman, Phys. Rev. Lett. **105**, 255302 (2010).

[78] L. Mazza, A. Bermudez, N. Goldman, M. Rizzi, M. A. Martin-Delgado, and M. Lewenstein, New J. Phys. **14**, 015007 (2012).

[79] K. Osterloh, M. Baig, L. Santos, P. Zoller, and M. Lewenstein, Phys. Rev. Lett. **95**, 010403 (2005).

[80] B. Béri and N. R. Cooper, Phys. Rev. Lett. **107**, 145301 (2011).

[81] L.-K. Lim, C. Morais Smith, and A. Hemmerich, Phys. Rev. Lett. **100**, 130402 (2008).

[82] L.-K. Lim, A. Hemmerich, and C. Morais Smith, Phys. Rev. A **81**, 023404 (2010).

[83] N. Goldman, A. Kubasiak, A. Bermudez, P. Gaspard, M. Lewenstein, and M. A. Martin-Delgado, Phys. Rev. Lett. **103**, 035301 (2009).

[84] A. Bermudez, L. Mazza, M. Rizzi, N. Goldman, M. Lewenstein, and M. A. Martin-Delgado, Phys. Rev. Lett. **105**, 190404 (2010).

[85] Z. Lan, N. Goldman, A. Bermudez, W. Lu, and P. Öhberg, Phys. Rev. B **84**, 165115 (2011).

[86] C. Chin, R. Grimm, P. Julienne, and E. Tiesinga, Rev. Mod. Phys. **82**, 1225 (2010).

[87] I. Bloch, J. Dalibard, and W. Zwerger, Rev. Mod. Phys. **80**, 885 (2008).

[88] J. Bellissard and B. Simon, J. Funct. Anal. **48**, 408 (1982).

[89] Y. Hatsugai, Phys. Rev. B **48**, 11851 (1993).

[90] M. Büttiker, Y. Imry, R. Landauer, and S. Pinhas, Phys. Rev. B **31**, 6207 (1985).

[91] M. Kohmoto, Ann. Phys. **160**, 343 (1985).

[92] Y. Hatsugai, Phys. Rev. Lett. **71**, 3697 (1993).

[93] P. Středa, J. Phys. C **15**, L717 (1982).

[94] P. Středa, J. Phys. C **15**, L1299 (1982).

[95] R. O. Umucalılar, H. Zhai, and M. Ö. Oktel, Phys. Rev. Lett. **100**, 070402 (2008).

[96] A. Bermudez, N. Goldman, A. Kubasiak, M. Lewenstein, and M. A. Martin-Delgado, New J. Phys. **12**, 033041 (2010).

[97] L. Onsager, Philos. Mag. **43**, 1006 (1952).

[98] I. M. Lifshitz and A. M. Kosevich, Sov. Phys. JETP **2**, 636 (1956).

[99] A. H. Castro Neto, F. Guinea, N. M. R. Peres, K. S. Novoselov, and A. K. Geim, Rev. Mod. Phys. **81**, 109 (2009).

[100] D. N. Sheng, Z. Y. Weng, L. Sheng, and F. D. M. Haldane, Phys. Rev. Lett. **97**, 036808 (2006).

[101] E. Prodan, Phys. Rev. B **80**, 125327 (2009).

[102] M. O. Goerbig, Rev. Mod. Phys. **83**, 1193 (2011).

[103] Y. Hatsugai, T. Fukui, and H. Aoki, Phys. Rev. B **74**, 205414 (2006).

[104] X.-L. Qi and S.-C. Zhang, Physics Today **63** (1), 33 (2010).

[105] W. Beugeling, C. X. Liu, E. G. Novik, L. W. Molenkamp, and C. Morais Smith, Phys. Rev. B **85**, 195304 (2012).

[106] M. Zarea and N. Sandler, Phys. Rev. B **79**, 165442 (2009).

[107] R. van Gelderen and C. Morais Smith, Phys. Rev. B **81**, 125435 (2010).

[108] R. de Gail, M. O. Goerbig, and G. Montambaux, Phys. Rev. B **86**, 045407 (2012).

[109] Z. Qiao, S. A. Yang, W. Feng, W.-K. Tse, J. Ding, Y. Yao, J. Wang, and Q. Niu, Phys. Rev. B **82**, 161414 (2010).

[110] Z. Qiao, H. Jiang, X. Li, Y. Yao, and Q. Niu, Phys. Rev. B **85**, 115439 (2012).

[111] G. Murthy, E. Shimshoni, R. Shankar, and H. A. Fertig, Phys. Rev. B **85**, 073103 (2012).

[112] E. I. Rashba, Phys. Rev. B **79**, 161409 (2009).

[113] D. A. Abanin, P. A. Lee, and L. S. Levitov, Phys. Rev. Lett. **96**, 176803 (2006).

[114] Y. S. Dedkov, M. Fonin, U. Rüdiger, and C. Laubschat, Phys. Rev. Lett. **100**, 107602 (2008).

[115] D. Gosálbez-Martínez, J. J. Palacios, and J. Fernández-Rossier, Phys. Rev. B **83**, 115436 (2011).

[116] N. Levy, S. A. Burke, K. L. Meaker, M. Panlasigui, A. Zettl, F. Guinea, A. H. Castro Neto, and M. F. Crommie, Science **329**, 544 (2010).

[117] C. Brüne, C. X. Liu, E. G. Novik, E. M. Hankiewicz, H. Buhmann, Y. L. Chen, X. L. Qi, Z. X. Shen, S. C. Zhang, and L. W. Molenkamp, Phys. Rev. Lett. **106**, 126803 (2011).

[118] M. König, H. Buhmann, L. W. Molenkamp, T. Hughes, C.-X. Liu, X.-L. Qi, and S.-C. Zhang, J. Phys. Soc. Jpn **77**, 031007 (2008).

[119] B. Büttner, C. X. Liu, G. Tkachov, E. G. Novik, C. Brüne, H. Buhmann, E. M. Hankiewicz, P. Recher, B. Trauzettel, S. C. Zhang, and L. W. Molenkamp, Nature Phys. **7**, 418 (2011).

[120] G. De Simoni, A. Singha, M. Gibertini, B. Karmakar, M. Polini, V. Piazza, L. N. Pfeiffer, K. W. West, F. Beltram, and V. Pellegrini, Appl. Phys. Lett. **97**, 132113 (2010).

[121] S. Melinte, M. Berciu, C. Zhou, E. Tutuc, S. J. Papadakis, C. Harrison, E. P. De Poortere, M. Wu, P. M. Chaikin, M. Shayegan, R. N. Bhatt, and R. A. Register, Phys. Rev. Lett. **92**, 036802 (2004).

[122] Y. Zhang, Z. Jiang, J. P. Small, M. S. Purewal, Y.-W. Tan, M. Fazlollahi, J. D. Chudow, J. A. Jaszczak, H. L. Stormer, and P. Kim, Phys. Rev. Lett. **96**, 136806 (2006).

[123] D. Makogon, I. B. Spielman, and C. Morais Smith, EPL **97**, 33002 (2012).

[124] L. Sanchez-Palencia and M. Lewenstein, Nature Phys. **6**, 87 (2010).

[125] E. Alba, X. Fernandez-Gonzalvo, J. Mur-Petit, J. K. Pachos, and J. J. Garcia-Ripoll, Phys. Rev. Lett. **107**, 235301 (2011).

[126] E. Zhao, N. Bray-Ali, C. J. Williams, I. B. Spielman, and I. I. Satija, Phys. Rev. A **84**, 063629 (2011).

[127] T. D. Stanescu, V. Galitski, J. Y. Vaishnav, C. W. Clark, and S. Das Sarma, Phys. Rev. A **79**, 053639 (2009).

[128] X.-J. Liu, X. Liu, C. Wu, and J. Sinova, Phys. Rev. A **81**, 033622 (2010).

[129] N. Goldman, J. Beugnon, and F. Gerbier, Phys. Rev. Lett. **108**, 255303 (2012).

[130] M. Buchhold, D. Cocks, and W. Hofstetter, Phys. Rev. A **85**, 063614 (2012).

[131] M.-C. Chang and M.-F. Yang, Phys. Rev. B **69**, 115108 (2004).

[132] B. A. Bernevig and S.-C. Zhang, Phys. Rev. Lett. **96**, 106802 (2006).

[133] D. A. Abanin, R. V. Gorbachev, K. S. Novoselov, A. K. Geim, and L. S. Levitov, Phys. Rev. Lett. **107**, 096601 (2011).

[134] R. Yu, W. Zhang, H.-J. Zhang, S.-C. Zhang, X. Dai, and Z. Fang, Science **329**, 61 (2010).

[135] G. Y. Cho and J. E. Moore, Phys. Rev. B **84**, 165101 (2011).

[136] H. Jin, J. Im, and A. J. Freeman, Phys. Rev. B **84**, 134408 (2011).

[137] W.-K. Tse, Z. Qiao, Y. Yao, A. H. MacDonald, and Q. Niu, Phys. Rev. B **83**, 155447 (2011).

[138] T.-W. Chen, Z.-R. Xiao, D.-W. Chiou, and G.-Y. Guo, Phys. Rev. B **84**, 165453 (2011).

[139] M. Taillefumier, V. K. Dugaev, B. Canals, C. Lacroix, and P. Bruno, Phys. Rev. B **84**, 085427 (2011).

[140] J. P. Eisenstein, K. B. Cooper, L. N. Pfeiffer, and K. W. West, Phys. Rev. Lett. **88**, 076801 (2002).

[141] M. O. Goerbig, P. Lederer, and C. Morais Smith, Phys. Rev. B **68**, 241302 (2003).

[142] M. O. Goerbig, P. Lederer, and C. Morais Smith, Phys. Rev. B **69**, 115327 (2004).

[143] J. H. Smet, Nature **422**, 391 (2003).

[144] M. O. Goerbig, P. Lederer, and C. Morais Smith, Phys. Rev. Lett. **93**, 216802 (2004).

[145] U. Zeitler, H. W. Schumacher, A. G. M. Jansen, and R. J. Haug, Phys. Rev. Lett. **86**, 866 (2001).

[146] R. J. Nicholas, K. Takashina, M. Lakrimi, B. Kardynal, S. Khym, N. J. Mason, D. M. Symons, D. K. Maude, and J. C. Portal, Phys. Rev. Lett. **85**, 2364 (2000).

[147] I. Knez and R.-R. Du, Front. Phys. **7**, 200 (2012).

[148] E. O. Kane, J. Phys. Chem. Solids **1**, 249 (1957).

[149] Y. S. Gui, C. R. Becker, J. Liu, V. Daumer, V. Hock, H. Buhmann, and L. W. Molenkamp, Europhys. Lett. **65**, 393 (2004).

[150] Y. S. Gui, J. Liu, K. Ortner, V. Daumer, C. R. Becker, H. Buhmann, and L. W. Molenkamp, Appl. Phys. Lett. **79**, 1321 (2001).

[151] G. Tkachov and E. M. Hankiewicz, Phys. Rev. Lett. **104**, 166803 (2010).

[152] X. Lou, C. Adelmann, S. A. Crooker, E. S. Garlid, J. Zhang, K. S. M. Reddy, S. D. Flexner, C. J. Palmstrom, and P. A. Crowell, Nature Phys. **3**, 197 (2007).

[153] Y. K. Kato, R. C. Myers, A. C. Gossard, and D. D. Awschalom, Science **306**, 1910 (2004).

[154] C. Brüne, A. Roth, E. G. Novik, M. König, H. Buhmann, E. M. Hankiewicz, W. Hanke, J. Sinova, and L. W. Molenkamp, Nature Phys. **6**, 448 (2010).

[155] C. Brune, A. Roth, H. Buhmann, E. M. Hankiewicz, L. W. Molenkamp, J. Maciejko, X.-L. Qi, and S.-C. Zhang, Nature Phys. **8**, 486 (2012).

[156] D. G. Rothe, R. W. Reinthaler, C.-X. Liu, L. W. Molenkamp, S.-C. Zhang, and E. M. Hankiewicz, New J. Phys. **12**, 065012 (2010).

[157] W. Beugeling, M. O. Goerbig, and C. Morais Smith, Phys. Rev. B **81**, 195303 (2010).

[158] B. I. Halperin, P. A. Lee, and N. Read, Phys. Rev. B **47**, 7312 (1993).

[159] X. G. Wen and A. Zee, Phys. Rev. B **46**, 2290 (1992).

[160] X. G. Wen and A. Zee, Phys. Rev. Lett. **69**, 1811 (1992).

[161] V. W. Scarola and J. K. Jain, Phys. Rev. B **64**, 085313 (2001).

[162] D. Orgad, Phys. Rev. B **75**, 035301 (2007).

[163] M. O. Goerbig, P. Lederer, and C. Morais Smith, Physica E **34**, 57 (2006).

[164] C. L. Kane, S. Kivelson, D. H. Lee, and S. C. Zhang, Phys. Rev. B **43**, 3255 (1991).

[165] M. O. Goerbig and N. Regnault, Phys. Rev. B **75**, 241405(R) (2007).

[166] D. P. Arovas, R. Schrieffer, F. Wilczek, and A. Zee, Nucl. Phys. B **251**, 117 (1985).

[167] D. Bohm and D. Pines, Phys. Rev. **92**, 609 (1953).

[168] R. de Gail, N. Regnault, and M. O. Goerbig, Phys. Rev. B **77**, 165310 (2008).

[169] A. López and E. Fradkin, Phys. Rev. B **69**, 155322 (2004).

[170] W. Kohn, Phys. Rev. **123**, 1242 (1961).

[171] A. H. MacDonald and S.-C. Zhang, Phys. Rev. B **49**, 17208 (1994).

[172] K. Moon, H. Mori, K. Yang, S. M. Girvin, A. H. MacDonald, L. Zheng, D. Yoshioka, and S.-C. Zhang, Phys. Rev. B **51**, 5138 (1995).

[173] C. Tőke and J. K. Jain, Phys. Rev. B **75**, 245440 (2007).

[174] S. M. Girvin, A. H. MacDonald, and P. M. Platzman, Phys. Rev. B **33**, 2481 (1986).

[175] H. L. Stormer, A. Chang, D. C. Tsui, J. C. M. Hwang, A. C. Gossard, and W. Wiegmann, Phys. Rev. Lett. **50**, 1953 (1983).

[176] A. M. Chang, P. Berglund, D. C. Tsui, H. L. Stormer, and J. C. M. Hwang, Phys. Rev. Lett. **53**, 997 (1984).

[177] R. Willett, H. L. Stormer, D. C. Tsui, A. C. Gossard, J. H. English, and K. W. Baldwin, Surf. Sci. **196**, 257 (1988).

[178] V. J. Goldman, M. Shayegan, and D. C. Tsui, Phys. Rev. Lett. **61**, 881 (1988).

[179] E. E. Mendez, L. L. Chang, M. Heiblum, L. Esaki, M. Naughton, K. Martin, and J. Brooks, Phys. Rev. B **30**, 7310 (1984).

[180] R. G. Clark, J. R. Mallett, A. Usher, A. M. Suckling, R. J. Nicholas, S. R. Haynes, Y. Journaux, J. J. Harris, and C. T. Foxon, Surf. Sci. **196**, 219 (1988).

[181] J. P. Eisenstein, G. S. Boebinger, L. N. Pfeiffer, K. W. West, and S. He, Phys. Rev. Lett. **68**, 1383 (1992).

[182] Y. W. Suen, L. W. Engel, M. B. Santos, M. Shayegan, and D. C. Tsui, Phys. Rev. Lett. **68**, 1379 (1992).

[183] J. Jo, Y. W. Suen, L. W. Engel, M. B. Santos, and M. Shayegan, Phys. Rev. B **46**, 9776 (1992).

[184] A. H. MacDonald, Surf. Sci. **229**, 1 (1990).

[185] S. P. Shukla, Y. W. Suen, and M. Shayegan, Phys. Rev. Lett. **81**, 693 (1998).

[186] J. Ye, Phys. Rev. B **71**, 125314 (2005).

[187] J. Ye, Ann. Phys. **323**, 580 (2008).

[188] S. V. Kravchenko, W. Mason, J. E. Furneaux, and V. M. Pudalov, Phys. Rev. Lett. **75**, 910 (1995).

[189] K. Lai, W. Pan, D. C. Tsui, S. Lyon, M. Mühlberger, and F. Schäffler, Phys. Rev. Lett. **93**, 156805 (2004).

[190] E. Tutuc, M. Shayegan, and D. A. Huse, Phys. Rev. Lett. **93**, 036802 (2004).

[191] M. Kellogg, J. P. Eisenstein, L. N. Pfeiffer, and K. W. West, Phys. Rev. Lett. **93**, 036801 (2004).

[192] L. Tiemann, W. Dietsche, M. Hauser, and K. von Klitzing, New J. Phys. **10**, 045018 (2008).

[193] R. Penrose, Proc. Cambridge Philos. Soc. **51**, 406 (1955).

[194] A. Ben-Israel and T. N. E. Greville, *Generalized Inverses: Theory and applications*, Pure and Applied Mathematics (Wiley, New York, 1974).

[195] D. Bercioux, N. Goldman, and D. F. Urban, Phys. Rev. A **83**, 023609 (2011).

[196] N. Goldman, D. F. Urban, and D. Bercioux, Phys. Rev. A **83**, 063601 (2011).

[197] W. Beugeling, J. C. Everts, and C. Morais Smith, "Topological phase transitions induced by next-nearest-neighbor hopping in two-dimensional lattices," (2012), arXiv:1207.6545 .

[198] Z. Wang and S.-C. Zhang, Phys. Rev. X **2**, 031008 (2012).

[199] L. Fidkowski and A. Kitaev, Phys. Rev. B **81**, 134509 (2010).

[200] X.-L. Qi, "A new class of (2+1)-d topological superconductor with $\mathbb{Z}_8$ topological classification," (2012), arXiv:1202.3983 .

Samenvatting

In de klassieke mechanica van Newton beschrijft men deeltjes in termen van bijvoorbeeld zijn plaats en zijn snelheid. Deze grootheden zijn continue variabelen: Zij kunnen binnen zekere grenzen alle mogelijke waarden aannemen. In de golfmechanica zien we grootheden die een zeker aantal discrete waarden aannemen; denk bijvoorbeeld aan de frequentie van de trillingen in een snaar van een muziekinstrument. Zo op het eerste gezicht gedragen golven en deeltjes zich dus heel verschillend. Aan het begin van de twintigste eeuw heeft men echter aangetoond dat ook deeltjes zich gedragen als golven. De grootheden zoals plaats, snelheid en energie zijn geen continue variabelen, maar ook zij kunnen slechts bepaalde waarden aannemen. De theorie die dit beschrijft heet de *kwantummechanica*. Hierin refereert het woord "kwantum" aan het feit dat de grootheden gekwantiseerd zijn, ofwel, dat ze alleen in vaste, discrete stapjes voorkomen.

In het dagelijks leven werkt de klassieke mechanica heel goed, en zien we van de kwantummechanica weinig terug. De kwantisatiestappen van de eerder genoemde grootheden zijn zo klein, dat het lijkt alsof ze continue variabelen zijn. Pas op microscopisch niveau speelt kwantummechanica een belangrijke rol, bijvoorbeeld bij de beschrijving van de structuur van atomen. In dit proefschrift beschrijven we echter systemen waarbij de kwantummechanica ook observeerbaar is "in het groot"; de grootheden die hierbij een rol spelen zijn gekwantiseerd in stappen die met "huis-, tuin-, en keukenapparatuur" te meten zijn.

Een voorbeeld hiervan is het kwantum-Halleffect, waar dit proefschrift o.a. om draait. Dit effect is de kwantummechanische versie van het klassieke Halleffect, dat in 1879 is ontdekt door Edwin Hall. In zijn experiment in 1879 heeft hij stroom laten lopen door een plat stuk goudfolie, terwijl hij loodrecht daarop een magnetisch veld heeft aangebracht. Hall observeerde dat hij loodrecht op de stroom een spanning kon meten, die evenredig is met het product van de stroomsterkte en de sterkte van het magnetisch veld. Of vanuit een ander oogpunt gezien, is de zogenaamde *Hallweerstand* (de verhouding tussen het gemeten voltageen de aangelegde stroom) evenredig met het magnetisch veld. Ongeveer een eeuw later heeft Klaus von Klitzing een soortgelijk experiment gedaan, alleen dan met als geleider een dunne laag elektronen[22] op

[22] Elektronen zijn de geladen deeltjes die voor de elektrische stroom zorgen. Elektronen behoren tot de

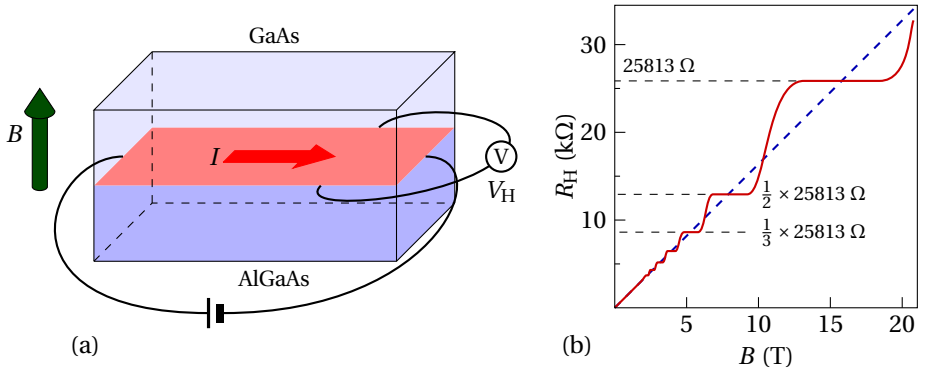

Figuur 1: (a) Een kwantum-Hallsysteem. Op het grensvlak (rood in de figuur) tussen de halfgeleidermaterialen GaAs en AlGaAs ontstaat een dunne laag die geleidend is voor elektronen. Loodrecht op dit grensvlak wordt een magnetisch veld **B** aangebracht, en in het vlak laat men een stroom I lopen. Dan wordt met een voltmeter loodrecht op de stroom het Hallvoltage V_H gemeten. De Hallweerstand is de verhouding tussen spanning en stroom $R_H = V_H/I$. (b) De Hallweerstand R_H als functie van het magnetisch veld B. De stippellijn geeft aan wat men in een klassiek systeem meet (het experiment van Hall in 1879), nl. dat de Hallweerstand evenredig is met het magnetisch veld. Bij een zeer zuiver systeem bij lage temperaturen, zoals bij het experiment van Von Klitzing in 1980, gedraagt de Hallweerstand zich zoals weergegeven door de continue lijn: Men ziet een trapvormige curve, met "treden" op $25813\,\Omega$, $\frac{1}{2} \times 25813\,\Omega$, $\frac{1}{3} \times 25813\,\Omega$, een teken dat er kwantisatie in het spel is.

het grensvlak tussen twee halfgeleiders [zie Fig. 1(a)]. Als de halfgeleiders zeer zuiver zijn, en als de temperatuur dicht bij het absolute nulpunt (ongeveer $-273\,^\circ$C) ligt, dan blijkt de Hallweerstand niet meer evenredig te zijn met het magnetisch veld, maar stapjes te vertonen op $25813\,\Omega$, $\frac{1}{2} \times 25813\,\Omega$, $\frac{1}{3} \times 25813\,\Omega$, etc., zoals weergegeven in Fig. 1. Deze waarden zijn niet microscopisch klein, maar heel alledaags. Zulke weerstandswaarden liggen ruim binnen het bereik van algemeen verkrijgbare voltmeters (bijv. de multimeters bij de doe-het-zelfzaak).

Het experiment van Von Klitzing laat zien dat de *Hallgeleiding* (1 gedeeld door de Hallweerstand) gekwantiseerd is in gelijke stappen, nl. $1/(25813\,\Omega)$. Deze waarde, het zogenaamde *geleidingskwantum*, is eenvoudig uit te drukken in universele natuurconstanten: Het is e^2/h, waarbij e de lading is van het elektron en h de constante van Planck. Opvallend genoeg hangt de waarde van het geleidingskwantum alleen af van universele natuurconstanten en niet van andere variabelen zoals de grootte van het systeem of van de materialen die worden gebruikt. Vanwege de universaliteit van het geleidingskwantum zijn kwantum-Hallexperimenten zeer bruikbaar om weerstandswaarden te ijken. De universele waarde, de Von Klitzingconstante, is bekend tot een

fermionen, een meer algemene groep deeltjes, waaraan de titel van dit proefschrift refereert.

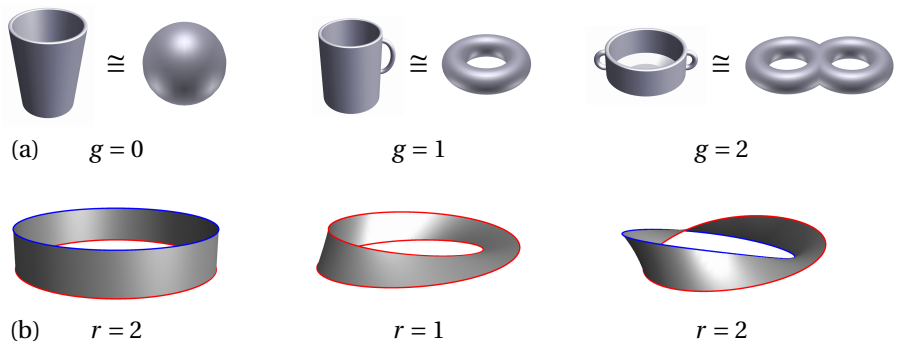

Figuur 2: Topologie. (a) Driedimensionale objecten die in elkaar omgevormd kunnen worden door te "kneden" zonder te scheuren, gaten te maken of te plakken zijn topologisch equivalent, aangegeven met het symbool "≅". Zo is een beker zonder oor equivalent met een bol, een mok met één oor equivalent met een torus (donut), en een soepkom met twee oren equivalent met een dubbele torus. Het "aantal oren" (ofwel het "genus") g is een topologische invariant, want het aantal oren kan niet veranderd worden door te "kneden". (b) Een strook papier kan aan de uiteinden aan elkaar worden geplakt tot een cilinder (links), maar door de uiteinden één slag of twee slagen te draaien ontstaan nieuwe, topologisch inequivalente structuren. Het aantal randen r van het oppervlak is een topologische invariant, maar kan anders dan het genus in (a) slechts twee waarden aannemen, $r = 1$ of $r = 2$. Dit is een voorbeeld van een "even-oneven" topologische invariant.

precisie van 1 op 3 miljard.[23]

Dat de kwantisatie van de Hallgeleiding zo nauwkeurig is bepaald komt doordat de waarde van de Hallgeleiding niet kan worden beïnvloed door kleine verstoringen zoals onzuiverheden in het materiaal of afwijkingen in de vorm van het systeem. Vanwege deze eigenschap wordt het kwantum-Halleffect *topologisch* genoemd. Deze term is ontleend aan het vakgebied *topologie* in de wiskunde. In dit onderdeel van de meetkunde bestudeert men van objecten de eigenschappen die niet veranderen bij een continue vervorming: Twee oppervlakken of lichamen worden beschouwd als topologisch equivalent als zij in elkaar om te vormen zijn zonder te "scheuren" of te "plakken", zie Fig. 2. In de topologie spelen *topologische invarianten* een belangrijke rol. Dit zijn getallen die nauw verbonden zijn aan de topologische structuur van een object: Als twee objecten topologisch equivalent zijn, dan moeten die topologische invarianten gelijk zijn.[24] Een continue vervorming van een object verandert zijn topologische eigenschappen niet, en daarom blijven ook de topologische invarianten behouden. In die zin is de Hallgeleiding een topologische invariant, omdat kleine (continue) veran-

[23] Naast zijn eigen constante heeft Von Klitzing voor zijn werk ook de Nobelprijs voor Natuurkunde van 1985 gekregen.

[24] Omgekeerd hoeft het niet altijd te gelden.

deringen geen invloed erop hebben. Hierbij moet vermeld worden dat deze topologische invariant los staat van de topologische structuur van het kwantum-Hallsysteem zelf; de topologie die verband houdt met de Hallgeleiding heeft een abstractere definitie (die ter sprake komt in hoofdstuk 2 van dit proefschrift).

We hebben nu vastgesteld dat de Hallgeleiding gekwantiseerd en topologisch is, maar we hebben nog geen antwoord gegeven op de vraag waarom. Het magnetisch veld zorgt ervoor dat alleen de elektronen die zich aan de rand bevinden kunnen bijdragen aan de stroom. Elektronen ver van de rand blijven op dezelfde plaats. Dit is een bijzonderheid van het kwantum-Hallsysteem: Het inwendige ("de bulk") van het systeem is isolerend (d.w.z. er loopt daar geen stroom) terwijl de randen elektrisch geleidend zijn. Het feit dat de stromen alleen langs de randen kunnen lopen en dat het magnetische veld deze stromen in één bepaalde richting dwingt heeft een belangrijke consequentie. Als een elektron botst tegen een onzuiverheid in het materiaal, dan kan onmogelijk zijn bewegingsrichting omdraaien. Botsingen hebben dus geen effect op de stroom. Aangezien deze randstromen verantwoordelijk zijn voor de Hallgeleiding, is deze dus immuun voor de aanwezigheid van zulke onzuiverheden. In vergelijking: In een normale geleider veroorzaken onzuiverheden een elektrische weerstand doordat elektronen botsen met deze onzuiverheden. Bij zulke botsingen kunnen de elektronen teruggekaatst worden in een willekeurige richting, wat zorgt voor een afname in de elektrische stroom, en dus een toename in de elektrische weerstand.

Een ander voorbeeld van topologie in een tweedimensionaal systeem is het kwantum-spin-Halleffect, theoretisch beschreven en experimenteel aangetoond rond 2005. Het kwantum-spin-Halleffect is een variant van het kwantum-Halleffect waarbij de randstromen niet veroorzaakt worden door een magnetisch veld, maar door een materiaaleigenschap die *intrinsieke spin-baankoppeling* genoemd wordt. Hierdoor hebben elektronen met tegengestelde spin[25] een tegengestelde bewegingsrichting op de rand, waardoor er netto geen elektrische lading verplaatst wordt, maar wel "spinlading". De bijbehorende topologische invariant is in dat geval de spin-Hallgeleiding. Anders dan de gewone Hallgeleiding kan deze invariant slechts twee waarden aannemen, "even" en "oneven" [zie Fig. 2(b)]. Materialen die het kwantum-spin-Halleffect vertonen worden ook wel *topologische isolatoren* genoemd; op dit moment wordt er zeer veel onderzoek gedaan naar zulke materialen en hun eigenschappen, zowel in tweedimensionale als in driedimensionale systemen.

In dit proefschrift onderzoek ik verschillende tweedimensionale (d.w.z. platte) systemen met topologische invarianten zoals de Hallgeleiding en spin-Hallgeleiding. In hoofdstuk 2 onderzoek ik systemen waarin zowel een magnetisch veld (dat aanleiding geeft tot het kwantum-Halleffect) als spin-baankoppeling (dat leidt tot het kwantum-

[25] Deeltjes zoals elektronen hebben in de kwantummechanica een extra vrijheidsgraad genaamd "spin". Spin heeft geen klassiek analogon, maar gedraagt zich als een impulsmoment (rotatie om zijn as). Het elektron heeft kan twee spintoestanden hebben ,"up" of "down".

spin-Halleffect) aanwezig zijn. Hierbij laat ik zien dat er ook toestanden bestaan waarbij tegelijkertijd de Hallgeleiding en de spin-Hallgeleiding gekwantiseerd zijn (en niet nul). Dit doe ik door een analyse te maken van de kwantumtoestanden van de elektronen op de rand. Ik geef ook een overzicht van het soort systemen waarin zulke toestanden experimenteel geobserveerd kunnen gaan worden. Hierbij passeren bijvoorbeeld grafeen en optische roosters de revue, beide ook vakgebieden waarin op dit moment zowel op theoretisch als op experimenteel gebied zeer veel interesse is.

In hoofdstuk 3 bestudeer ik een systeem van het materiaal HgTe, dat een sterke spin-baankoppeling heeft. Als het niet wordt blootgesteld aan een magnetisch veld, dan is in dit systeem het kwantum-spin-Halleffect te meten. In een magnetisch veld gedraagt het zich als een kwantum-Hallsysteem. Door Mn ionen toe te voegen veranderen de magnetische eigenschappen van het materiaal, wat leidt tot een bijzonder verloop van de Hallgeleiding als functie van het magnetisch veld.

In hoofdstuk 4 beschrijf ik een formalisme waarmee het *fractioneel* kwantum-Halleffect kan worden verklaard. Het fractioneel kwantum-Halleffect is zichtbaar in een meting van de Hallgeleiding van een kwantum-Hallsysteem als kwantisatiestappen die niet op een geheel veelvoud maal het geleidingskwantum e^2/h liggen, maar op een breuk maal e^2/h. Dit wordt veroorzaakt doordat het magnetisme aan de elektronen "kleeft". Dit effect wordt beschreven met het zogenaamd *Chern-Simonsformalisme*. In dit proefschrift geef ik aan hoe dit formalisme moet worden toegepast wanneer de interne vrijheidsgraden van de elektronen, zoals spin, een niet verwaarloosbare bijdrage leveren aan de fysische eigenschappen (bijv. de Hallgeleiding).

De motivatie om deze onderwerpen te onderzoeken ligt in de (toekomstige) toepasbaarheid van topologische toestanden bijvoorbeeld bij kwantumcomputers. De topologische bescherming van zulke toestanden, namelijk de immuniteit voor kleine verstoringen, zou een van de belangrijkste problemen uit dit vakgebied, het verloren gaan van de kwantumdata door invloeden van buitenaf, kunnen oplossen. Tevens zijn er mogelijkheden om topologische toestanden te gebruiken in de *spintronica*, waarbij niet de elektrische lading van de elektronen, maar hun spin wordt gebruikt om schakelingen mee te maken.

Dankwoord

Er was mij van tevoren verteld dat het leven van een promovendus bestond uit hard werken en lange dagen maken. Terugkijkend op die periode van bijna vier jaar kan ik nu niet zeggen dat het me is tegengevallen of dat het heel zwaar is geweest. Zoals dat met meer levensfasen gaat, zal ik later nog met plezier aan deze tijd terugdenken. Het plezier in het werk als promovendus komt natuurlijk met name door de fijne werkomgeving. Ik ben dankbaar voor ieder die daaraan een bijdrage heeft geleverd. Hier bedank ik in het bijzonder de mensen die een grote of kleine, directe of indirecte rol hebben gespeeld bij de totstandkoming van dit proefschrift.

First of all, let me thank my PhD advisor Cristiane, for her insights, ideas, advices, care, and encouragement. It has been really a pleasure to work with her in the past four years, both in research and in educational activities. The collaboration has been very productive, and I hope we could continue this good collaboration in the future.

I am also indebted to the other co-authors of the papers on which this thesis is based, Mark Goerbig, Nathan Goldman, Chao-Xing Liu, Alena Novik, and Laurens Molenkamp, for the fruitful collaborations and for the many useful suggestions that have certainly improved the quality of these works.

Laat ik ook al mijn huidige en voormalige collega's bedanken die het ITF tot een fijne werkplek maken en hebben gemaakt, zowel bij het werk zelf als bij de wat meer ontspannen momenten daarbuiten, zoals lunches, borrels en andere extra-institutionele activiteiten. Ik noem hier nog enkele mensen die ik in het bijzonder wil bedanken. First, I thank the fellow PhD students and postdoc in Cristiane's group, Lih-King, Dima, Achilleas, Olivier, Ralph, and Marco. Verder dank ik mijn kamergenoot Martijn, met wie ik vier jaar lang met plezier het kantoor heb gedeeld. Uiteraard ben ik ook dank verschuldigd aan de mensen die het instituut draaiende houden in administratief en technisch opzicht, Geertje, Wilma, Biene, Olga, Els, Joost, Marion en Riny.

Niet minder belangrijk zijn de mensen buiten het instituut, die misschien wel minder direct betrokken zijn bij het promotieonderzoek zelf, maar juist meer bij het leven daarbuiten. Allereerst noem ik mijn studievrienden Wilfred, Jan Willem, Martijn, Marius en Wouter; hoewel we nu ver uit elkaar leven—dat hoort er nou eenmaal bij in de academische wereld—blijven we toch een hechte club. Ik wil ook de vrienden noemen

die ik heb overgehouden aan mijn periode in de studentenflat van de Warande in Zeist, in het bijzonder Hans, Ingrid, Els, Chris, Imam en Hilde.

En tot slot bedank ik mijn ouders Willem en Ina en mijn broer Steven, voor al hun zorg en steun, maar toch vooral voor de gezelligheid.

Curriculum vitae

Ik ben geboren op 21 maart 1982 in Winkel, gemeente Niedorp. Van 1994 tot 2000 heb ik vwo gevolgd aan het Murmelliusgymnasium in Alkmaar. In 2000 ben ik begonnen met de TWIN-studie Natuurkunde en Wiskunde aan de Universiteit Utrecht. Mijn doctoraaldiploma voor Wiskunde heb ik in 2005 behaald (*cum laude*) na het schrijven van een scriptie over de Heisenberggroep en pseudodifferentiaaloperatoren, onder begeleiding van Joop Kolk. In 2008 heb ik de masterstudie Theoretical Physics (eveneens *cum laude*) afgerond met een scriptie over supergravitatie, begeleid door Bernard de Wit. In september 2008 ben ik begonnen met het promotieonderzoek bij Cristiane Morais Smith waarvan dit proefschrift het resultaat is.

Publications

This thesis is based on the following publications:

- W. Beugeling, M. O. Goerbig, and C. Morais Smith, *Chern-Simons theory of multi-component quantum Hall systems*, Phys. Rev. B **81**, 195303 (2010).
- N. Goldman, W. Beugeling, and C. Morais Smith, *Topological phase transitions between chiral and helical spin textures in a lattice with spin-orbit coupling and a magnetic field*, EPL **97**, 23003 (2012).
- W. Beugeling, C. X. Liu, E. G. Novik, L. W. Molenkamp, and C. Morais Smith, *Reentrant topological phases in Mn-doped HgTe quantum wells*, Phys. Rev. B **85**, 195304 (2012).
- W. Beugeling, N. Goldman, and C. Morais Smith, *Topological phases in a two-dimensional lattice: Magnetic field versus spin-orbit coupling*, Phys. Rev. B **86**, 075118 (2012).
- W. Beugeling, M. O. Goerbig, and C. Morais Smith, *Generalisation of Murthy and Shankar's Hamiltonian theory to multi-component systems*, in preparation.

Other publications to which the author has contributed:

- W. Beugeling, J. C. Everts, and C. Morais Smith, *Topological phase transitions induced by next-nearest-neighbor hopping in two-dimensional lattices*, preprint arXiv:1207.6545 [cond-mat.mes-hall].
- R. van Gelderen, W. Beugeling, and C. Morais Smith, *Electronic states in twisted bilayer graphene in a commensurate periodic magnetic field*, in preparation.